

THE PENNSYLVANIA STATE UNIVERSITY
SCHREYER HONORS COLLEGE

DEPARTMENT OF BIOENGINEERING

Development of a Magnetic Bead Microrheometry System to Study Thrombus Rheology

ANDREW ROGERS
SPRING 2013

A thesis
submitted in partial fulfillment
of the requirements
for a baccalaureate degree
in Bioengineering
with honors in Bioengineering

Reviewed and approved* by the following:

Keefe Manning
Associate Professor of Bioengineering and Surgery
Thesis Supervisor and Honors Adviser

Peter Butler
Associate Professor of Bioengineering
Thesis Supervisor

Steven Deutsch
Senior Scientist Emeritus
Faculty Reader

* Signatures are on file in the Schreyer Honors College.

ABSTRACT

The primary objective of this study was to develop a magnetic bead microrheometry system to measure spatially heterogeneous thrombus elasticity. Elasticity of a thrombus may affect the time and location of embolism, leading to stroke or heart attack. Previous studies in thrombus rheology studied entire thrombi as one homogeneous material, but have not accounted for the heterogeneous composition of thrombi. The spatial variation in magnetic force developed by a computer controlled electromagnet was calibrated by measuring the displacement of 45 μm fluorescent paramagnetic beads embedded in polyacrylamide hydrogels of homogeneous tunable elasticity. Nm-scale displacements of beads were measured using bead tracking software that cross-correlated bead position between recorded frames. Polyacrylamide hydrogels with an elasticity of 0.2 kPa and 1.61 kPa were used to calibrate the working area of the system and gather displacement data for beads in that area. These values were chosen to represent the upper and lower bounds of previous thrombus rheology studies. This force distribution in the gel due to magnetic force on the bead was then derived by integrating the total force of the gel on the bead after a prescribed displacement using finite element analysis. The force calculations were interpolated to map force as a function of position within the working area in order to test samples of spatially non-uniform elasticity. By studying thrombus rheology using magnetic bead microrheometry, localized measurements of elasticity can be used to correlate with local cellular and fibrin composition and flow dynamics on thrombus elasticity.

TABLE OF CONTENTS

List of Figures	iii
List of Tables	iv
Acknowledgements.....	v
Chapter 1 Introduction	1
Coagulation Cascade.....	3
Importance of Clot Rheology.....	5
Clot Rheology	6
Magnetic Bead Microrheology	7
Chapter 2 Methods.....	9
Overview	9
Hydrogel formation.....	10
Magnet and Experimental Setup	12
Fluorescent Microscopy, Image Capture, and Bead Tracking	15
Experimental testing with hydrogel	17
Position Calculation	18
Data Processing.....	20
COMSOL modeling.....	22
Chapter 3 Results	27
COMSOL Modeling for force calculation	27
Bar Magnet Placement Reproducibility	28
Bead Location Calculations	29
Initial results of bead tracking.....	31
Results with Electromagnet.....	35
Chapter 4 Discussion	49
Bar Magnet.....	50
Bead Response Categories	53
Analysis of Different Response Types.....	56
Spatial Distribution of Response Categories.....	58
COMSOL Modeling of Magnetic Force	60
Conclusion and Future Directions.....	62
Bibliography.....	64
Appendix A: Solidworks figures and schematics of slide and electromagnet holders	67
Appendix B: Bead displacement data for 1.61 kPa Hydrogel.....	69
Appendix C: Bead displacement data for 0.2 kPa Hydrogel.....	128
Academic Vita.....	173

LIST OF FIGURES

Figure 1:	Blood Coagulation Cascade	4
Figure 2:	Experimental Setup for Bar Magnet	12
Figure 3:	Experimental Setup for Electromagnet	13
Figure 4:	Electromagnet Control System Setup	13
Figure 5:	Micrometer	15
Figure 6:	Working Area of Hydrogel	17
Figure 7:	Magnet Origin	18
Figure 8:	Position Calculation of Beads	19
Figure 9:	Initial COMSOL Model	21
Figure 10:	Simplified COMSOL Model	22
Figure 11:	COMSOL Model of Normal Stress on Bead	23
Figure 12:	Stress Distribution on Bead	25
Figure 13:	Magnetic Field Lines	26
Figure 14:	Initial COMSOL Force on Bead Results	28
Figure 15:	Beads Under Fluorescent Microscopy	29
Figure 16:	Preliminary Results with Bar Magnet	32
Figure 17:	Reproducibility Study with Bar Magnet	33
Figure 18:	Summary of Reproducibility Study	35
Figure 19:	Spatial Distribution of Beads in Hydrogels	38
Figure 20:	Representative Plots of Bead Response Categories	39
Figure 21:	Spatial Distribution of Beads by Response Type	42
Figure 22:	Magnetic Field Over Distribution of Beads by Response Type	43
Figure 23:	Side View of Experimental Setup with Field Lines	45

LIST OF TABLES

Table 1:	Polyacrylamide Hydrogel Substrates	10
Table 2:	Hydrogel Material Properties	22
Table 3:	Paramagnetic Bead Material Properties	22
Table 4:	Standard Deviation of Bar Magnet Placement	29
Table 5:	Bead Location Vernier Scale Values	30
Table 6:	Relating Bead Positions	30
Table 7:	Distance Component Calculations using ImageJ	30
Table 8:	Final Position of Beads	31
Table 9:	Bead Positions Relative to Magnet Origin	36
Table 10:	Number of Response Types by Category	41
Table 11:	Summary of Bead Positions, Displacements, and Forces	46
Table 12:	Back Calculation of Gel Elasticity	49

ACKNOWLEDGEMENTS

I would like to thank Gene Gerber and Gary Meyers for their manufacturing expertise and technical assistance. I would also like to thank Changjin Huang for his instruction and advice on making polyacrylamide hydrogels. I would also like to thank Prithvi Nilkant, my undergraduate assistant, for his patience and assistance in learning about this project and helping me tackle the endless spreadsheets of raw data.

In particular, I want to thank both Dr. Butler and Dr. Manning for all of the support and resources they have provided. This was a collaborative effort on their parts to mentor me through this project, each lending their particular expertise to educate and advise me as I progressed. A special thanks goes to Dr. Manning for allowing me to work in his lab in the first place, and I would also like to thank Dr. Butler for trusting me with his incredibly high tech – and expensive – microscope. I would also like to thank Dr. Butler, Dr. Manning and Dr. Deutsch for taking the time to read this thesis and provide feedback.

Finally, I want to thank my family for their continued support throughout my education. Even though you do not understand most of the details of this research, the effort to try to understand means all the world.

Chapter 1

Introduction

Cardiovascular Disease is the leading cause of death in the United States, causing about one out of every three deaths.^{1,2} Cardiovascular disease includes ischemic heart diseases such as myocardial infarction and atherosclerotic cardiovascular disease, heart failure, endocarditis, hypertension, cerebrovascular disease (stroke), and atherosclerosis.¹ Of these, several are directly related to, or a result of, atherosclerosis. Atherosclerosis is a disease process characterized by inflammation and hardening of the vascular walls as a result of a buildup of fatty deposits, cells, and scar tissue.² This buildup leads to progressive occlusion of the lumen leading to stenosis. Also, the hardening of the vascular walls reduces the arterial compliance, decreasing the ability for dynamic regulation of local pressure and conditions. As a result, atherosclerosis can be a catalyst for various cardiovascular pathologies and is considered a significant indicator of risk for cardiovascular disease as a whole.³

Stenoses that form as a result of atherosclerosis can play a significant role in disease formation by altering the fluid mechanics of the blood flow. Narrowing of the lumen requires flow velocity through the stenosis to increase, creating a jet. In the sudden expansion downstream of the stenosis, velocity must decrease due to principles related to flow continuity and Bernoulli's equation. The mix of suddenly changing velocities and pressures may create a region of turbulent flow characterized by separation of the high velocity jet through the stenosis that leads to recirculations.⁴⁻⁶ Recirculation

regions can lead to stagnating flow that allows for cell and platelet aggregation that can initiate thrombus formation.⁶ Residence time in recirculations have been related to fibrin polymerization in shear flow.⁴ *In vivo*, platelets are concentrated near the vessel wall, a proximity that combined with stagnation in recirculation regions, allows activated platelets maximum time to adhere to the vessel wall.⁵ Thus, the altered fluid mechanics through and downstream of an arterial stenosis directly lead to thrombus formation.

Thrombus formation itself can occlude vessels, leading to adverse cardiac events that may end in hospitalization or mortality. Another major concern is thromboembolism, the breakage of part or all of a thrombus as a result of stress from blood flow.⁴ The presence of aortic atherosclerotic lesions increases risk of embolic events in patients by 10% per patient-year.⁷ Emboli can be carried downstream where they can subsequently block arteries, potentially causing stroke, pulmonary embolism, or myocardial infarction.

Shear stress due to viscous blood flow over blood clots can result in embolization as the stress dislodges or breaks off part of a clot. This stress is related to velocity and vessel diameter,⁵ so various geometries and flow patterns can affect shear stress and potential for embolization. Some research suggests that reversal and rotational blood flow in the thoracic aorta can lead to cerebral embolism from distal aortic atherosclerotic plaques.⁸

Thromboembolism is of particular concern in the development of artificial cardiac devices. Left ventricular assist devices (LVADs), total artificial hearts, and prosthetic heart valves have all been linked to increased risk of thromboembolism.^{9,10} In addition to the way these devices alter flow patterns, this increased risk stems from the interaction

between blood and the biomaterials. Biomaterials cannot, as of yet, mimic the endothelium and therefore have different interactions with blood.¹¹ Thrombus formation is initiated by proteins adsorbing to the biomaterial surface, which can lead to platelet activation to initiate the coagulation cascade.¹¹ Thromboembolism is a challenge to study owing to the variability in geometry, pulsatile fluid flow, and the cellular components of blood, however given the significance of thromboembolism as it relates to atherosclerosis, cardiovascular disease, and medical devices, this is a process that merits further study. In particular, studying the material properties of blood clots is valuable in understanding the mechanical response of thrombi to shear stress due to blood flow.

Coagulation Cascade

When a blood vessel is damaged and collagen exposed, platelets bind and are activated to release a series of proteins including adenosine diphosphate, serotonin, platelet-activating factor, von Willebrand Factor, thromboxane A₂, and platelet Factor IV.¹² These proteins further recruit platelets and mediate adhesion, forming a platelet plug. This platelet plug is the immediate response to tissue injury, but is rapidly replaced by a chemically stable fibrin blood clot.¹³

Blood clots form as a result of the coagulation cascade (Figure 1). This cascade has two starting pathways (intrinsic and extrinsic) that lead to a common pathway for final clot formation. The extrinsic pathway results from damage to the endothelium and is the primary pathway for homeostatic blood coagulation. The intrinsic pathway is

surface mediated and is the pathway most related to thrombus formation as a result of cardiovascular devices.

The extrinsic pathway initiates with tissue thromboplastin (or tissue factor) activating Factor VII, which in turn activates Factor X.^{13,14} The intrinsic pathway results from activation of Factor XII by kallikrein on a negatively charged surface, which subsequently activates Factors XI, IX, and VIII before activating Factor X.^{13,14} The activation of Factor X is the beginning of the common pathway coagulation. Activated Factor X (FXa) binds with activated Factor V (FVa) to cleave prothrombin to thrombin. Thrombin acts as an agonist in activating platelets, and platelets release phospholipids to accelerate thrombin generation.¹² The key function of thrombin is to convert fibrinogen to fibrin. Fibrin monomers then quickly polymerize to form a complex, stable fibrin network.^{13,15,16} This network can entrap platelets and erythrocytes as it forms a stable blood clot in place of the platelet plug.

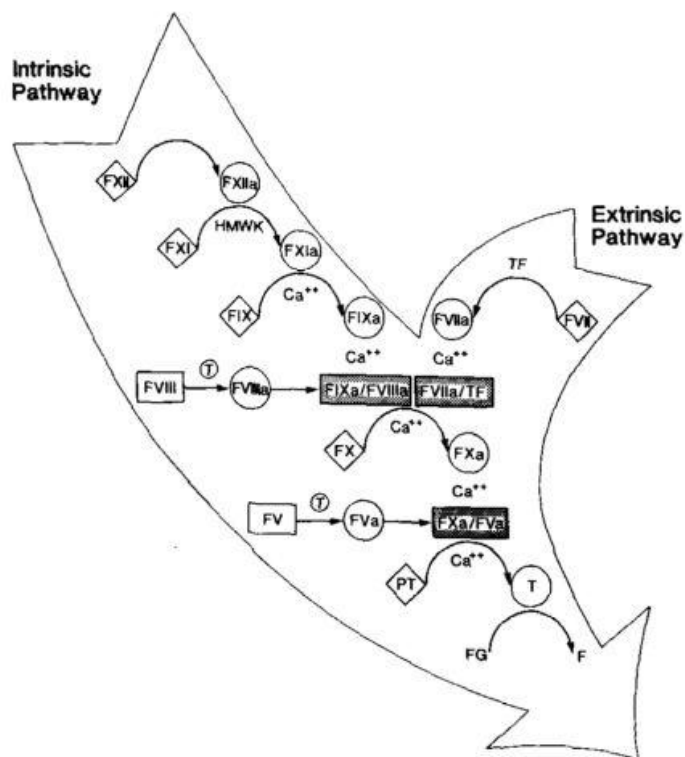


Figure 1:¹⁴ Blood coagulation cascade. The extrinsic pathway is initiated by the activation of Factor VII (FVII) by tissue factor (TF), leading to the activation of Factor X (FX). The intrinsic pathway is initiated by activation of Factor XII (FXII) followed by subsequent activation of Factors XI (FXI), IX (FIX), VIII (FVIII), and X (FX). Activated Factor X (FXa) binds with activated Factor V (FVa) to cleave prothrombin (PT) to thrombin (T). Thrombin then activates fibrinogen (FB) to fibrin (F) initiating clot formation.

Importance of Clot Rheology

As embolization is a result of a stress deforming a material to fracture, it is important to understand the rheological properties of that material. Rheology is the study of the relationship between an applied stress and resulting deformation of a material.¹⁷ In thrombi formed *in vivo*, that applied stresses are the shear stress from blood flow and normal stresses from hydrostatic pressure. The resultant deformation can lead to

embolization. By understanding the rheological properties of blood clots, the mechanical response to shear stress from blood flow can be better understood and computational fluid dynamics can be used to better predict clot formation and embolization.

Clot Rheology

Previous clot rheology studies have looked at whole clot rheology^{18,19} and in studied fibrin fiber rheology.²⁰ These studies, however, are limited in several respects. The work done on whole clots utilized cone and plate rheometers,^{18,19} which only provide an average measurement of the overall response.¹⁷ While this may give a good approximate value, it does not accurately represent spatially non-homogeneous materials. Blood clots are inhomogeneous networks composed of platelets, erythrocytes, leukocytes, fibrin, and other proteins and clotting factors. This composition is dependent on a number of factors including calcium ions,²¹ Factor XIIIa,^{15,21} hematocrit,^{5,18} and fibrin network.¹⁸⁻²⁰ The factors can be highly complex as Factor XIIIa can catalyze isopeptide bonds between fibrin molecules, resulting in clots up to 5 times stiffer than unligated counterparts,¹⁵ and clot elasticity is thought to be strongly dependent on fibrin fiber thickness, branchpoint density, and fibrin concentration.¹⁹ In short, to assume clots are homogenous and can be characterized by an average elasticity is a flawed assumption due to the variability in factors affecting clot composition. As such, it is important to study clot rheology on a localized level to account for inhomogeneity and to potentially correlate local elasticity to local composition.

Another flaw to previous work in clot rheology is the manner in which the clots under examination were formed. In some studies, the clots were formed by simply allowing whole blood to coagulate for 30 minutes to 2 hours.^{18,19} This is by no means a physiological representation of thrombogenesis. *In vivo* thrombus formation is often a result of areas of recirculation in blood flow due to geometries of vascular bifurcations, branching, and curvatures, as well as following stenosis and atherosclerotic lesions, as previously described.^{4,5} Factors affecting clot composition are often related to flow conditions and can dynamically change the clot composition as it forms. For example, varied relative concentrations of red blood cells can affect fibrin network density as clots form, resulting in a varied structure and locally different rheological properties.¹⁸ As such, forming clots by flow phenomena in a bench top blood flow loop is important to simulate physiologic clot formation conditions.

Magnetic Bead Microrheology

Most previous studies in clot rheology utilized cone and plate rheometers that produced average values for whole clot elasticity.^{18,19} In order to study clot rheology on a localized level to account for inhomogeneity, a microrheology technique must be used. Microrheology is rheology but on a smaller scale to locally deform a material and test local elasticity, often using embedded micron-sized probes.¹⁷ Some work has been done using microrheology techniques to study fibrin fiber elasticity by attaching $\sim 1\mu\text{m}$ polystyrene latex beads to individual fibers. The beads were then trapped by optical tweezers and oscillated to deflect the fiber.²⁰ This study looked specifically at the

elasticity of individual fibrin clots, but the same principles of microrheology can be applied to look a little larger at a region of a thrombus.

Magnetic bead microrheology is a microrheological technique that embeds paramagnetic micron-sized beads in a material.¹⁷ By introducing a magnetic field, a magnetic force acts on the beads, placing a load on the material as it resists displacement of the beads. This load can be in pico- or nano-Newton range, depending on magnet strength, bead size, and distance to magnet.^{22,23} Magnetic bead microrheology has been used to test viscoelastic parameters of adherent cell surfaces and cytoskeletal deformations.^{22,23} Advantages of the magnetic bead microrheology system is that it can be constructed at relatively low cost, is repeatable, and does not require major or permanent microscope adjustments.

The purpose of this project is to develop a magnetic bead microrheometry system to study the elasticity of blood clots formed in a backwards-facing step blood flow model. Polyacrylamide hydrogels of tunable homogenous elasticity were used to develop and calibrate this system that uses a computer controlled electromagnet.

Chapter 2

Methods

Overview

Elasticity is a relationship between stress (due to a force) and strain (due to a displacement or deformation). In order to study the unknown elasticity of a material, there must be a known stress (σ) and known strain (ϵ) to relate via the elasticity (E) (Equation 1).

$$\sigma = E * \epsilon \quad (\text{Equation 1})$$

In terms of magnetic bead microrheology, the stress comes from the magnetic force applied to the paramagnetic beads embedded in the material. The strain is then the displacement of the paramagnetic beads as a result of that force. To calculate elasticity, the force acting on the beads and displacement of the beads must be known.

Displacement of the beads can be measured directly using fluorescent microscopy and tracking software to track bead movement. Determining the force acting on a given bead is not simple. Magnetic fields from an electromagnet are nonuniform, so the magnetic force changes with distance and position relative to the magnet. As such, the force must be experimentally determined. To do this, a material of known elasticity must be used as the test subject so that a force can be calculated from a known displacement and known elasticity. Polyacrylamide hydrogels were used as the material of known elasticity to determine the magnetic force by position. By solving for magnetic force by

position, a map of forces can be interpolated between experimental values, allowing for the magnetic force to be known for a given location within the working range. With a known force and a measurable displacement, the elasticity of unknown samples can be calculated.

Hydrogel formation

Polyacrylamide hydrogels have been used to mimic extracellular matrix for studying cell-substrate mechanical interactions and applications in tissue engineering.²⁴⁻²⁶ These gels are popular as they produce a linear deformation and complete, rapid recovery in response to the addition and removal of a wide range of stress. They are also clear, nonfluorescent, and the rigidity of hydrogels can be easily manipulated.^{24,25} These traits make polyacrylamide hydrogels an excellent material to test and calibrate the magnetic bead microrheometry system as it will display an elastic deformation in response to bead displacement, will not interfere with fluorescent imaging of the magnetic beads, and allows for an elastically tunable material for initial testing. Polyacrylamide hydrogels have been used previously to develop a portable magnetic tweezer device using magnetic bead microrheometry.²³

Coverslips and glass slides were activated to bind securely to the hydrogel solution. Coverslips (18 mm x 18 mm, VWR, Radnor, Pennsylvania) and glass slides (3" x 1" x 1 mm, Fisher Scientific, Pittsburgh, Pennsylvania) were passed over the inner flame of a Bunsen burner, smeared with 0.1N NaOH (VWR) and air dried in a chemical safety hood. The coverslips and slides were then immersed in 2% 3-

aminopropyltrimethoxysilane (Sigma-Aldrich, St. Louis, Missouri) in isopropanol for 10 minutes while gently swirled in a glass dish. The coverslips and slides were washed in double distilled water (ddH₂O) 4 times for 5 minutes each wash. The coverslips and slides were then immersed in 1% glutaraldehyde (VWR) solution in ddH₂O and swirled for 30 minutes. Following 3 5-minute washes of ddH₂O, the coverslips and slides were left to dry at room temperature, covered with foil to prevent dust from sticking.

A microchamber was made to form the gel for viewing under fluorescent microscopy. Micrometers were used to measure to half the length of a treated glass slide, and this halfway point was marked using a diamond scribe pen (SPI Supplies, West Chester, Pennsylvania). This reference point aligns the gel in the center of the slide for consistent positioning. One strip of double sided tape (80 μ m thick) was used on either side of an activated coverslip to attach the coverslip to the slide, and the coverslip edge was aligned on the center mark.

Stock solutions of acrylamide/bis-acrylamide mixtures were made based on the relative concentrations of acrylamide, bis-acrylamide, and ddH₂O for the desired Young's Modulus of the hydrogel (Table 1);²⁴ however, a small volume of water was withheld to be made up when adding the beads at 0.1% w/v (weight per volume). This was done as the magnetic beads are dissolved in water, so the relative concentration of water will remain correct for the desired elasticity. Hydrogel substrate elasticity's were chosen to reflect the range of elasticity's experimentally determined in previous clot rheology studies.

Table 1.^{24,27} Four polyacrylamide hydrogel substrates used to calibrate and test the hydrogel system.

Acrylamide %	Bis-Acrylamide %	E \pm St. Dev. (kPa)
3	0.03	0.2 \pm 0.03
3	0.06	0.48 \pm 0.16
3	0.1	1.10 \pm 0.34
8	0.08	1.61 \pm 0.11

Acrylamide/bis-acrylamide solution was degassed in a vacuum chamber for 20 minutes. A 10% ammonium persulfate solution (VWR) was made with ddH₂O. Following degassing, 45 μ m diameter yellow-green fluorescent magnetic beads (Spherotech, Lake Forest, Illinois) were added to a final concentration of 0.1% w/v. To initiate gel polymerization, tetramethylethylenediamine (TEMED, VWR) and ammonium persulfate solution were added at concentrations of 0.15% and 0.5%, respectively. After briefly mixing with a pipette, the gel solution was transferred to the microchamber, where capillary action allowed the gel solution to be spread throughout between the coverslip and slide. The chamber was then sealed with clear nail polish to prevent dehydration of the gel. Gels were allowed to polymerize at room temperature for 30 minutes to ensure complete polymerization.

Magnet and Experimental Setup

A Neodymium Rare-Earth bar magnet (N50, 0.25 x 0.25 x 1 in; Applied Magnets, Plano, Texas) was initially chosen as the source of the magnetic force given success in previous work with a similar magnet.²³ This magnet produces a maximum flux of 14500 Gauss, or a 1.45 Tesla magnetic field. An electromagnet was fabricated by wrapping

24AWG magnet wire (Belden, St. Louis, Missouri) 393 times about a 6.35 mm (0.25 in) diameter soft iron core to minimize hysteresis loss. Equation 2 was used to determine the operating conditions of the electromagnet to generate a pull force equivalent to that of the N50 Neodymium bar magnet²⁸ to create a qualitatively equivalent strength magnet.

$$F = \frac{(N * I)^2 * \mu_0 * A}{(2 * g^2)} \quad (\text{Equ}$$

Electromagnetic force is a function of the number of turns of the wire (N), current (I, in amperes), the cross sectional area of the magnetic core (A), the length gap between the electromagnet and a piece of ferromagnetic metal (g), and the permeability of free space ($\mu_0 = 4\pi \times 10^{-7} \text{ V*s}/(\text{A*m})$).²⁹ This equation cannot be used to determine magnetic force acting on the magnetic beads as it does not take into account bead volume or relative permeability.

To study the displacement of beads, the magnetic force is introduced to the system while the beads are viewed under fluorescent microscopy using a 10X objective and an IX71 Olympus Epifluorescent Microscope (Olympus, Center Valley, Pennsylvania) on a vibration isolation workstation. To further minimize noise due to vibration, special acrylic clamps were custom made to hold down the test slide and include a notch for precision placement of the bar magnet such that it would align with the edge of the gel (Appendix A.1). Figure 2 shows the full experimental setup of clamps, a test slide, and bar magnet in place.

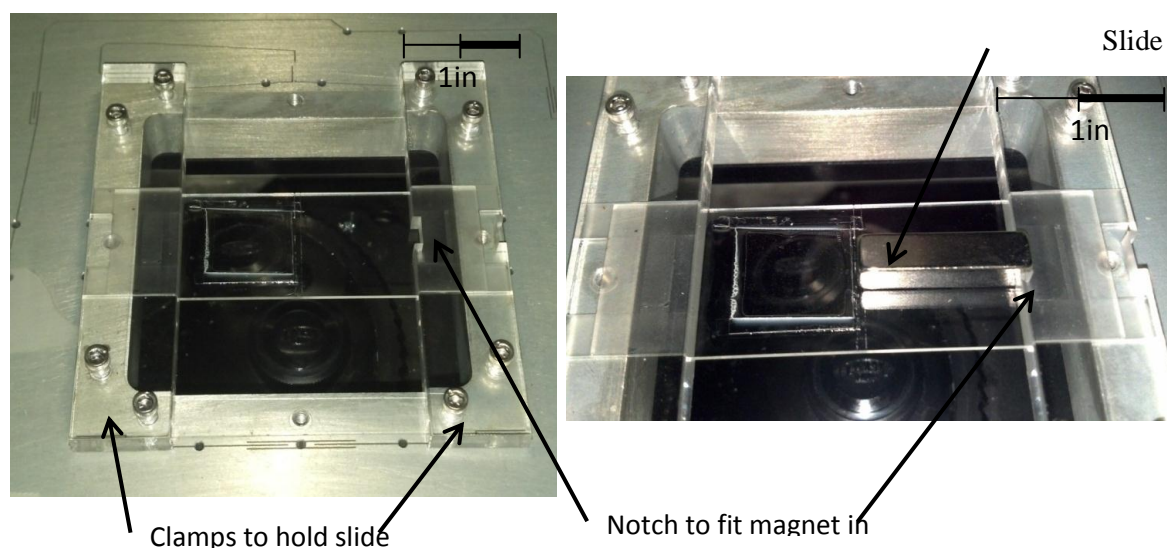


Figure 2 – Experimental setup showing custom clamps, slide with gel, and magnet fitted into notch in clamp. The magnet is manually inserted into the notch to introduce the magnetic field to the system.

Similarly, a special ABS thermoplastic clamp was custom made to secure the test slide and hold the electromagnet in place on the microscope stage (Figure 3, Appendix A). The electromagnet was connected to a DC power source supplying 9.75A current via a DC solid state relay (Futurlec, New York, New York) to allow for computer control of magnet activation using Labview Software (Figure 4).

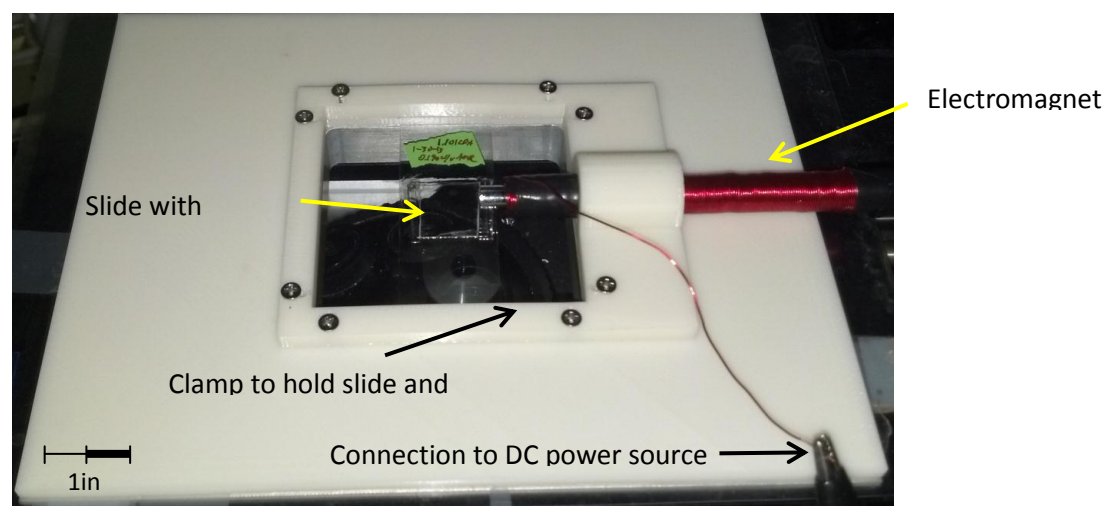


Figure 3: Experimental setup of electromagnet on microscope stage.

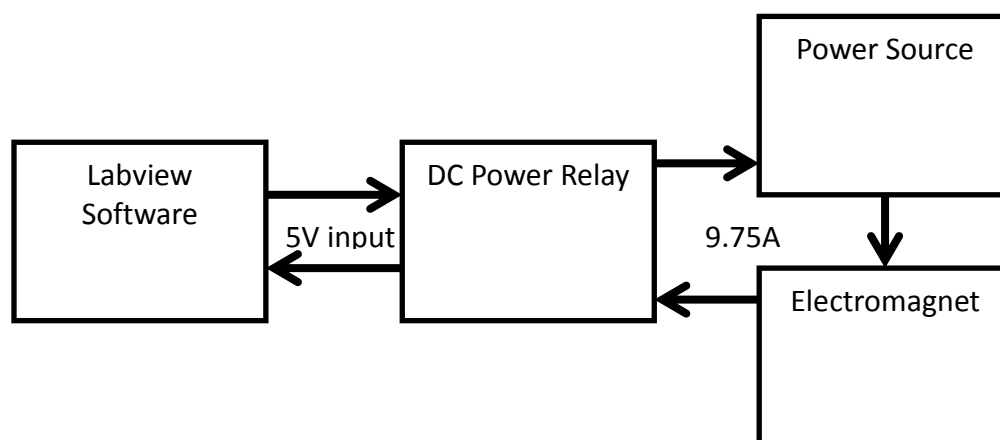


Figure 4: Diagram of electromagnet control system setup. The electromagnet is switched on by activating the DC relay with a 5V input, controlled from the computer using Labview Software.

Fluorescent Microscopy, Image Capture, and Bead Tracking

As previously mentioned, the beads were viewed using the 10X objective under fluorescent microscopy. The beads excite at 488 nm and emit at 520 nm. Fluorescent beads were chosen so they can be viewed even within an opaque material. Images were captured using a high speed, low light CCD camera (Cooke Sensicam) and analyzed in CamWare software (PCO). Images captured through the CamWare software were then analyzed in a Labview program that tracks two-dimensional bead movement using an intensity-weighted, centroid-based particle-tracking algorithm.³⁰ This centroid-based particle tracking algorithm compares the centroid of two successive images of each bead and is based on Equation 3.³¹

$$C_y = \frac{\sum_{i=1}^n \sum_{j=1}^m (y_i \cdot I_{ij})}{\sum_{i=1}^n \sum_{j=1}^m I_{ij}} \quad (\text{Equation 3})$$

Equation 3 shows the centroid calculation for a single axis where I is a matrix of intensities, y_i is the coordinate of a pixel on the y-axis, I_{ij} is the intensity of that pixel, and C_y is the distance an object has moved in the y-direction. A similar equation is done for the x-direction for two dimensional tracking. This tracking software is able to track to the tenth of a pixel, allowing for small displacements to be quantified.

A photo of a micrometer slide was used to determine the resolution of the 10X objective (Figure 5). The image of the micrometer was analyzed in ImageJ (National Institute of Health) and it was determined that the resolution of the 10x objective is 641.97 nm/pixel. This means that the tracking software is able to track displacements of around 64 nm.

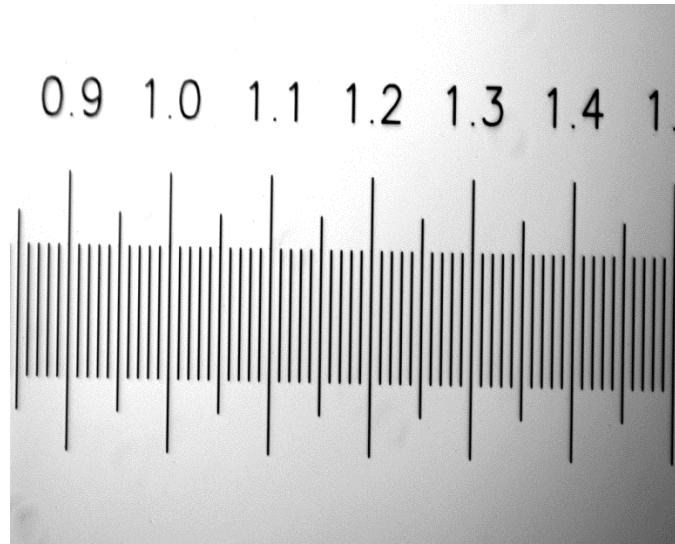


Figure 5 – Micrometer under 10X objective for determining resolution of the objective.

Experimental testing with hydrogel

Hydrogels with beads at a concentration of 0.1% w/v were used to test and calibrate the magnetic bead microrheometry system. This concentration was chosen such that each imaging position would contain several beads without excessive use of materials. The CamWare software was set up for no delay in image capture and an appropriate exposure such that the bead image intensities were distinct from the background without saturating the sensor. Initial trials with the N50 Neodymium rare-earth bar magnet recorded the following readings:

- One Baseline Control– recording of the system with no change.
- One Mass Control – recording of the system with a nonmagnetic mass, similar to the magnet, is placed on the slide. This was done to study the effect on bead movement by simply adding a mass, potentially deflecting the slide.
- One Elasticity reading – system is initially at baseline before manually placing the bar magnet into place for 3 seconds. The magnet was then manually removed from the system to return to baseline position. This was done to look for an elastic response where the beads returned to baseline position following the removal of the bar magnet.
- One Steady State reading – system is initially at baseline before manually placing the bar magnet into place. The magnet remained in place for position calculation.

Each reading with the bar magnet was 10 seconds. Subsequent trials were done to specifically study replicability of results for a given position and of the positioning of the magnet.

Initial trials with the electromagnet also used hydrogels with beads at a concentration of 0.1% w/v to determine working range of the magnet. One hydrogel each with Young's Moduli of 0.2kPa and 1.61kPa were used to determine the full working range of the system, representing the upper and lower bounds of experimentally determined elasticity's of previous clot rheology work.^{18,19,32} All recordings were taken

within the range of the width of the magnet such that it can be assumed all relevant bead motion is in the y-direction (Figure 6). For each image position, the position of the center bead in the image was recorded. Then three of the following 15 s reading was recorded at each position:

- Step response readings - system is initially at baseline for 3 seconds before turning on the electromagnet for 3 seconds. The magnet was then switched off to return to baseline conditions while the camera software continued to record bead movement for a total of 15 s. This was done to look for an elastic response where the beads returned to baseline position, and record a sample (n=3) of steady state displacements of the beads.

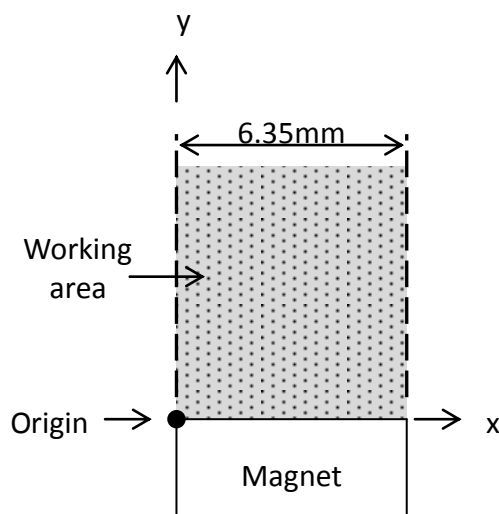


Figure 6: Working area of hydrogel used in the magnetic bead microrheometry system. This region is within the width of the magnet, allowing for an assumption of the magnetic force to act solely in the y direction, neglecting x-displacement. The origin position is also shown with the nominally determined coordinate axes labeled. Bead positions were calculated based on this set of axes.

Position Calculation

Bead positions were defined relative to a coordinate axes with an origin at the top left corner of the magnet (Figure 7). The vernier scales (± 0.001 mm) on the microscope

stage (Mad City Labs, Madison Wisconsin) were used to determine the location of the beads relative to this origin by recording the values of the stage position at the center bead's location and the magnet origin location. For trials with the bar magnet, this required leaving the magnet in place following introduction to the system, measuring bead position, and then measuring magnet position as the magnet origin could move each time it is placed into position. For trials with the electromagnet, magnet origin position was recorded at the start, and then each image's position was recorded at the start of each trial.

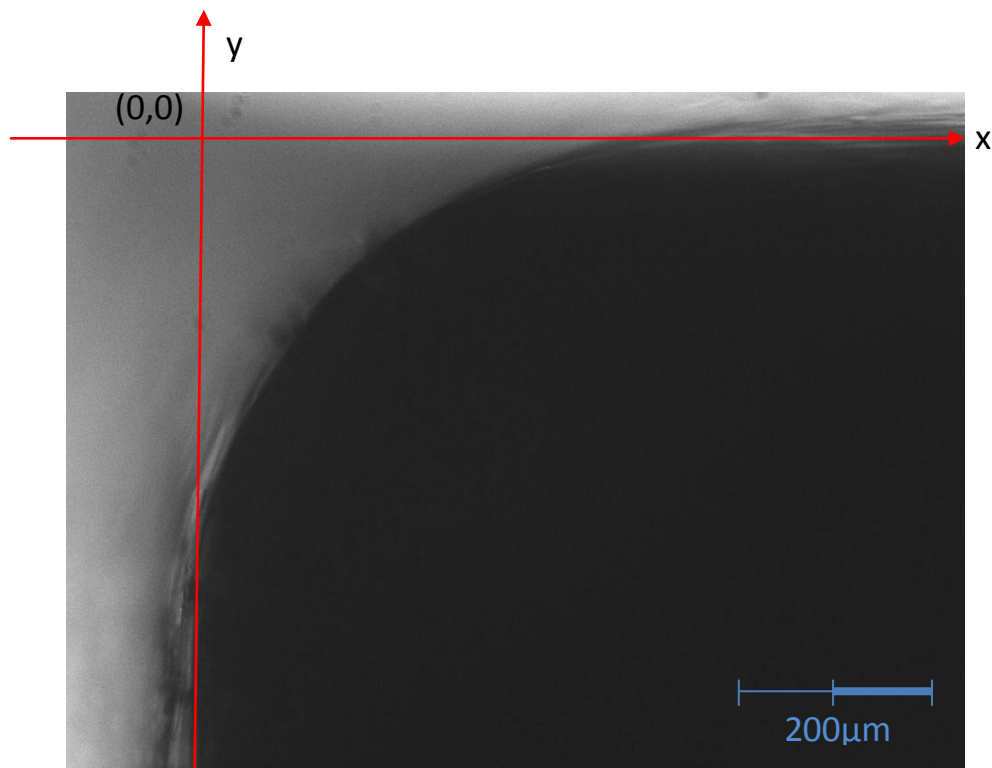


Figure 7 – Coordinate axes on which bead locations were determined. The origin was the top left corner of the magnet (when viewed in images captured with the CamWare software) as defined by extending the straight sides of the magnet until intersection.

If there were multiple beads in the frame, the position of the center bead was measured using the vernier scales and recorded. ImageJ was then used to calculate the distances between that bead and the other beads in the same frame (Figure 8).

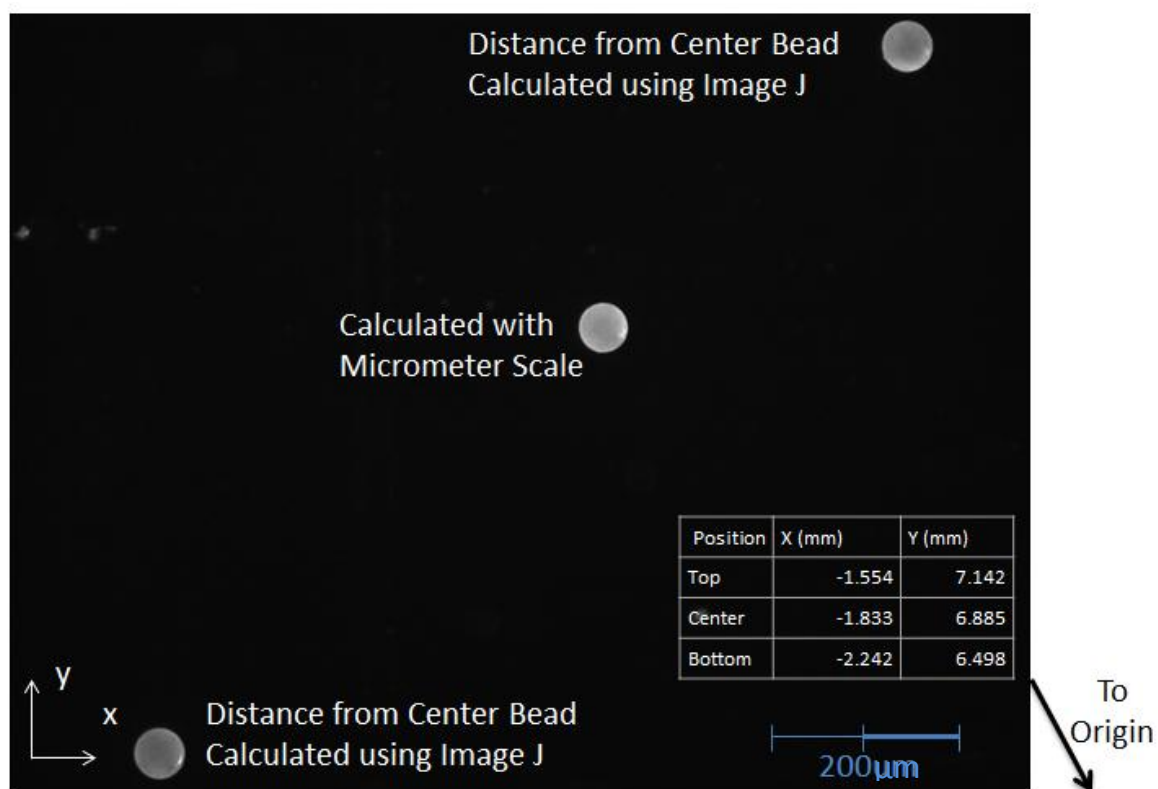


Figure 8 – Beads under fluorescent microscopy with positions calculated relative to the magnet origin (Figure 7). The center bead's position was calculated using the vernier scales on the microscope stage. The top and bottom bead positions were calculated using ImageJ to calculate the distance from the center bead.

Data Processing

Data points generated by the tracking software were loaded into Microsoft Excel and plotted for analysis. As data was only taken on beads within the working area (Figure 6), displacements in the x-direction were neglected. The y-position was plotted versus time to show displacement in each direction during the length of each trial. When

the bar magnet or non-magnetic mass control was added or removed to the system, a definitive and obvious spike was shown indicating clear outliers due to the extra movement and vibration (Figure 9a). These data points were not considered for calculating average values of position and removed from plots to more accurately represent the pertinent data (Figure 9).

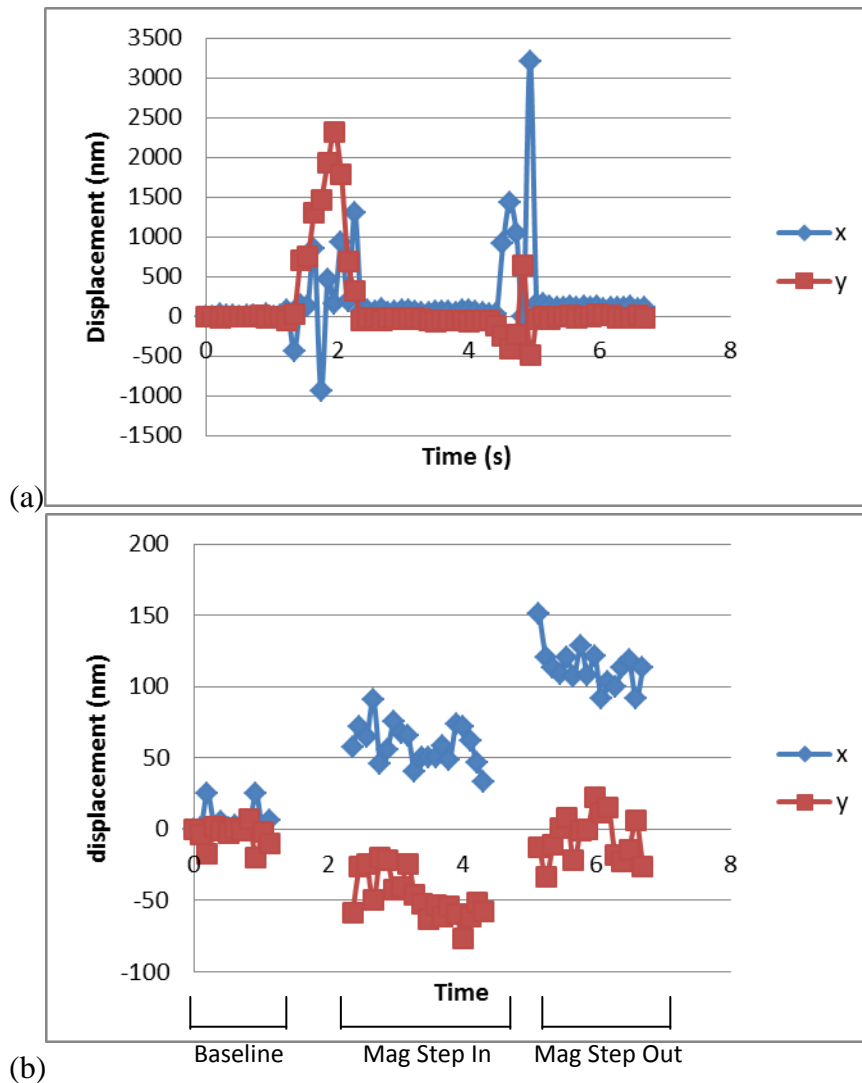


Figure 9 – Sample of raw data of baseline, magnet step in, and magnet step out results using the bar magnet. (a) shows the full raw data and (b) represents the data after removing the outlier data points due to the vibration and weight of manually adding and removing the magnet.

Steady state data at baseline and at an elastic displacement due to magnetic force were averaged separately for each run. A net displacement was determined by subtracting the displacement from the baseline. For trials with the electromagnet, three such data sets were measured for each position. The three net displacement values were averaged for an average displacement for each position. This average displacement was used to calculate the magnetic force acting on the bead.

COMSOL modeling

Finite element analysis computer modeling with COMSOL 4.3 (COMSOL AB) was used to model the magnetic force acting on the beads. Initially, COMSOL was used to model the entire system with a full magnet, beads, and hydrogel using the *Magnetic Fields, No Current* and *Solid Mechanics* modules (Figure 10). The bead position was moved in an array using a parametric sweep, and data for force acting on the beads was acquired. Mesh and converging issues that resulted in poor data could not be resolved. As a result, the magnetic force acting on the beads could not accurately be solved for directly when modeling the entire physical system.

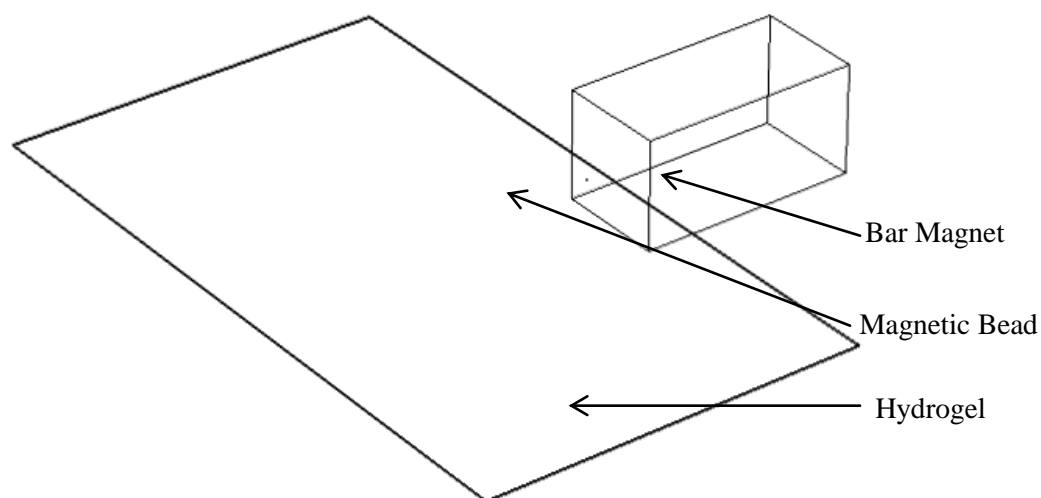


Figure 10 – Initial setup of COMSOL model of magnetic bead, gel, and bar magnet.

To simplify the model for force calculation, the magnet was removed entirely and the model was focused on a single bead in a small, $250\ \mu\text{m} \times 250\ \mu\text{m} \times 80\ \mu\text{m}$ area of gel (Figure 11). This COMSOL Multiphysics model only utilized the *Solid Mechanics* module to simplify the system and reduce solving time. A prescribed displacement equal to calculated displacement of beads from the tracking software was assigned to the bead. The top and bottom of the gel domain was set as a fixed constraint to model binding to the coverslip and microscope slide. The other sides of the domain were set as free boundaries to simulate the gel's ability to deform in any direction. It was assumed that the bead was sufficiently far enough away a gel boundary in the x and y directions.

Material properties of the hydrogels and paramagnetic beads are listed in Tables 2 and 3. The Poisson's ratio of the hydrogels was assumed 0.5 as the hydrogels are incompressible and in a fixed volume with no volume lost.^{33,34} The Young's Modulus

and Poisson's ratio of the paramagnetic beads was based on the polystyrene core of the beads.

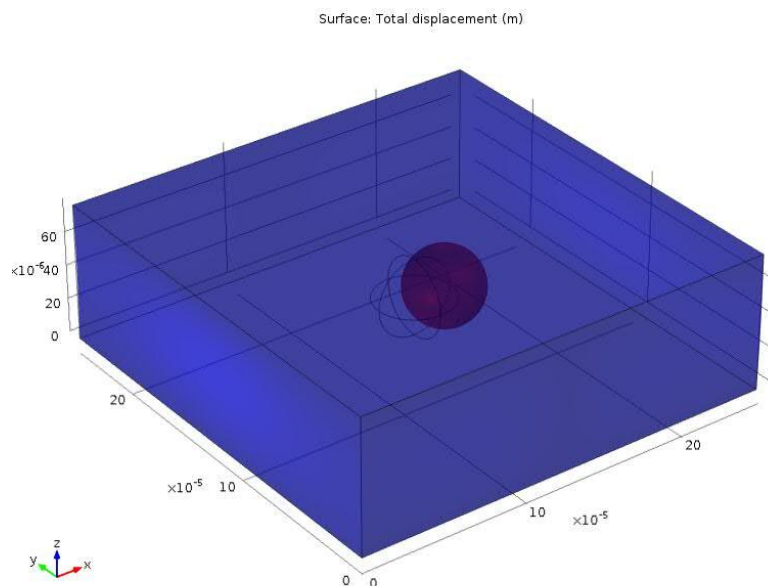


Figure 11 – Simplified COMSOL model of a bead displaced in a gel. This model uses a prescribed displacement input on the bead to model experimental displacement data.

Table 2: Hydrogel material properties used in the COMSOL Multiphysics model used to relate force, displacement, and elasticity.

Young's Modulus	0.2 – 1.61 kPa
Poisson's ratio	0.5
Density ²⁴	1004 kg/m ³

Table 3: Paramagnetic bead material properties used in the COMSOL Multiphysics model used to relate force, displacement, and elasticity.

Young's Modulus	3.25 GPa
Poisson's ratio	.35
Density ²⁴	1580 kg/m ³

The force (F_y) was then calculated by COMSOL by integrating the normal stress tensor y-component (σ_y) over the surface area (A) of the bead (Figure 12, Equation 4).

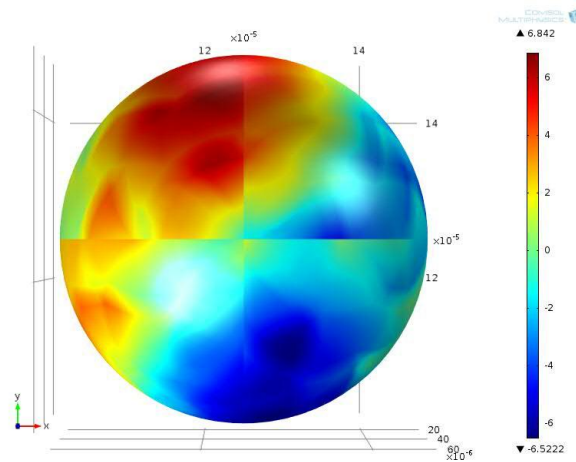


Figure 12 – COMSOL model results for normal stress tensor calculation acting on a magnetic bead particle surface due to a prescribed displacement. This model is used to determine the magnetic force acting on a bead.

$$F_y = \iint_A \sigma_y dA \quad (\text{Equation 4})$$

COMSOL Multiphysics was also used to model the electromagnet and plot the magnetic field lines (Figure 13). This was done using the *Magnetic Field, No Current* module using a prescribed remnant flux density of 1.45T on the end inch of the cylinder. This was done to help visualize the magnetic field to see how it would overlay with beads within the gel and correlate with response.

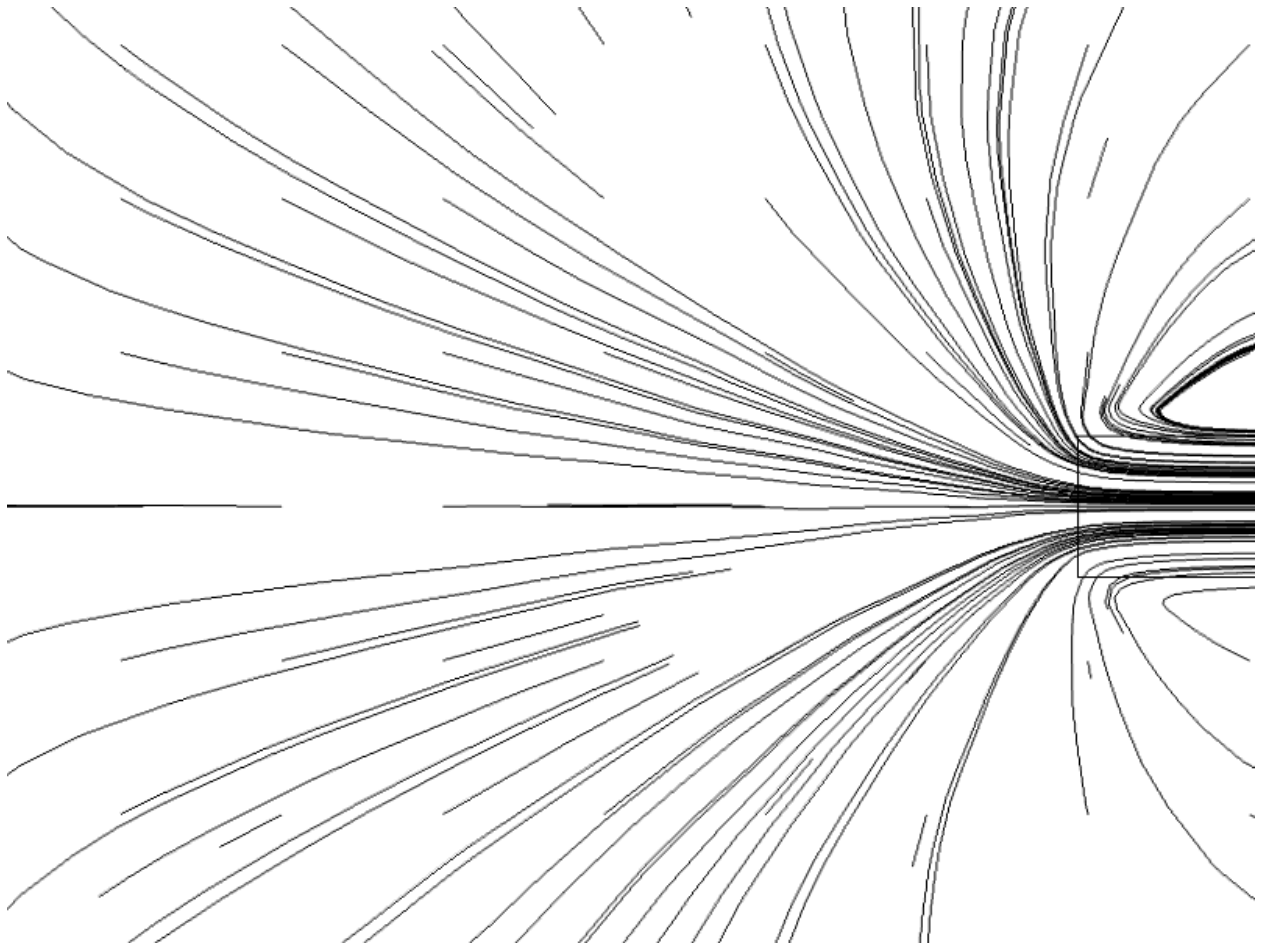


Figure 13: Magnetic field lines of the electromagnet modeled using COMSOL Multiphysics.

COMSOL Force Calculation and Force Mapping

This model was used to calculate the force of the gel acting on a bead at any given position based on experimental data of bead displacement in the hydrogels of known elasticity. This force is equivalent to the magnetic force being applied to the bead at that location by the magnet. By knowing the material properties of the hydrogels and using the experimental displacements as inputs, the magnetic force at many positions in the working area can be determined. The composite data of these forces known by position can then be interpolated using Matlab (Mathworks, Natlick, Massachusetts) software to

“map” electromagnet force by position. This map can then be used to test samples of spatially non-uniform elasticity. The force acting on a bead in an unknown sample can be known by calculating the position relative to the magnet. This force, along with the experimental displacement calculated by the bead tracking software, are input variables into the COMSOL Multiphysics model to solve for elasticity of the unknown sample.

To validate the force calculation method, the force (F_y) and the displacement were used to back-calculate the modulus of elasticity (E) using Equation 5.

$$E = \frac{\sigma_y}{\varepsilon_y} = \frac{\left(\frac{F_y}{\text{Bead Surface Area}} \right)}{\left(\frac{\text{Displacement}}{\text{Diameter of bead}} \right)} \quad \text{Equation 5}$$

Equation 5 is manipulation of Equation 1, using Equation 4 to solve for stress acting on the bead (σ_y). To calculate strain (ε), the displacement was divided by the diameter of the bead (the characteristic length). To be able to validate the methods for solving force, this calculation should return the elasticity that was programmed into COMSOL initially, namely the known elasticity of the hydrogel.

Chapter 3

Results

COMSOL Modeling for force calculation

Initially, the entire system of magnet, hydrogel, and beads were modeled in an attempt to solve for magnetic force on beads directly (Figure 10). As shown in Figure 14,

these results did not meet expectations as the force on the beads was not symmetrical about the centerline of the magnet and shows random spikes rather than a smooth curve. For the y-component of force (Figure 14a), it was expected that force would be highest along the centerline of the magnet where the magnetic field is entirely in the y-direction. For the x-component of force, it was expected that forces would be pointing toward the magnet, so pointing positively at positions less than $x=0\text{mm}$ and negatively at positions greater than $x=0\text{mm}$.

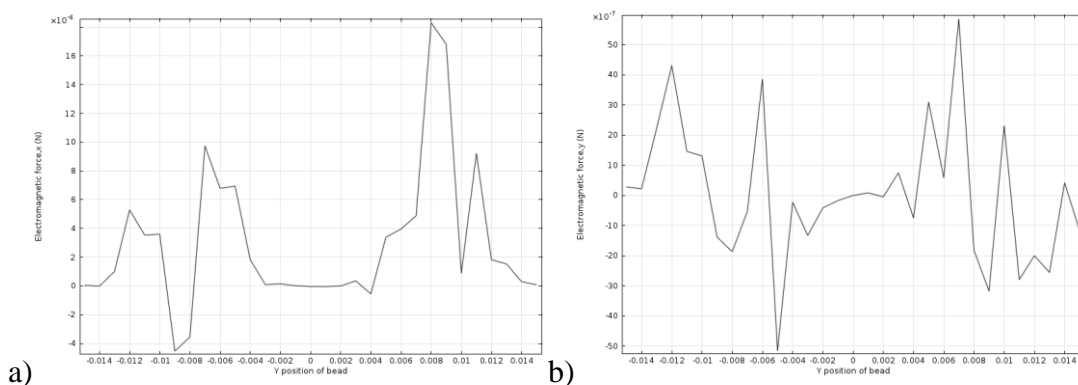


Figure 14 – Initial results of magnetic force acting on beads in the (a) y and (b) x directions.

Bar Magnet Placement Reproducibility

To determine reproducibility of magnet placement, the magnet was placed in the notch of the slide clamps repeatedly and the position of the magnet origin (Figure 7) was calculated using the vernier scales of the microscope stage. Table 4 summarizes the standard deviation in millimeters for magnet position in both the x and y directions. Due to the imprecision of magnet placement, it is necessary to leave the magnet in place for calculating bead position and magnet origin position with the vernier scales.

Table 4 – Standard deviation in both x and y directions of the magnet origin location. Positions were calculated using the vernier scales (± 0.001 mm).

Direction	Standard Deviation (mm)
X	0.144
Y	0.761

Bead Location Calculations

As described previously, bead locations were determined relative to the magnet origin using the vernier scales. Table 5 shows raw values for the center bead of Figure 15 and origin locations using the vernier scales. These values are related in Table 6, and Table 7 shows the relative distances between the top and bottom beads from the center bead calculated with ImageJ. Table 8 summarizes the position of the three beads to the magnet origin.

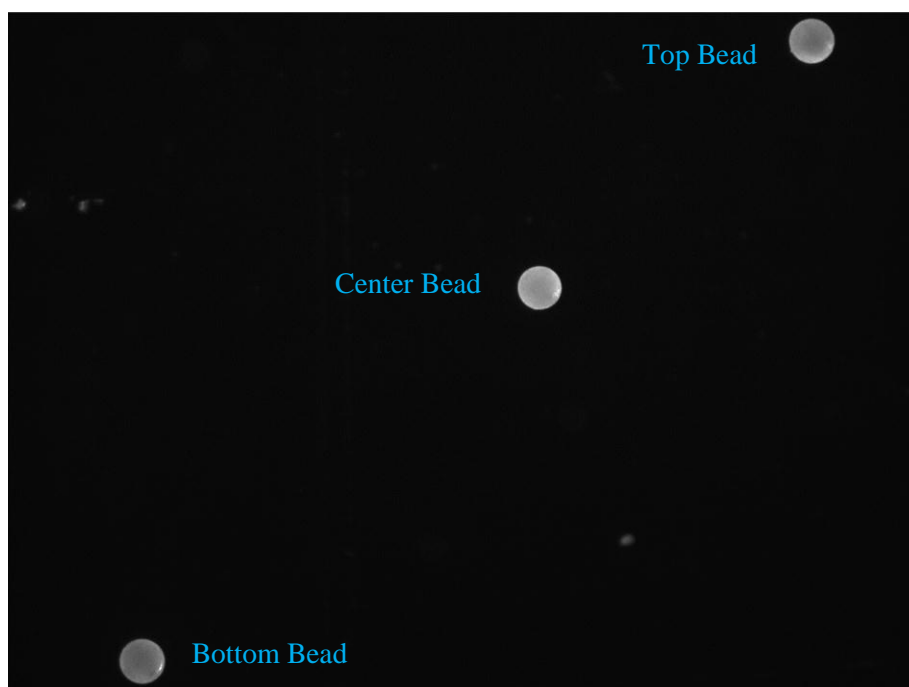


Figure 15 – Image of 3 beads labeled by their relative positions.

Table 5 – Values from the vernier scales for the (a) center bead and (b) magnet origin.

a) Center bead locations

	X	Value (mm)	Y	Value (mm)
Sleeve reading	8.5	8.5	16	16
Thimble Reading	12	0.12	21	0.21
Vernier Reading	0	0	6	0.006
Total		8.620		16.216

b) Magnet origin locations

	X	Value (mm)	Y	Value (mm)
Sleeve reading	9	9	13.5	13.5
Thimble Reading	34	0.34	0	0
Vernier Reading	2	0.002	5	0.005
Total		9.342		13.505

Table 6 – Relating the position of the center bead to the magnet origin.

	X (mm)	Y (mm)
Magnet coordinates	9.342	13.505
Center bead coordinates	8.620	16.216
Center bead location relative to magnet origin	-0.722	2.711

Table 7 – Calculating the distance components between the center bead and the top and bottom beads using ImageJ.

	Length (μm)	Angle (rad)	X comp (mm)	Y comp (mm)
Top bead	379.4	0.744	0.279	0.257
Bottom bead	563.4	0.759	0.408	0.387

Table 8 – Final positions of all three beads relative to the magnet origin.

	X (mm)	Y (mm)
Top	-0.443	2.968
Center	-0.722	2.711
Bottom	-1.130	2.324

Initial results of bead tracking

Initial trials were conducted as outlined previously. Data for a baseline, nonmagnetic mass control, displacement with the magnet in place (mag in), and displacement upon removal of the magnet (mag out) were all acquired using the bead tracking software. Figure 16 shows preliminary results indicating a definite step response in y displacement as a result of the magnet being introduced. The x displacement can be correlated to the mass of the magnet deflecting the slide as there is no significant difference between the mass control and mag in displacement. Upon removing the magnet (step mag out) the bead returned to an average position comparable to the baseline showing an elastic response. The final displacement is calculated by subtracting the displacement due to the mass control from the displacement with the magnet in place (mag in).

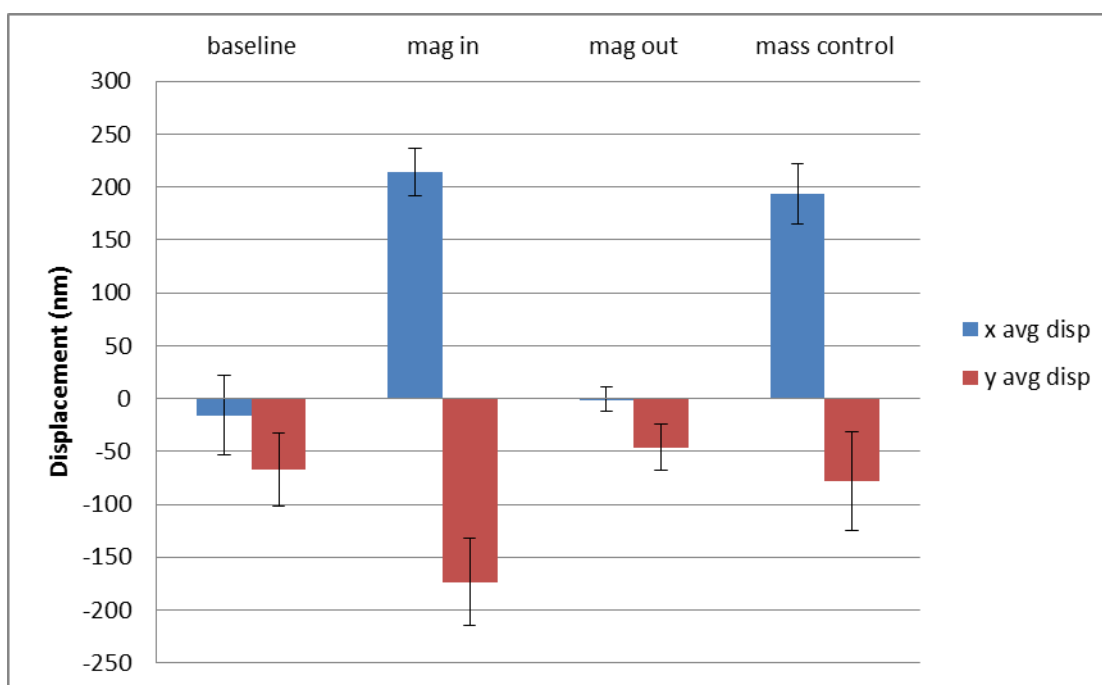
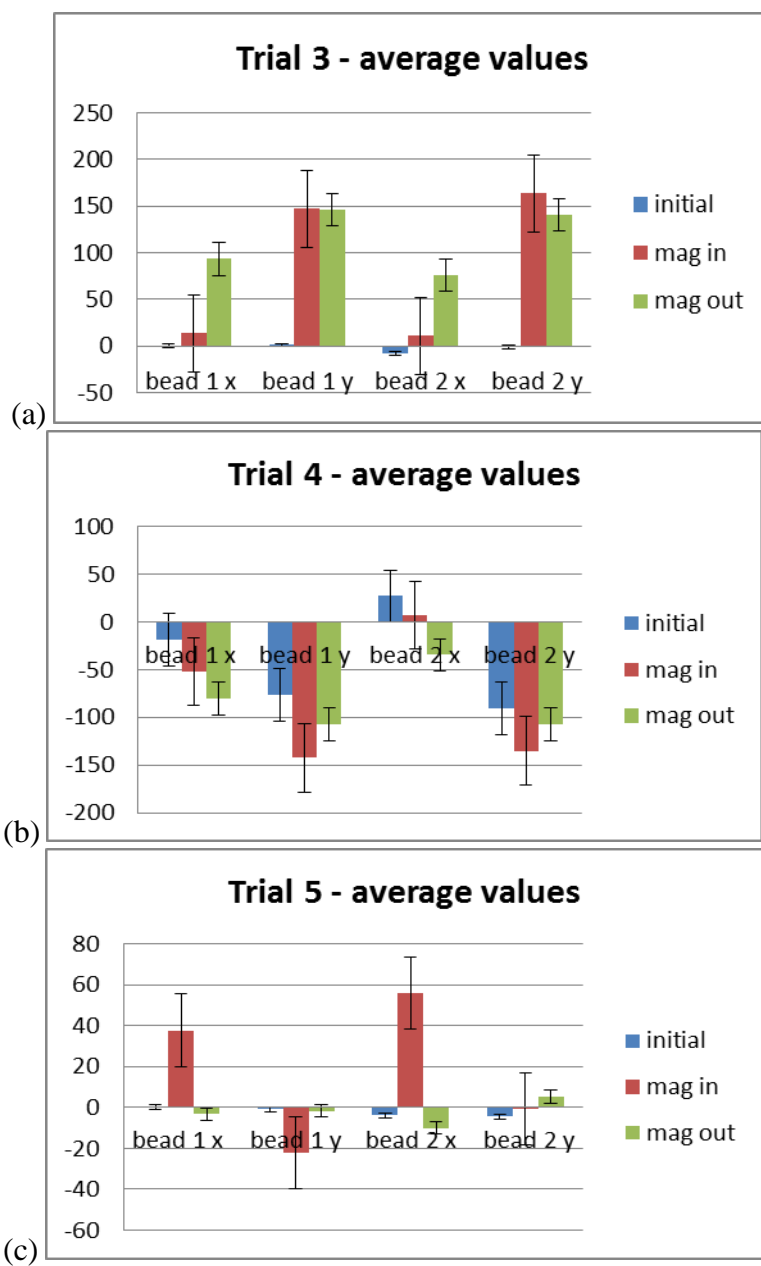


Figure 16 – Preliminary results of bead testing in a 1.10kPa hydrogel. Baseline is the average displacement with no magnet or mass introduced to the system. Mag in is the response after the magnet has been added to the system. Mag out is the data after removing the magnet. Mass control is the displacement when a nonmagnetic mass was added to the system to deflect the slide.

To corroborate these preliminary results, a study was done which repeated these methods of placing the magnet and removing it to look for a step in and step out response. This trial was done on an image with 2 beads, and repeated 5 times. Figure 17 shows the average values of each region in both the x and y directions for each bead for all 5 trials. From this, we can see that the responses are not always consistent in magnitude or direction.



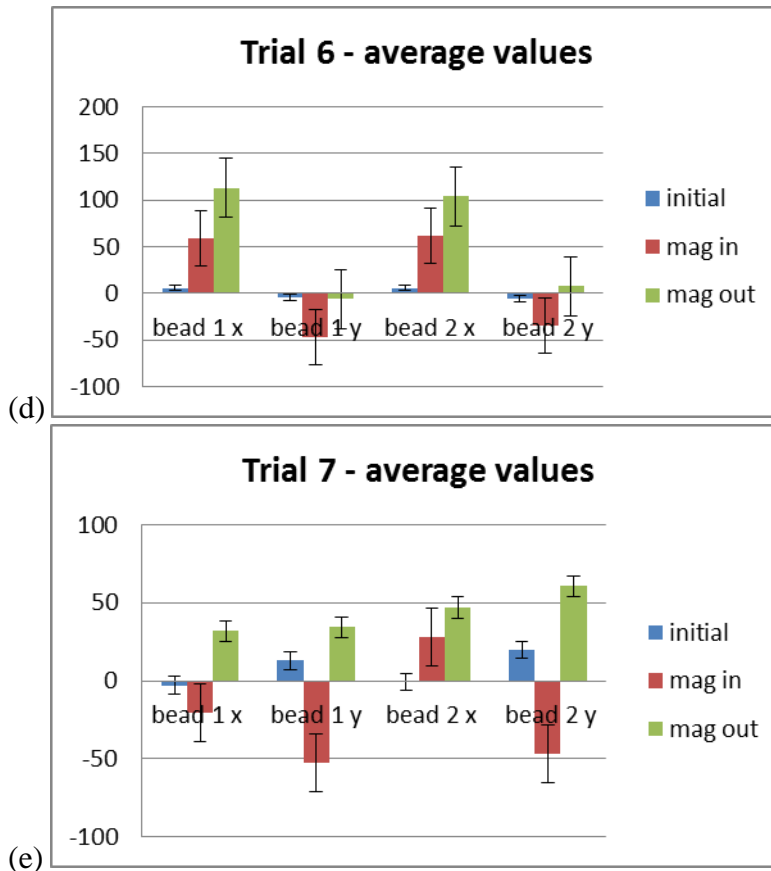


Figure 17 – Results of extended study of step response at the same location by placing bar magnet into and out of the system. Error bars represent standard error. All displacements are in nm.

An additional 5 trials were performed to measure the displacements due to the magnetic force (Figure 18). Again, these results show variation in magnitude between trials, and one trial (Trial 8) is completely in the opposite direction from the others. The reason for this variability could be due to general motion of the system due to vibration, the imprecision of magnet placement, or added movement from manually placing the magnet on the slide.

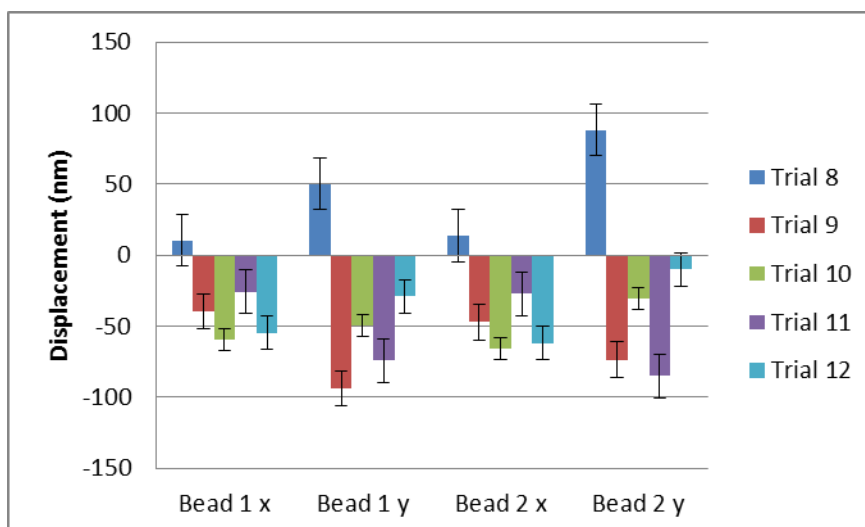


Figure 18 – Summary of net displacement of additional 5 trials.

This variability and inability to have repeatable results led to the decision to use an electromagnet to replace the bar magnet.

Results with Electromagnet

A 1.61 kPa hydrogel and a 0.2 kPa hydrogel were used to calculate bead displacement in the working area of the electromagnet (Figure 6). For the 1.61 kPa hydrogel, data was collected at 28 positions within the working area that contained a total of 57 beads. For the 0.2 kPa hydrogel, data was collected at 27 positions that contained a total of 49 beads. Data for positions 3, 4, and 5 (containing a total of 6 beads) was discarded as these beads were outside of the working area. Table 9 contains the coordinates of each bead relative to the magnet origin for the 1.61 kPa (Table 9a) and the 0.2 kPa (Table 9b) gels. Figure 19 shows the distribution of beads within the working area for each gel.

Table 9 – Bead positions relative to the magnet origin for both the (a) 1.61 kPa gel and the (b) 0.2 kPa gel. Beads were labeled by position and bead number. Each position represents a separate image captured using the fluorescent microscope and analyzed in the bead tracking software.

(a) Position	Bead	Bead Position	
		X (mm)	Y (mm)
1	1	1.881	0.678
2	1	2.872	0.785
	2	3.284	0.711
3	3	3.547	0.215
	1	4.137	0.970
4	2	4.429	0.478
	1	6.010	1.079
5	2	6.295	0.821
	1	6.317	1.783
6	2	6.056	1.229
	3	5.771	1.389
7	1	4.191	2.046
8	1	3.227	2.028
	2	3.069	1.853
9	1	3.453	2.593
	2	3.312	2.359
10	1	3.279	1.976
11	1	0.145	1.558
12	1	0.097	3.974
	2	0.267	3.541
	3	0.345	3.673
13	1	1.254	3.737
	2	1.547	3.707
14	1	2.093	4.146
	2	2.289	3.999
	3	2.318	3.922
15	1	3.104	4.013
	2	3.286	3.547
	3	3.295	3.704
	4	3.803	4.181

Position	Bead	Bead Position	
		X (mm)	Y (mm)
15	1	4.612	3.909
	2	5.167	3.459
16	1	0.776	0.469
	2	0.943	0.196
17	1	2.180	1.455
	2	2.320	1.559
	3	2.622	1.263
18	1	2.469	2.477
	2	2.406	2.058
19	1	3.580	0.925
20	1	4.393	1.589
21	1	3.820	2.224
22	1	5.365	1.929
23	1	4.683	2.729
	2	4.949	2.835
	3	4.964	2.522
24	1	4.371	3.178
	2	4.378	2.736
25	1	4.761	4.059
	2	4.693	3.632
26	1	3.523	4.281
27	1	1.839	3.921
	2	1.902	3.721
28	1	0.673	3.917
	2	1.010	4.089
	3	1.196	3.911
	4	1.435	4.171

(b)

Position	Bead	Bead Position	
		X (mm)	Y (mm)
1	1	4.000	1.294
2	1	4.808	0.927
	2	4.963	0.352
6	1	4.812	2.330
	2	5.046	1.594
7	1	3.097	1.945
8	1	0.675	2.105
9	1	0.881	3.047
10	1	1.157	3.709
	2	1.438	3.453
11	1	2.038	2.990
12	1	2.559	3.381
	2	2.898	2.899
13	1	3.839	3.560
	2	4.445	3.369
14	1	5.135	2.819
15	1	5.643	3.100
	2	6.170	3.173
16	1	5.889	4.129
	2	5.665	3.773
	3	5.649	3.393

Position	Bead	Bead Position	
		X (mm)	Y (mm)
17	1	5.888	5.079
	2	5.798	4.494
	3	5.151	4.482
18	1	5.362	5.161
19	1	4.459	4.813
	2	4.724	4.760
	3	4.957	4.914
20	1	4.242	5.212
	2	4.552	5.469
21	1	3.389	5.229
	2	3.428	4.741
	3	3.981	4.872
22	1	3.285	4.771
23	1	3.209	5.312
24	1	2.197	4.833
	2	2.425	5.165
25	1	1.277	4.330
	2	1.808	4.170
	3	1.980	4.702
26	1	1.386	4.261
	2	0.862	4.423
27	1	0.847	4.721

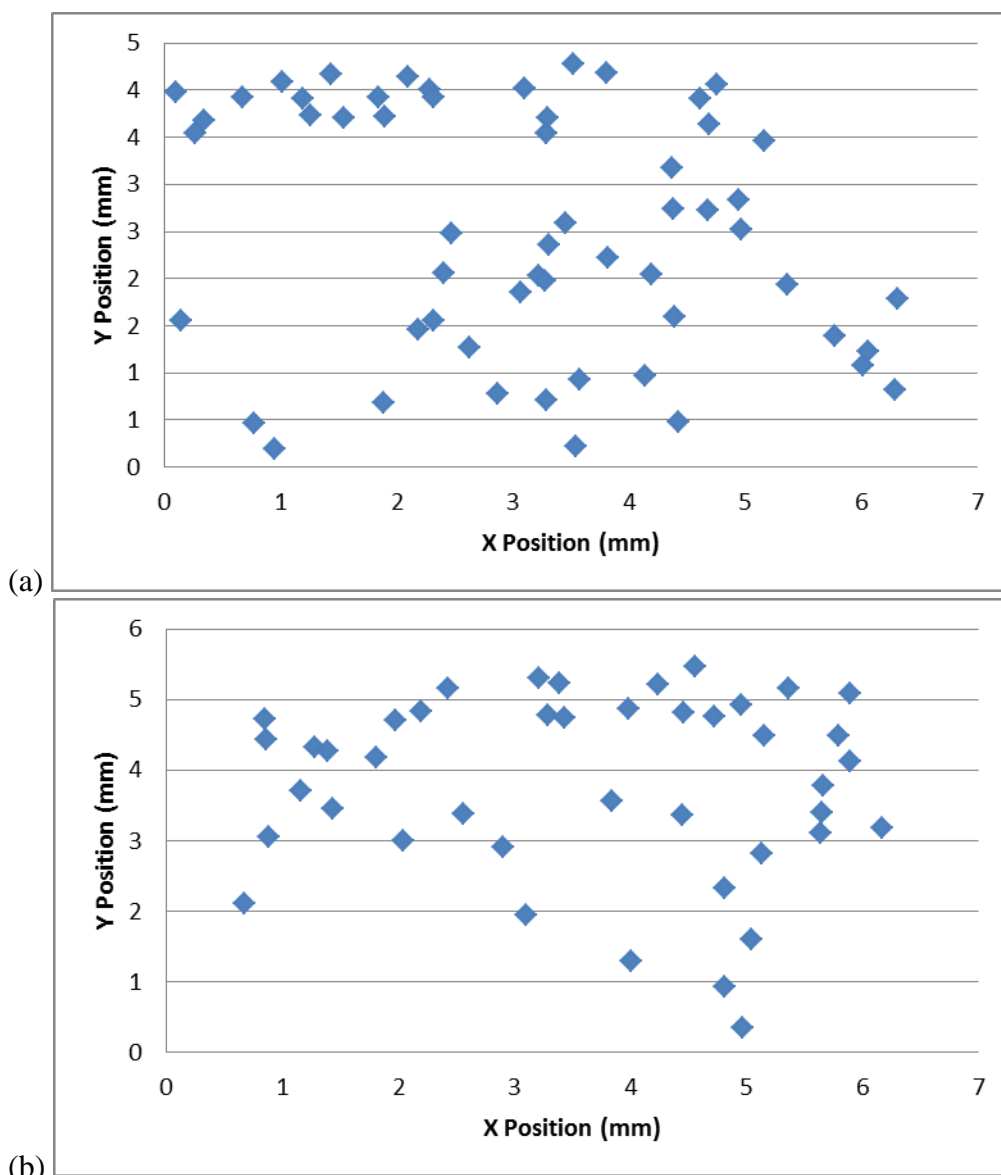
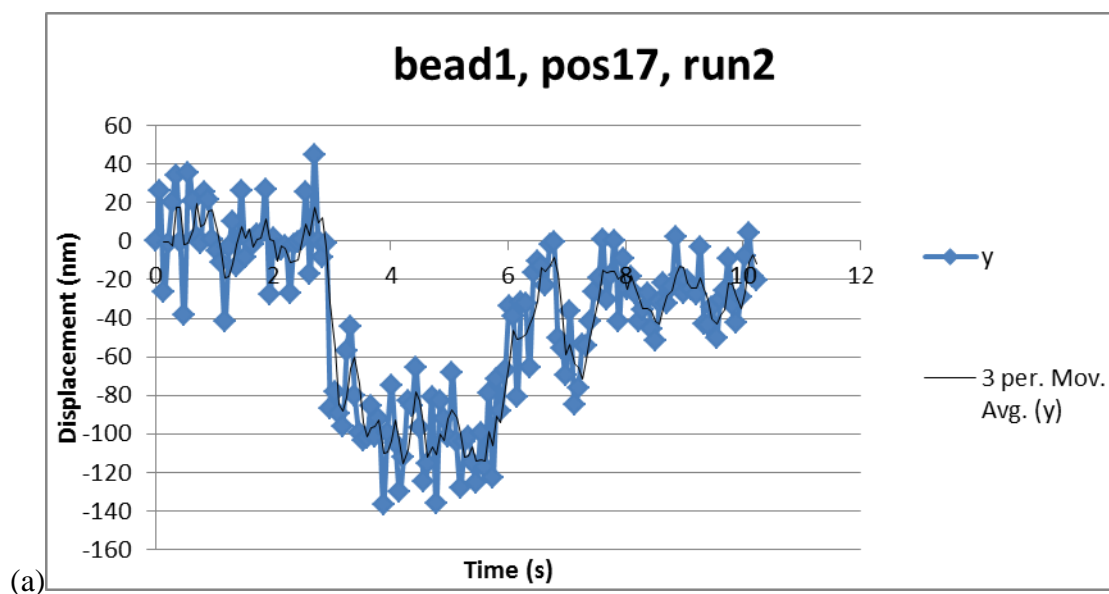


Figure 19 – Scatter plot of bead locations for the (a) 1.61 kPa gel and the (b) 0.2 kPa gel. The magnet width is from $x=0$ mm to $x=6.35$ mm. Y position references distance from the magnet face.

The beads showed varied responses in both gels and at different locations. Figure 20 shows representative plots of some common response patterns. Some responses clearly showed an elastic response (Figure 20a) with a distinct, immediate displacement upon activating the electromagnet (at $t=3$ s), a constant displacement, and an elastic

response back to the baseline when the magnet was turned off (at $t=6$ s). Figure 20b is an example of a viscoelastic response where there was an elastic displacement upon activating the electromagnet followed by a time-dependent viscous displacement while the electromagnet remained on. This viscous displacement plateaued in some runs, however in others it continued after the electromagnet was switched off. Once the electromagnet was turned off, there was an elastic, then viscous, recoil. Not all responses were obvious to categorize. Some did not show a response when the magnet was activated, but did show a positive displacement (away from the magnet) when the magnet was switched off (Figure 20c).



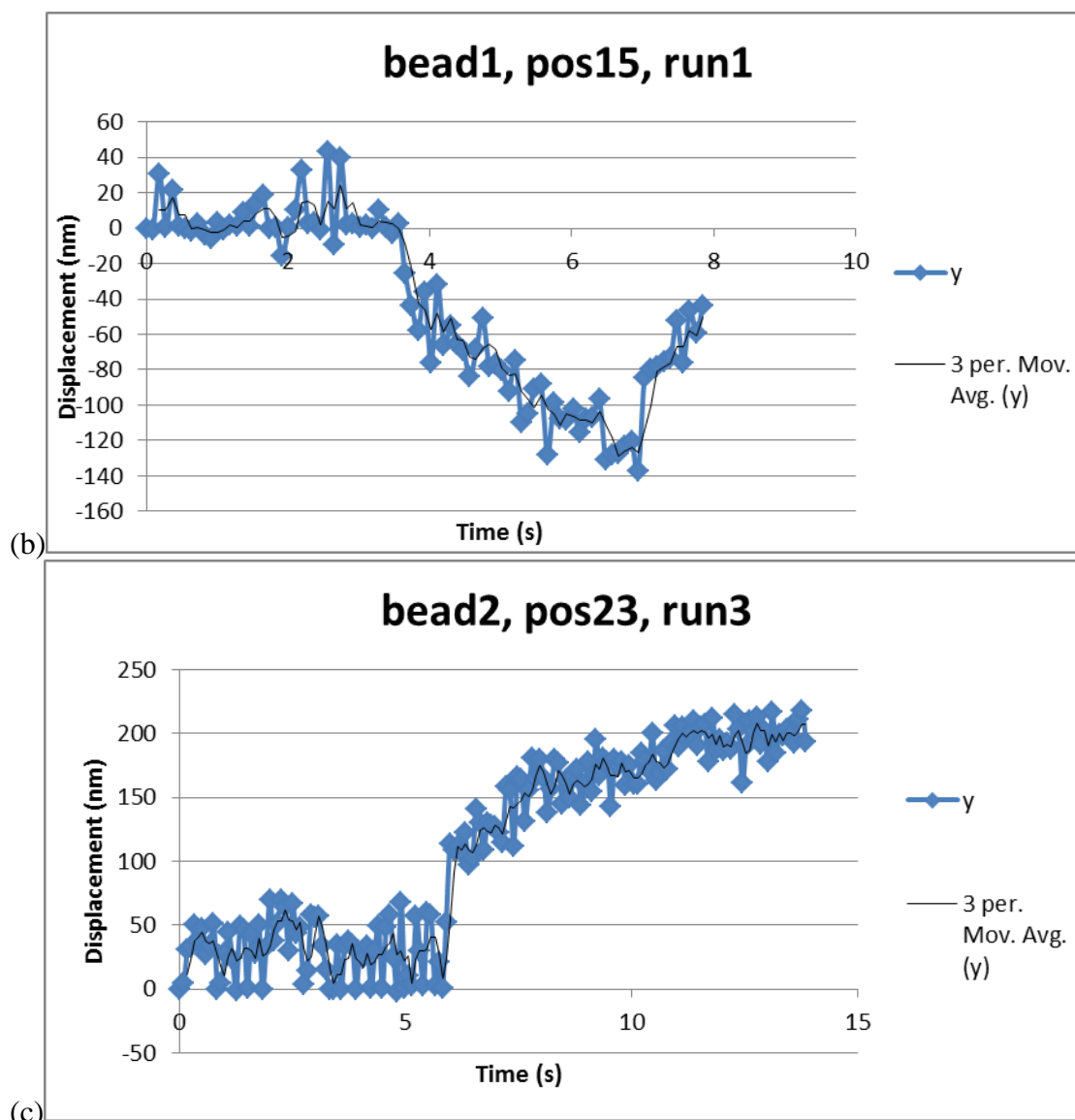


Figure 20 – Representative plots of bead responses to activation of the electromagnet. Shown are an (a) elastic response, (b) viscoelastic response, and (c) no response until the magnet was turned off. The electromagnet was activated at $t=3\text{s}$ and turned off at $t=6\text{s}$. Displacements are in the y-direction, and 3 period moving average is shown to better show the data trend.

The response for each bead was categorized as “elastic”, “viscoelastic”, or “other”. Responses categorized as “elastic” resembled Figure 20a where there was a distinct elastic response to activation of the electromagnet, a constant displacement, and an elastic response to deactivation of the electromagnet. Responses categorized as

“viscoelastic” resembled Figure 20b where there was a distinct response followed by a displacement that changed with time. Responses categorized as “other” were those responses that did not fit the elastic or viscoelastic categories. It is important to note that in some instances, a bead did not show a consistence response across all three runs. In those cases, if a response type was consistent in two out of three runs, the bead’s response was categorized as that response. Table 10 summarizes a count of each response category for each gel. Figure 21 shows the spatial distribution of the beads by response category for the (a) 1.61 kPa hydrogel and the (b) 0.2 kPa hydrogel, and Figure 22 overlays the magnetic field lines over these distributions.

Table 10 – Number of each response type for each hydrogel

Gel	Elastic	Viscoelastic	Other	Total
0.2 kPa	6	11	26	43
1.61 kPa	25	21	11	57

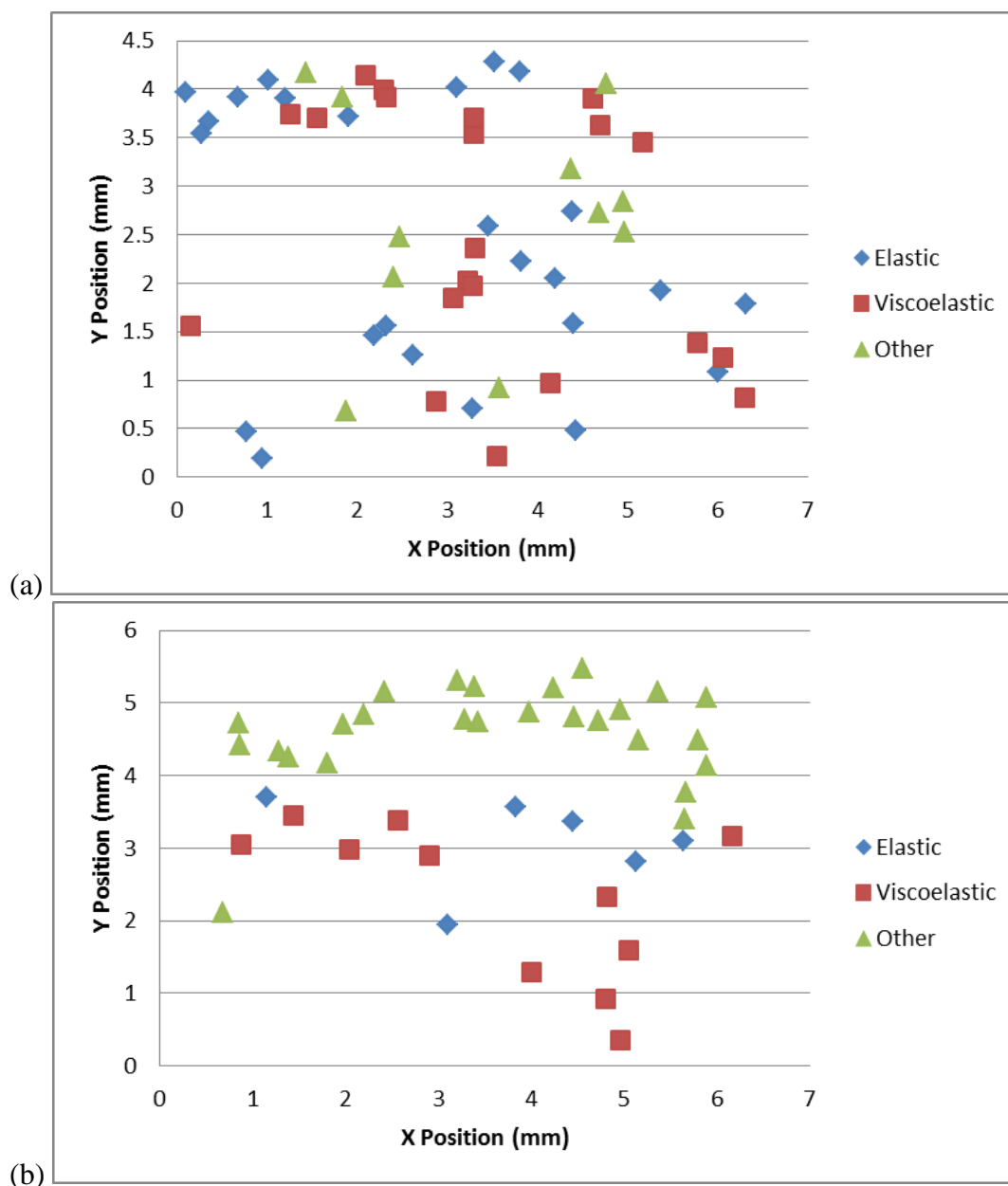
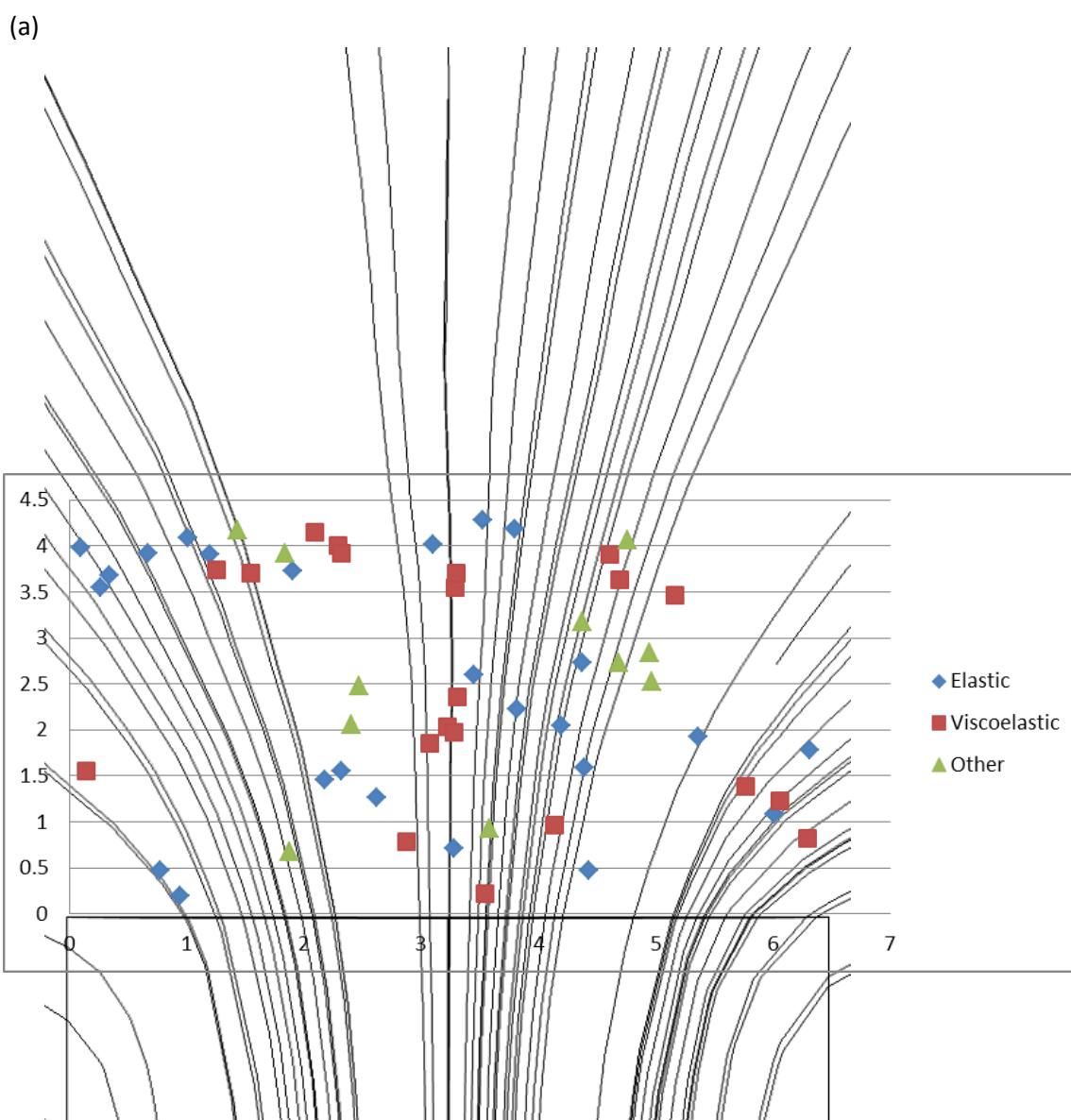


Figure 21 – Spatial distribution of beads labeled by their response categories in the (a) 1.61 kPa and (b) 0.2 kPa hydrogels.



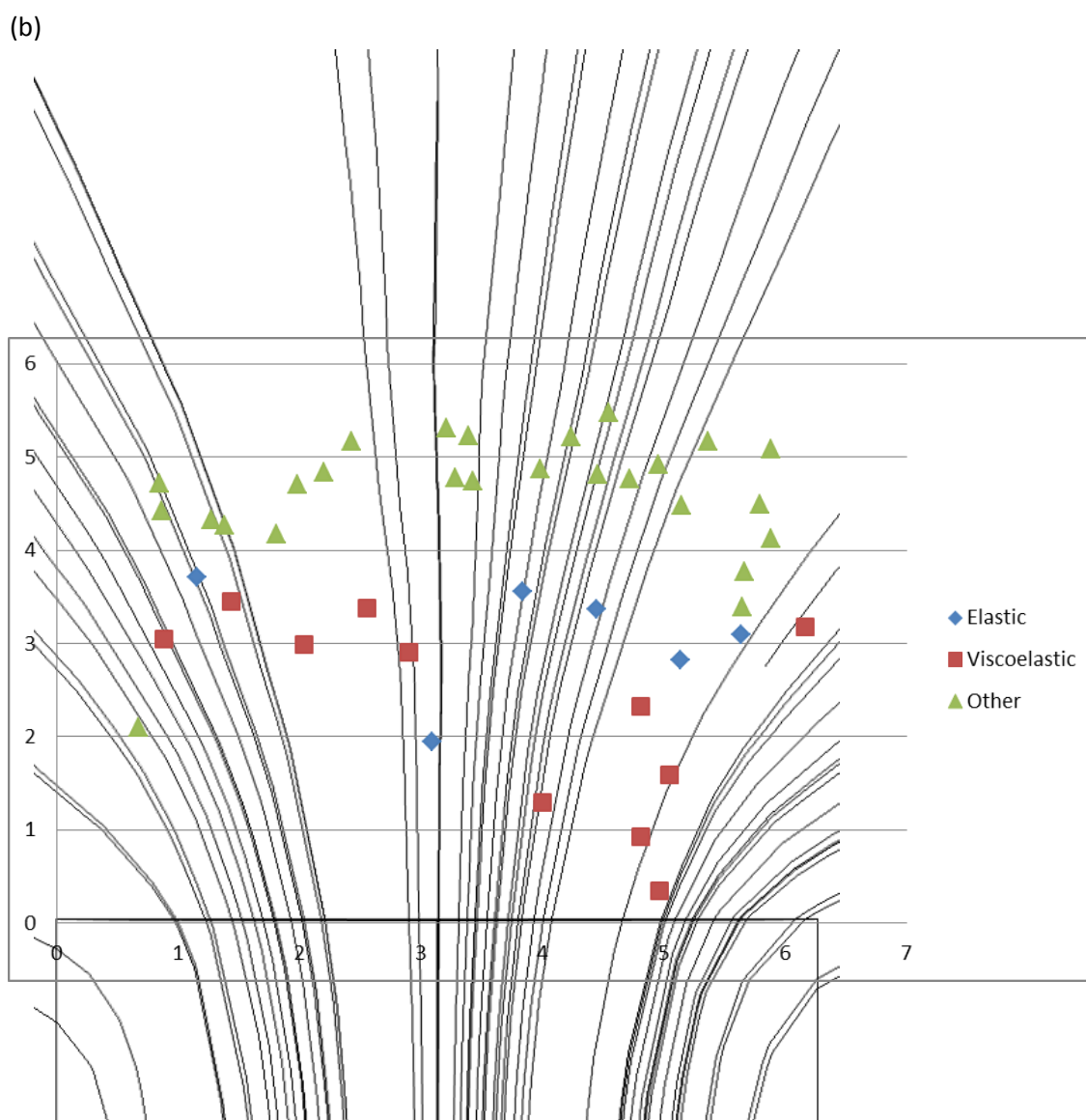


Figure 22 – Magnetic field lines superimposed over distribution plot of bead locations labeled by response type for the (a) 1.61 kPa and (b) 0.2 kPa hydrogels.

The overlay of the magnetic field (Figure 22) sparked interest in the field's fringing effects in the z-direction. Figure 23 shows the experimental setup from the side with the magnetic field in the z-direction overlaid.

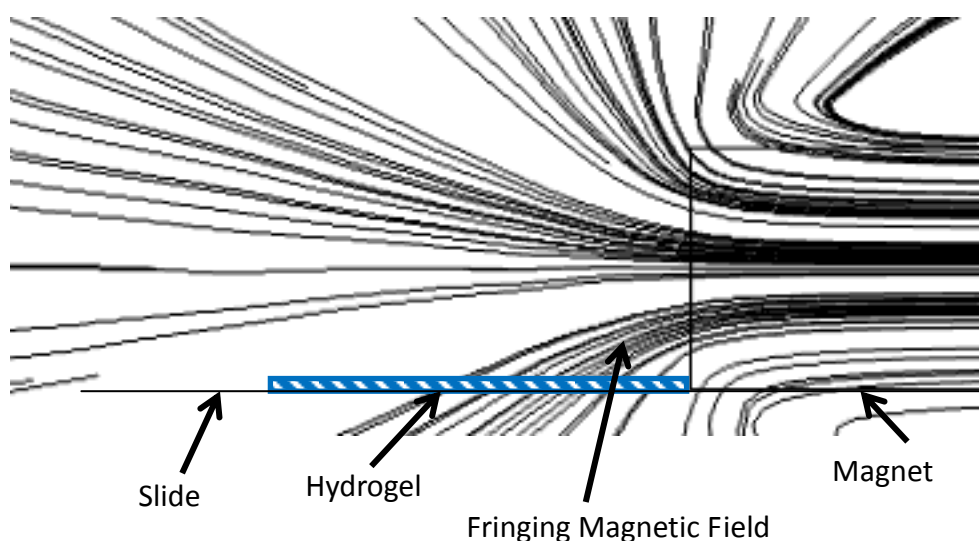


Figure 23: Side sketch of the experimental setup with the magnetic field lines in the z -direction overlaid. This shows the magnetic field is bending or fringing downwards through the hydrogel.

Elastic displacement values were calculated for each bead based on the bead tracking data. The net displacement was determined by the difference between the data points at the baseline and at the displacement upon magnet activation. The baseline value was calculated by averaging the data points for up to 1 s prior to activation. The displacement value for responses categorized as “elastic” was determined by averaging the displacement for the first second while the magnet was activated. The displacement value for responses categorized as “viscoelastic” looked specifically at the data points surrounding the elastic jump in position when the magnet was switched either on or off. Not all runs showed this distinct response, so only data sets that showed this response were used to calculate an elastic displacement. Displacement values for responses categorized as “other” were determined using a similar method as the “viscoelastic” responses if they showed an elastic response when the magnet was turned either on or off.

For example, Figure 20c shows a response when the magnet is turned off (at $t=6s$) that resembles the recoil of the bead from the elastic response of Figure 21a.

Net displacement values were calculated for each run of each bead that showed a response able to be analyzed in this way. The net displacements for each run of each bead were then averaged, and the average displacement value was programmed into the COMSOL Multiphysics model (Figure 11) to calculate the magnetic force acting on the bead. Table 11 summarizes the average bead displacement, bead position, and force.

Table 11 – Summary of bead position, displacement, and magnetic force acting on the beads in the (a) 1.61kPa hydrogel and the (b) 0.2kPa hydrogel. N represents the number of displacement data points averaged into the final displacement. Two beads, position 1 bead 1 and position 3 bead 1 in the 1.61kPa hydrogel, did not have response data from which an elastic displacement could be discerned.

(a) 1.61kPa hydrogel

Position	Bead	Bead Position		N	Average Displacement (nm)	Force (pN)
		X	Y			
1	1	1.881	0.678	3	**	**
2	1	2.872	0.785	3	-97.389	123.25
	2	3.284	0.711	2	-87.632	110.91
	3	3.547	0.215	2	-87.809	111.13
3	1	4.137	0.970	3	**	**
	2	4.429	0.478	2	-47.770	60.46
4	1	6.010	1.079	3	-94.135	119.14
	2	6.295	0.821	2	-89.664	113.48
5	1	6.317	1.783	3	-81.277	102.86
	2	6.056	1.229	2	-72.930	92.30
	3	5.771	1.389	2	-104.265	131.96
6	1	4.191	2.046	3	-198.210	250.85
7	1	3.227	2.028	3	-86.760	109.80
	2	3.069	1.853	2	-92.752	117.39
8	1	3.453	2.593	3	-104.234	131.91
	2	3.312	2.359	2	-109.790	138.95
9	1	3.279	1.976	3	-78.097	98.84
10	1	0.145	1.558	3	-68.190	86.30

11	1	0.097	3.974	3	-117.390	148.57
	2	0.267	3.541	2	-115.430	146.09
	3	0.345	3.673	2	-121.130	153.30
12	1	1.254	3.737	3	-83.567	105.76
	2	1.547	3.707	2	-77.298	97.83
13	1	2.093	4.146	3	-74.342	94.09
	2	2.289	3.999	2	-62.725	79.38
	3	2.318	3.922	2	-82.539	104.46
14	1	3.104	4.013	3	-84.519	106.97
	2	3.286	3.547	2	-110.182	139.44
	3	3.295	3.704	2	-78.248	99.03
	4	3.803	4.181	2	-93.545	118.39
15	1	4.612	3.909	3	-83.579	105.78
	2	5.167	3.459	2	-79.267	100.32
16	1	0.776	0.469	3	-101.571	128.55
	2	0.943	0.196	2	-193.602	245.02
17	1	2.180	1.455	3	-88.020	111.40
	2	2.320	1.559	2	-68.223	86.34
	3	2.622	1.263	2	-109.347	138.39
18	1	2.469	2.477	3	-103.303	130.74
	2	2.406	2.058	2	-76.269	96.53
19	1	3.580	0.925	3	-75.207	95.18
20	1	4.393	1.589	3	-108.606	137.46
21	1	3.820	2.224	3	-70.240	888.95
22	1	5.365	1.929	3	-81.435	103.06
23	1	4.683	2.729	3	-63.569	80.45
	2	4.949	2.835	2	-88.078	111.47
	3	4.964	2.522	2	-61.341	77.63
24	1	4.371	3.178	3	-59.861	75.76
	2	4.378	2.736	2	-105.901	134.03
25	1	4.761	4.059	3	-78.989	99.97
	2	4.693	3.632	2	-82.110	103.92
26	1	3.523	4.281	3	-45.990	58.20
27	1	1.839	3.921	3	-62.604	79.23
	2	1.902	3.721	2	-77.080	97.55
28	1	0.673	3.917	3	-99.840	126.36
	2	1.010	4.089	2	-53.402	67.59
	3	1.196	3.911	2	-125.140	158.38
	4	1.435	4.171	2	-66.287	83.89

(b) 0.2kPa hydrogel

Position	Bead	Bead Position		N	Average Displacement (nm)	Force (pN)
		X	Y			
1	1	4.000	1.294	0	-83.182	13.08
2	1	4.808	0.927	3	-92.762	14.58
	2	4.963	0.352	3	-92.733	14.58
6	1	4.812	2.330	2	-64.291	10.11
	2	5.046	1.594	3	-86.006	13.52
7	1	3.097	1.945	2	-78.273	12.31
8	1	0.675	2.105	3	-132.209	20.78
9	1	0.881	3.047	3	-114.153	17.95
10	1	1.157	3.709	3	-111.253	17.49
	2	1.438	3.453	3	-133.763	21.03
11	1	2.038	2.990	2	-128.594	20.22
12	1	2.559	3.381	3	-110.263	17.33
	2	2.898	2.899	3	-112.572	17.70
13	1	3.839	3.560	2	-94.162	14.80
	2	4.445	3.369	3	-71.045	11.17
14	1	5.135	2.819	2	-79.022	12.42
15	1	5.643	3.100	3	-88.060	13.84
	2	6.170	3.173	3	-72.988	11.47
16	1	5.889	4.129	2	-55.943	8.79
	2	5.665	3.773	3	-137.120	21.56
	3	5.649	3.393	2	-53.837	8.46
17	1	5.888	5.079	2	-114.130	17.94
	2	5.798	4.494	3	-81.070	12.75
	3	5.151	4.482	2	-98.701	15.52
18	1	5.362	5.161	2	-57.716	9.07
19	1	4.459	4.813	3	-109.339	17.19
	2	4.724	4.760	3	-78.566	12.35
	3	4.957	4.914	2	-74.775	11.76
20	1	4.242	5.212	2	-72.469	11.39
	2	4.552	5.469	3	-94.220	14.81
21	1	3.389	5.229	2	-95.212	14.97
	2	3.428	4.741	3	-90.493	14.23
	3	3.981	4.872	2	-84.890	13.35
22	1	3.285	4.771	2	-99.603	15.66
23	1	3.209	5.312	3	-80.514	12.66
24	1	2.197	4.833	3	-111.122	17.47

	2	2.425	5.165	3	-110.009	17.29
25	1	1.277	4.330	2	-75.995	11.95
	2	1.808	4.170	3	-106.473	16.74
	3	1.980	4.702	2	-90.309	14.20
26	1	1.386	4.261	2	-92.660	14.57
	2	0.862	4.423	3	-59.871	9.41
27	1	0.847	4.721	2	-92.662	14.57

The modulus of elasticity for each data point was back-calculated using Equation 5 to validate the model and methods. The results of this calculation were the same for all points in each gel. Table 12 summarizes these results.

Table 12: Comparison of known gel elasticity (from relative ratios of acrylamide/bis-acrylamide) and the results of back-calculating the Modulus of Elasticity for each gel using bead displacement data and calculated force value. The back-calculated values were the same for all data points in each gel.

Known Gel Elasticity	Back-Calculated Modulus of Elasticity
1.61 kPa	8.95 kPa
0.2 kPa	1.11 kPa

Chapter 4

Discussion

The purpose of this project is to develop a magnetic bead microrheometry system for studying local thrombus rheology. For a successful system able to calculate the local elasticity of a spatially inhomogeneous material like a thrombus, the magnetic force and displacement of magnetic beads embedded in the material must be known. To develop this system, the displacement of magnetic beads can be measured using bead tracking software. The magnetic force at a given spatial location was experimentally determined

using polyacrylamide hydrogels of known elasticity. These steps were evaluated to determine the success of the system as designed so far.

Bar Magnet

Initially, a neodymium rare-earth bar magnet was used to apply the magnetic force to the paramagnetic beads. The magnet was placed in the system manually by fitting it into the notch on the slide clamp holders (Figure 2). This manual process of adding the magnet into and out of the system presented several issues. First, the placement of the magnet was inconsistent. A study of magnet placement reproducibility (Table 4) showed a standard deviation of 0.144 mm in the x-direction and 0.761 mm in the y-direction. This presents an issue in repeating the response of a particular bead as the magnet is not necessarily the same distance from the beads for each trial. This most likely played a role in the variability in the study of response reproducibility (Figures 17 and 18).

The magnet placement variation also had practical implications. As the bead locations are determined relative to the magnet origin (defined as the top left corner of the magnet, Figure 7), the variation in magnet placement meant the origin changed in position relative to the beads of interest for each trial. To calculate bead location, the magnet would need to remain placed in the system while the origin position was calculated with the vernier scales, a process that often required at least a minute to complete. While this location data was acquired and recorded, all of the beads in the hydrogel were subject to the magnetic force. As seen in many trials, there was often a

viscous response as the beads continued to displace even after the initial elastic displacement. The effects of leaving the magnet in the system on viscous displacement of the beads are unknown as the microscope location had to change to identify the origin position. The effects of this repeated prolonged exposure to the magnetic force over long durations and multiple trials is also unknown. As some trials showed this viscous displacement to cause a plastic deformation of the hydrogel (the bead did not return to baseline position), it stands to reason that repeated, prolonged exposure to the magnetic force may have plastically deformed the hydrogel and compromised its elastic properties.

The manual placement of the bar magnet into position in the system also had an effect on the data collection and bead tracking results. As Figure 9a shows, placement and removal of the bar magnet introduced movement and noise into the system that appeared as clear outliers in the bead tracking results. These data points were removed (Figure 9b) to separate regions of baseline, after placement of the magnet (“mag in”), and after removal of the magnet (“mag out”). The difference between the averaged displacements of the baseline and “mag in” regions was calculated to determine the elastic displacement. This method works well for elastic displacements of the beads where the “mag in” region shows no viscous displacement. However, for those responses showing a viscous displacement in this region, averaging over this region for displacement calculations is not representative of the elastic displacement. In a viscoelastic response the only points that show the elastic displacement are when the magnet is introduced to the system and the beads displace in a time-independent manner. The noise caused by manual placement of the magnet masks this initial elastic response and leads to a loss of data.

Given the variability of magnet placement, practicality of calculating bead position, and data loss due to manual placement of the magnet, the decision was made to switch to an electromagnet. An electromagnet improves the system as it remains fixed throughout experimentation, requiring only one magnet origin measurement and removing any need for manual manipulation of the system. No outliers are created, allowing for the elastic response of the beads due to the introduction of the magnetic force to be calculated, even in viscoelastic or “other” responses (Figure 20). An electromagnet also allows for precise timing of introducing and removing the magnetic force from the system as it can be controlled by a computer (Figure 4).

An important result from the bar magnet experiments was the decision to limit the area of interest to within the width of the magnet. This working area (Figure 6), was thought to allow the assumption that all displacement due to magnetic force will be in the y-direction alone. This assumption halves data analysis and simplifies the COMSOL model for calculating force acting on the beads. The assumption was developed in trials with the bar magnet. For bead positions within this working area, displacement in the x-direction was shown to result only from the mass of the magnet being added to the system. In Figure 16, it can be seen that the displacement in the x-direction when the magnet was present was not significantly different than the displacement due to the mass control (a nonmagnetic mass comparable to the magnet placed on the slide). Displacement due to magnetic force was only significant in the y-direction.

Following all trials with the electromagnet, this assumption was then assessed in part by superimposing the magnetic field lines over the bead distribution (Figure 22). From this, it is observed that the assumption that we can limit our concern to the y-

direction only in the very center of the magnet area where field lines run only in the y-direction. Outside of this region, and the farther away from the magnet one goes, the field lines begin to curve away from the midline of the magnet, with an increasing x-component that challenges the assumption. Beyond these points, the x-component must also be considered.

Further analysis of the magnetic field shows a fringing field in the z-direction as well (Figure 23). This would require a 3 dimensional analysis of force and displacement. To limit the system to 2 dimensional analysis, the hydrogel and slide need to be raised to the midpoint of the magnet. These fringing fields and erroneous assumption of only looking in the y-direction may have seriously impacted results from this study and are key considerations for future work.

Bead Response Categories

Studies with the electromagnet utilized two hydrogels with a modulus of elasticity of 1.61 kPa and 0.2 kPa to represent the upper and lower bounds of experimentally determined elasticity's of previous thrombus rheology work.^{18,19,32} Responses were varied in many regards. Some showed a clearly elastic response (Figure 20a) or clearly viscoelastic response (Figure 20b). There was also a large number of "other" responses (Figure 20c is a representation of one common example) that did not clearly fit into an easily definable category.

Most of the "other" response types showed definite bead responses to application and/or removal of the magnetic force (at t=3s and t=6s). However, some runs showed the

beads displaced away from the magnet while the magnetic force was still being applied, while others did not show a response until the magnetic force was removed (Figure 20c). The responses that only showed an elastic displacement upon removal of the magnetic force indicate a force internal to hydrogel acted on the bead. This displacement is similar to the elastic recoil displayed in elastic responses (see Figure 20a), yet the overall response does not show the initial elastic displacement of the bead upon application of the magnetic force. It is possible that the bead was already displaced in such a way that there was an elastic potential energy stored in the hydrogel to recoil the bead away from the magnet once the magnet force was removed. This would indicate the bead displacement at baseline ($t=0s$ to $t=3s$) was already in equilibrium with the magnetic force. Repeated exposure to the magnetic force (the beads were exposed to magnetic force approximately 150 times for each gel for a total time of 450 s) may have had an effect on bead displacement to the point where they could not displace further, but the magnetic force acting on the bead, and the bead in turn on the hydrogel, built the potential energy for the elastic recoil upon removal of the magnetic force.

For those responses categorized as “other” in which the bead displaced away from the magnet while the magnetic force was still being applied, the cause is unclear. A displacement away from the magnet while the magnetic force is still being applied indicates either the bead is being repelled by the magnet or there is a force within the hydrogel acting on the bead. The beads are paramagnetic, meaning they are magnetized only in the presence of an external field. The electron spins of constituent atoms are aligned with the field, causing attraction. These dipole moments do not align such that the beads can be repelled by the field. Also, the beads often showed an initial elastic

response to the application of the magnetic field demonstrating attraction to the magnet (a displacement in the negative y-direction) and an elastic response to removal of the magnetic field (a jump in the positive y-direction) reminiscent of the elastic recoil that would indicate the magnetic force was attracting the bead.

In addition to the forces of the crosslinks on the bead, it is possible that the water within the hydrogel could be acting on the beads, playing a role in some of this behavior. The 1.61 kPa hydrogel and 0.2 kPa hydrogel are approximately 92% and 97% water, respectively. Movement of beads within the gel may cause liquid water to displace, the momentum of which can act on the beads. This “other” response type, where the beads displaced away from the magnet while the magnetic force was still being applied, occurred more in the 0.2 kPa gel, which does have a less dense crosslink network and a higher water concentration. It is unclear, however, to what extent movement of water in response to bead movement on a 100 nm scale level could create a force or momentum to significantly displace the bead, let alone in the direction opposite of the magnetic attraction. Additionally, if this was a key factor to the response, it would consistently have an impact on all responses, regardless of category type. As many of these response types displace the bead a distance greater than the initial elastic displacement, the reasons for this response remain unclear.

As mentioned previously, Figure 22 shows that for some bead locations, the assumption of neglecting the x-direction is not valid outside of the center half of the magnet. It may be possible that the x-component of the displacement and force play a role in the irregular response of some of these beads. However, given that these “other” response types occurred in both the center region for which one-directional assumption

was valid and the region for which this assumption is invalid, it is unlikely that the x-component not factored into the calculations has a significant effect on the bead response pattern.

Analysis of Different Response Types

Bead displacement was determined by tracking bead location through a series of recorded images as the beads were exposed to a magnetic force. As the COMSOL model was made to model a linearly elastic material, the bead displacement responses were analyzed to determine elastic displacement of beads. For each run of each bead, an elastic displacement was determined if there was a clear response occurring when the magnet was either turned on or off (at $t=3s$ or $t=6s$, respectively). For runs that did not show a response from which a displacement could be observed, no elastic displacement was determined. The elastic displacements for all runs of each bead were averaged, and that value was used to solve for force.

For both the 1.61 kPa and 0.2 kPa gel, displacements were on the same order of magnitude, varying from -53 nm to -193 nm. The resolution for bead tracking is 64.1 nm, meaning most displacements were barely outside the range considered discernible, although there were definitely responses to the presence of the magnetic field. To improve confidence in these displacements, resolution must be improved or the magnet needs to be stronger to exert a greater force on the beads. There was no noticeable difference in scale of the displacements for each gel. This reflects that the beads are too large to pass through the pores of the hydrogels (100 nm scale).²⁴ The only difference

between the gels is the density of the crosslinks and the resulting reaction force acting on the bead in response to the applied magnetic force.

The response category type determined how each elastic displacement was solved for each run. For those responses categorized as elastic, this was achieved by subtracting the averaged y-position for 1s after magnet activation from the averaged y-position of the bead for the 1s prior to magnet activation. For those responses categorized as viscoelastic and other, an average displacement after turning on the magnet could not be calculated due to the viscous displacement. Instead the two data points between the magnet being turned on and off had to be compared. As the magnet was controlled by the computer, this point could be determined with precision and accuracy. However, there is an uncertainty associated with each data point. When averaging the baseline and displacement values for the elastic response types, there was a standard deviation of 11-25nm for those points. That is why averaging a set of values over time is important comparing baseline and displacement values. Calculating an elastic displacement using two individual, adjacent data points in the viscoelastic and other response types is less accurate and causes the displacement value to carry an uncertainty.

For the purposes of this study, an elastic displacement was calculated from all runs that showed a distinct displacement, despite this uncertainty. The ideal scenario for determining elastic displacement is the elastic response type where values for baseline and displacement due to magnetic force can be averaged over a range of data points. For future work, if time permits it would be preferable to only keep and use displacement data that shows this elastic response type and can determine an elastic displacement based on more than 2 data points. Viscoelastic response types can also be further

analyzed and used if the COMSOL model were modified to be a viscoelastic solid. The regions of elastic displacement and viscous displacement could be fit with a line to experimentally determine more properties of the hydrogel or other unknown material acting on the bead. Time did not permit for this to be done for this study.

Spatial Distribution of Response Categories

When categorized into the three response type categories (elastic, viscoelastic, and other) and plotted by spatial location (Figure 21), some trends do occur. In the 0.2 kPa gel (Figure 21b), it is observed that the majority of “other” responses were at locations farther from the magnet. All elastic and viscoelastic responses occurred at positions within 4 mm of the magnet. In the 1.61 kPa gel, there is a less obvious trend. Elastic, viscoelastic, and other response types were found throughout the working area. When the spatial distribution of response types was overlaid with the magnetic field lines from the magnet (Figure 22), there did not appear to be a correlation between the field line shape and distribution with the response type. For both hydrogels, the response types were scattered evenly across the x-direction, showing no relation to the bending of the magnetic field at the wider sides of the working area where the field lines bent and the x-component became relevant. There was a greater number of elastic and viscoelastic responses in the 1.61 kPa gel than in the 0.2 kPa gel, accounting for over 80% of the responses. In the 0.2 kPa gel, over half of all responses were categorized as “other”.

This trend may be due to the different crosslink densities in each gel. The 1.61 kPa hydrogel has a higher density of crosslinks than the 0.2 kPa gel, the reason for the

higher modulus of elasticity. While the pores in both hydrogels are on the order of 100nm,²⁴ which is sufficiently small such that the beads (diameter of 45 μm) are not able to freely move through pores within the gel, there is a varied pore size and density of crosslinks. This difference may contribute to the varied responses in the gels, in addition to distribution of response types, at least for the 0.2 kPa gel where there was a clear pattern.

The distribution of response types is important when looking ahead to testing blood clots with this magnetic bead microrheometry system. It is important to know where to look for a response that can be well (and accurately) categorized and analyzed to find material elasticity. As previously described, elastic response types are best for statistically determining an elastic displacement, and viscoelastic response types can be further analyzed in conjunction with a viscoelastic COMSOL model for more accurate results.

It is expected that blood clot elasticity will be between 0.2 kPa and 1.61 kPa, so the results shown in Figure 21 indicate what regions to consider in testing an unknown material. Based on those results, for clots of lower elasticity, the area most likely to return an elastic or viscoelastic response easy to characterize and analyze is within 4 mm of the magnet, ideally between 2 and 4 mm. As the clot elasticity increases, there appears to be a greater working distance where elastic responses will appear. The region appearing most appropriate for more pliable clots (2 – 4 mm) is also a region where more stiff clots return elastic responses. This is not to say that an easily characterized response cannot be accurately analyzed outside of this range, however to accommodate a breadth of possible elasticity's, this working distance of 2-4 mm appears to be favorable for the

current system and magnet. A stronger electromagnet could extend this working range to be wider to reach distances a bit further from the magnet.

COMSOL Modeling of Magnetic Force

COMSOL Multiphysics was used to model magnetic force acting on beads in a hydrogel. Initial attempts sought to measure force direction by modeling the full system of magnet, gel, and beads (Figure 10). Results of this model did not make logical sense as the y-component of magnetic force was not at a maximum when directly in front of the magnet (Figure 14a) just as the x-component of magnetic force did point inwards toward the magnet when the bead was beyond the width of the magnet in the x-direction (Figure 12b). After failed attempts at refining the mesh and different iteration patterns, it was decided that the system needed to be simplified. As a result, magnetic force would need to be experimentally determined by looking at the displacement in a bead of known elasticity.

The new model was simplified to a bead within a gel with fixed constraints on the top and bottom (simulating adhesion of the hydrogel to the treated coverslip and glass slide) and free boundaries on the sides as it was assumed the beads would not be near the boundary of the gels. When the experimental setup was designed, the magnet origin was intentionally set away from the edge of the gel. The bead was given a prescribed displacement to calculate force. Using elastic displacement data, magnetic force was calculated for beads within the 1.61 kPa and 0.2 kPa gels (Table 11). All forces were in

the pN range. The magnetic forces calculated for the 0.2 kPa hydrogel was an order of magnitude less than the magnetic forces calculated for the 1.61 kPa hydrogel.

To validate the COMSOL model and force calculation methods, the calculated force and measured displacement for each bead were used to back-calculate the modulus of elasticity of the hydrogel using Equation 5. The results of these calculations (Table 12) did not match the elasticity known by the composition of the acrylamide/bis-acrylamide in the hydrogels and did not match the modulus of elasticity programmed into the COMSOL model used to calculate the force. This clearly indicates that there is a flaw in the force calculation methodology. If the displacement and gel elasticity were used to calculate the force, that same force and displacement should be able to calculate the same gel elasticity. The force was calculated by integrating the normal y-component of the stress tensor over the surface area of the bead (Equation 4). This method neglected all forces in the x-direction and the shear stress in the yx and yz directions. As discussed previously, the assumption of only considering the y-direction appears invalid for most locations when considering the displacement response. When calculating the force, this assumption also appears to fall short. The computer model for calculating force needs to acquire data for all 2D components of force and utilize these to be able to more accurately calculate the elasticity. Calculating force only in the normal y-direction is not adequate to represent the magnetic force on the bead and in turn calculate elasticity.

Conclusion and Future Directions

The purpose of this project was to develop a magnetic bead microrheometry system that can be used to study thrombus rheology. A computer controlled electromagnet system was developed to apply a magnetic force to paramagnetic beads embedded in a material while recording and tracking bead movement. Hydrogels with an elasticity of 1.61 kPa and 0.2 kPa were used to represent the upper and lower ranges of published thrombus rheology values. Experiments with these hydrogels showed varying bead displacement response types that were inconsistent spatially. Results showed that a distance of 2-4 mm from the magnet is optimal for yielding elastic or viscoelastic response types, especially in the more pliable hydrogels. The assumption that the x-component of magnetic force and bead displacement was shown to be invalid except in the center half of the working area, although this did not affect the variation in response type. Elastic response types were more accurately analyzed to determine an elastic displacement that could be used to determine magnetic force acting on the bead. An elastic displacement could also be determined from viscoelastic and “other” response types, albeit less accurately. The elastic displacements calculated for both gels were on the same order of magnitude. From these elastic displacements, magnetic forces acting on the beads at varying locations were determined to be on the 10-100 pN range. The force values for the stiff gel were an order of magnitude larger than the more pliable gel, showing that they are not consistent in calculating the magnetic force acting on the beads in the same general region. When these force values were used with the displacement values to calculate elasticity for system validation, the results did not match the known

elasticity of the hydrogels. From this, it was concluded that calculating the normal force in the y-direction alone fails to properly represent the total force acting on the bead.

This project has laid the groundwork for developing a magnetic bead microrheometry system for studying thrombus rheology, however there is much room for improvement. As the assumption of only the y-direction being relevant was shown to be invalid in terms of how the magnetic field lines pass through the working area and how the in normal y-component of force is inadequate for calculating elasticity, both x and y dimensions should be considered for future work. This includes analyzing displacement in the x direction, along with calculating the force in the normal x direction, as well as the xy shear force. The hydrogel or thrombus sample must also be elevated to the center of the magnet to avoid a fringing field in the z-direction. In order to have more significant displacement values, the resolution on bead tracking needs to be improved or the magnetic force needs to be increased. More elastic displacement data points need to be determined for each gel type in order to more accurately calculate and map out force. Better assessment of repeatability of elastic displacement can be achieved with shorter magnet duration and repeated application of force. With more accurate elastic displacement data, magnetic force can be calculated with better certainty to map the magnetic force on the beads spatially. When this force mapping is achieved, a hydrogel of known elasticity can be tested to validate and verify the accuracy of the system. From there, a thrombus of unknown elasticity can be characterized.

BIBLIOGRAPHY

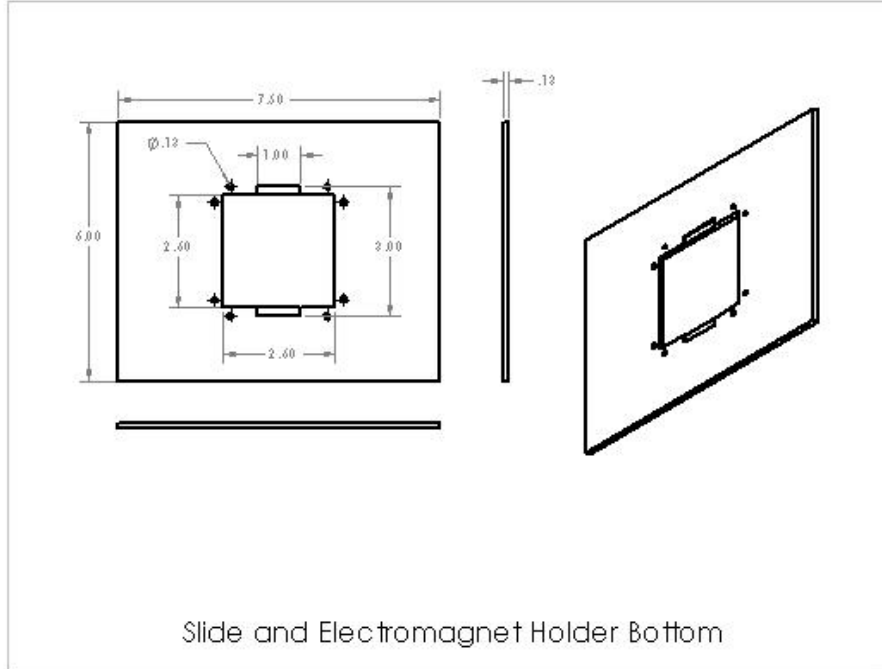
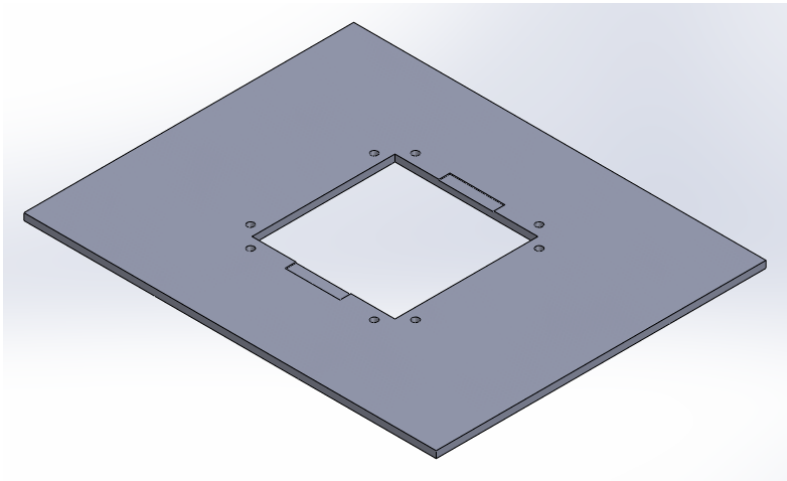
1. Kochanek KD, Xu J, Murphy SL, Minin AM. National Vital Statistics Reports Deaths : Final Data for 2009. 2011;60(3).
2. Roger VL, Go AS, Lloyd-Jones DM, et al. Heart disease and stroke statistics--2012 update: a report from the American Heart Association. *Circulation*. 2012;125(1):e2–e220.
3. Heidenreich P a, Trogdon JG, Khavjou O a, et al. Forecasting the future of cardiovascular disease in the United States: a policy statement from the American Heart Association. *Circulation*. 2011;123(8):933–44.
4. Wootton DM, Ku DN. Fluid Mechanics of Vascular Systems , Diseases , and Thrombosis. 1999:299–329.
5. Lowe GD. Rheological influences on thrombosis. *Baillière's best practice & research. Clinical haematology*. 1999;12(3):435–49.
6. Katritsis DG, Theodorakakos a, Pantos I, et al. Vortex formation and recirculation zones in left anterior descending artery stenoses: computational fluid dynamics analysis. *Physics in medicine and biology*. 2010;55(5):1395–411.
7. Mitusch R, Stierle U, Sheikhzadeh A. Aortic Atherosclerosis as a Source of arterial embolism. *Zeitschrift fur Kardiologie*. 1998;87(10):789–796.
8. Tenenbaum a, Motro M, Shapira I, et al. Retrograde embolism and atherosclerosis development in the human thoracic aorta: are the fluid dynamics explanations valid? *Medical hypotheses*. 2001;57(5):642–7.
9. Wagner WR, Johnson PC, Kormos RL, Griffith BP. Evaluation of bioprosthetic valve-associated thrombus in ventricular assist device patients. *Circulation*. 1993;88(5):2023–2029.
10. Akbarian M, Austen WG, Yurchak PM, Scannell JG. Thromboembolic Complications of Prosthetic Cardiac Valves. *Circulation*. 1968;37(5):826–831.
11. Courtney JM, Lamba NM, Sundaram S, Forbes CD. Biomaterials for blood-contacting applications. *Biomaterials*. 1994;15(10):737–44.

12. Hoffman R, Benz EJ, Shattil SJ, et al. *Hematology: Basic Principles and Practice, 3rd Edition.*; 2000:1753–1754.
13. Benz EJ, Hoffman R, Shattil SJ, et al. *Hematology: Basic Principles and Practice, 3rd Edition.*; 2000:1783–1786.
14. Furie B, Furie BC. The molecular basis of blood coagulation. *Cell*. 1988;53(4):505–18.
15. Ryan E a., Mockros LF, Stern AM, Lorand L. Influence of a Natural and a Synthetic Inhibitor of Factor XIIIa on Fibrin Clot Rheology. *Biophysical Journal*. 1999;77(5):2827–2836.
16. Furie B, Furie BC. Thrombus formation in vivo. *The Journal of Clinical Investigation*. 2005;115(12):3355–3362.
17. Gardel ML, Valentine MT, Weitz DA. 1 Microrheology. 1999:1–55.
18. Riha P, Wang X, Liao R, Stoltz JF. Elasticity and fracture strain of whole blood clots. *Clinical hemorheology and microcirculation*. 1999;21(1):45–9.
19. Ryan E a., Mockros LF, Weisel JW, Lorand L. Structural Origins of Fibrin Clot Rheology. *Biophysical Journal*. 1999;77(5):2813–2826.
20. Collet J-P, Shuman H, Ledger RE, Lee S, Weisel JW. The elasticity of an individual fibrin fiber in a clot. *Proceedings of the National Academy of Sciences of the United States of America*. 2005;102(26):9133–7.
21. Shen LL, Hermans J, Mcdonagh J, Mcdonagh RP, Carr M, Hill C. Effects of Calcium Ion and Covalent Crosslinking on Formation and Elasticity of Fibrin Gels. *Thrombosis Research*. 1975;6:255–265.
22. Bausch a R, Ziemann F, Boulbitch a a, Jacobson K, Sackmann E. Local measurements of viscoelastic parameters of adherent cell surfaces by magnetic bead microrheometry. *Biophysical journal*. 1998;75(4):2038–49.
23. Yang Y, Lin J, Meschewski R, Watson E, Valentine MT. Portable magnetic tweezers device enables visualization of the three-dimensional microscale deformation of soft biological materials. *BioTechniques*. 2011;51(1):29–34.
24. Tse JR, Engler AJ. Preparation of hydrogel substrates with tunable mechanical properties. *Current protocols in cell biology / editorial board, Juan S. Bonifacino ... [et al.]*. 2010;Chapter 10(June):Unit 10.16.

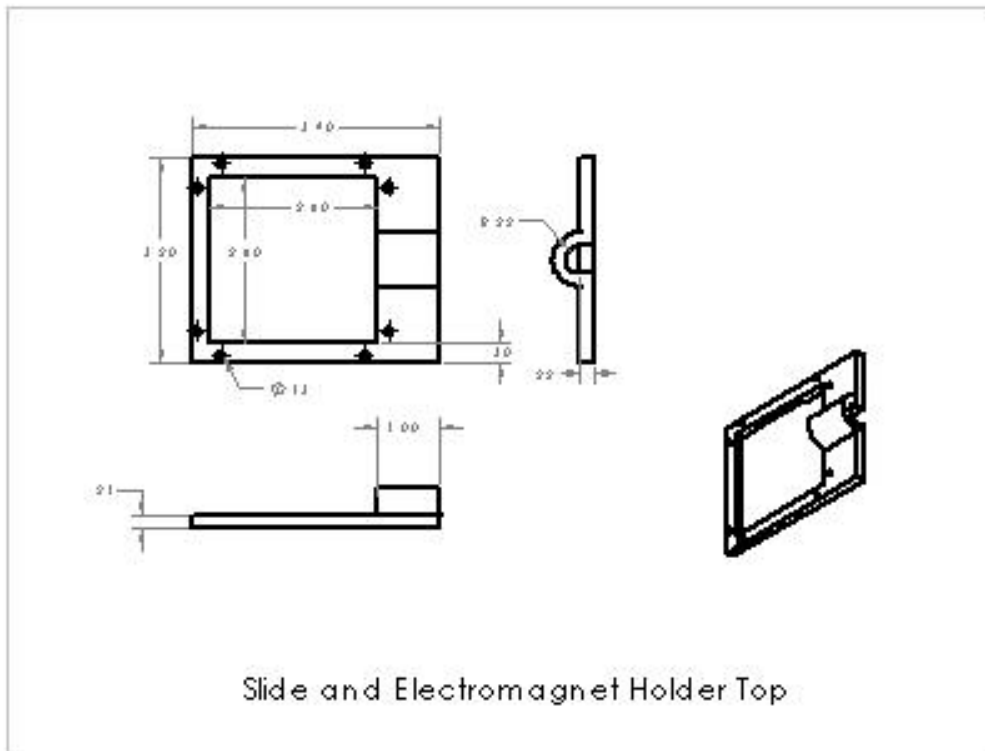
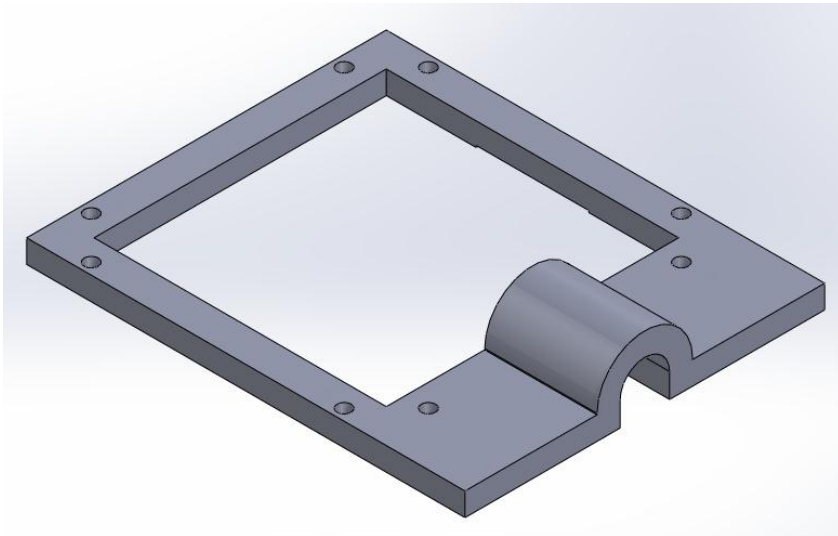
25. Kadow CE, Georges PC, Janmey P a, Beningo K a. Polyacrylamide hydrogels for cell mechanics: steps toward optimization and alternative uses. *Methods in cell biology*. 2007;83(07):29–46.
26. Kotlarchyk M a, Botvinick EL, Putnam a J. Characterization of hydrogel microstructure using laser tweezers particle tracking and confocal reflection imaging. *Journal of physics. Condensed matter : an Institute of Physics journal*. 2010;22(19):194121.
27. Huang C, Butler PJ, Tong S, Muddana HS, Bao G. Substrate Stiffness Regulates Cellular Uptake of Nanoparticles. 2013:1–16.
28. Anon. Magnet Calculator. *Magnetics, K&J*. Available at: <http://www.kjmagnetics.com/calculator.asp?calcType=block>.
29. Anon. Solenoid (Electromagnet) Force Calculator. *Daycounter, Inc. Engineering Services*. 2004. Available at: <http://www.daycounter.com/Calculators/Magnets/Solenoid-Force-Calculator.phtml>.
30. Dangaria JH, Butler PJ. Macrorheology and adaptive microrheology of endothelial cells subjected to fluid shear stress. *American journal of physiology. Cell physiology*. 2007;293(5):C1568–75.
31. Cheezum MK, Walker WF, Guilford WH. Quantitative comparison of algorithms for tracking single fluorescent particles. *Biophysical journal*. 2001;81(4):2378–88.
32. Evans P a., Hawkins K, Williams PR, Williams RL. Rheometrical detection of incipient blood clot formation by Fourier transform mechanical spectroscopy. *Journal of Non-Newtonian Fluid Mechanics*. 2008;148(1-3):122–126.
33. Kwon HJ, Rogalsky AD. Mechanical characterization of hydrogel. *Society of Plastics Engineers*. 2010:3–5.
34. Ahearne M, Yang Y, El Haj AJ, Then KY, Liu K-K. Characterizing the viscoelastic properties of thin hydrogel-based constructs for tissue engineering applications. *Journal of the Royal Society, Interface / the Royal Society*. 2005;2(5):455–63.

Appendix A: Solidworks figures and schematics of slide and electromagnet holders

Bottom Part:

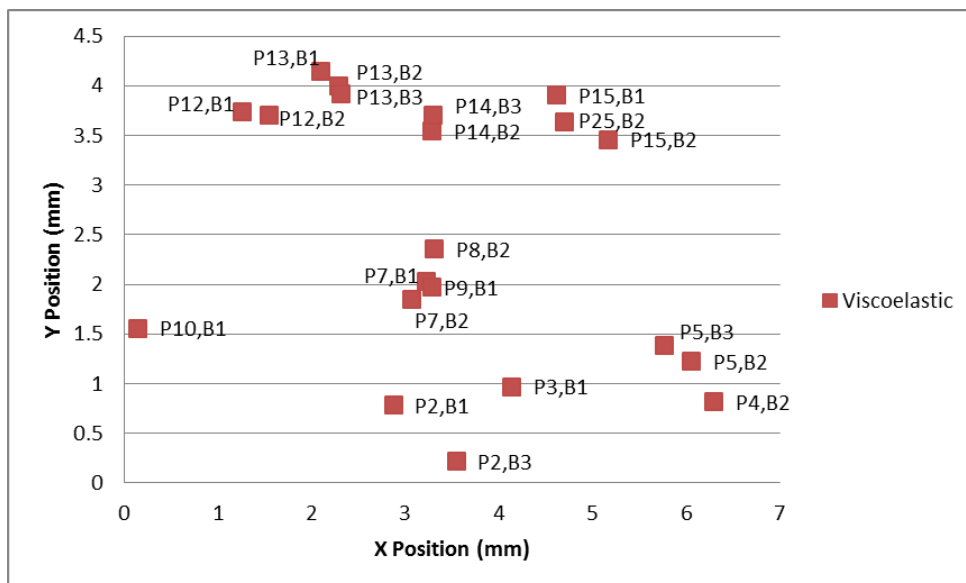
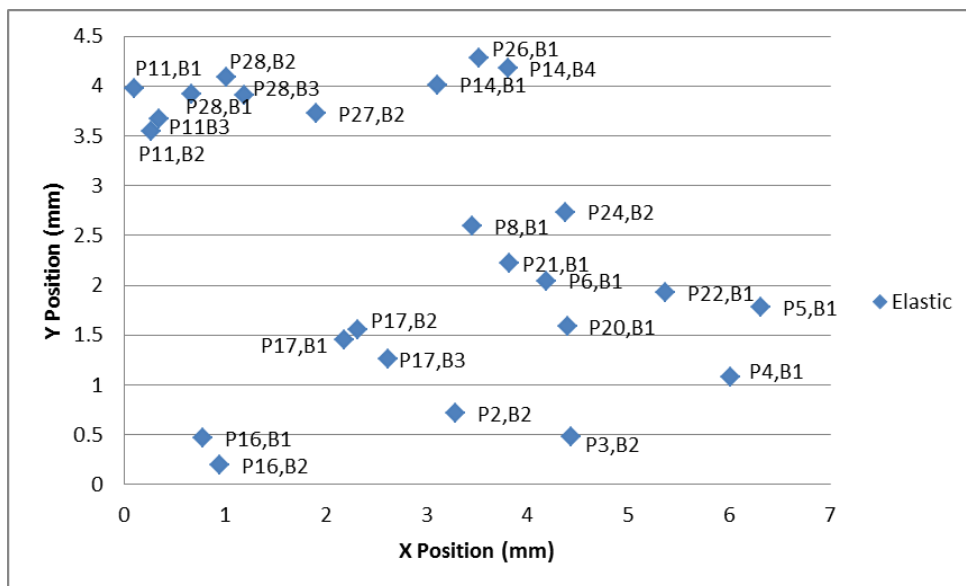


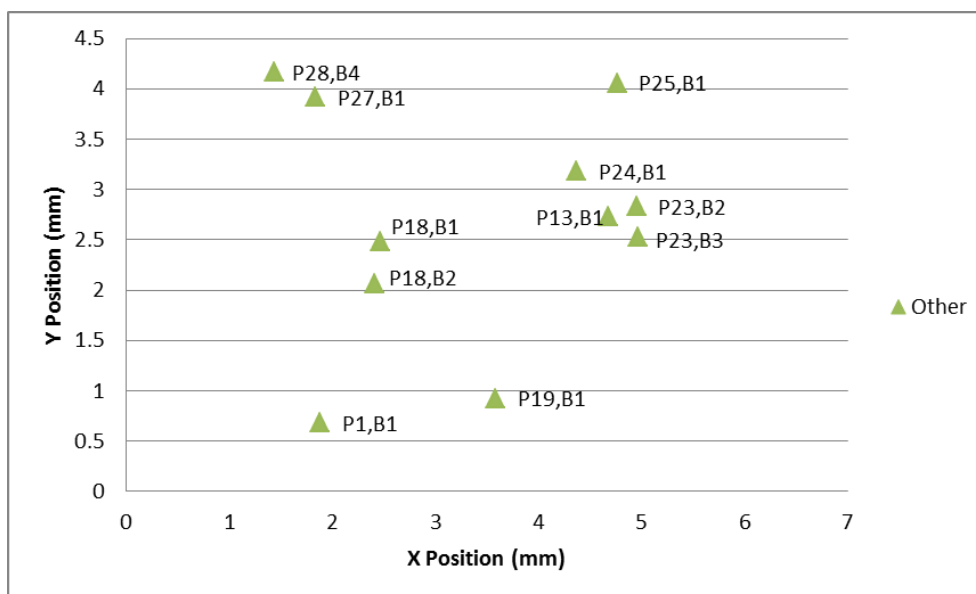
Top Part:



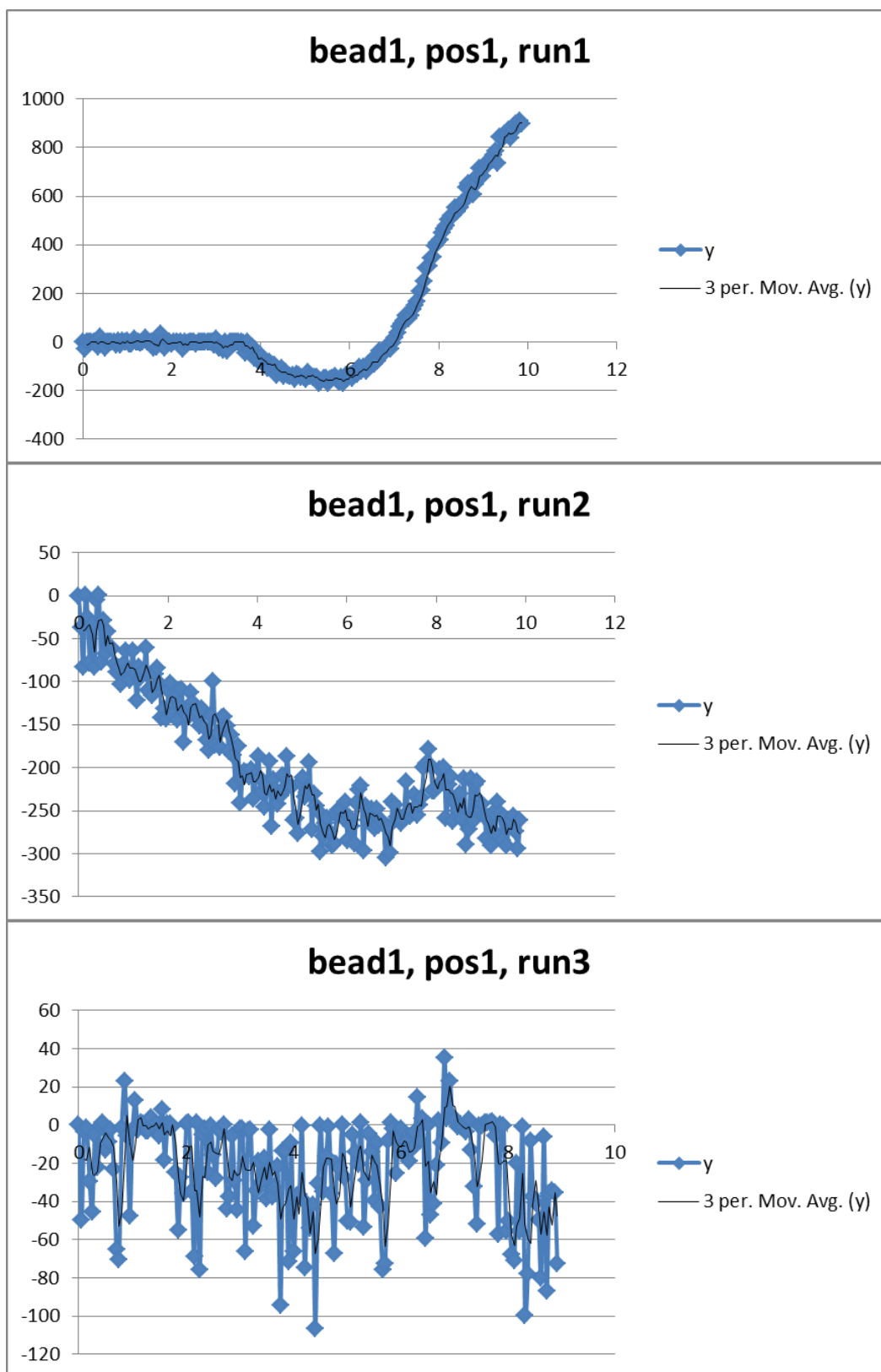
Appendix B: Bead displacement data for 1.61 kPa Hydrogel

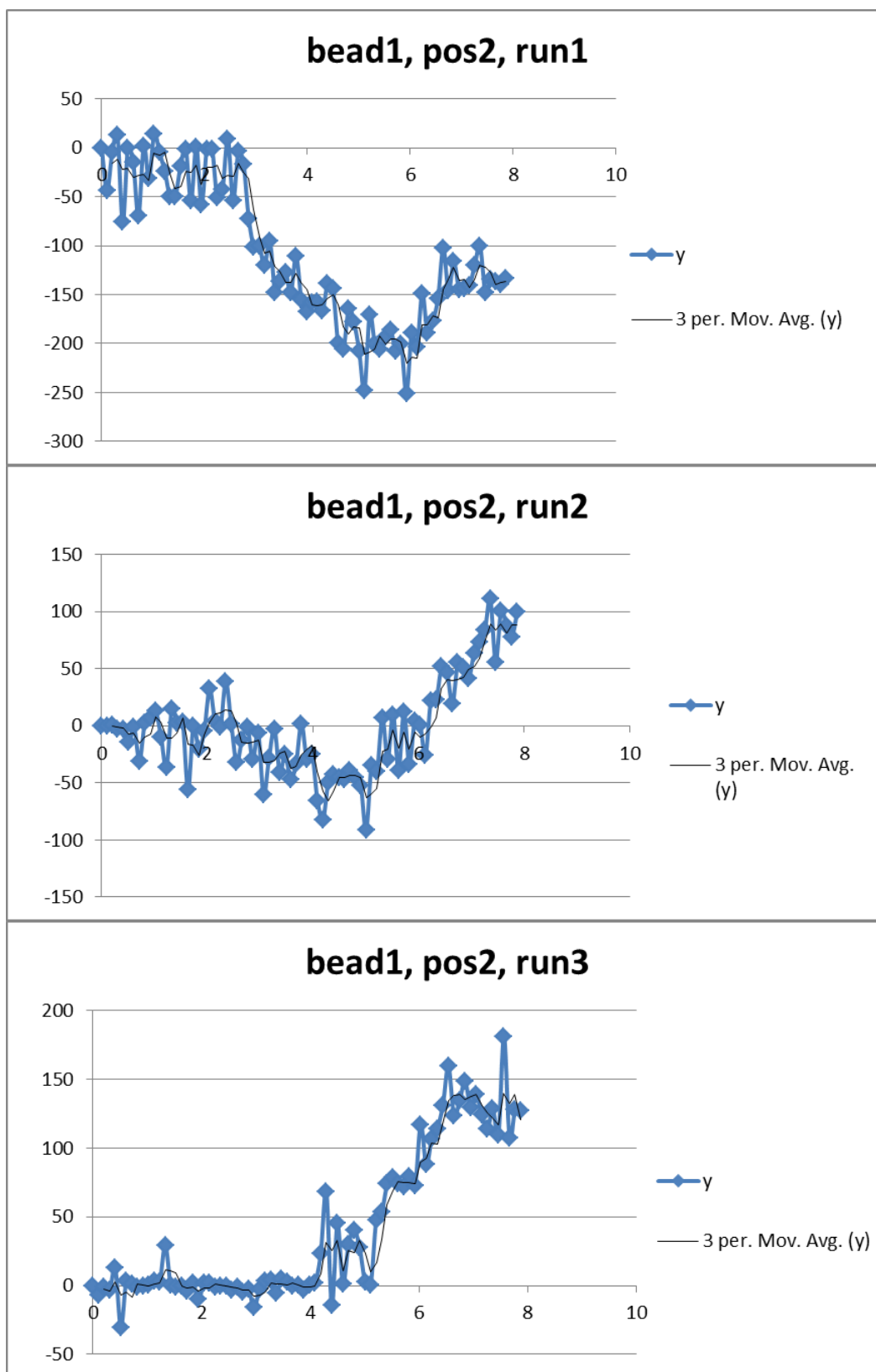
For reference, beads are labeled by Position (P) and Bead (B) on the spatial distribution plots below.

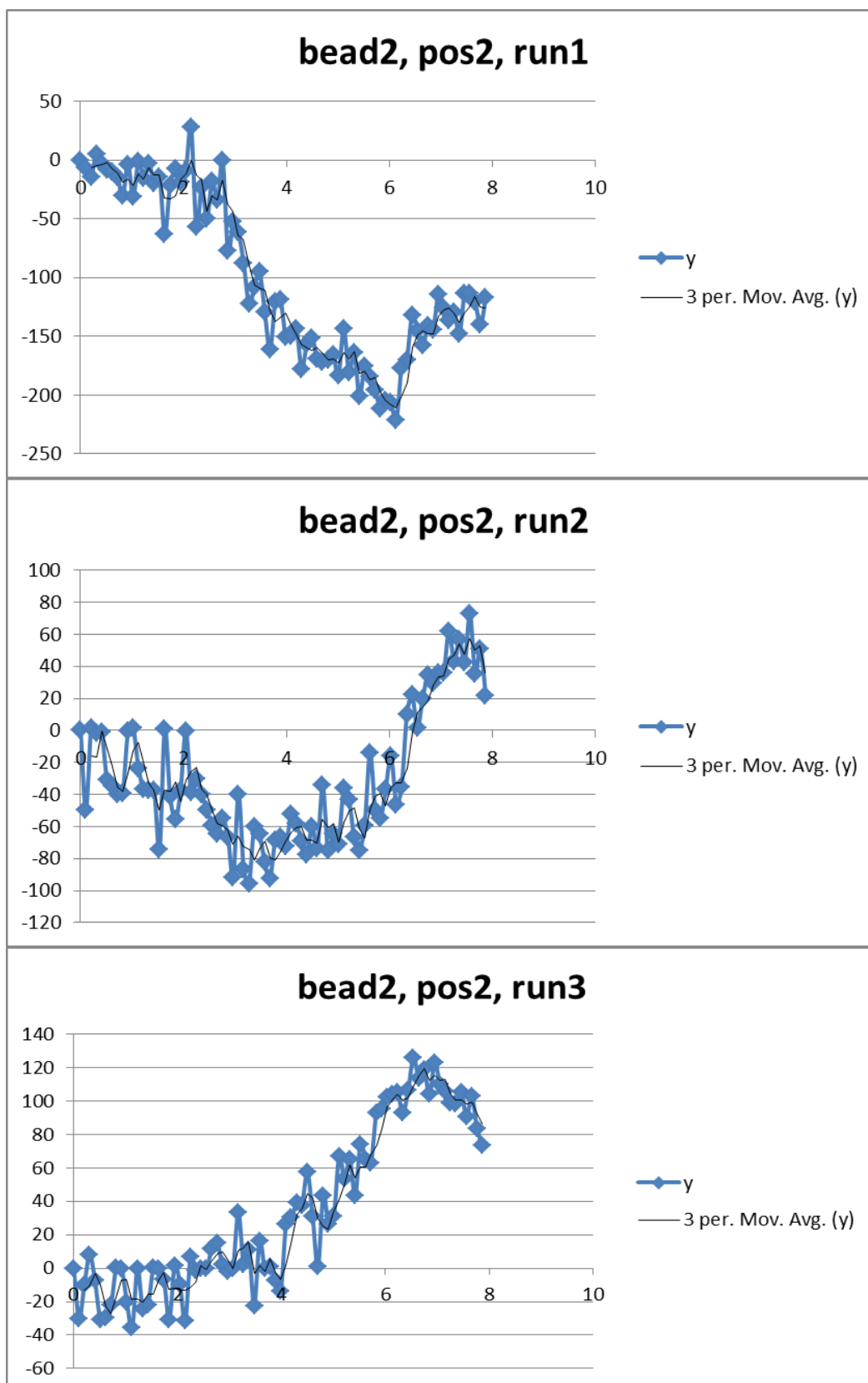


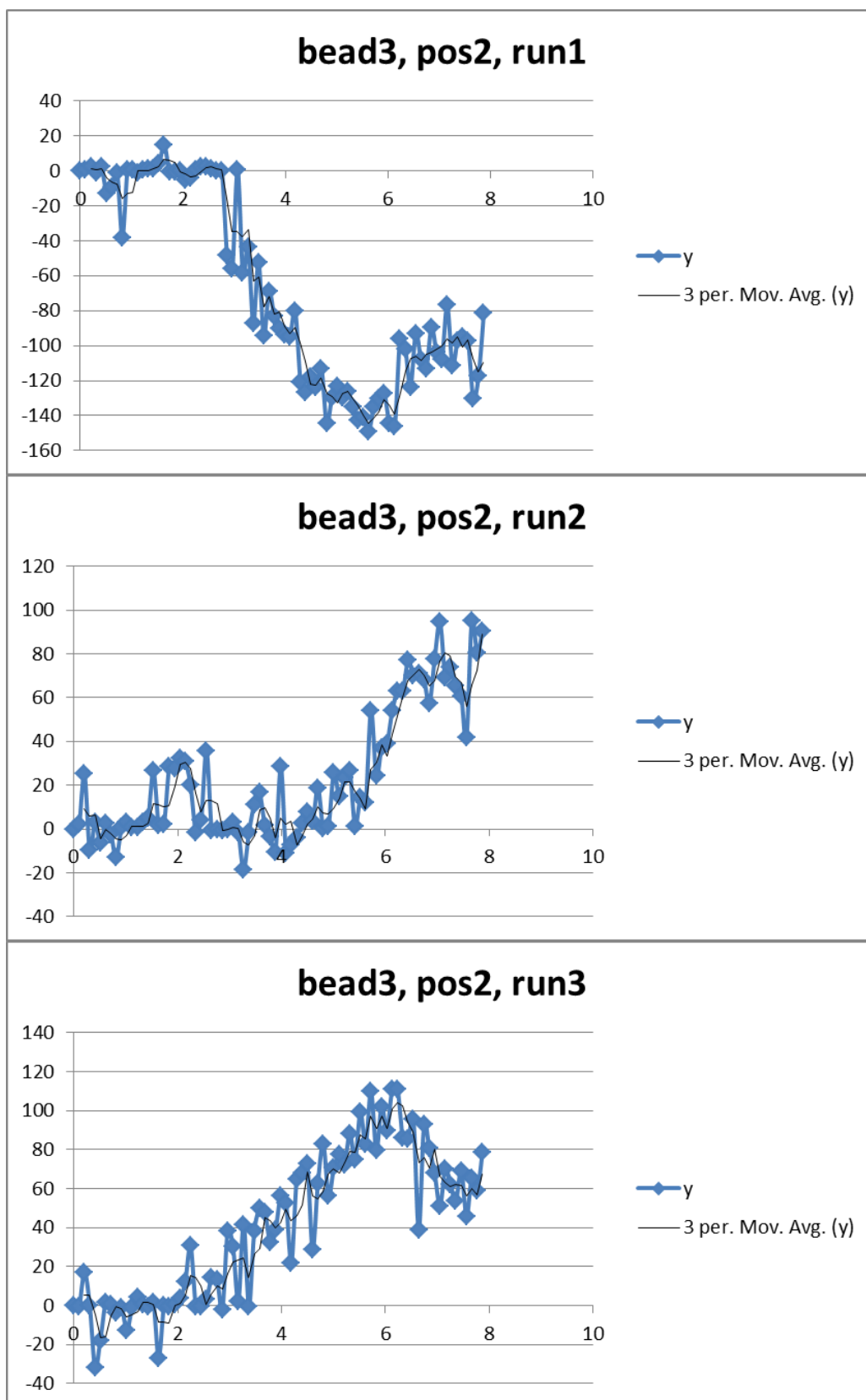


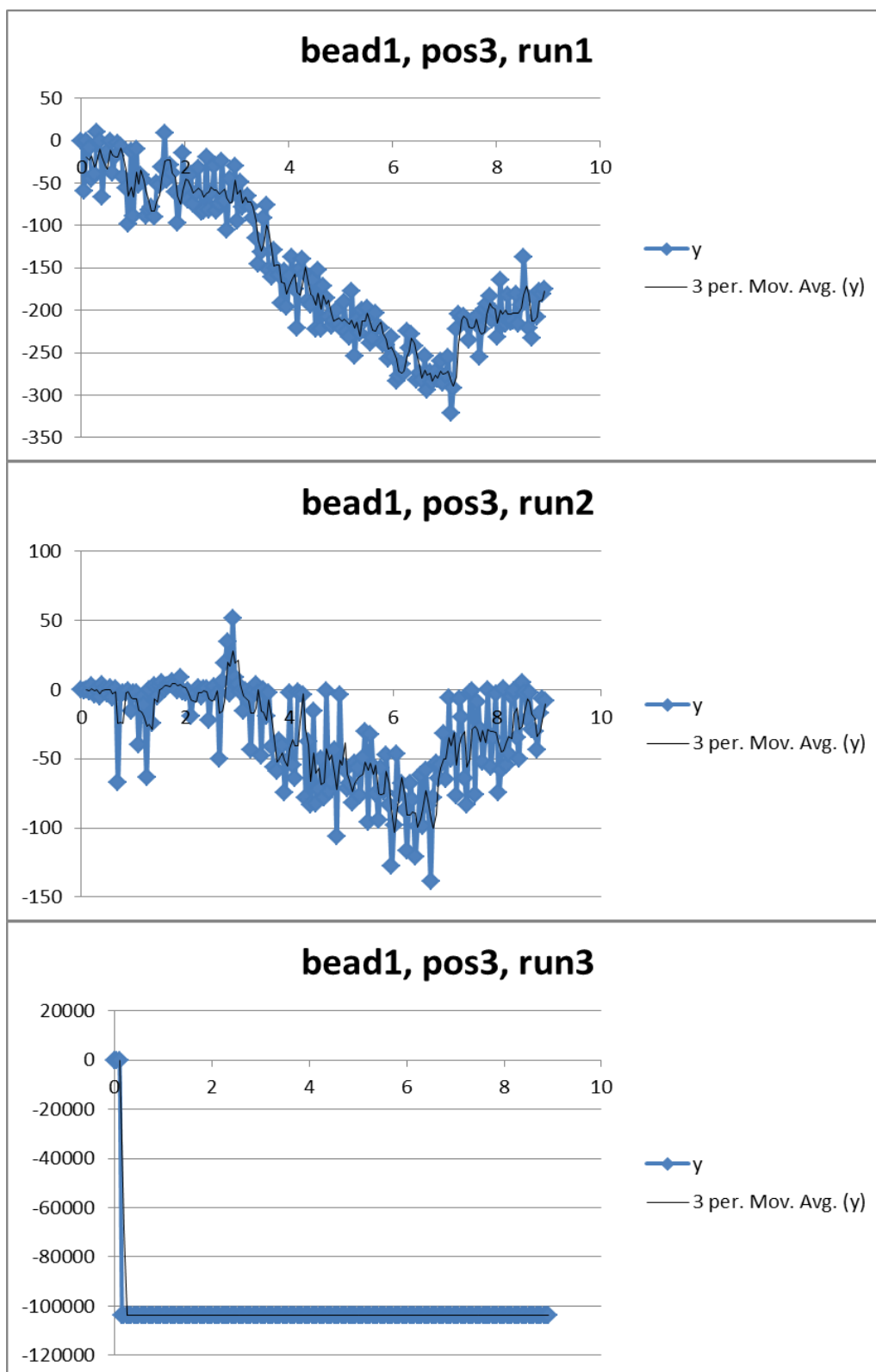
All plots represent Y-Displacement (nm) vs. Time

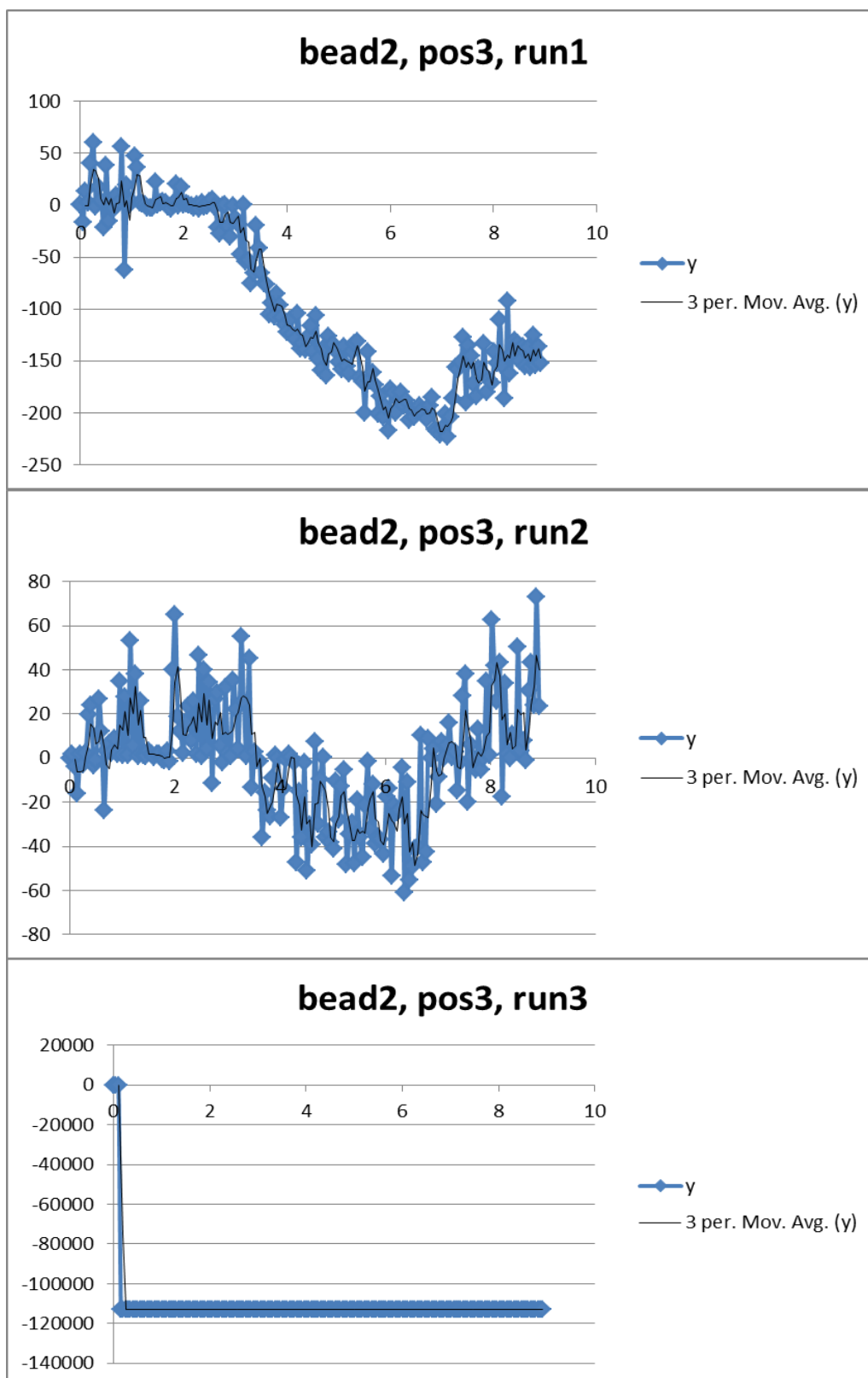


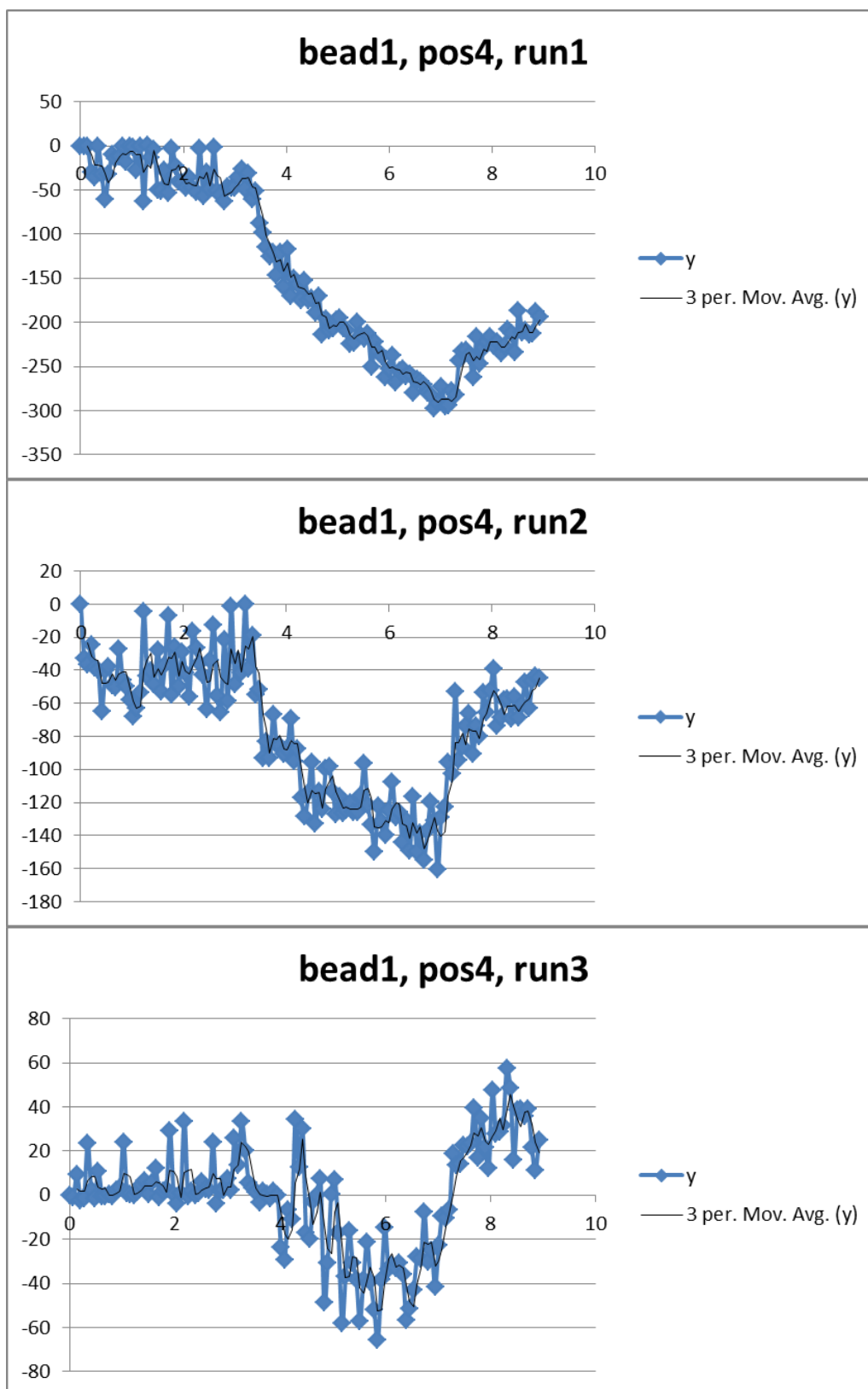


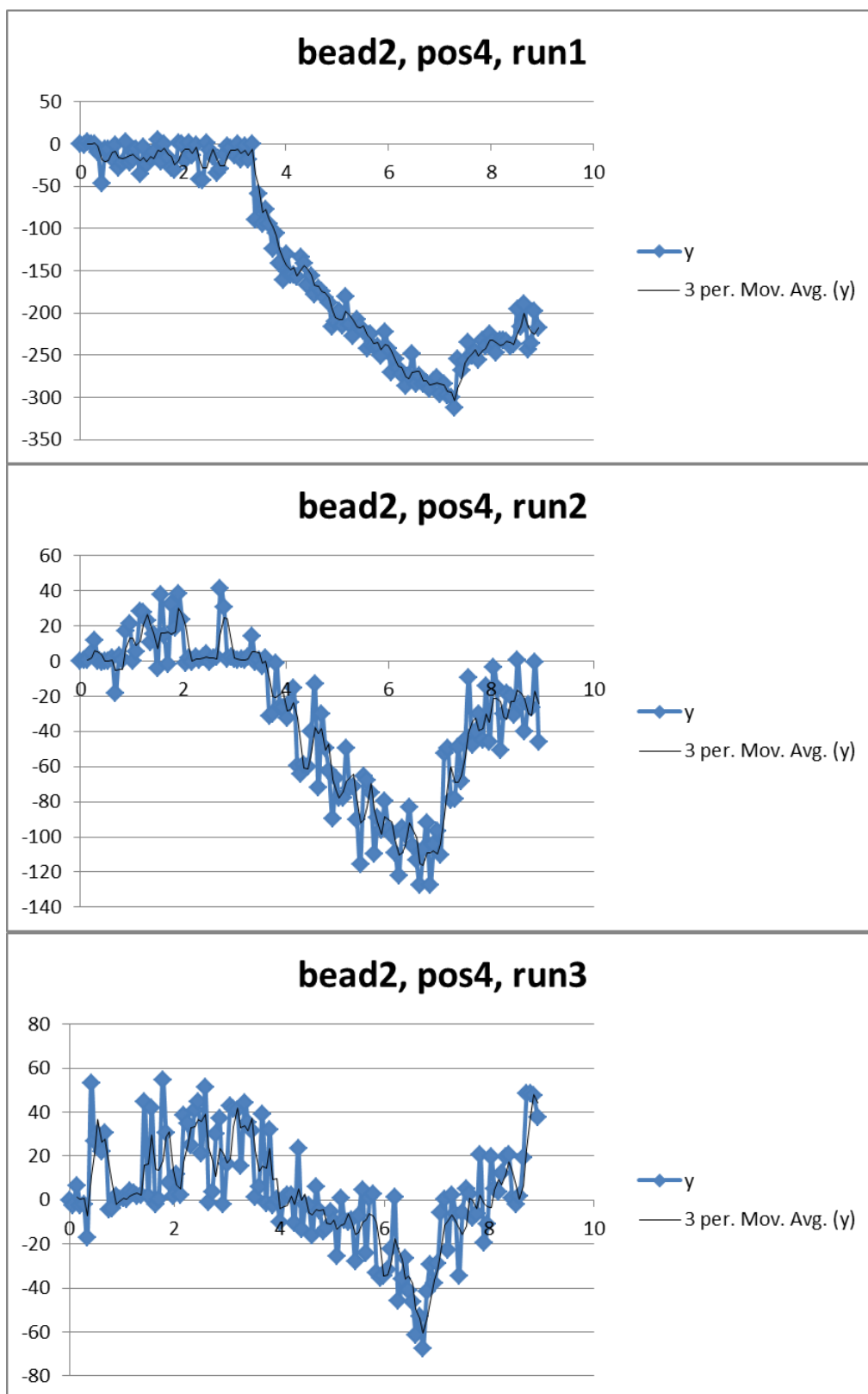


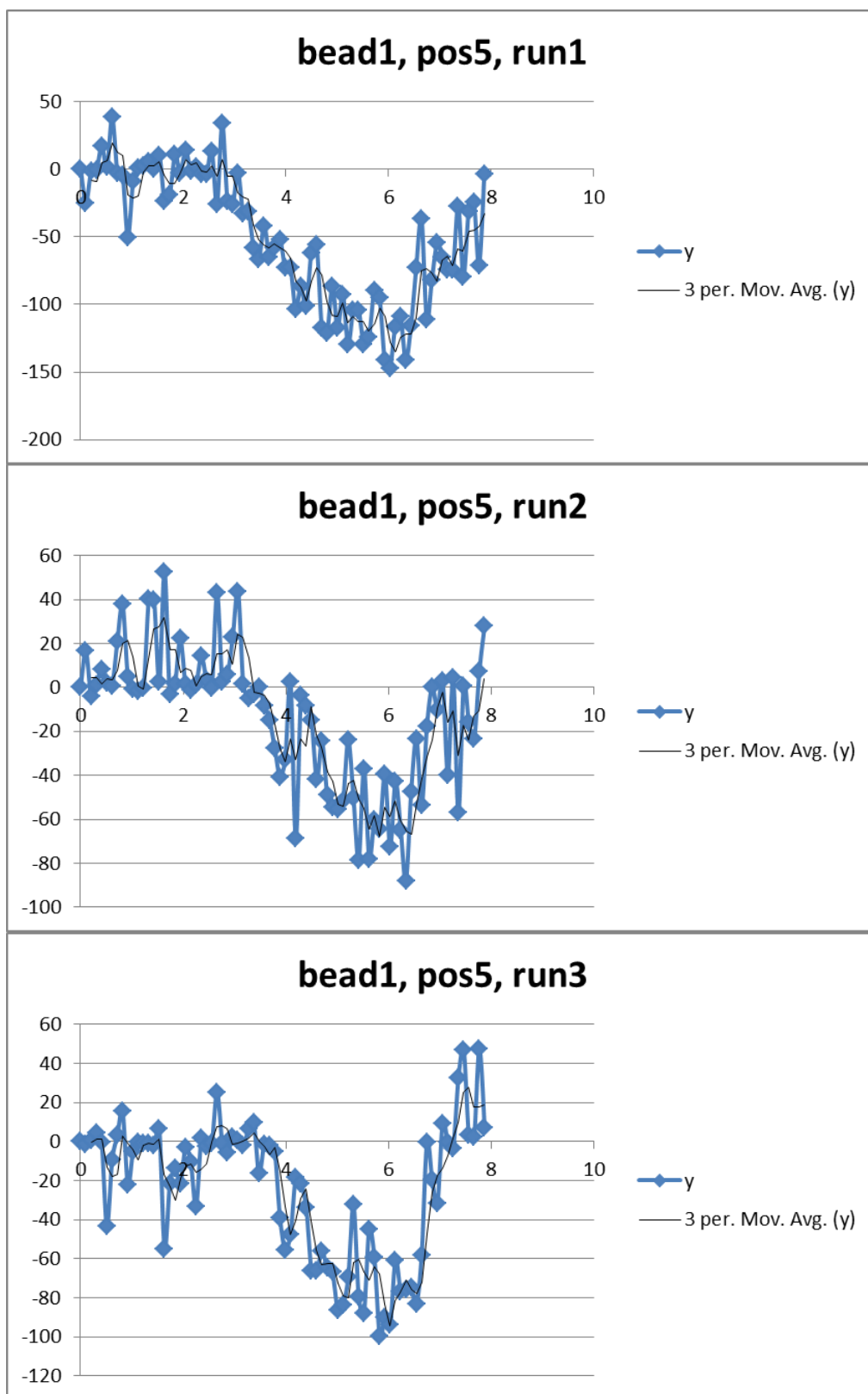


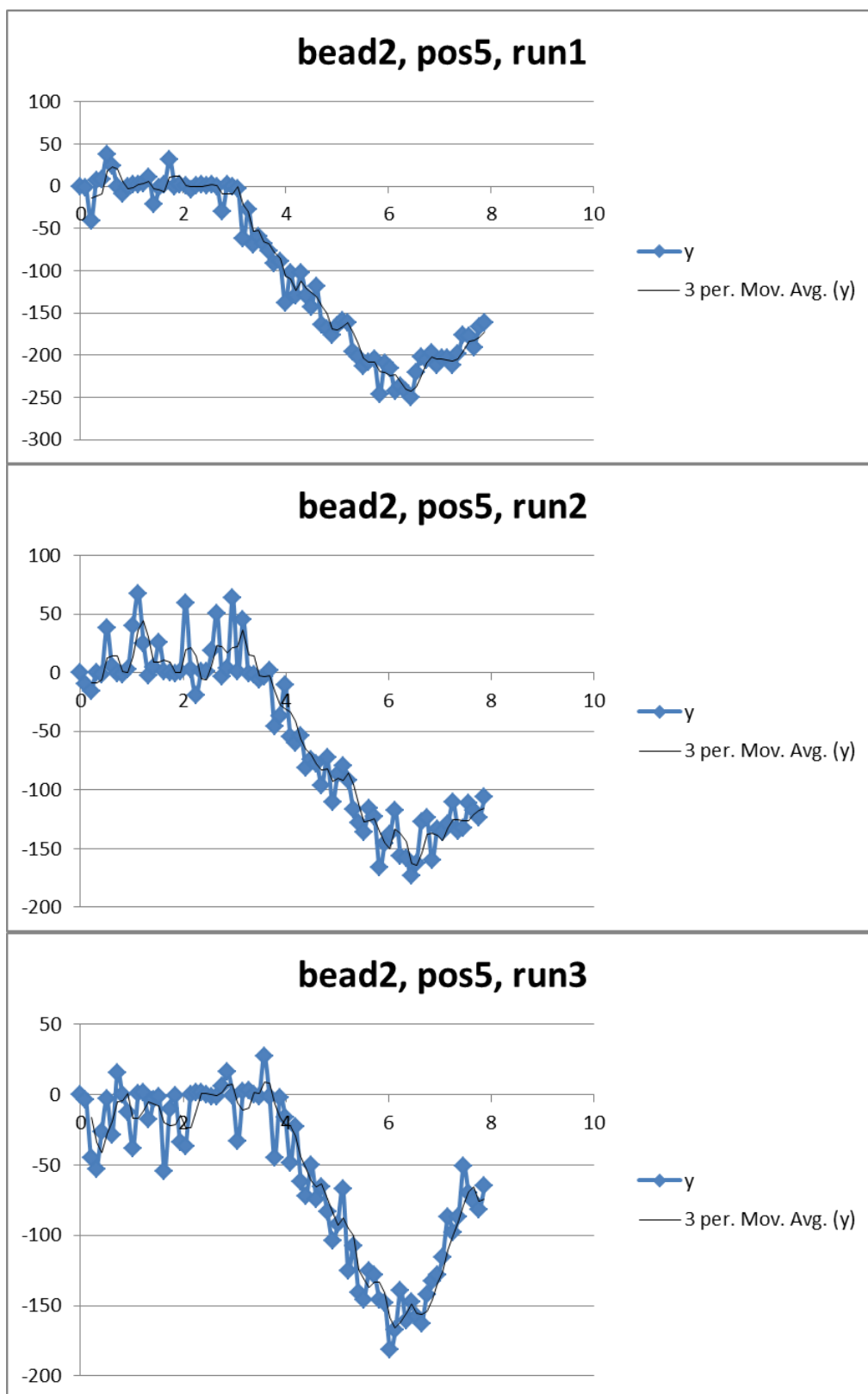


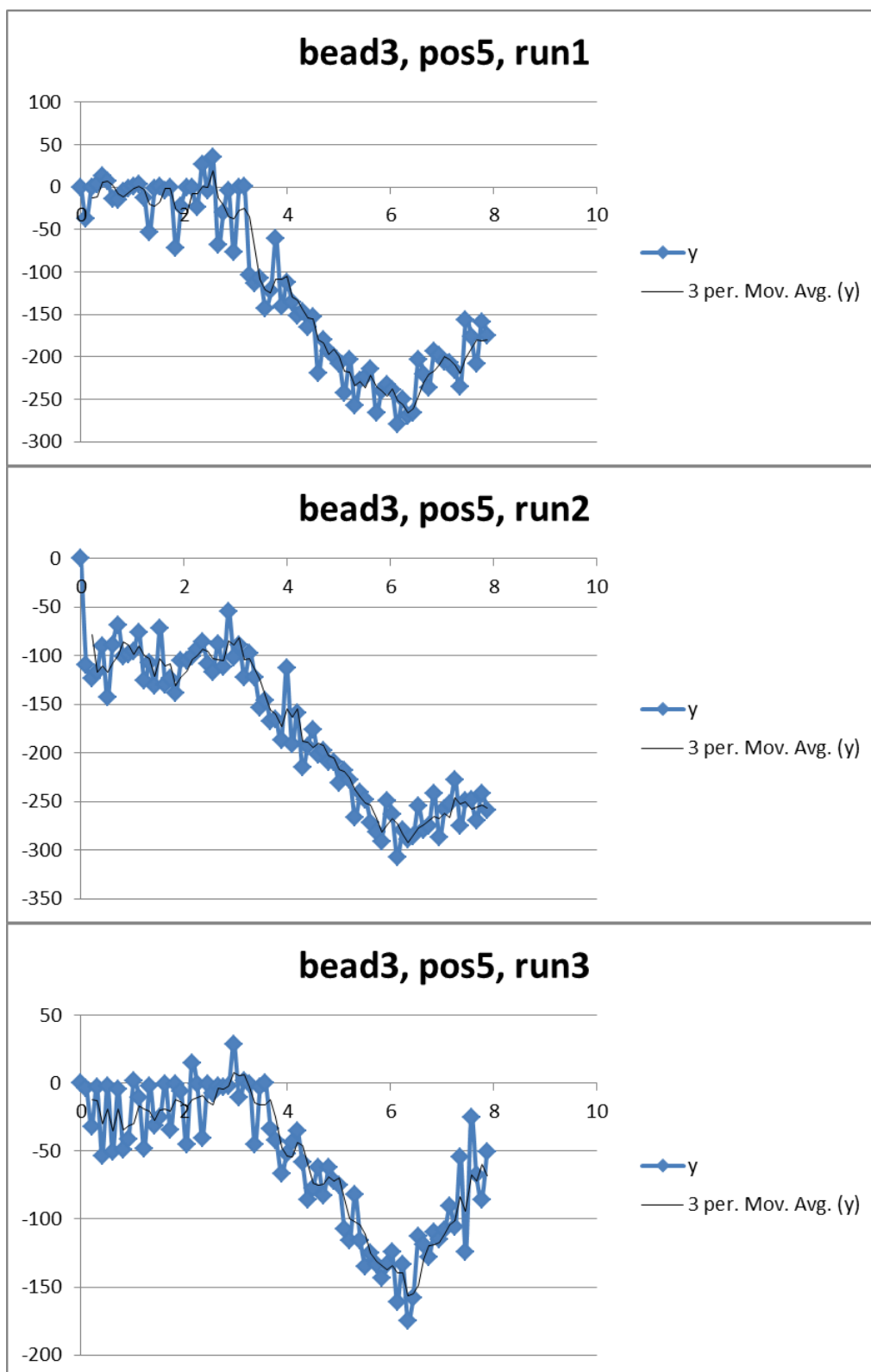


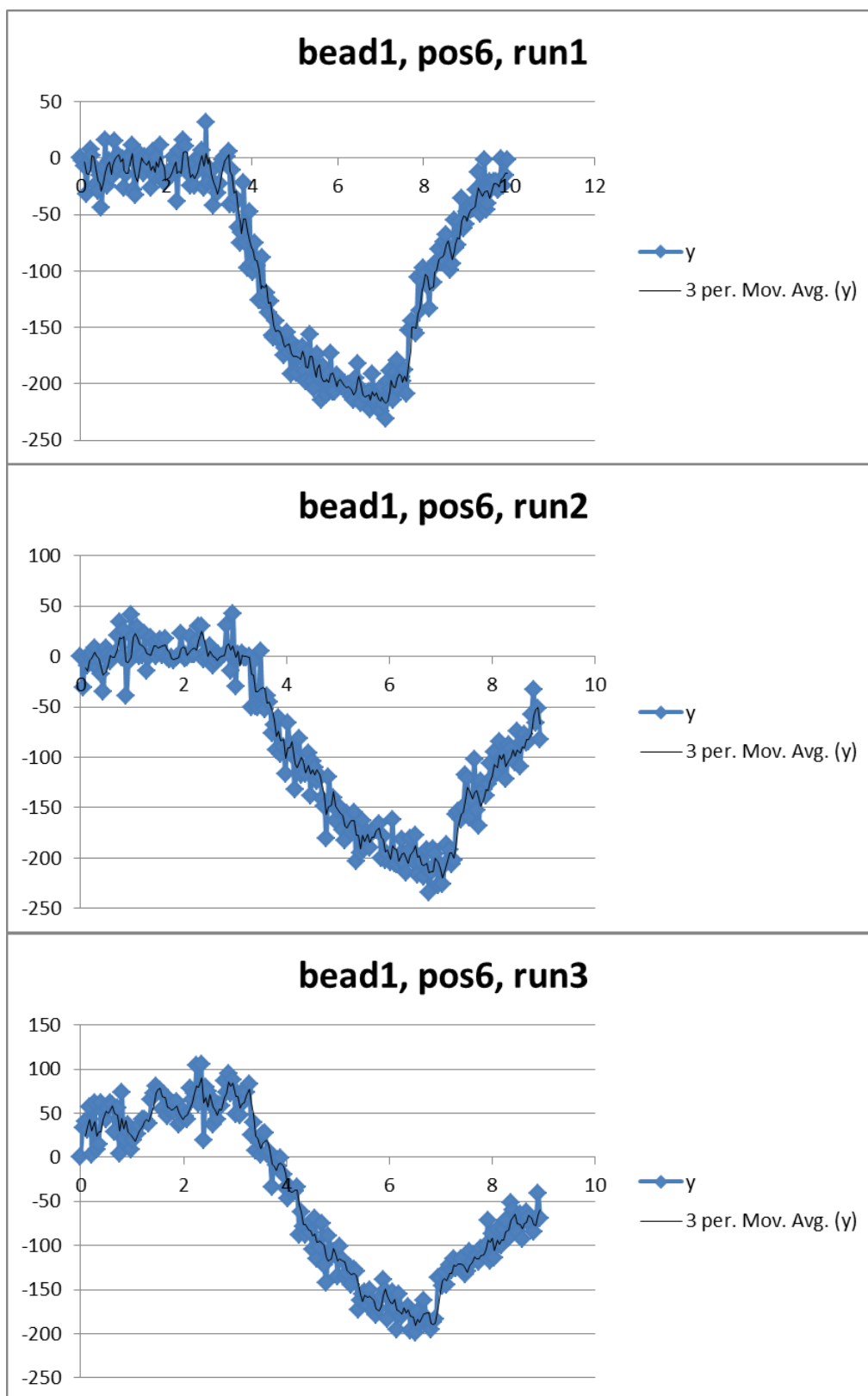


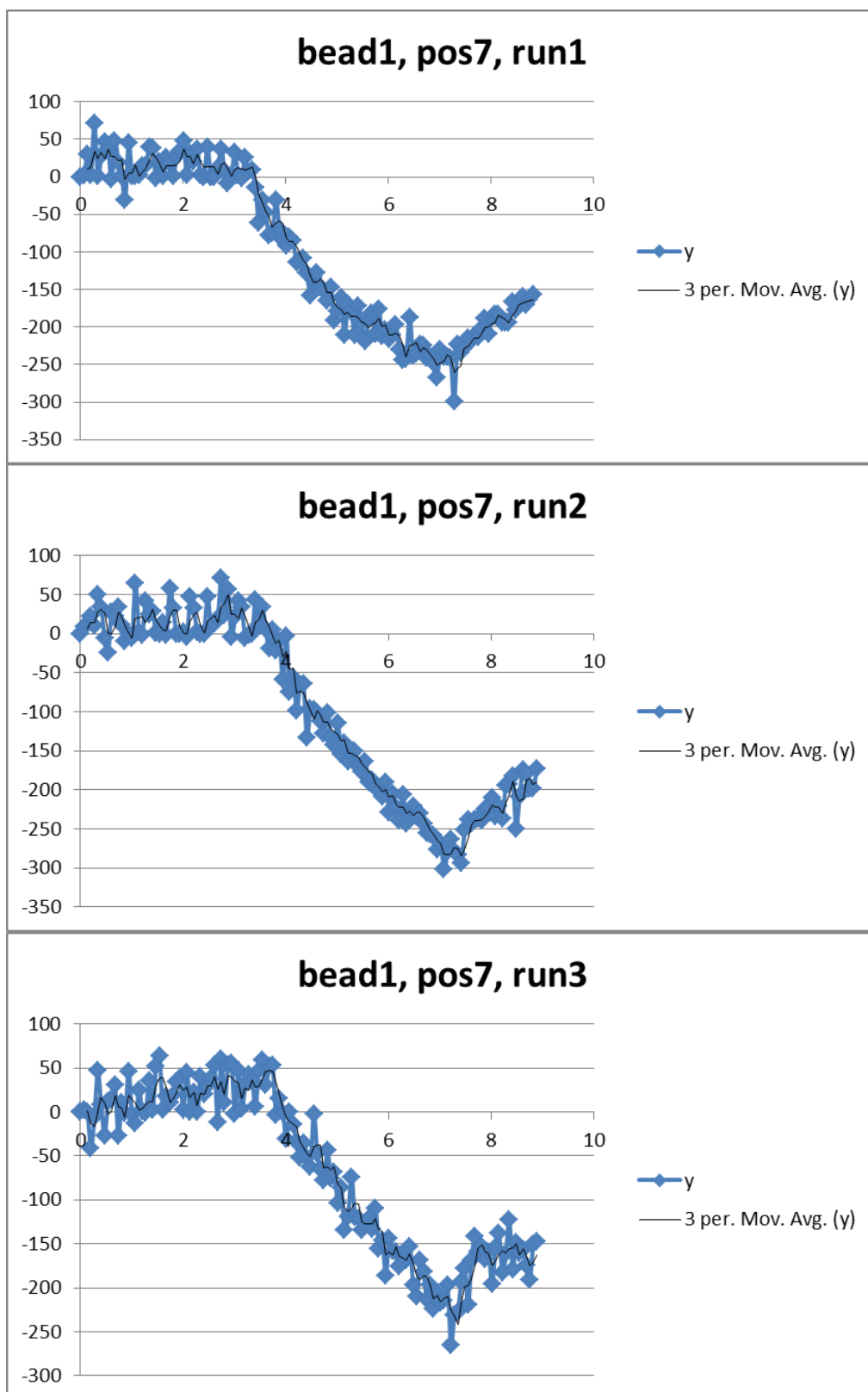


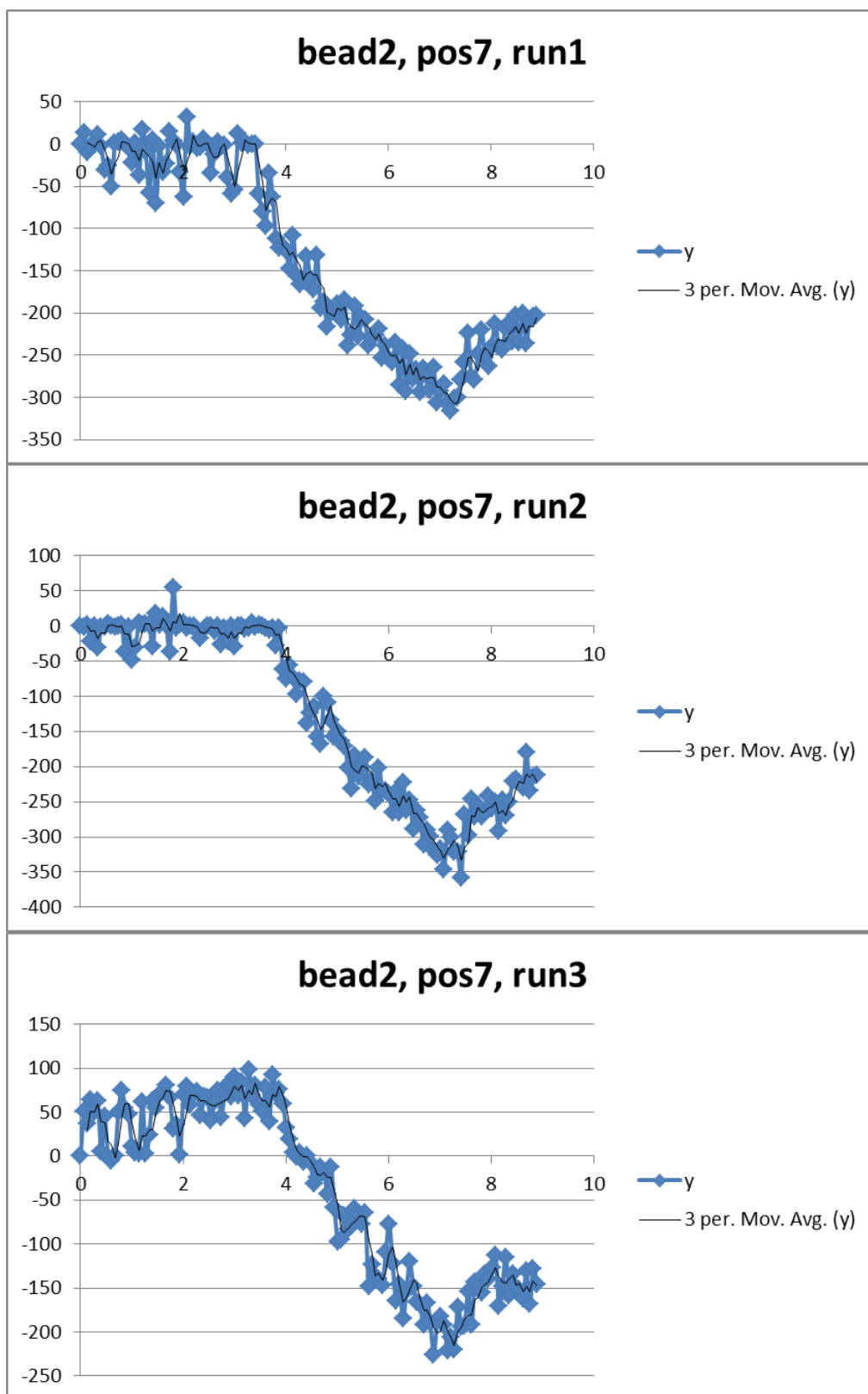


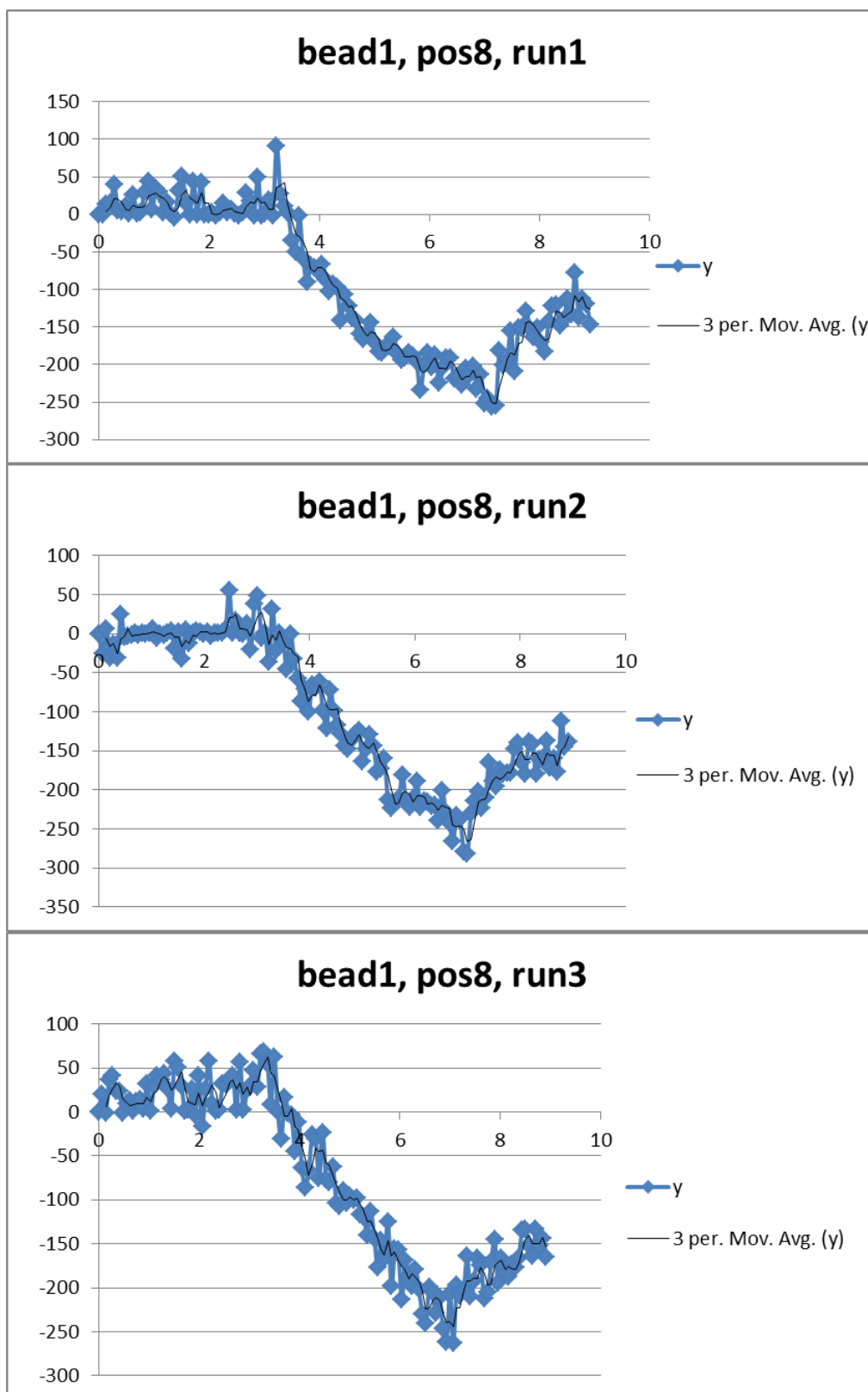


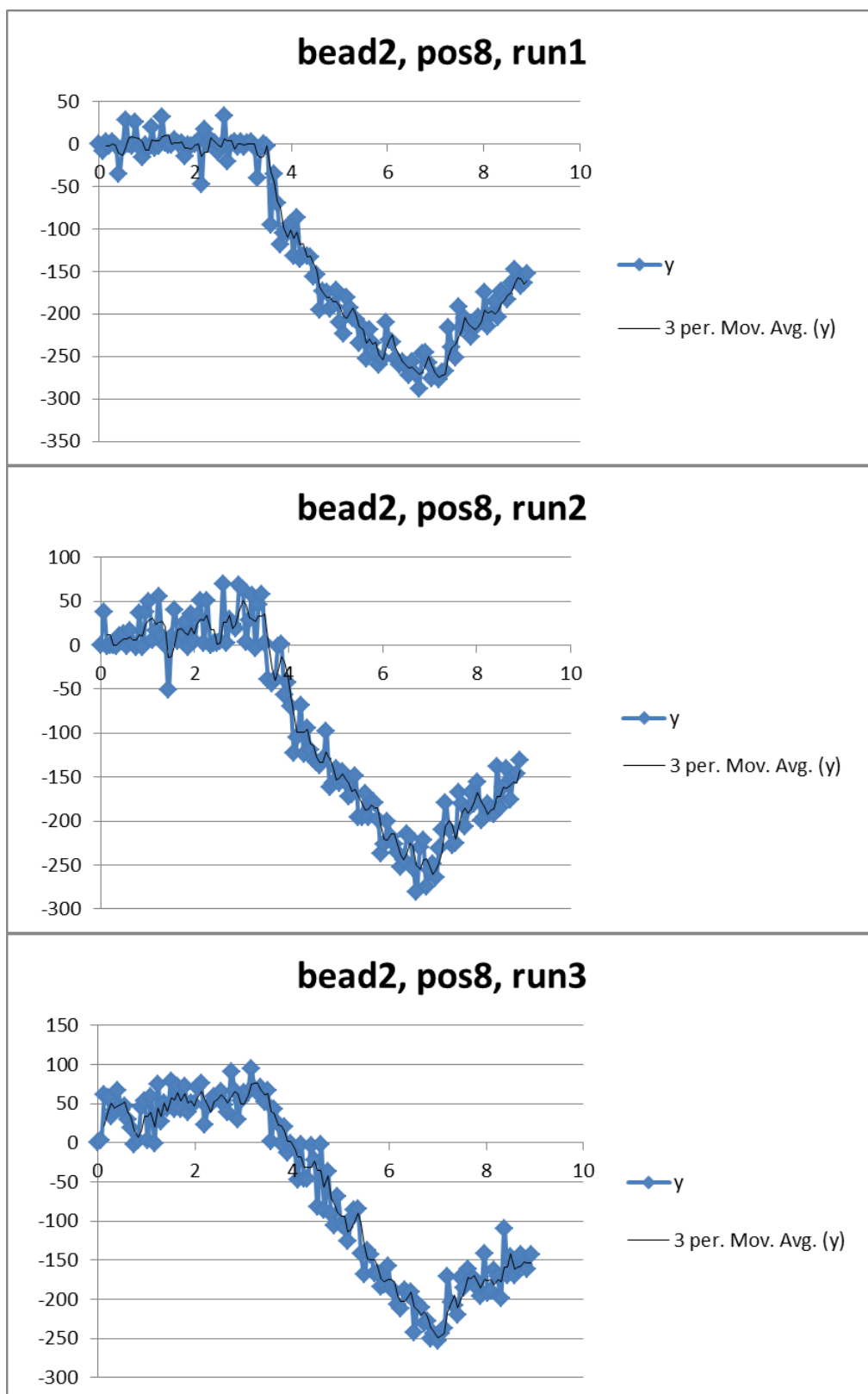


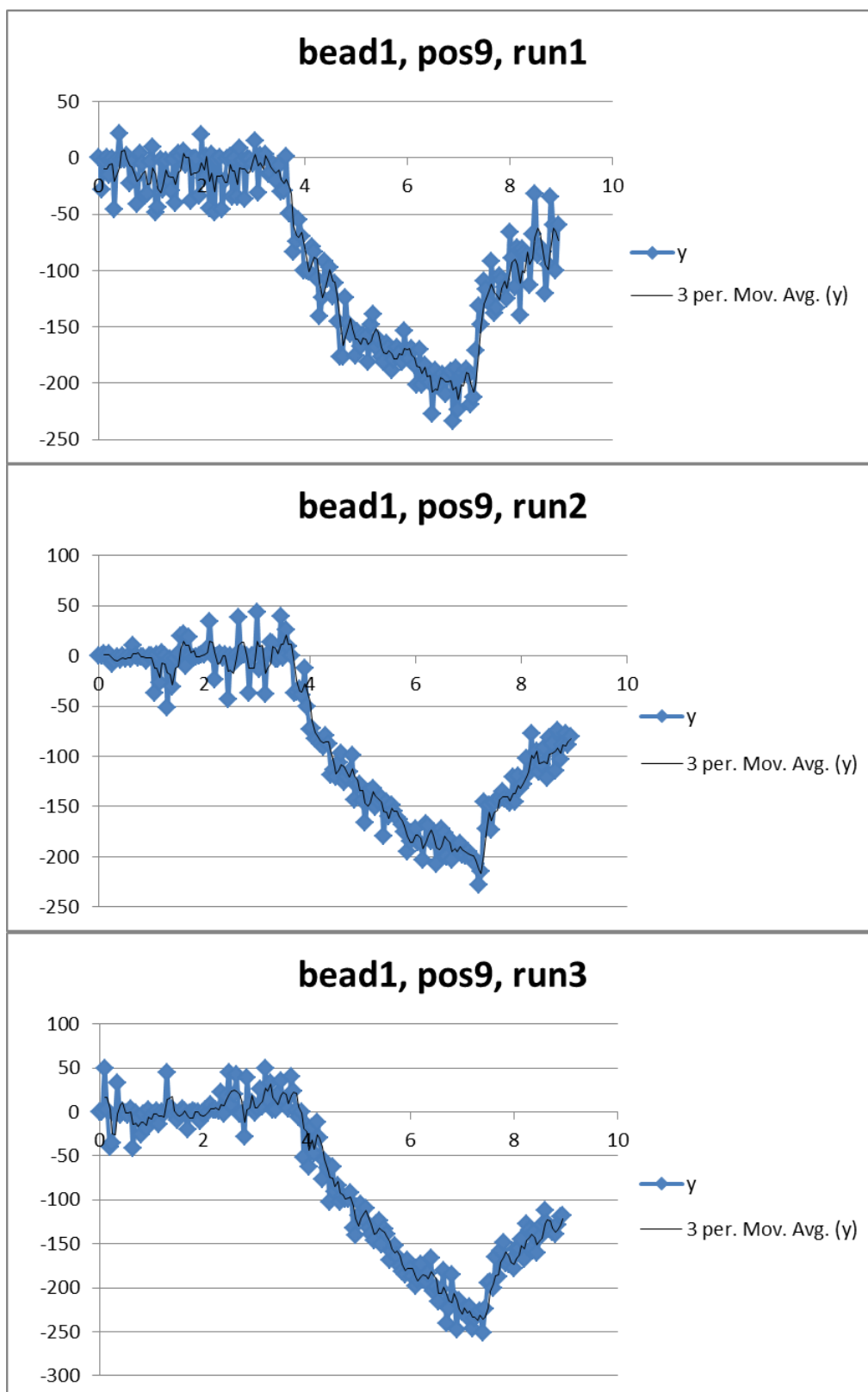


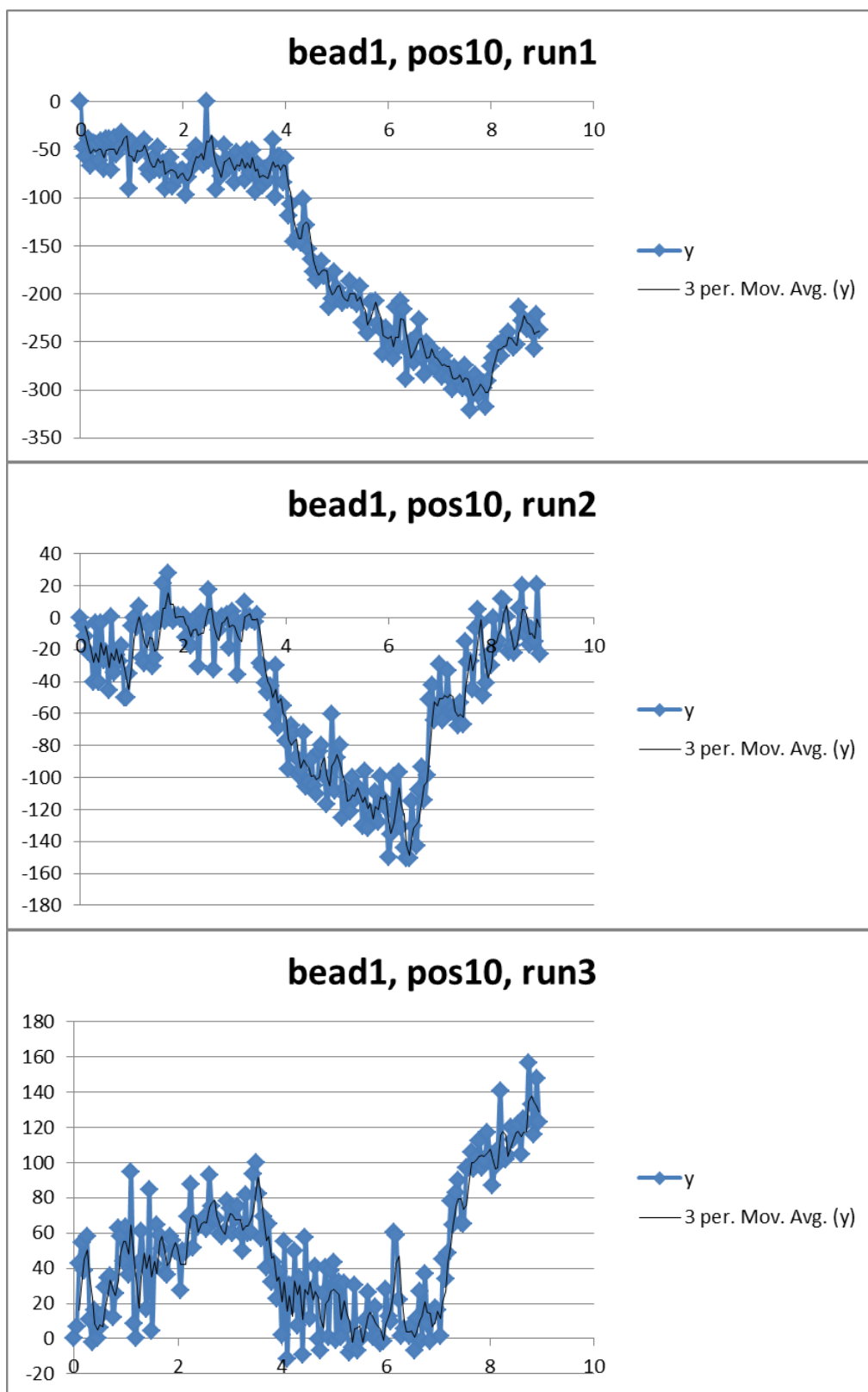


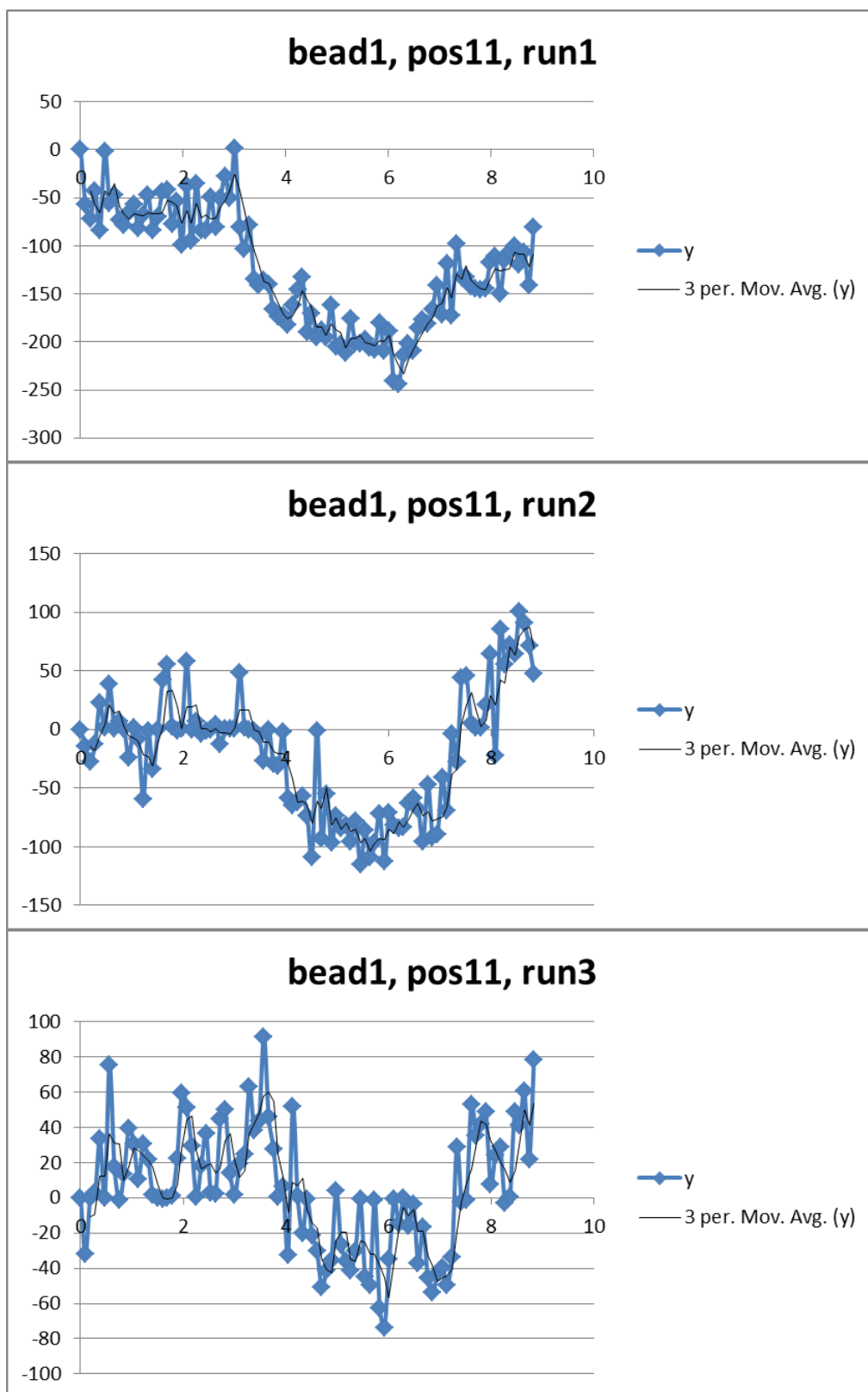


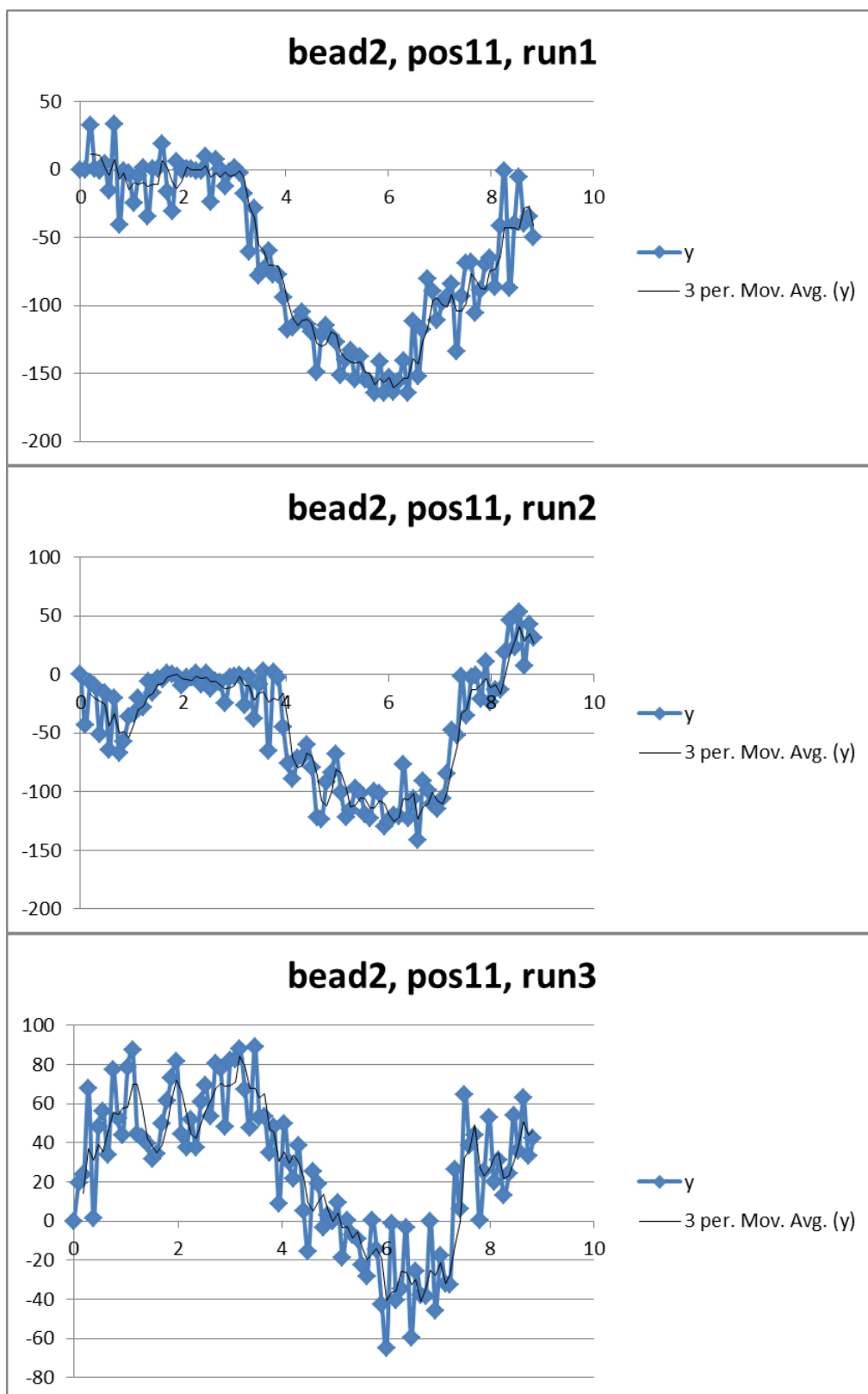


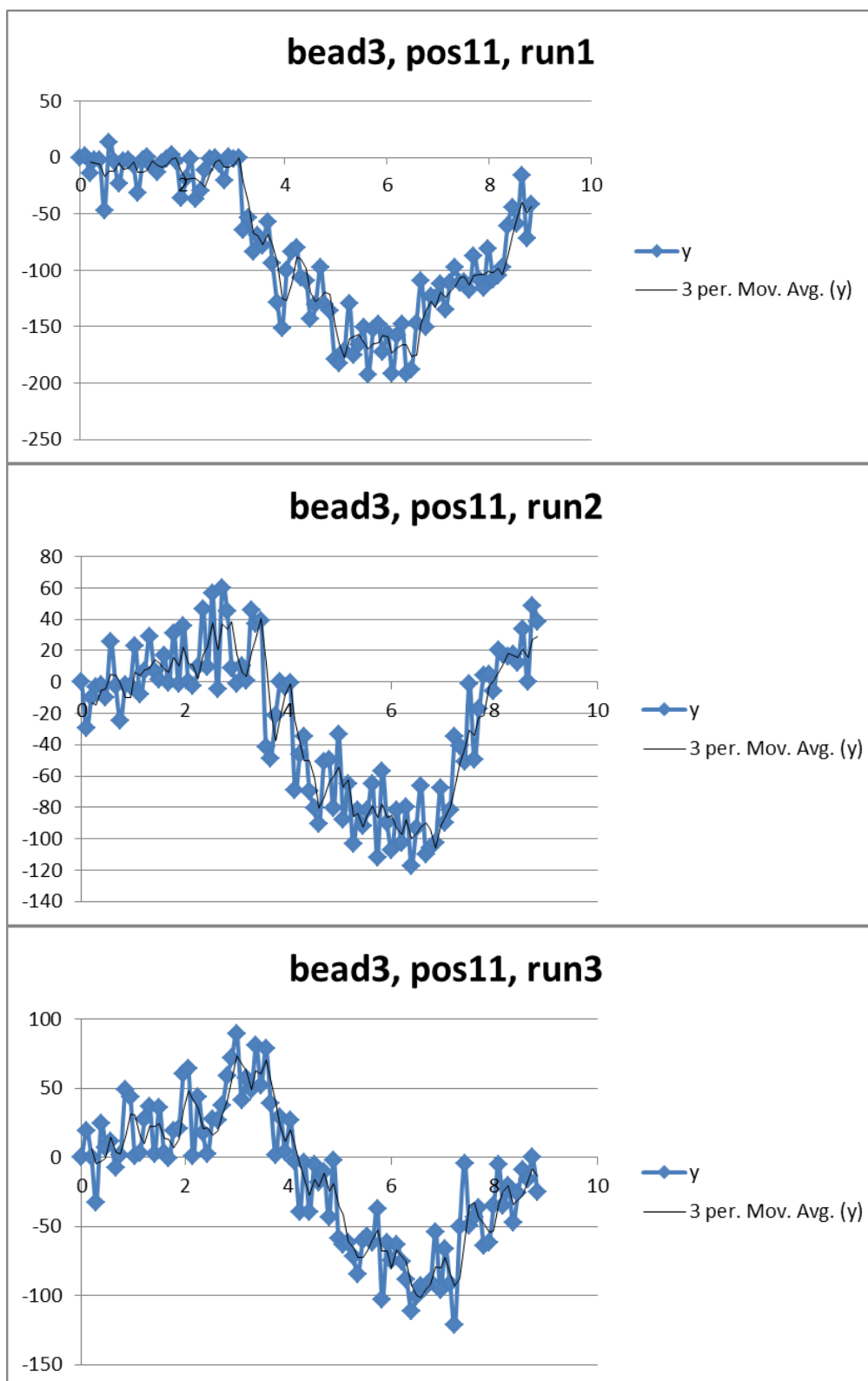


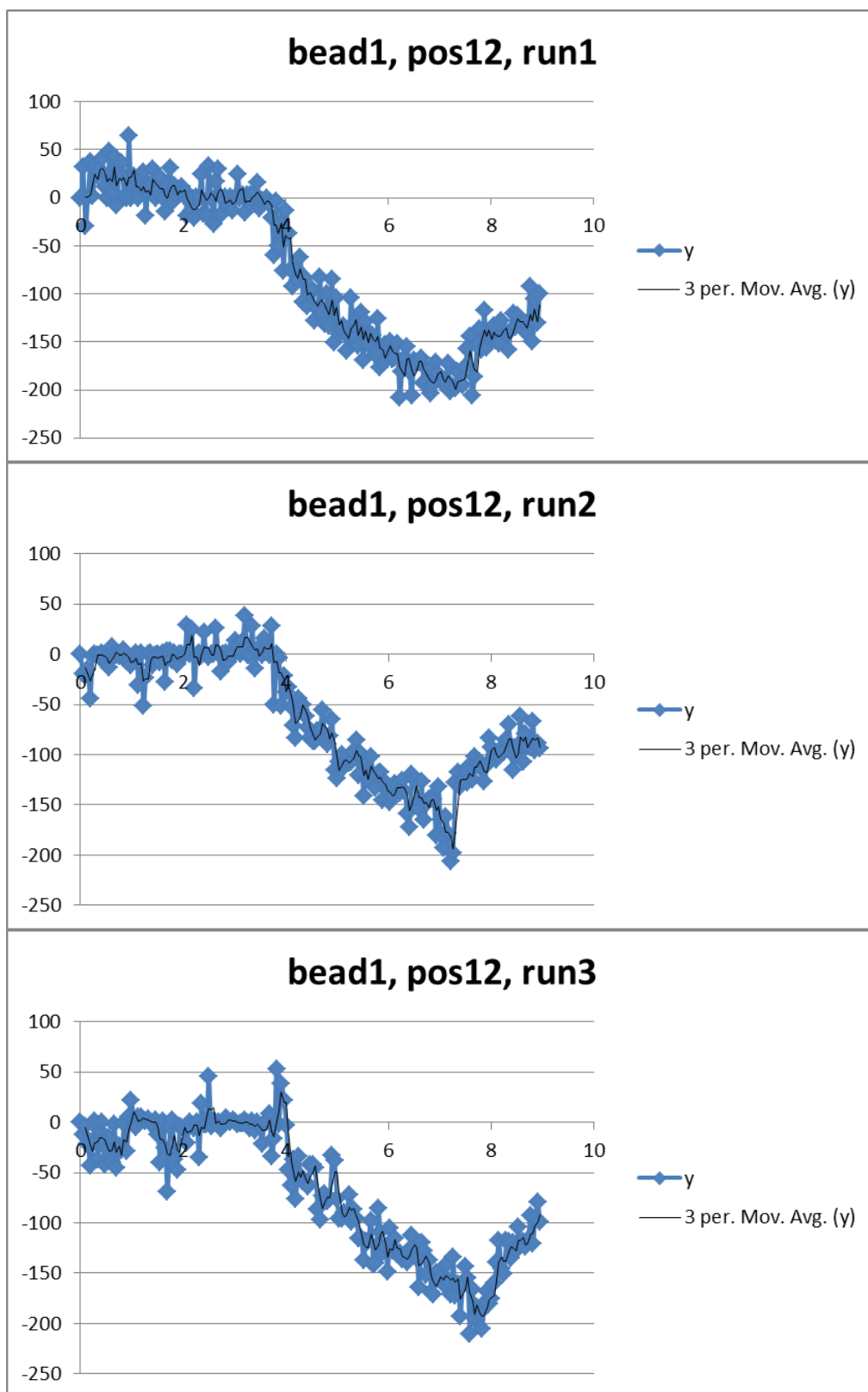


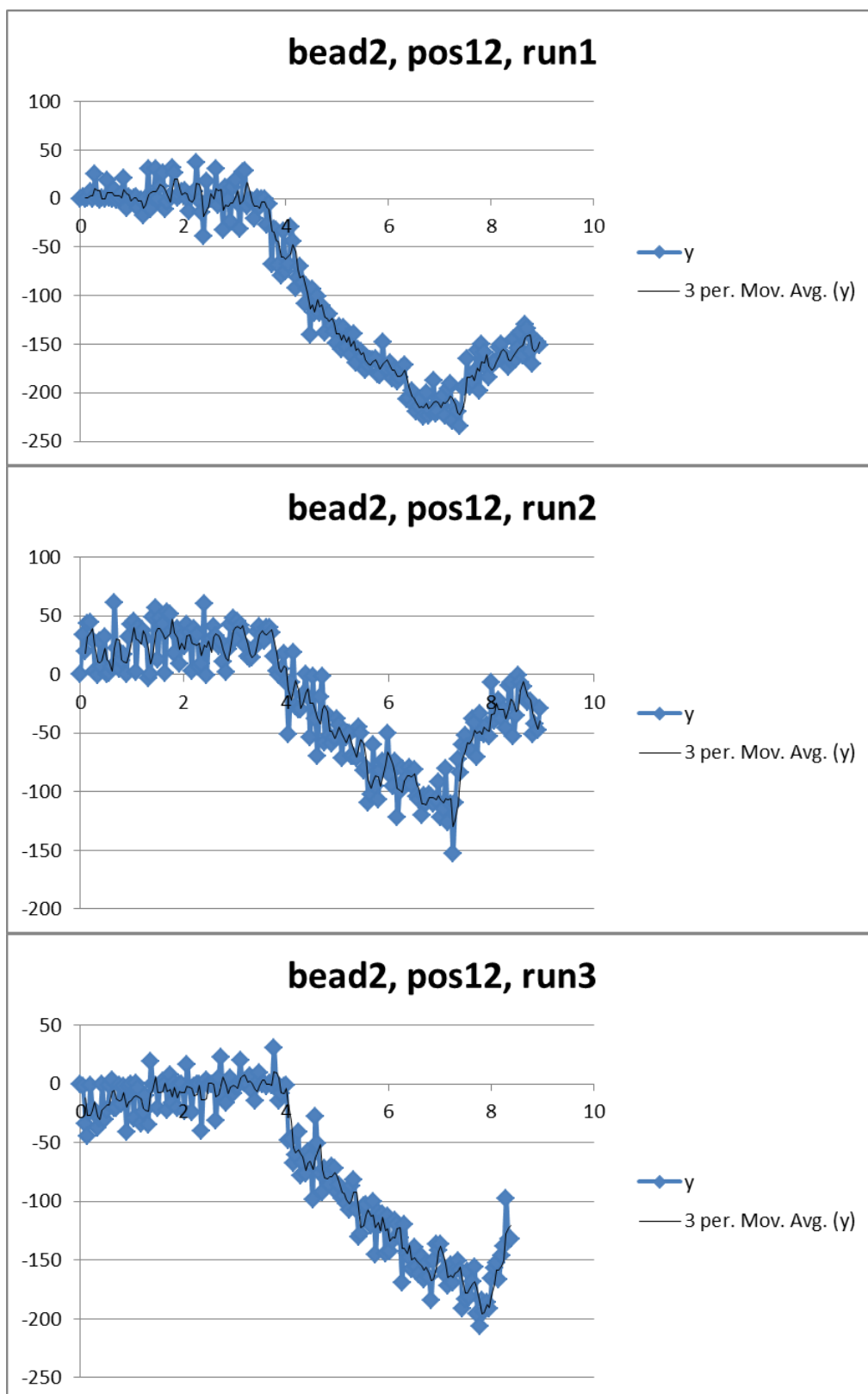


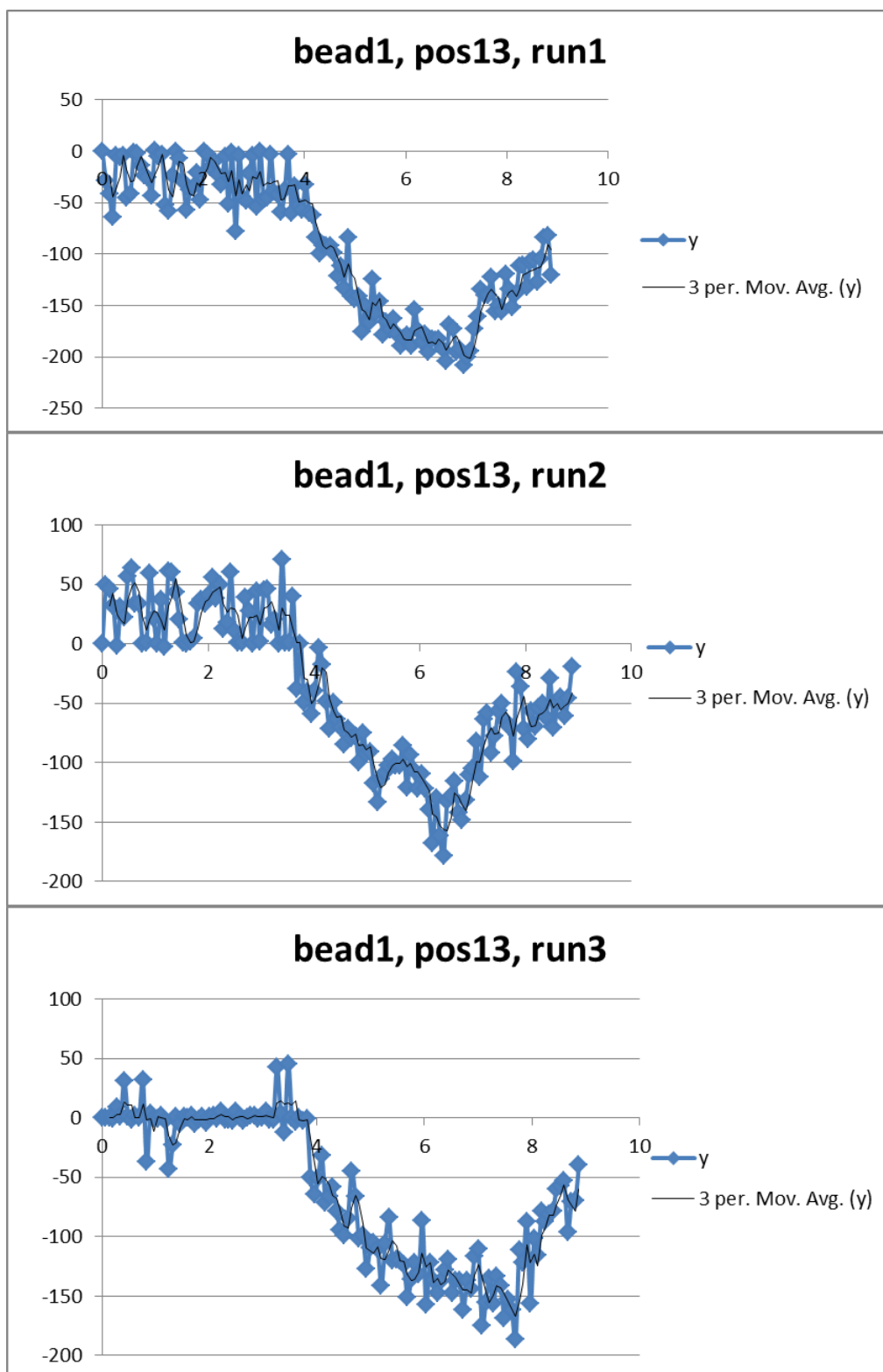


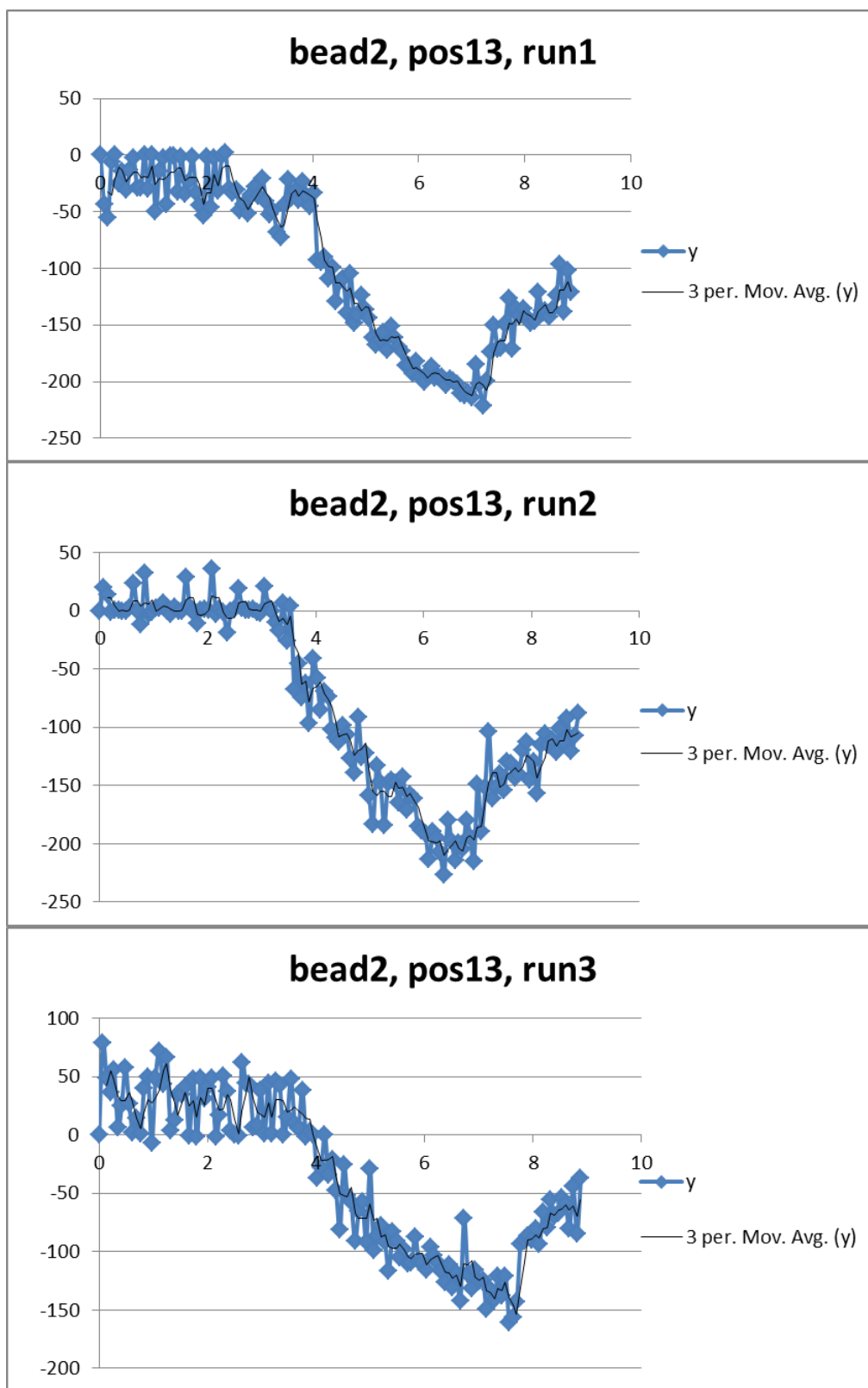


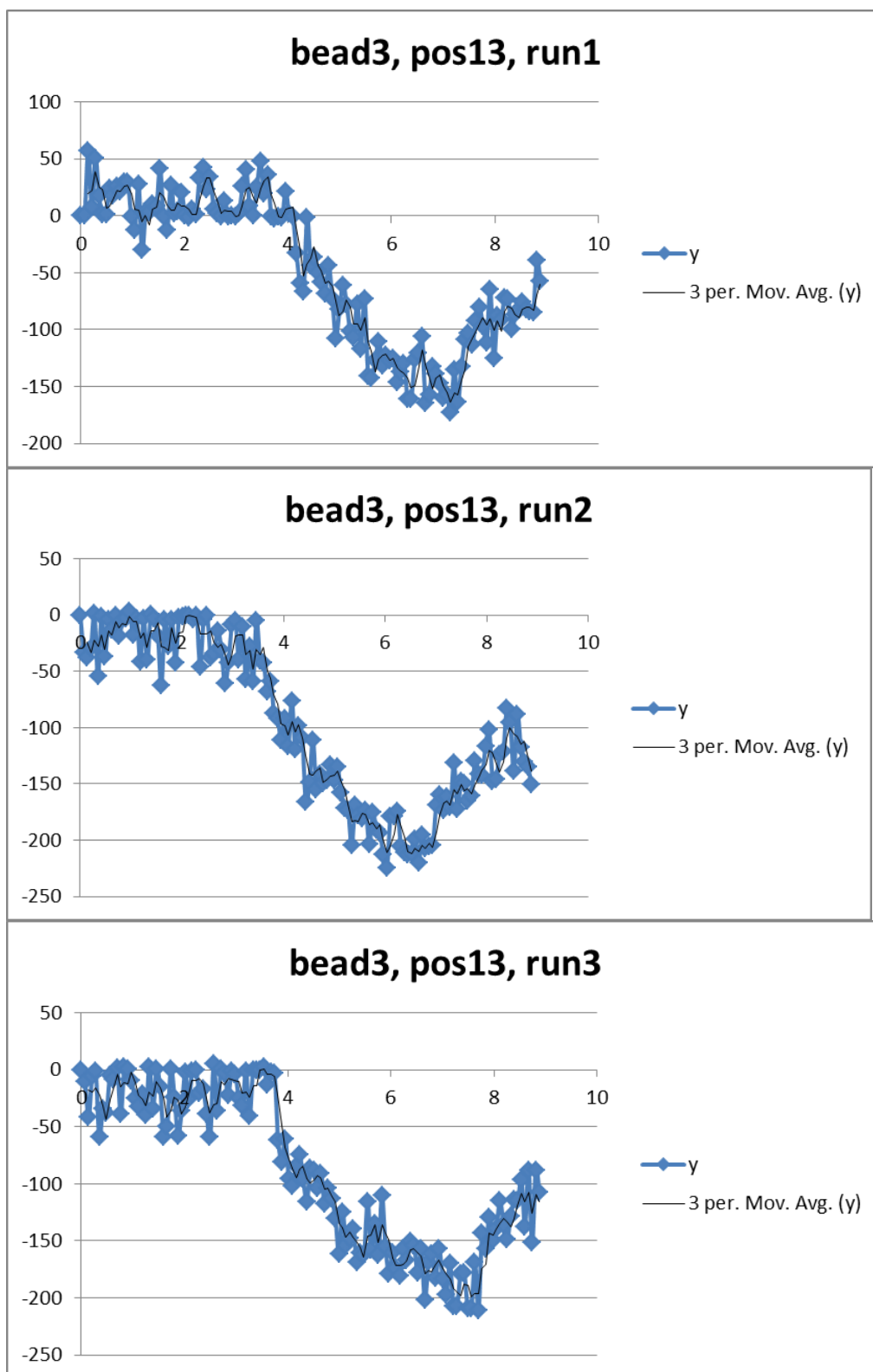


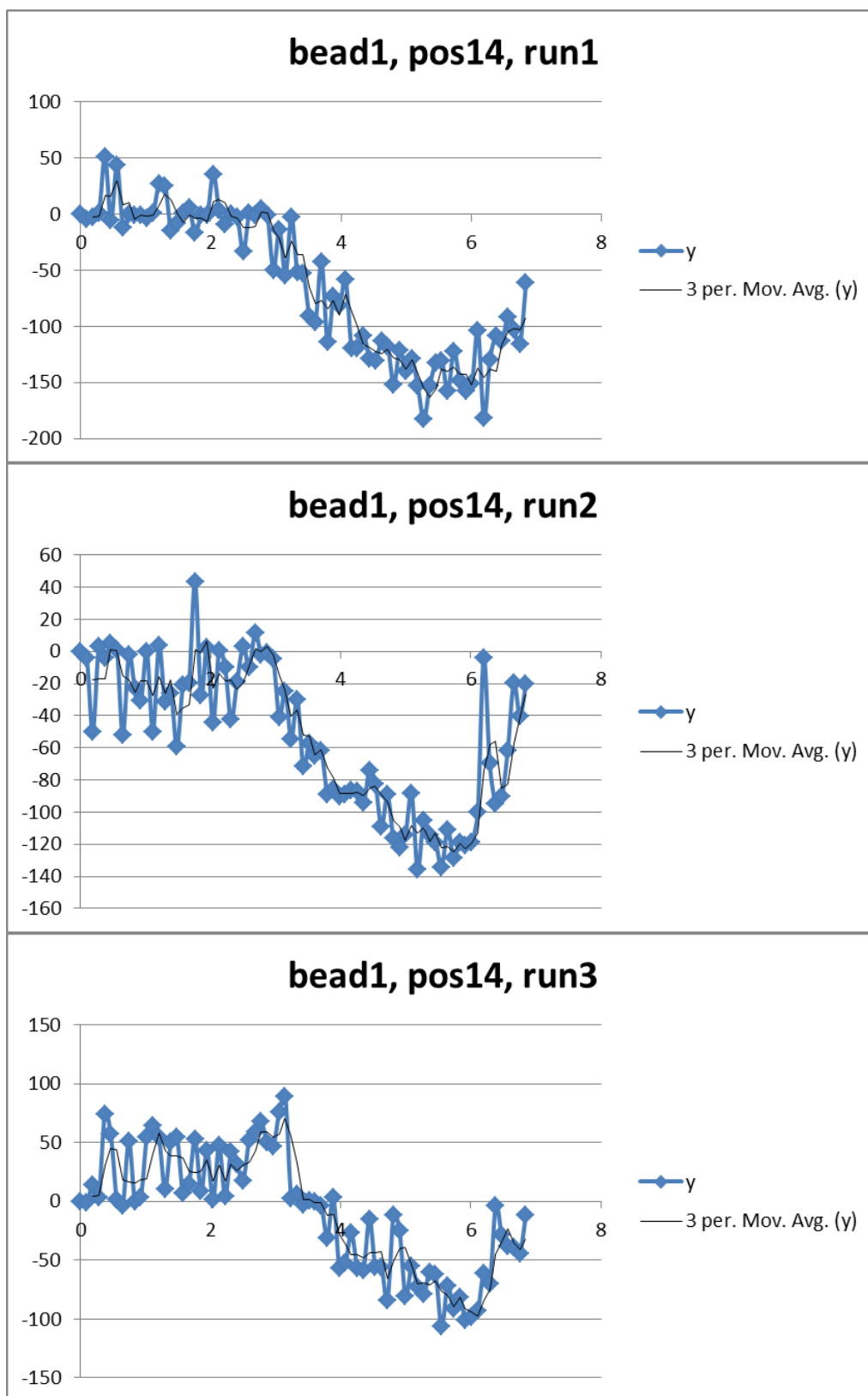


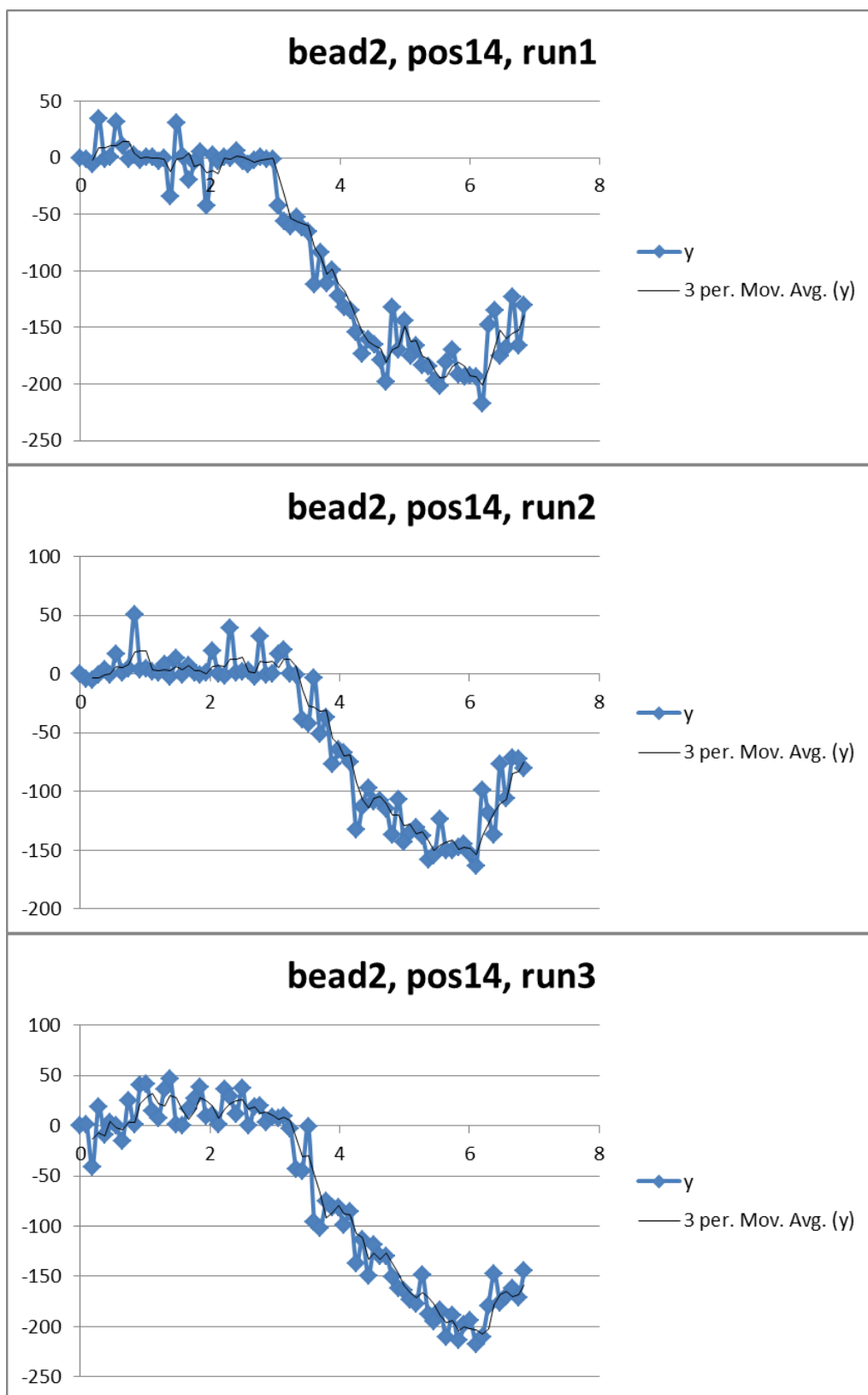


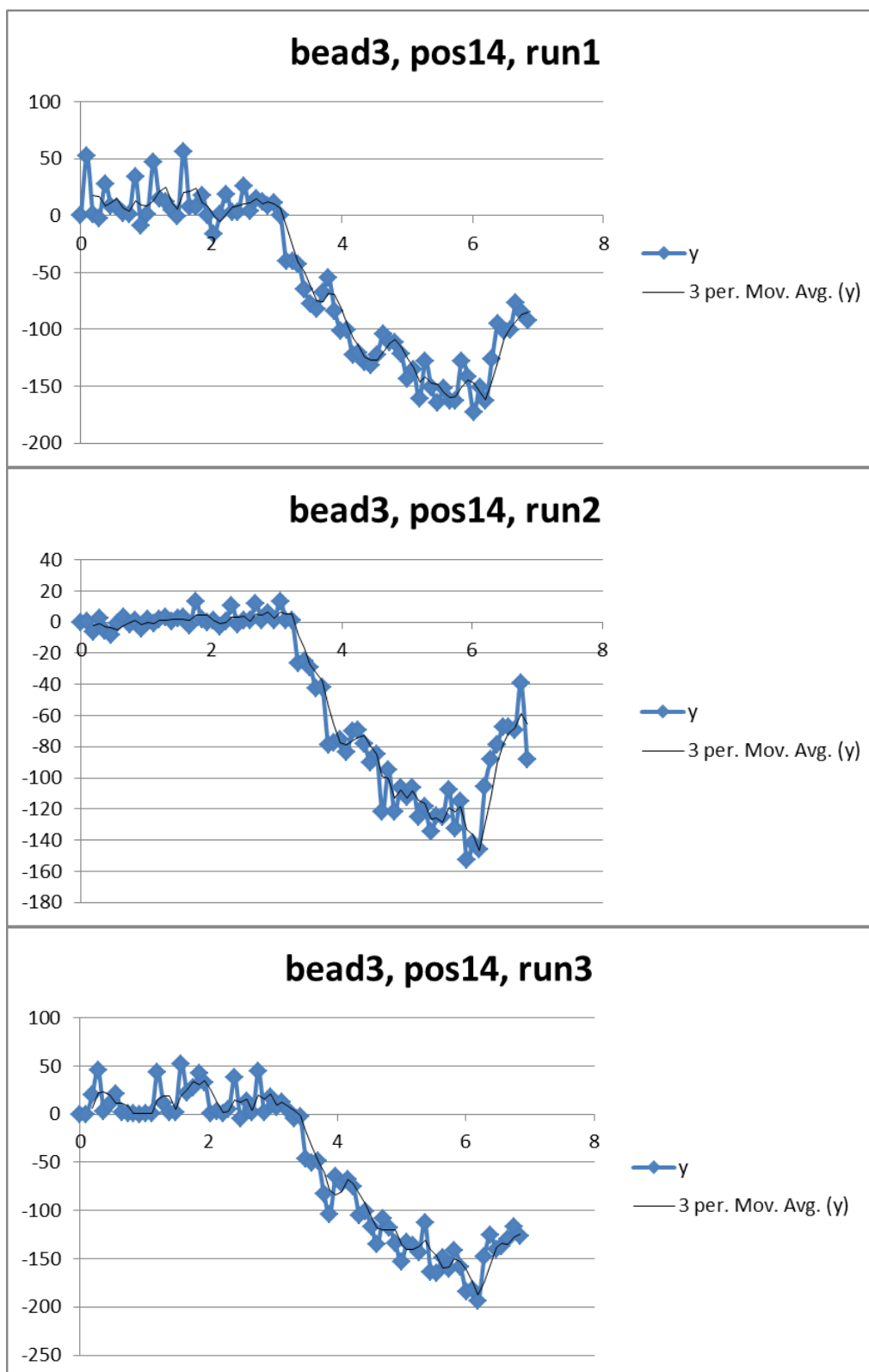


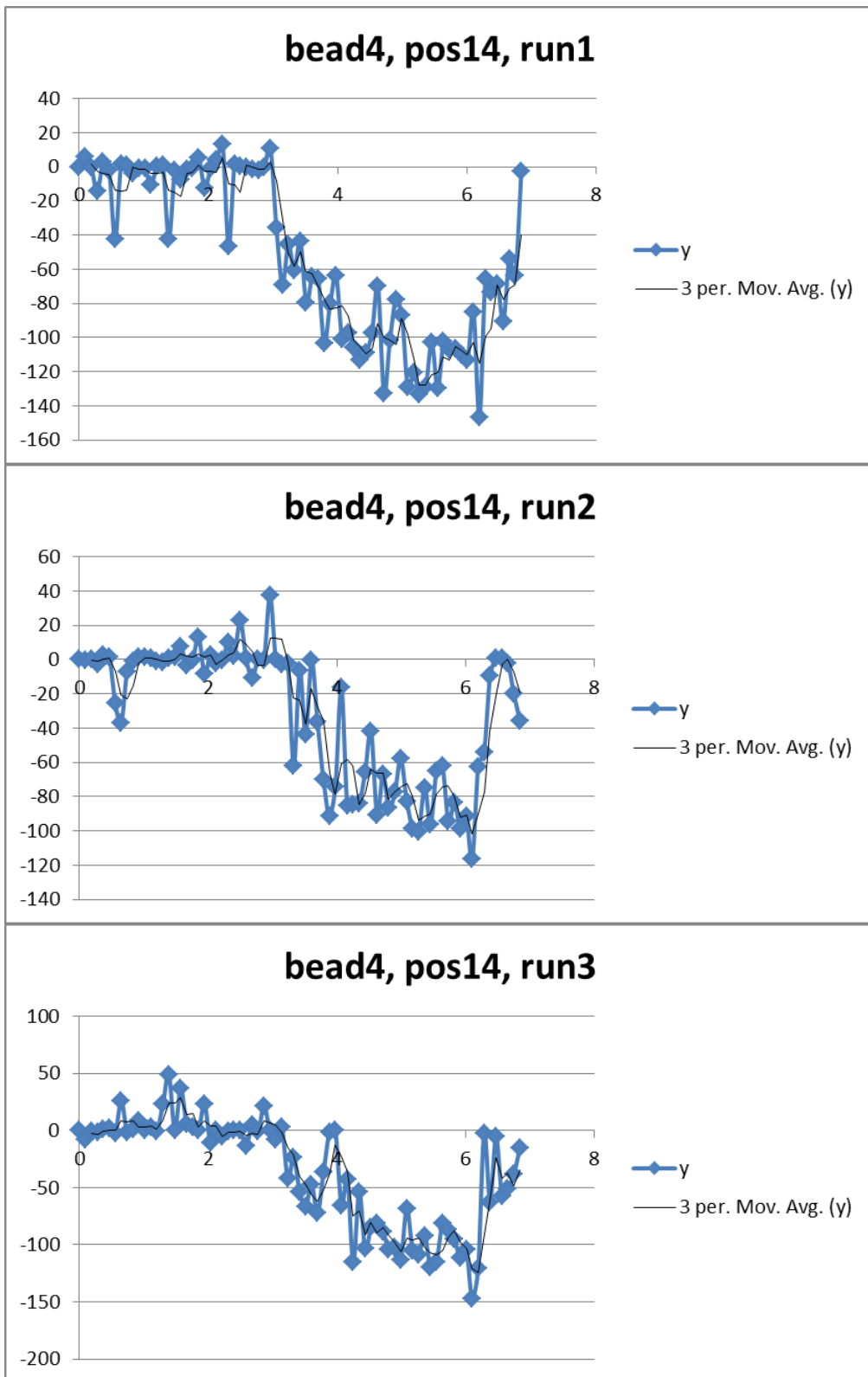


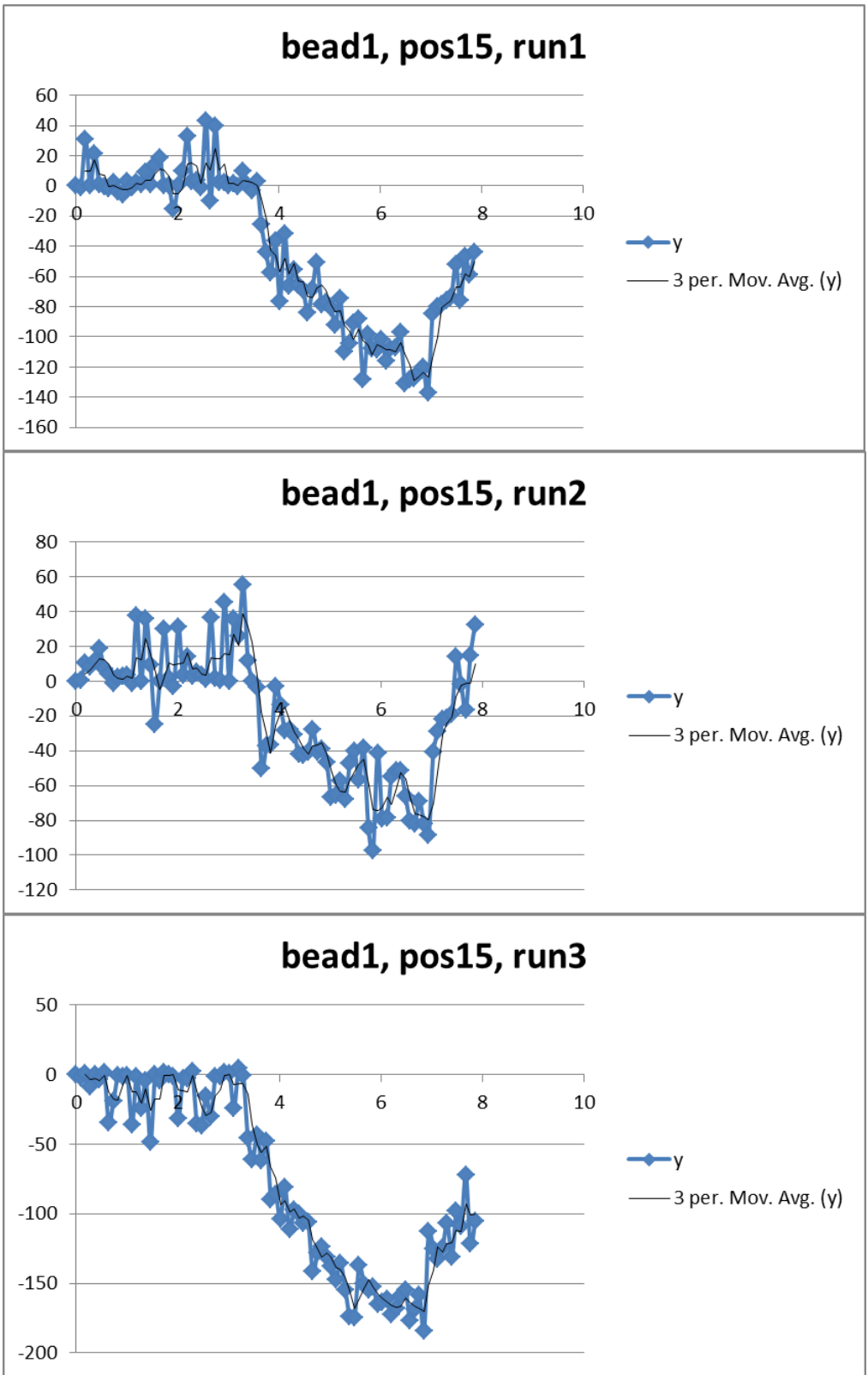


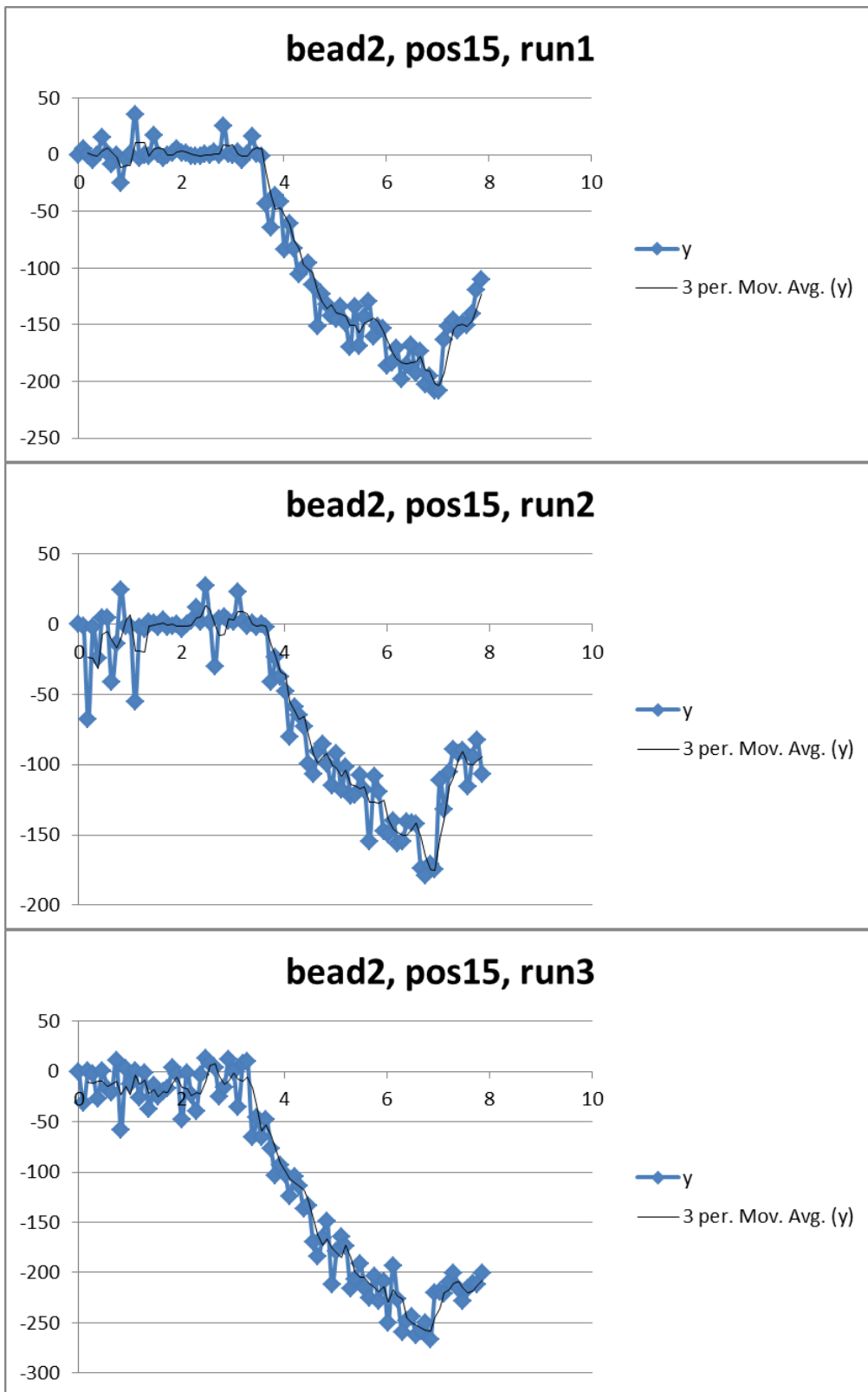


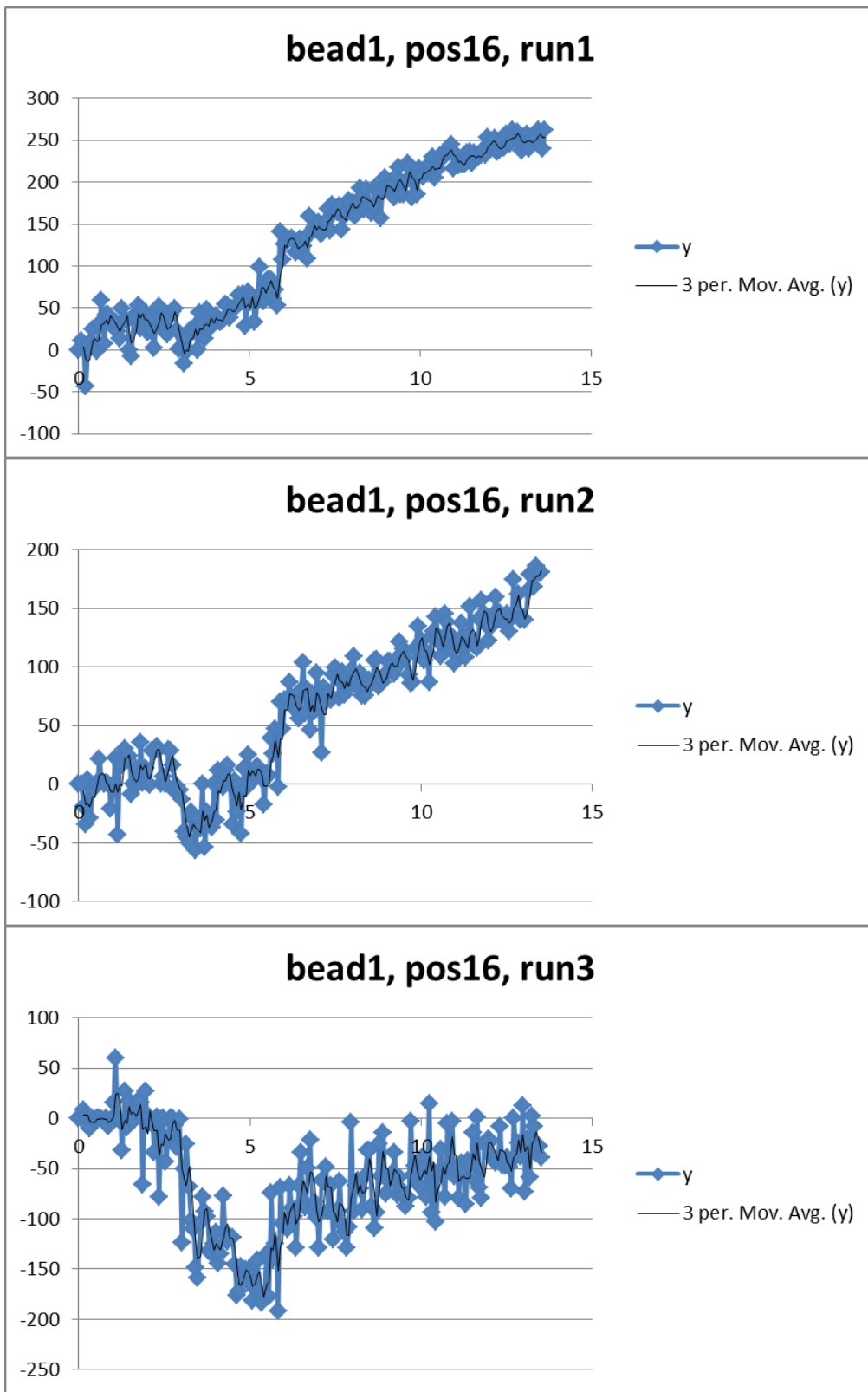


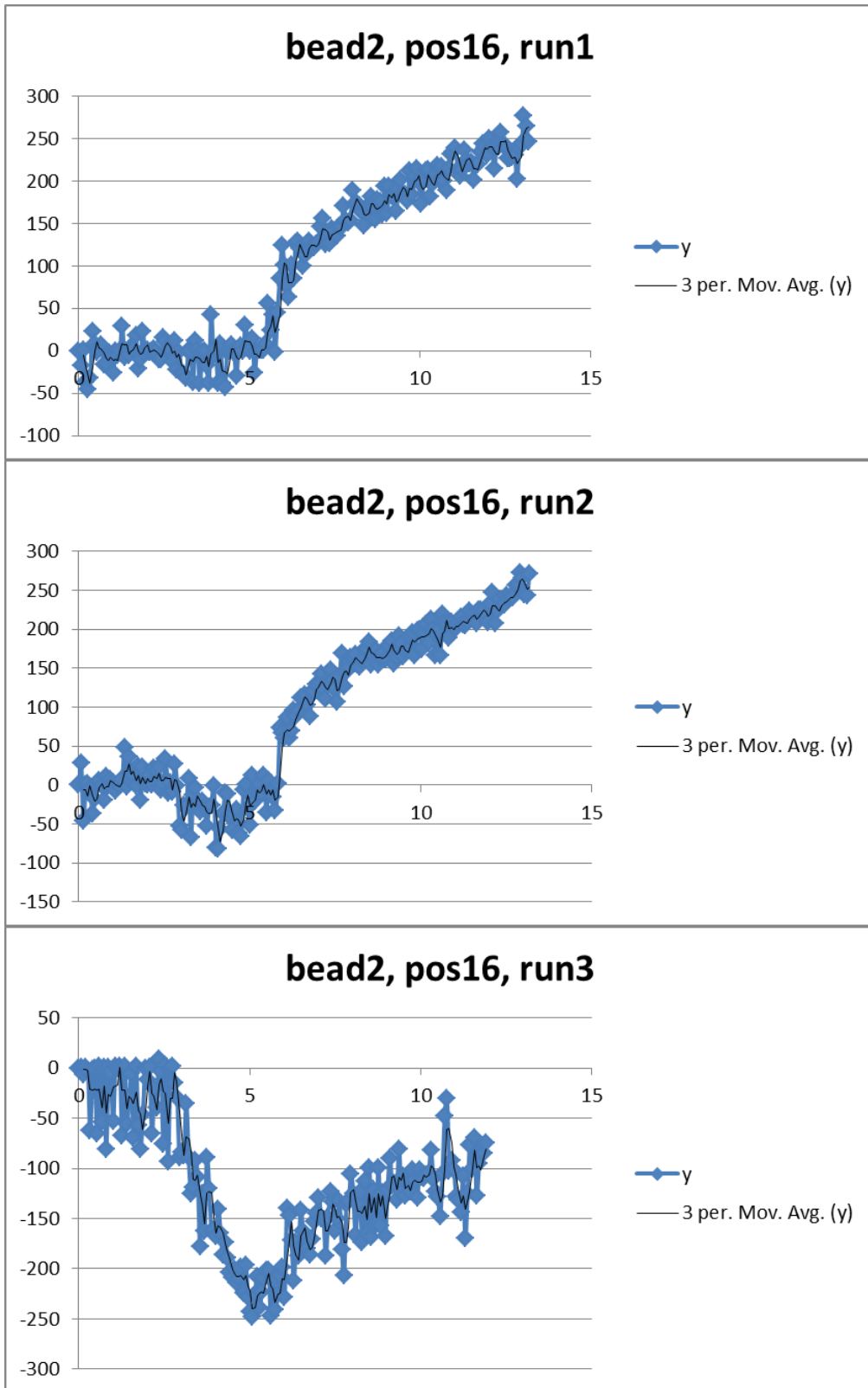


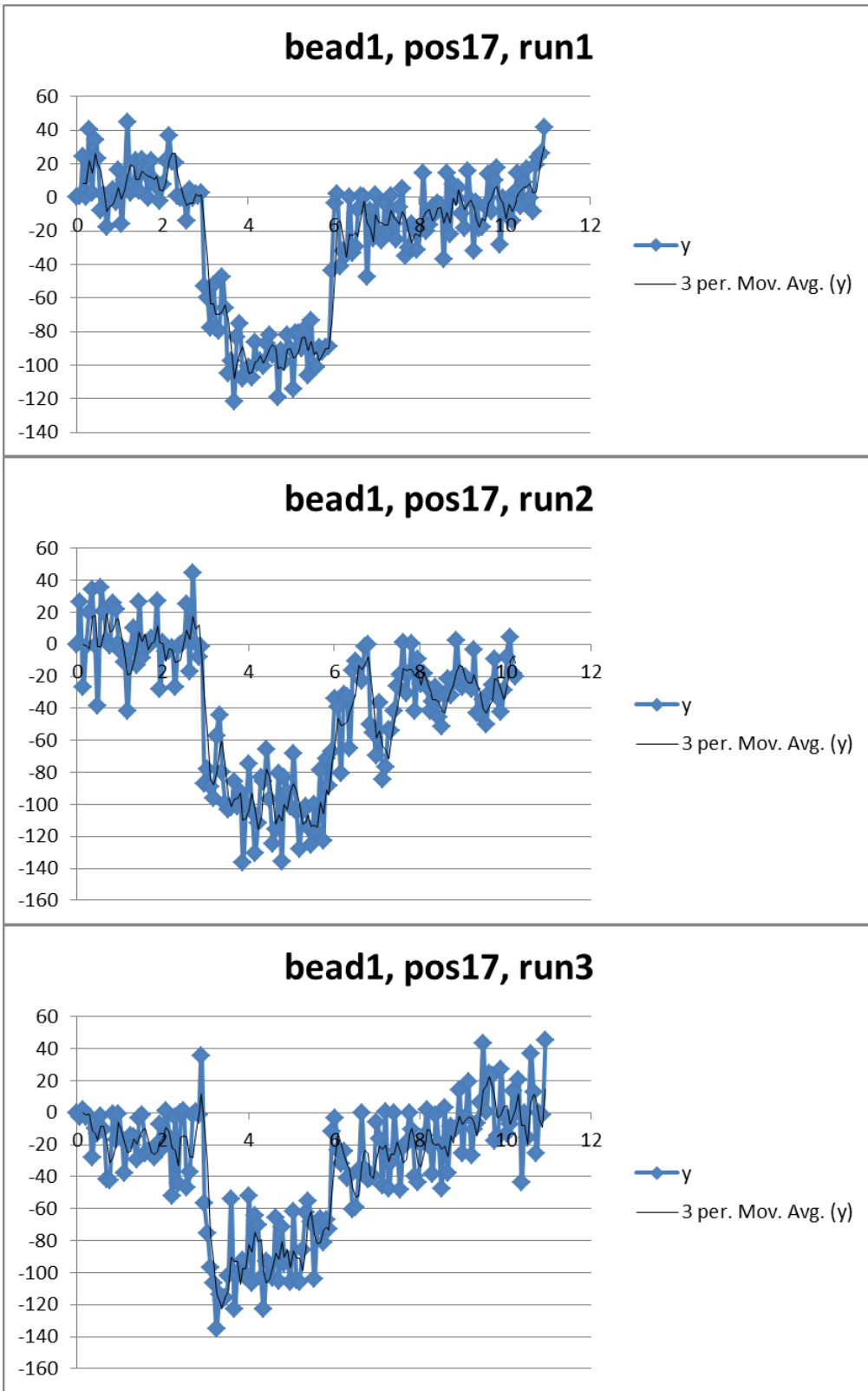


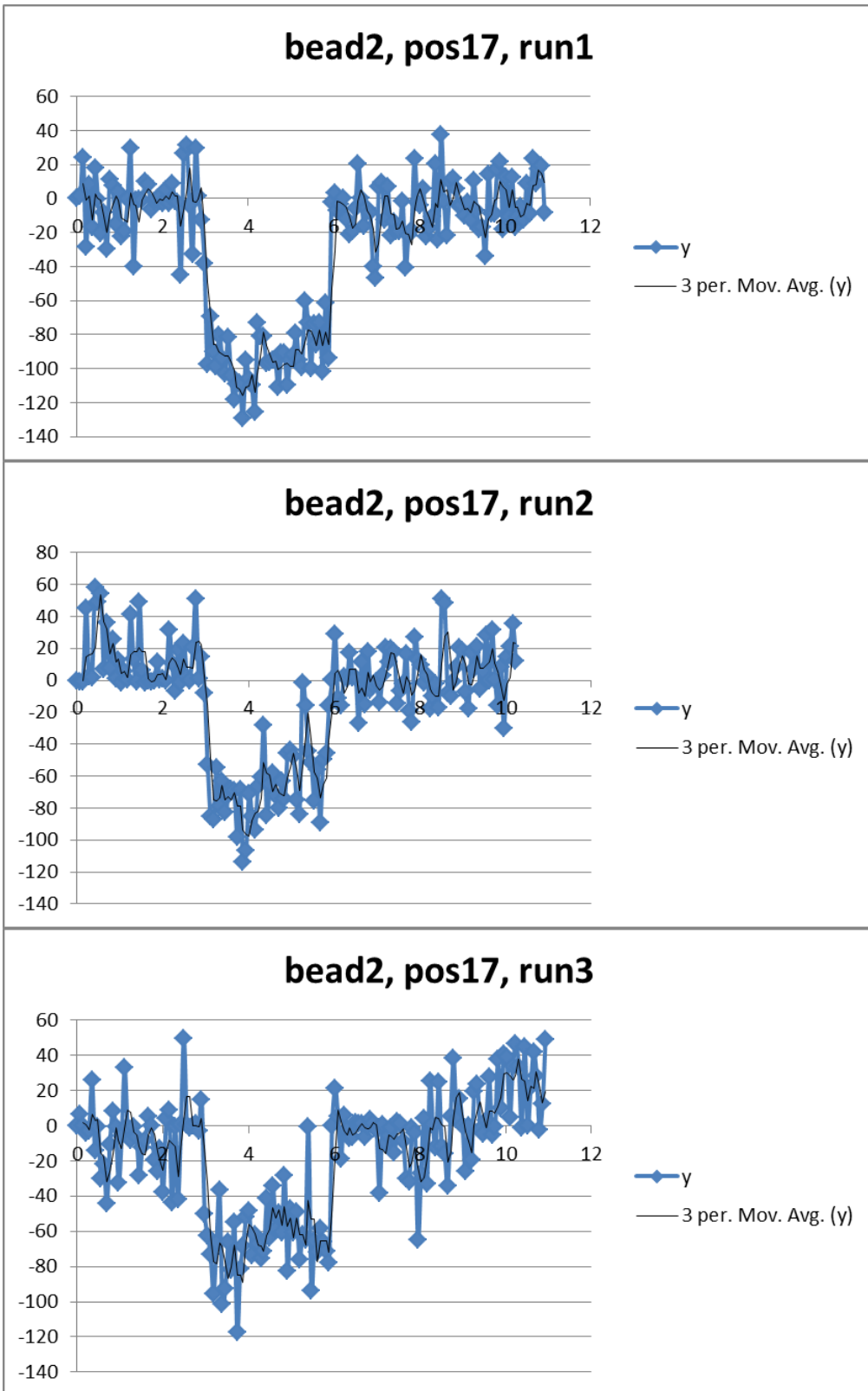


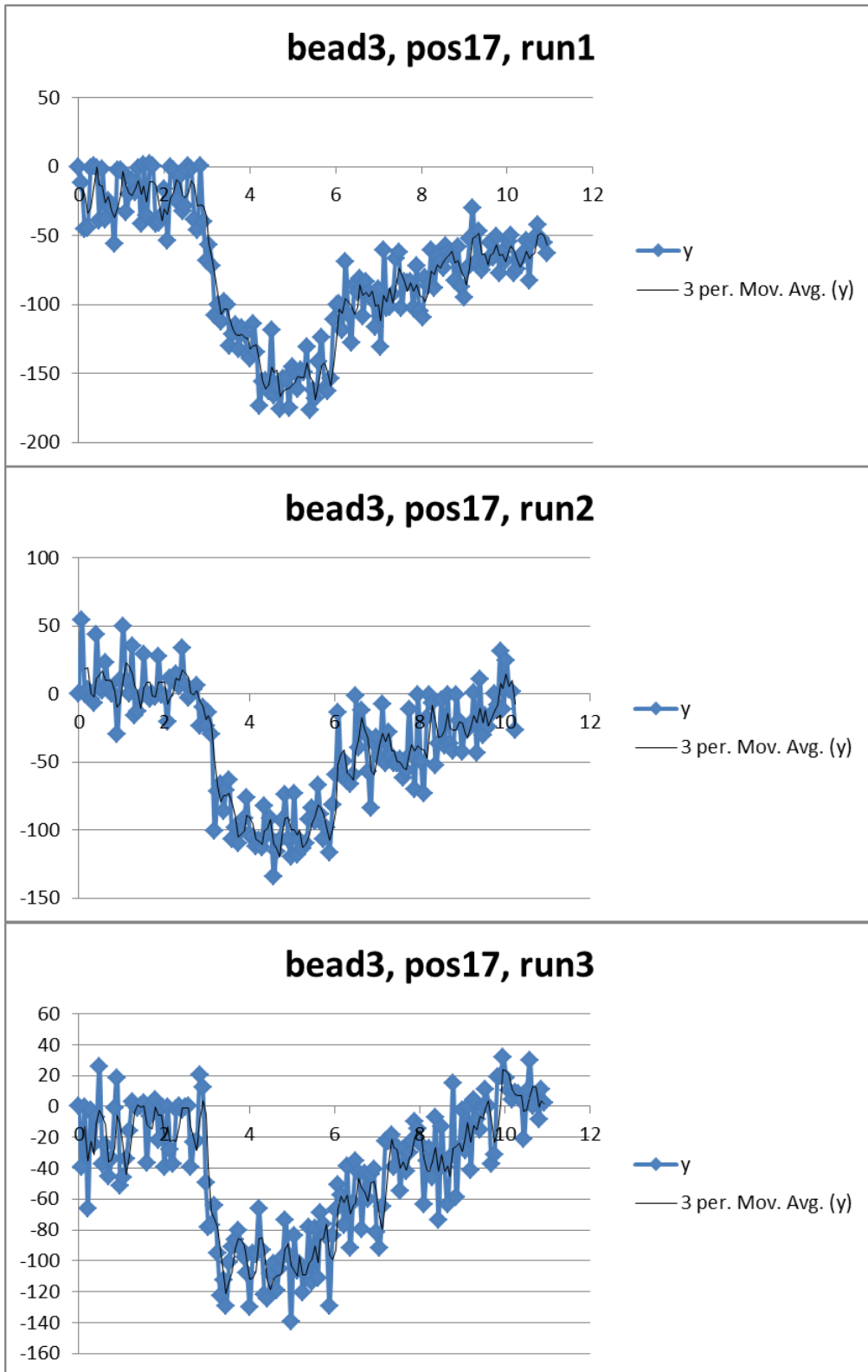


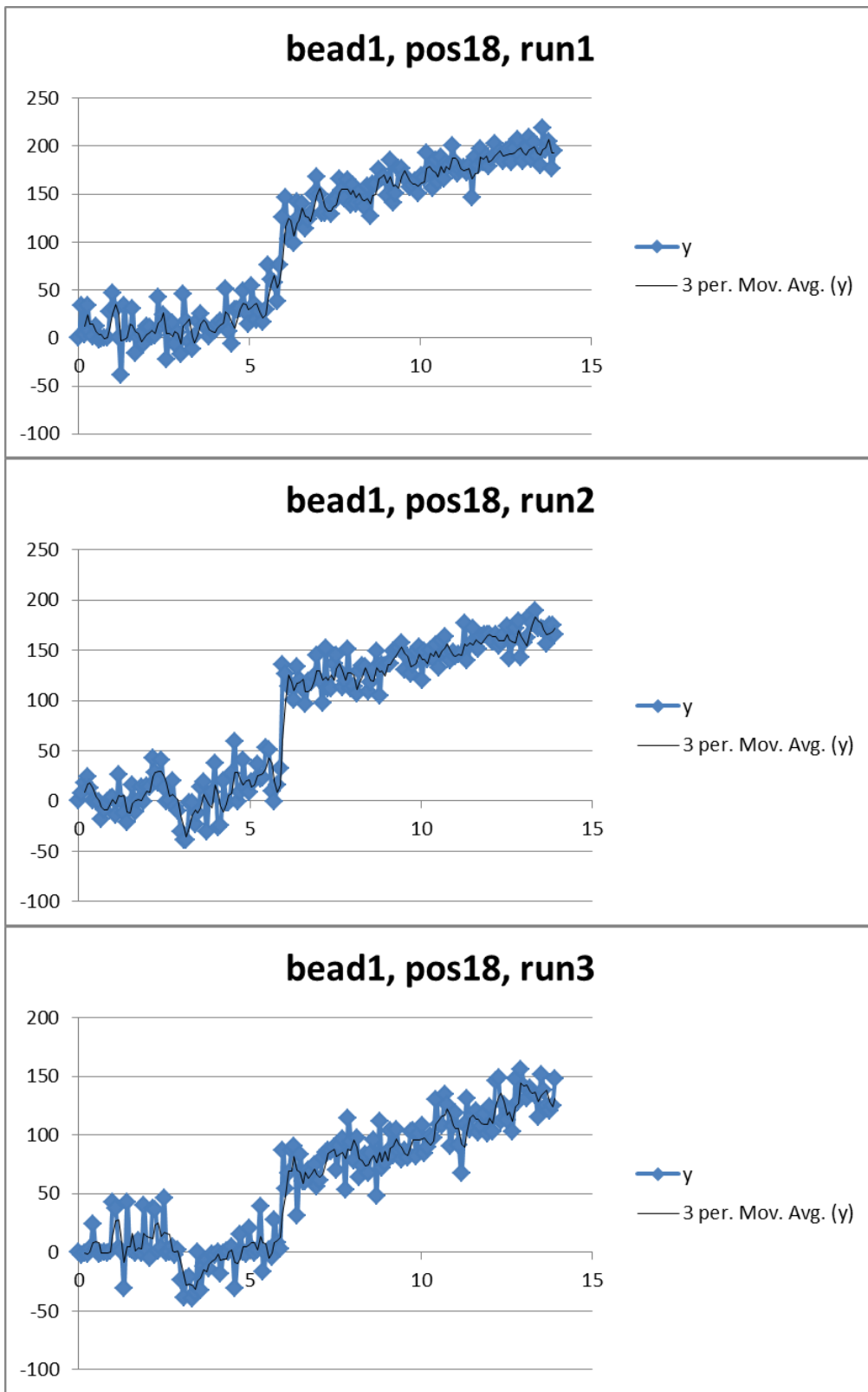


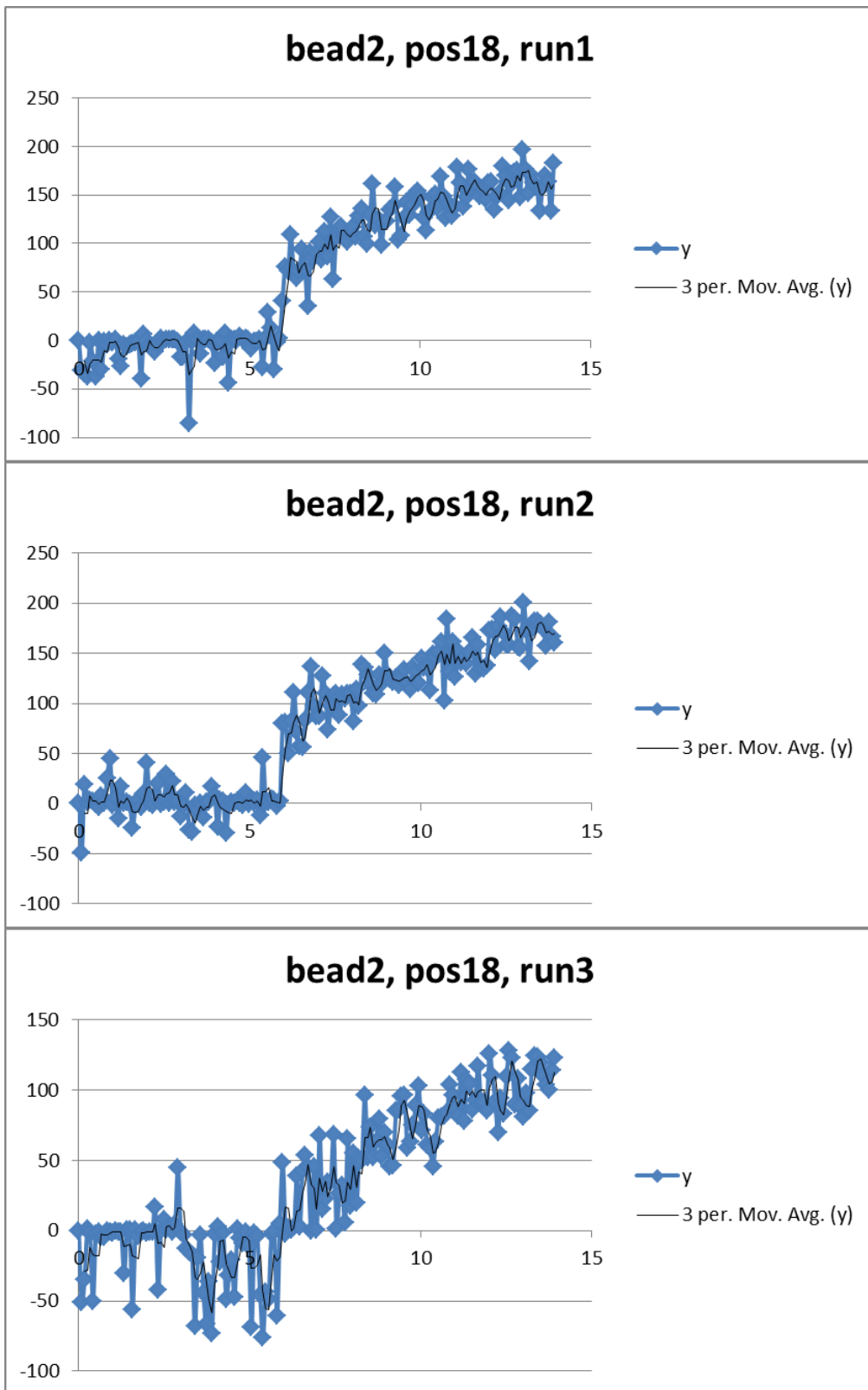


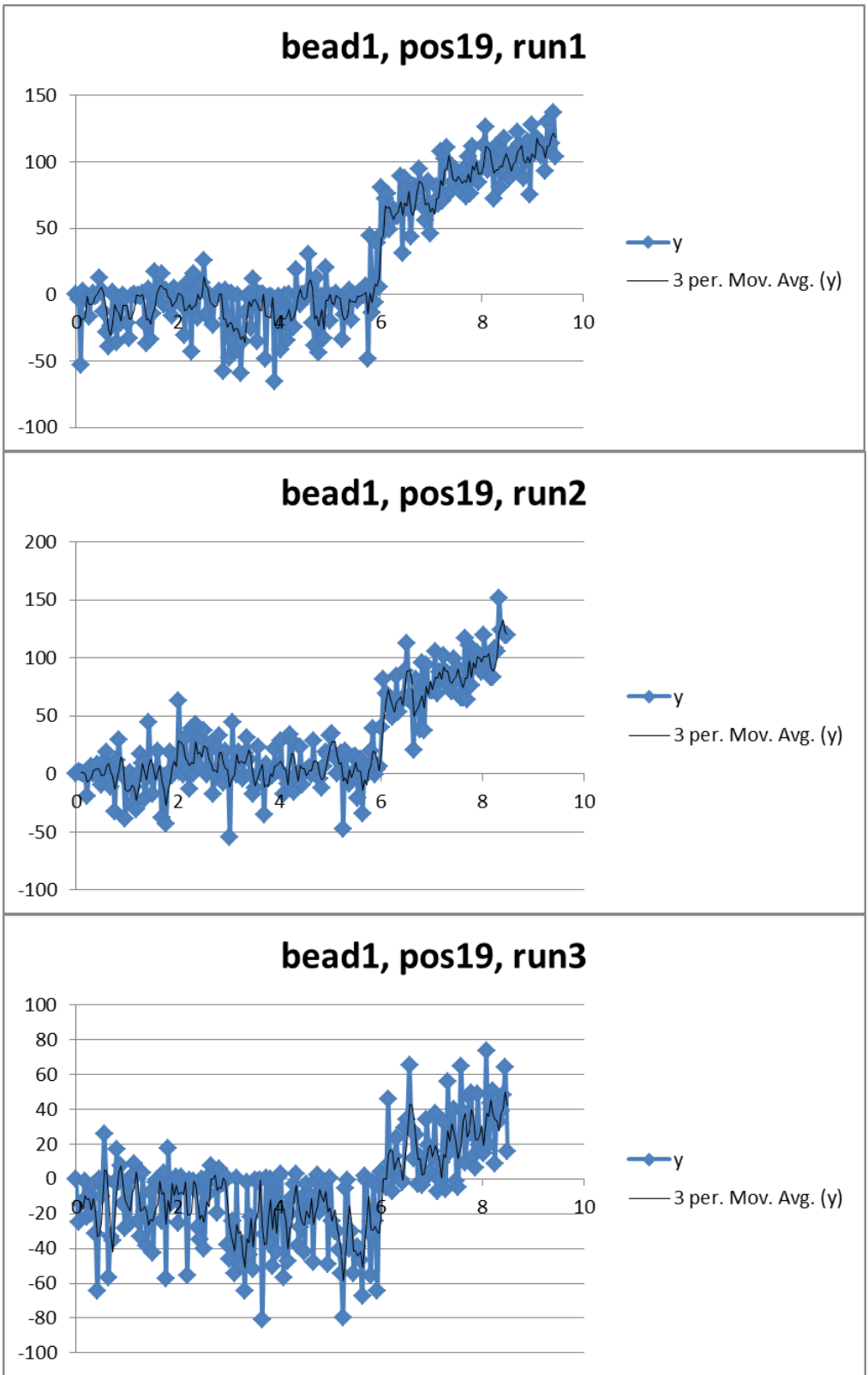


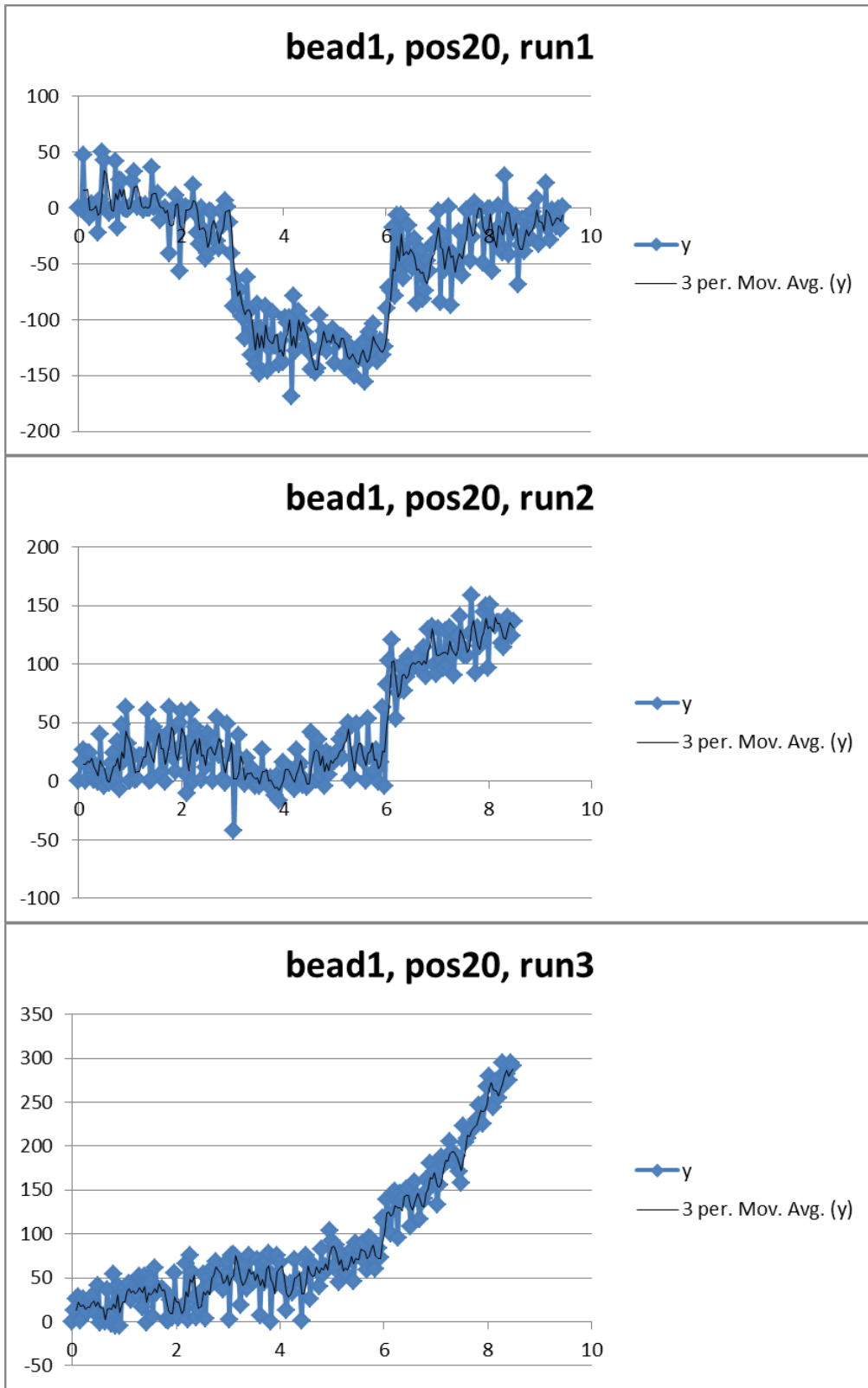


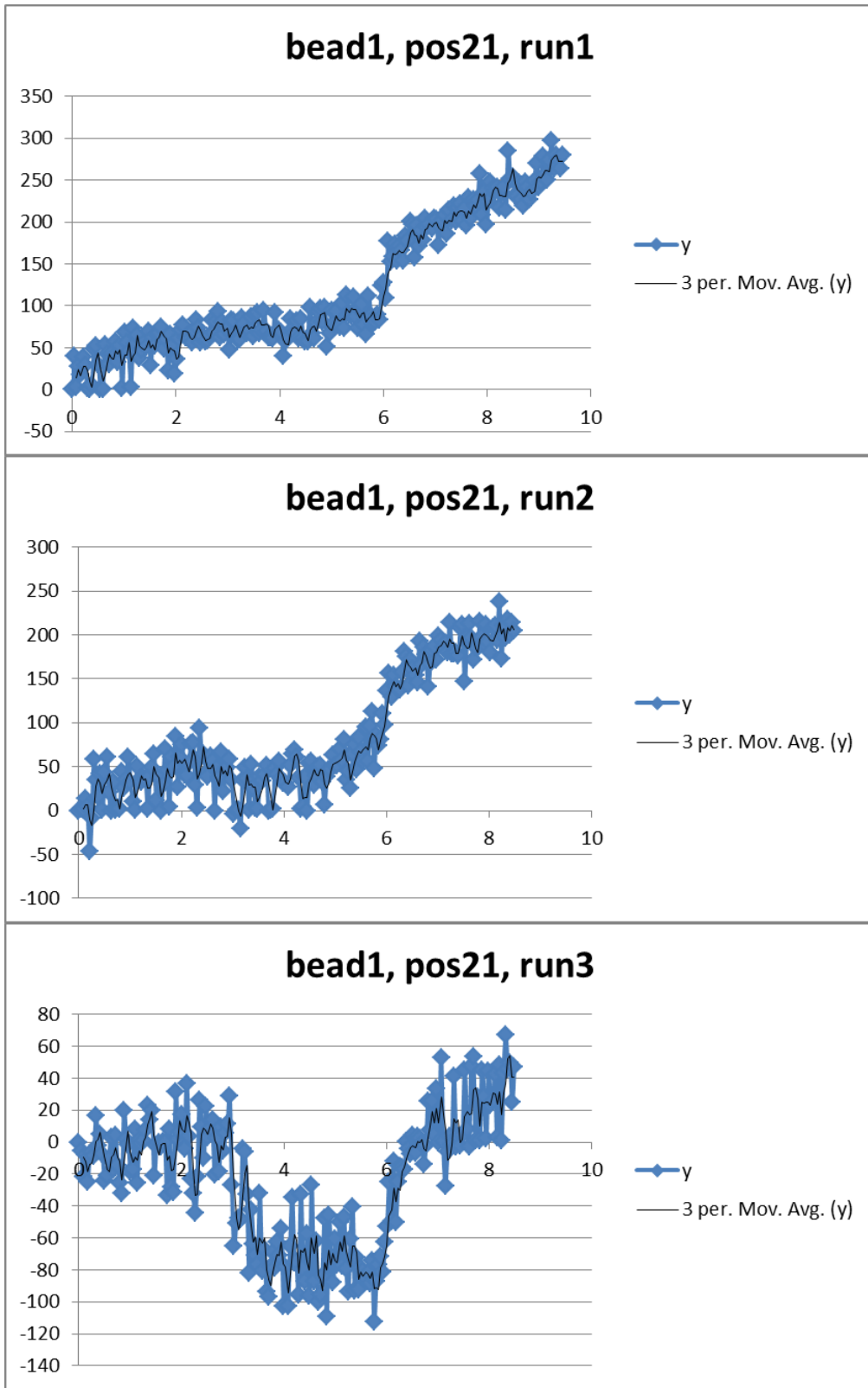


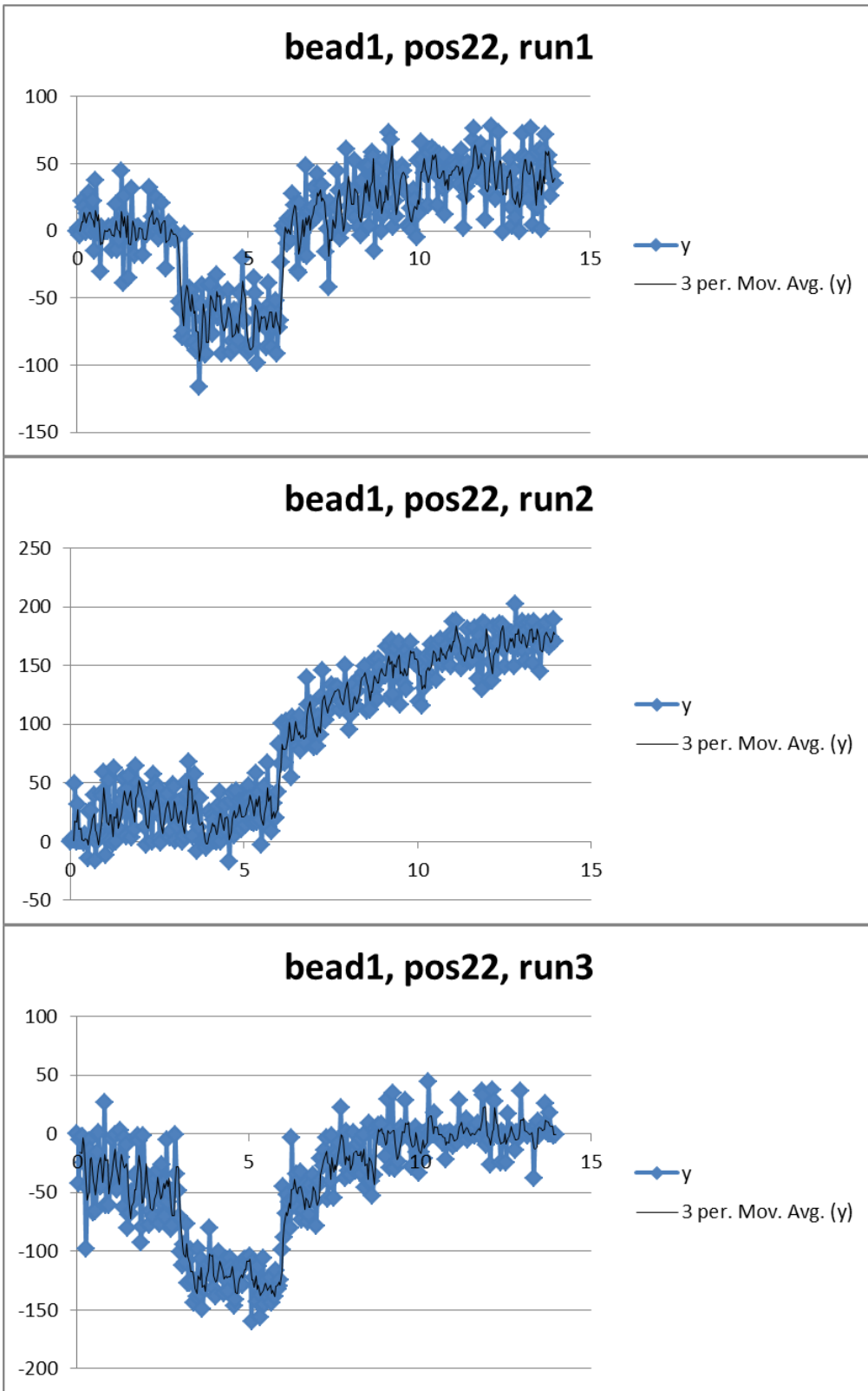


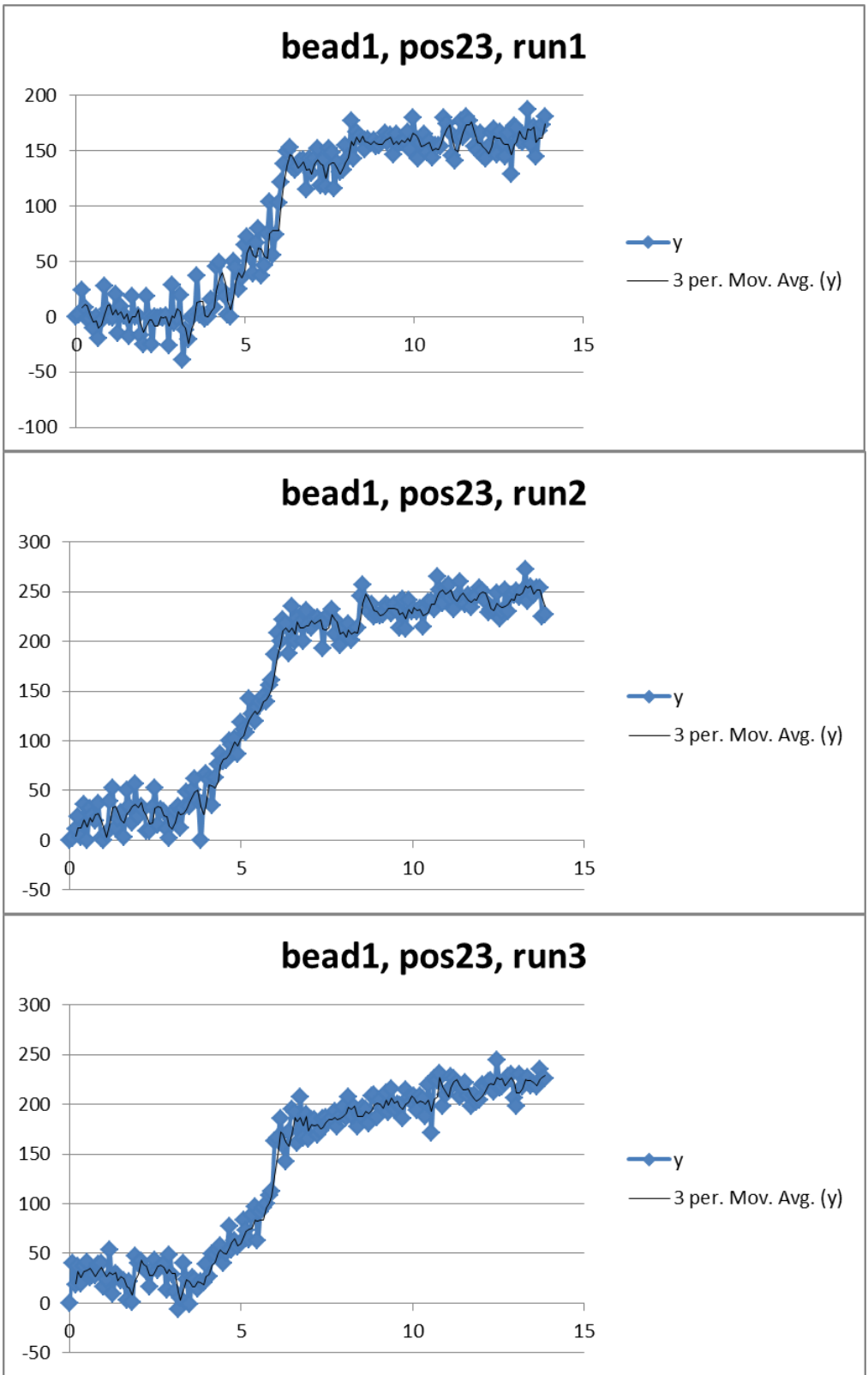


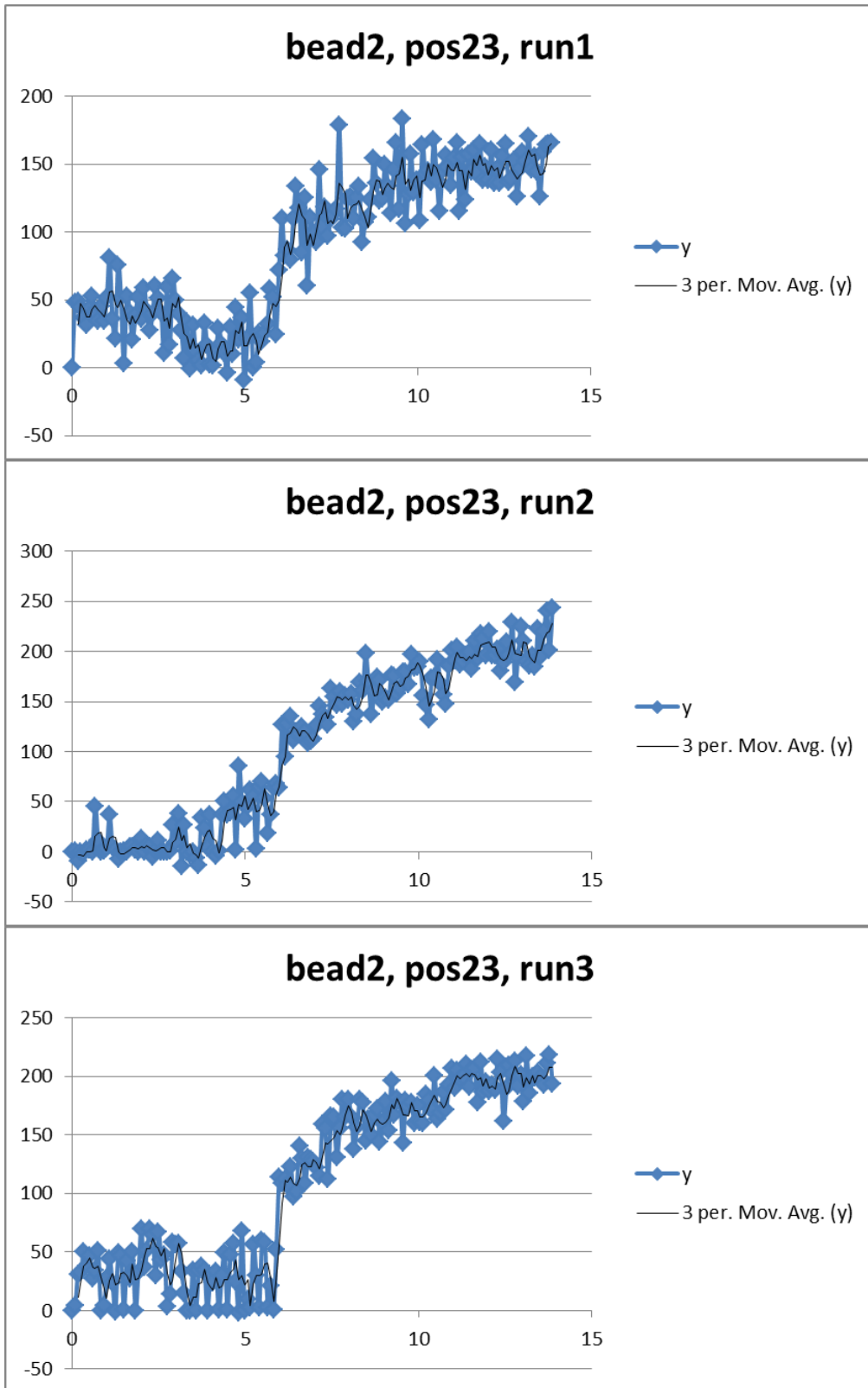


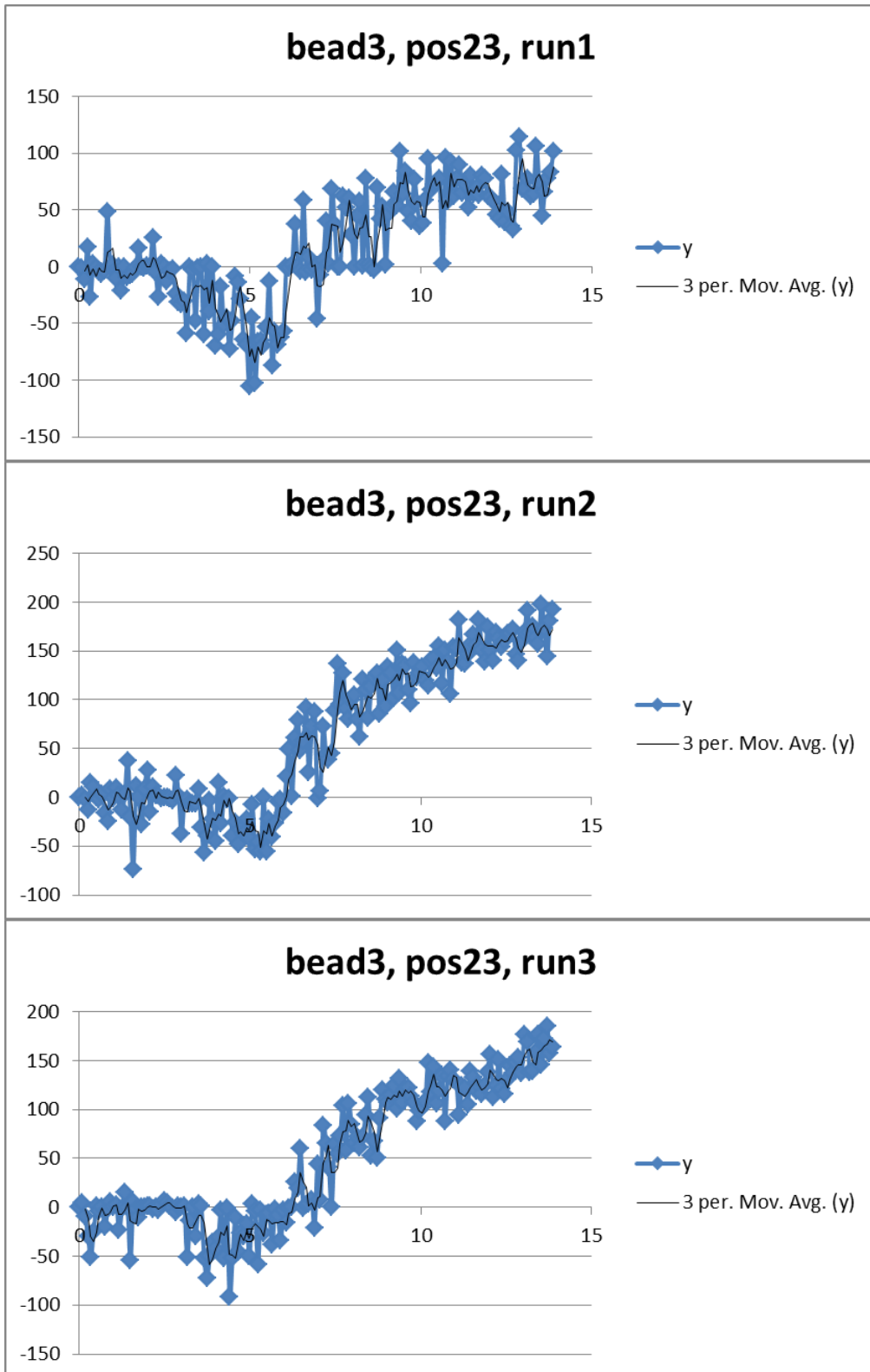


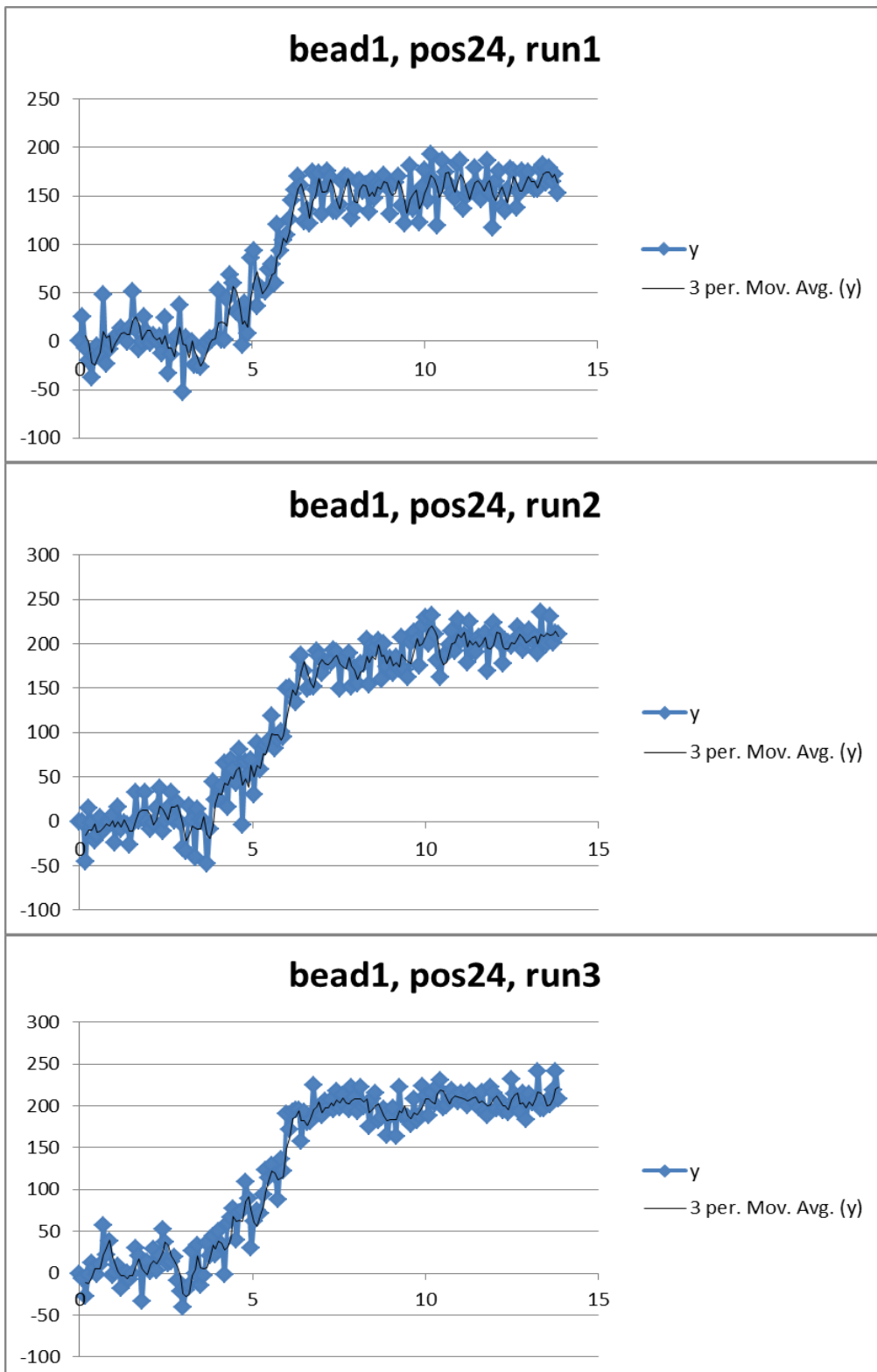


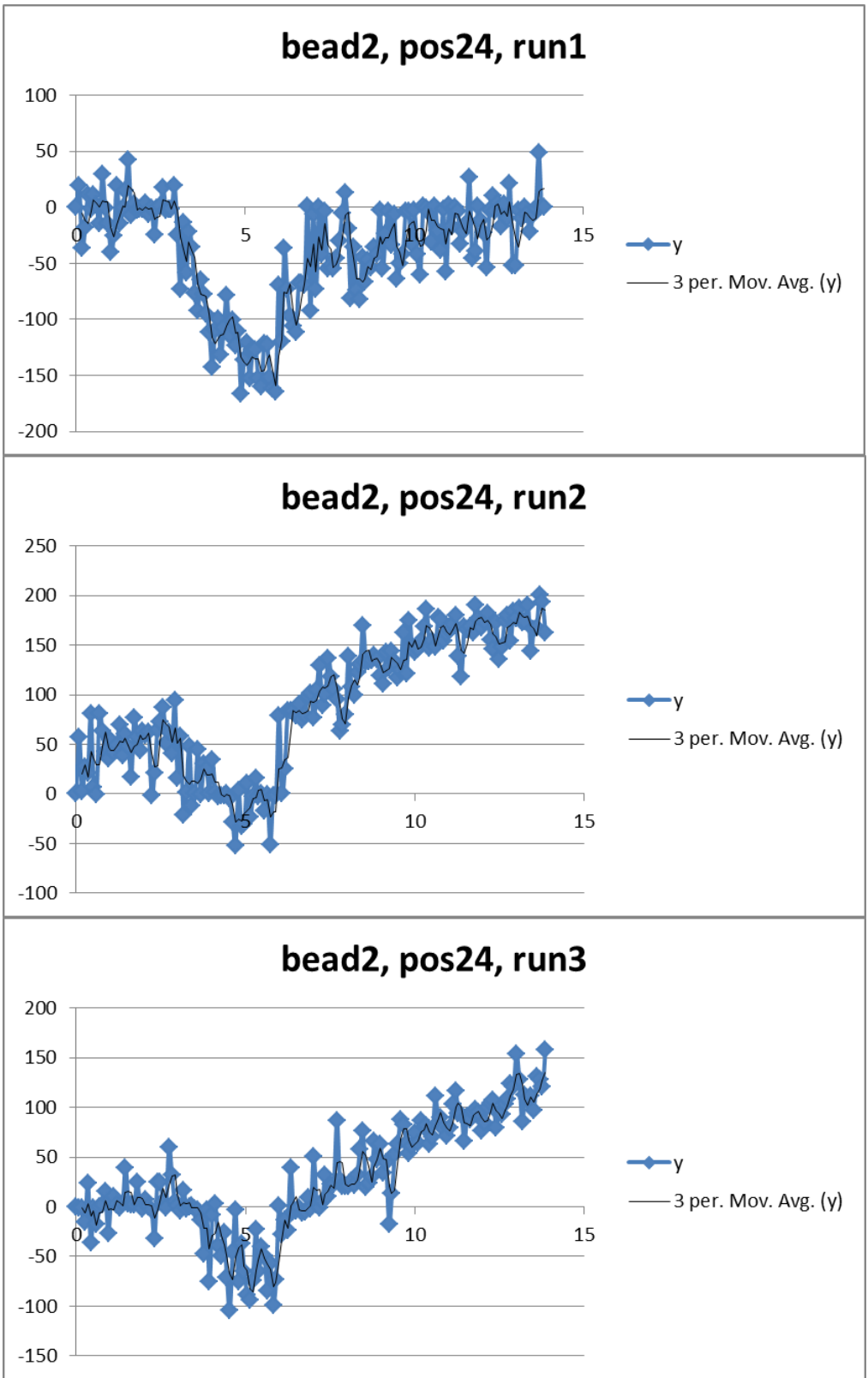


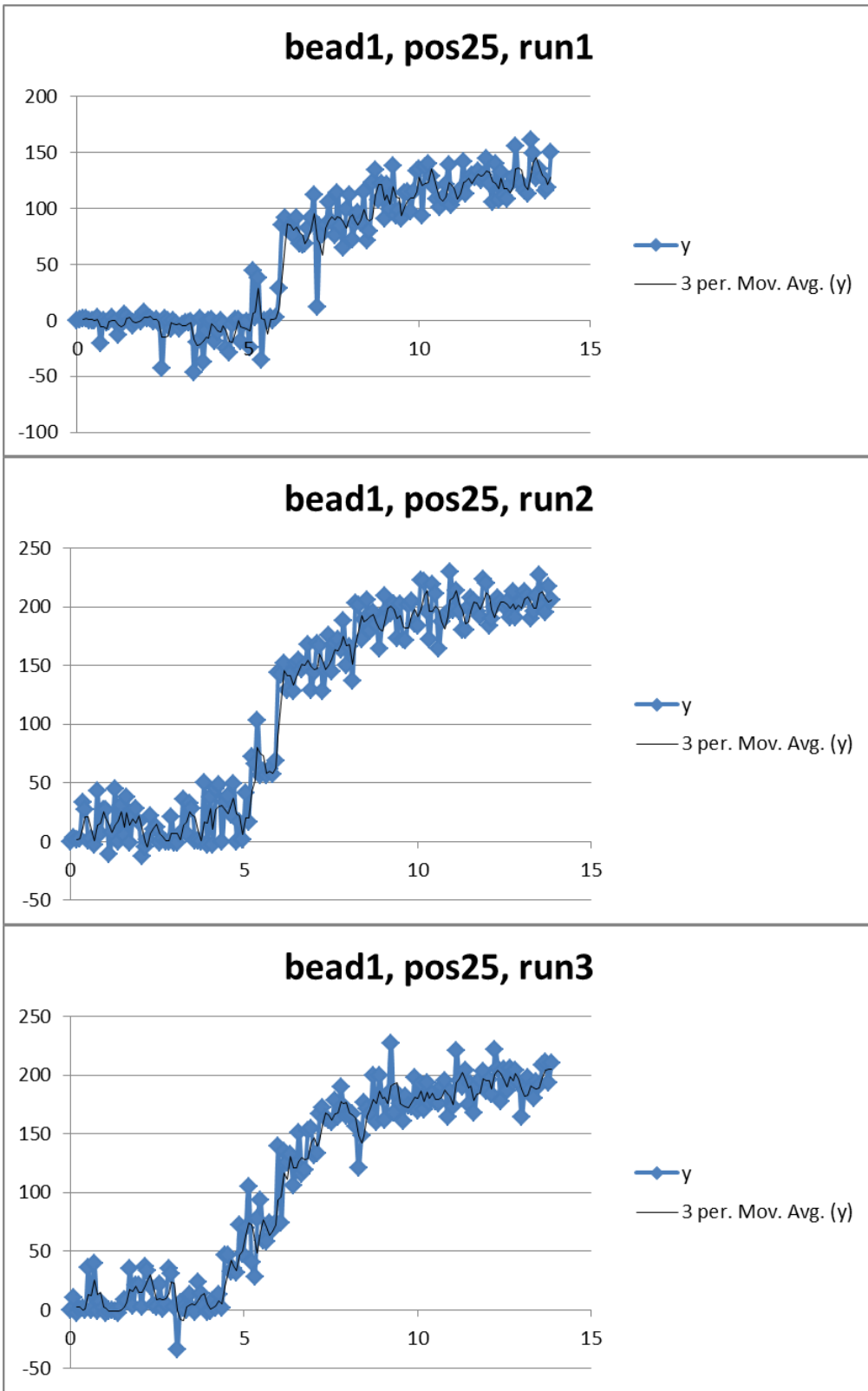


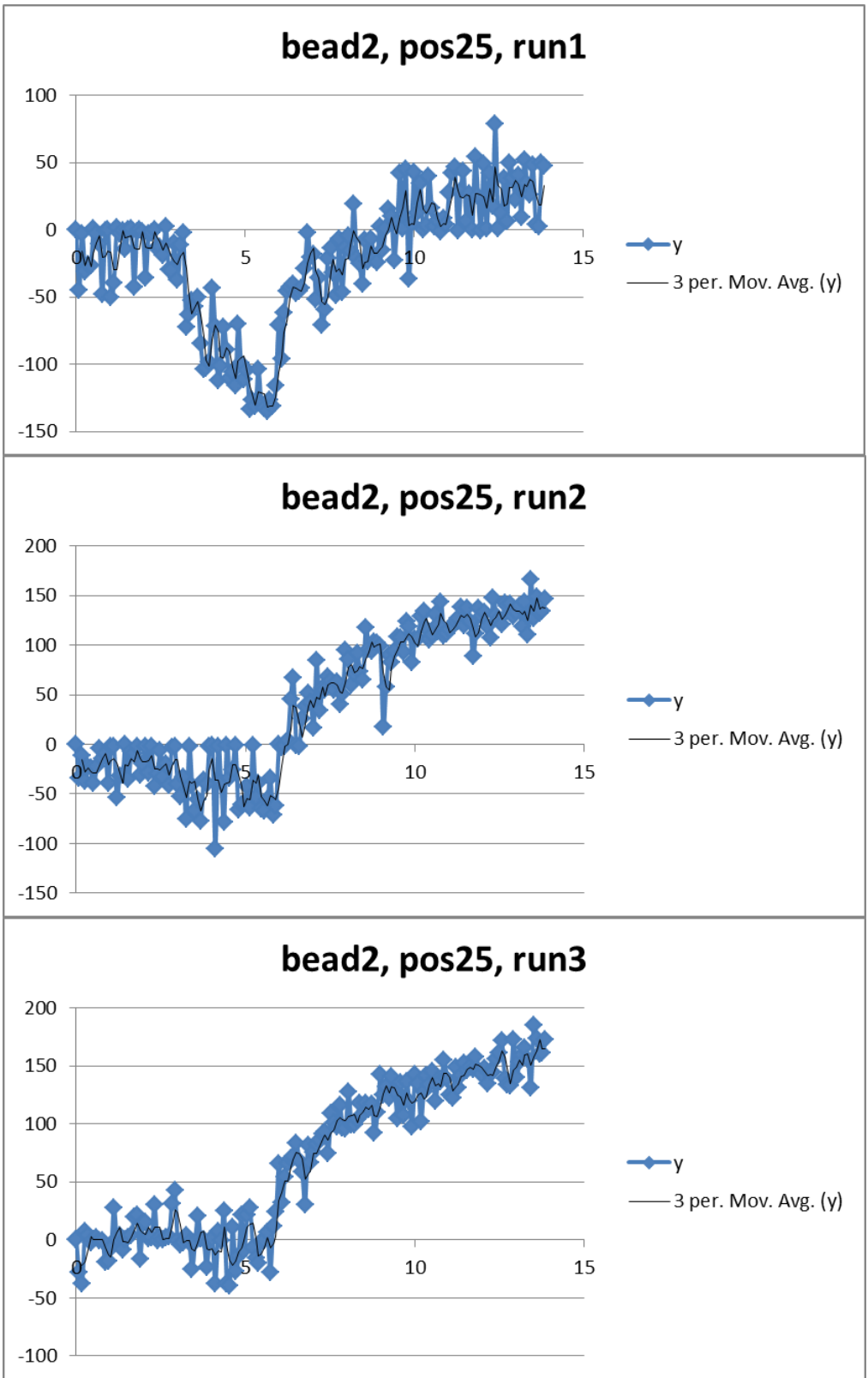


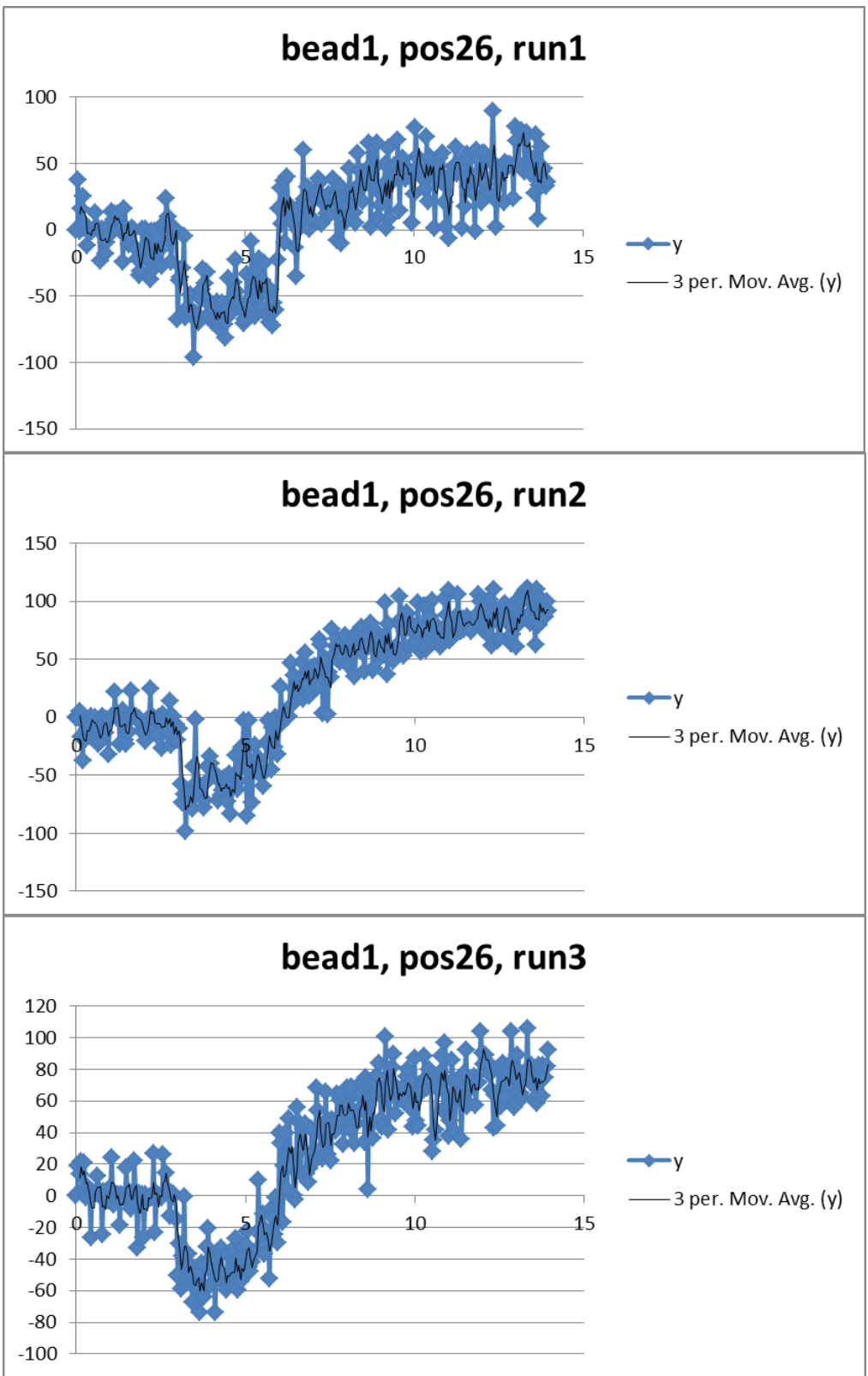


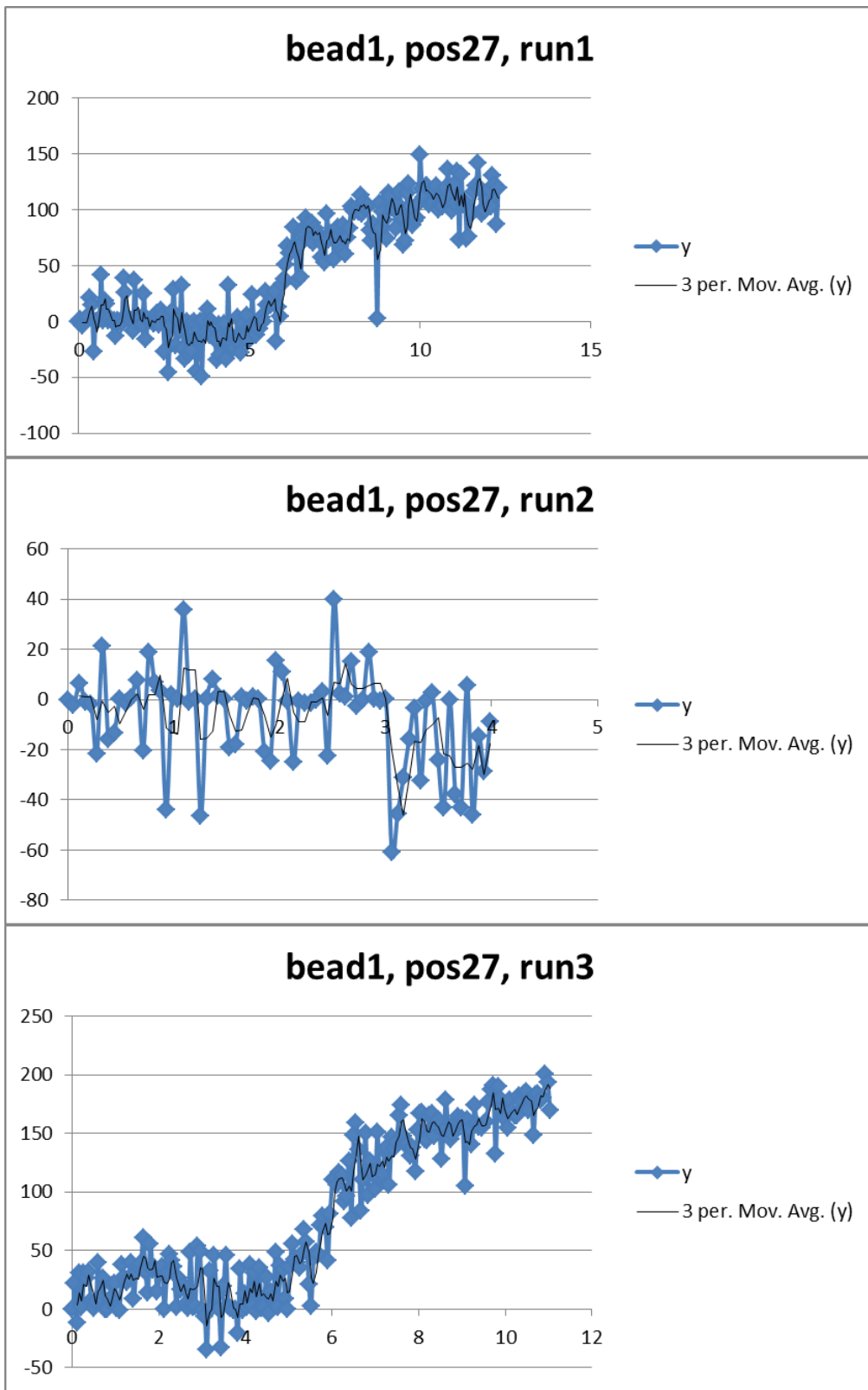


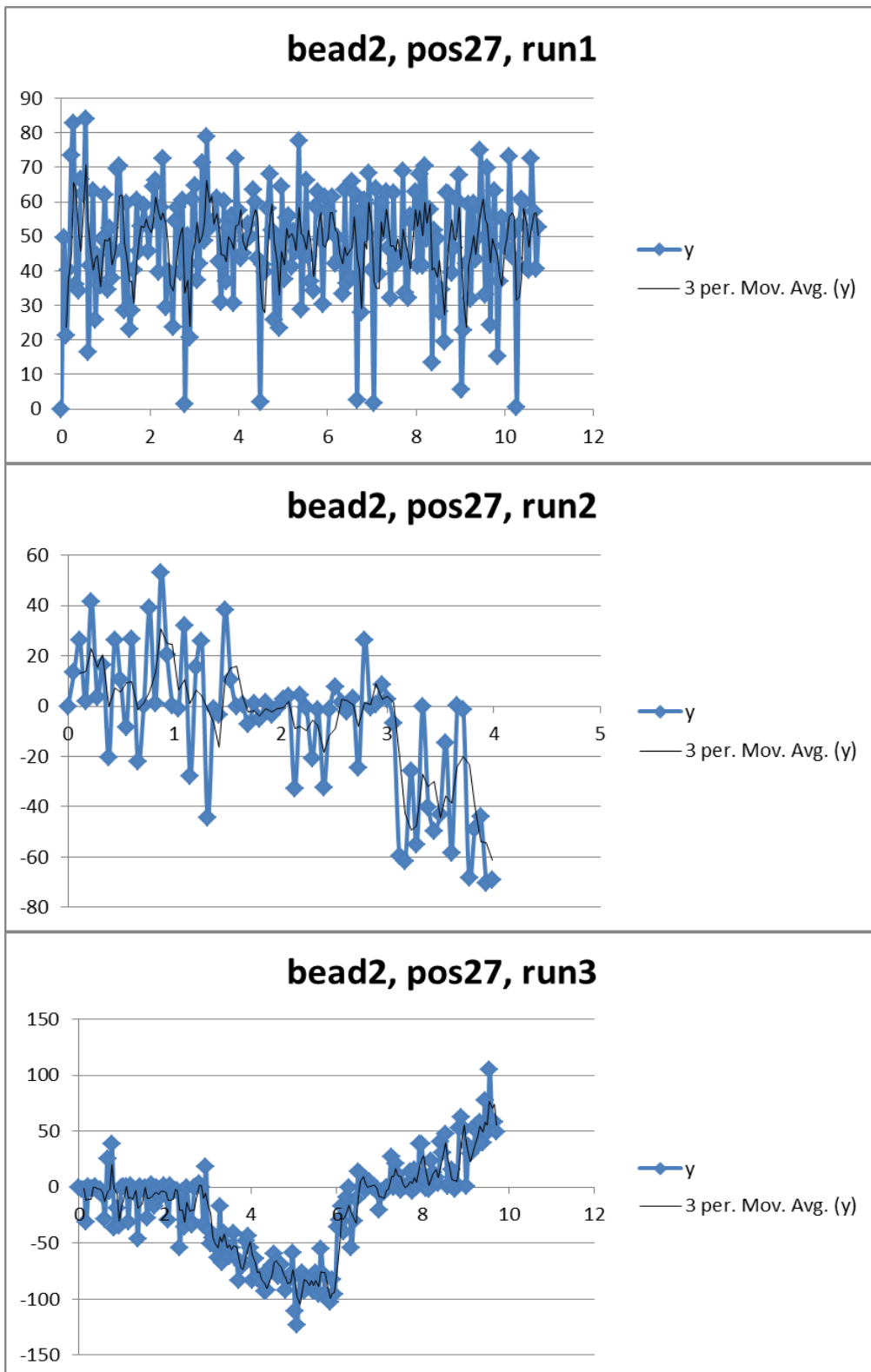


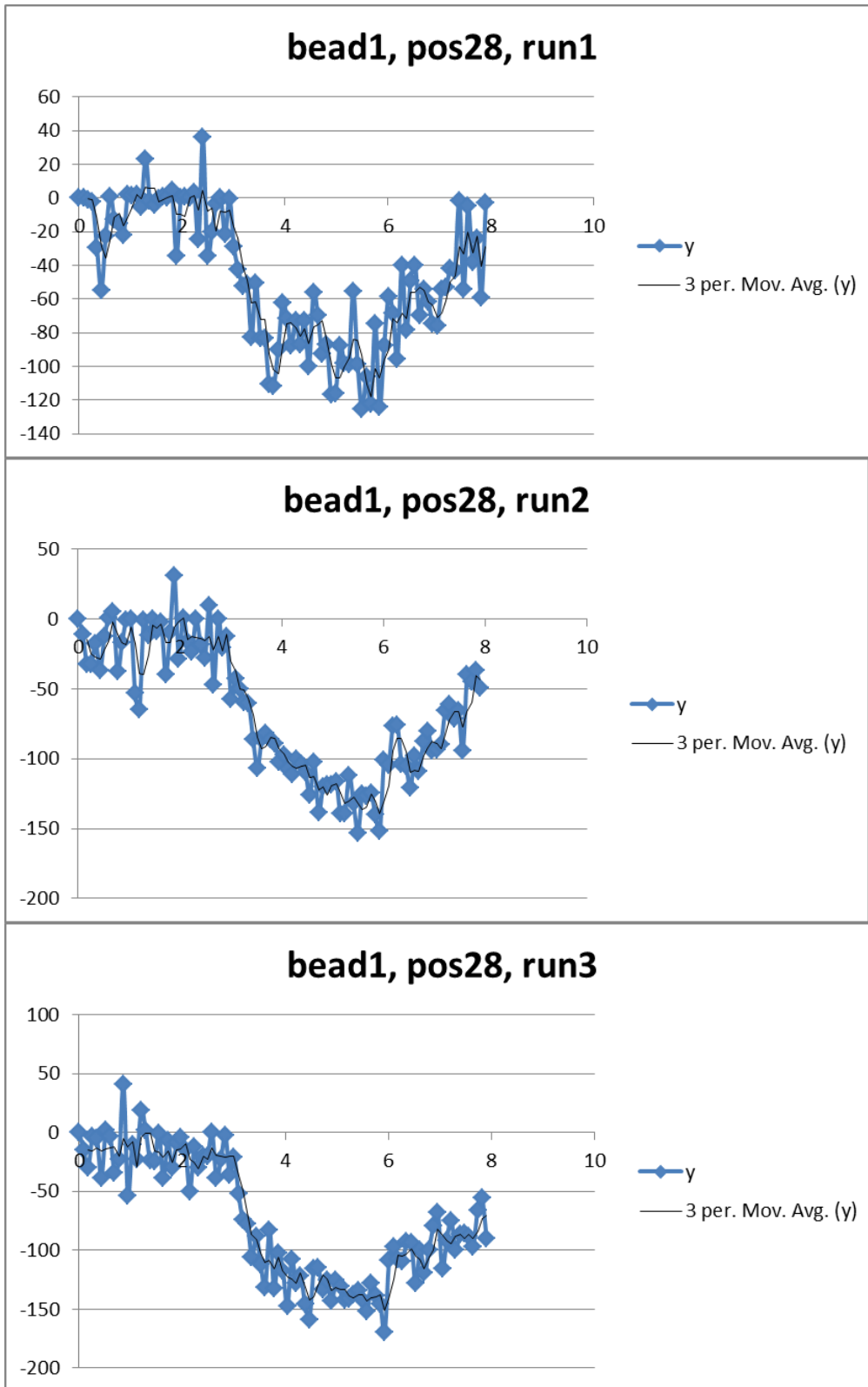


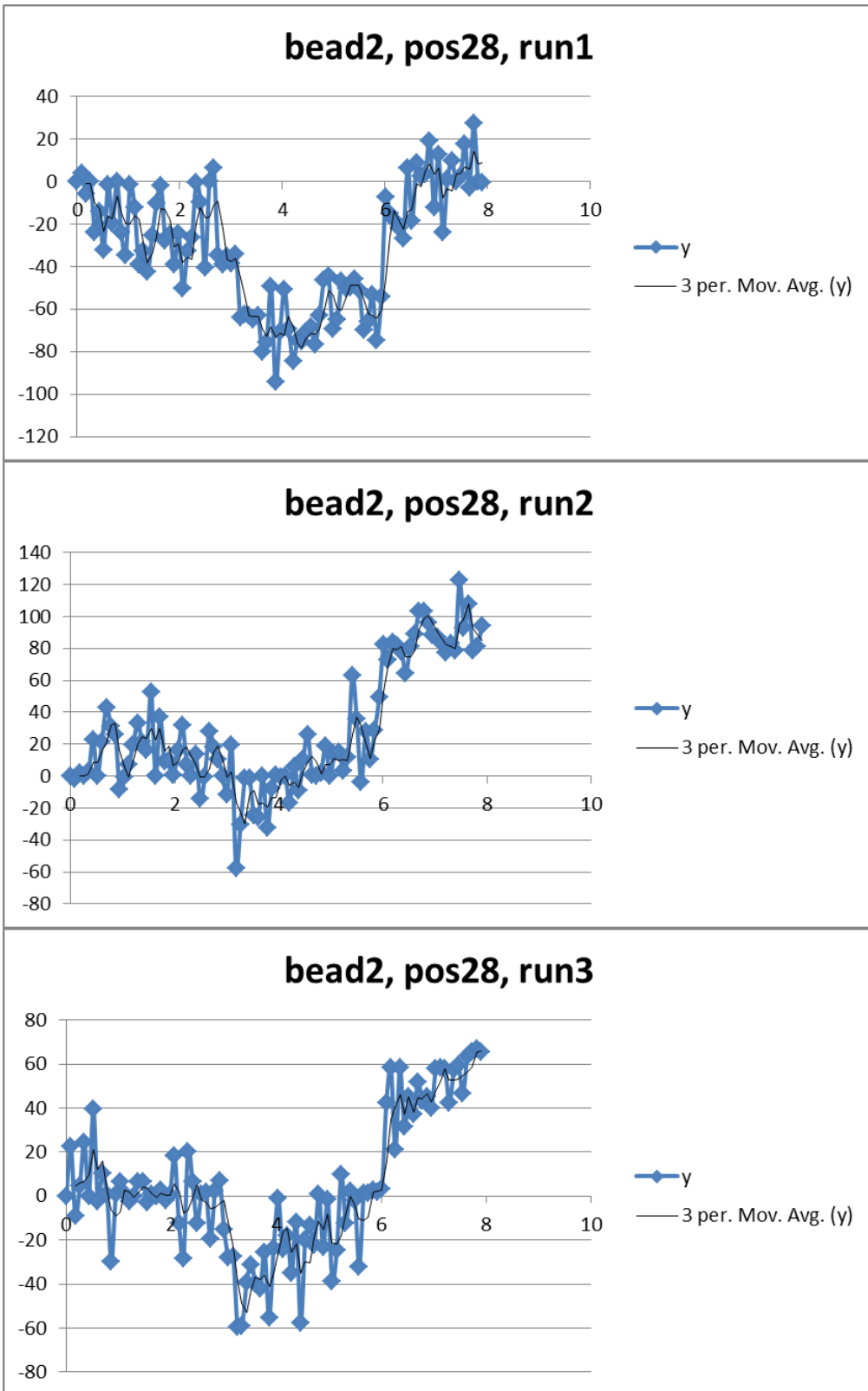


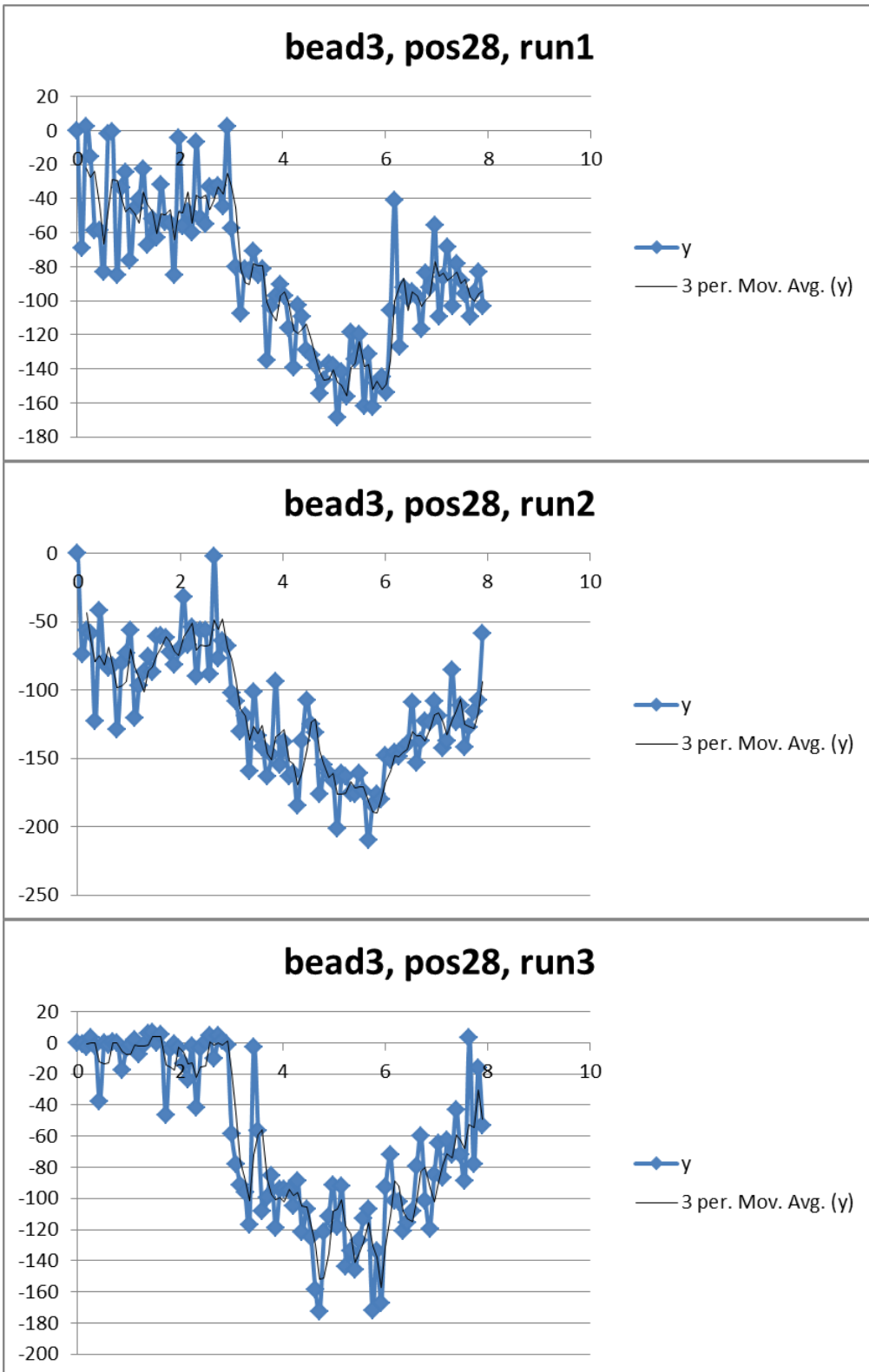


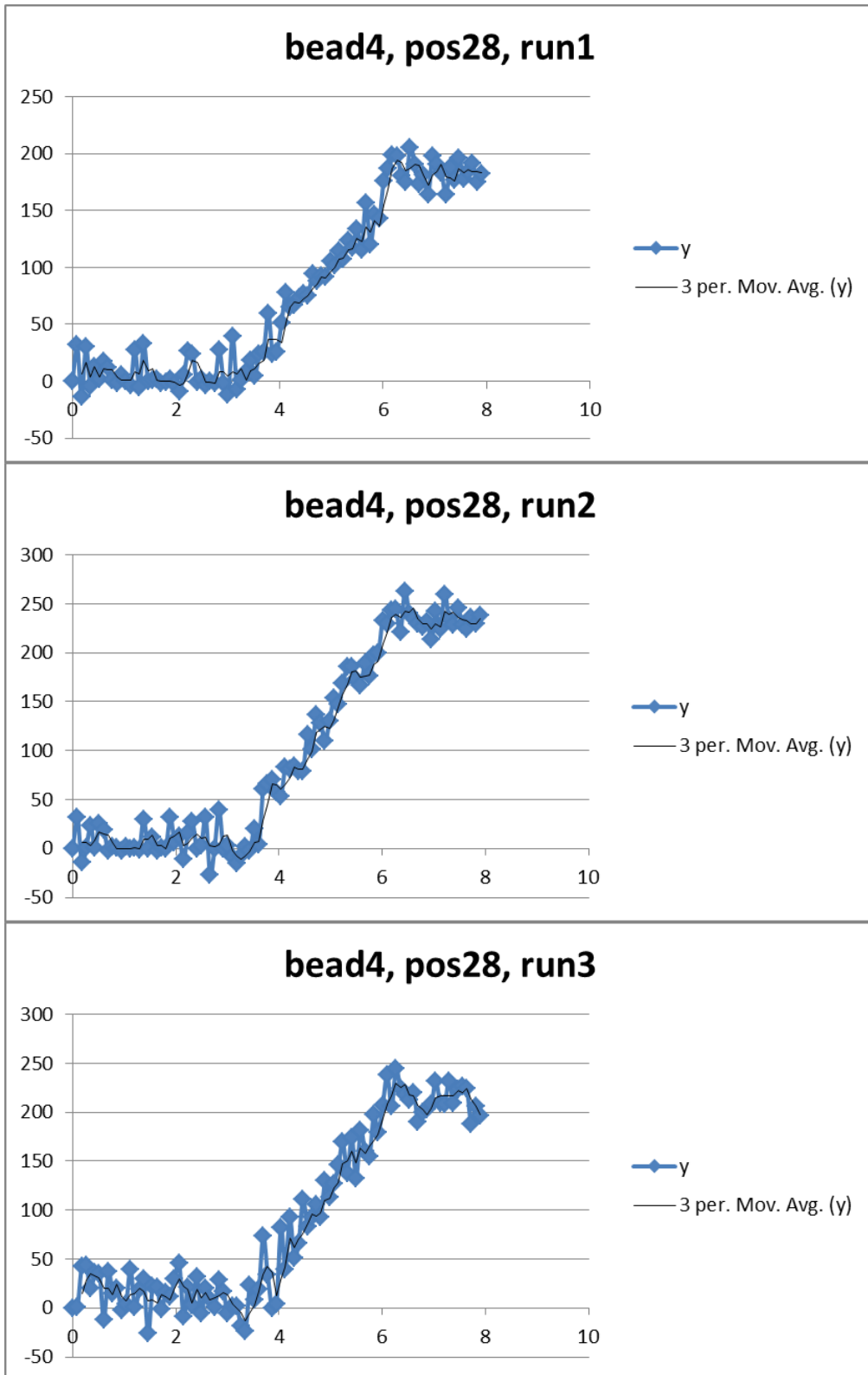






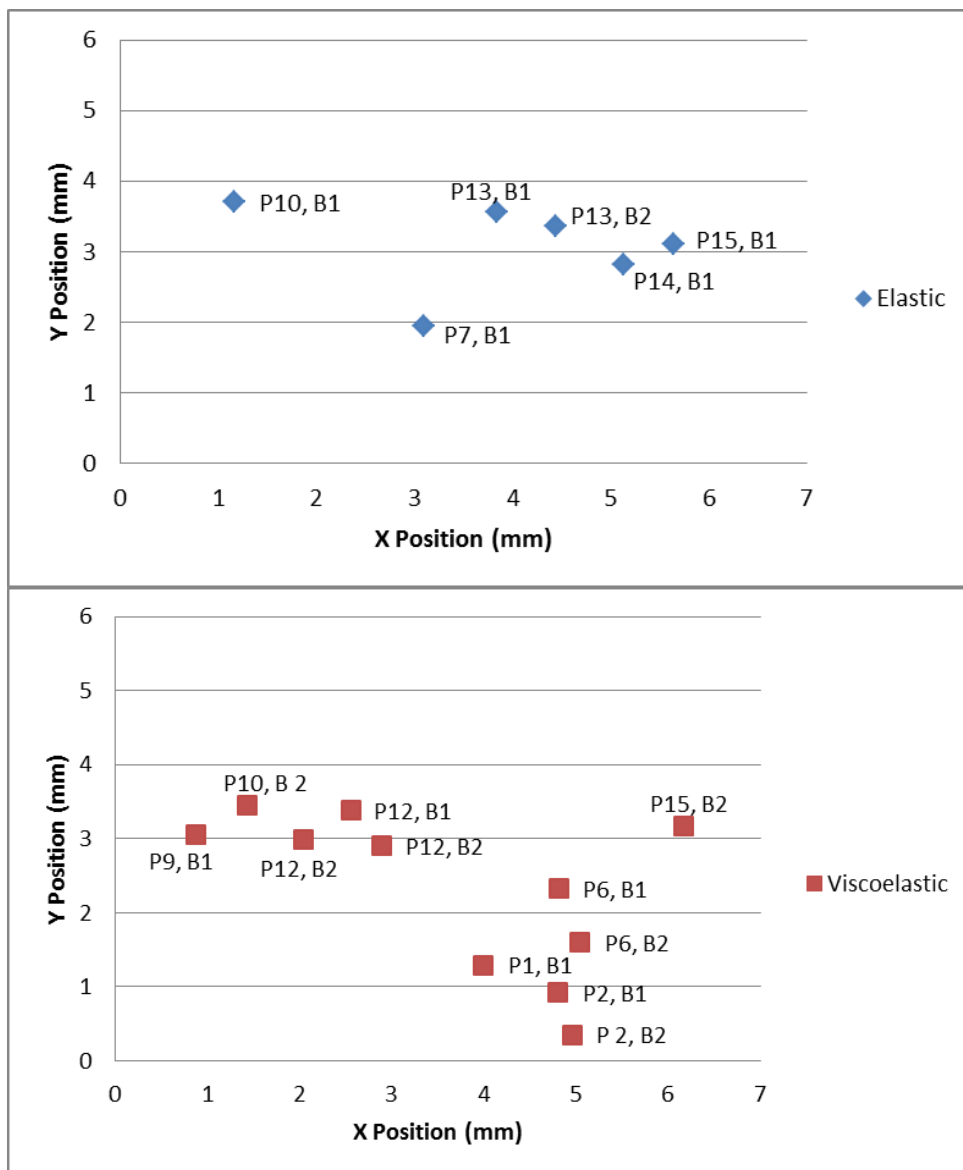


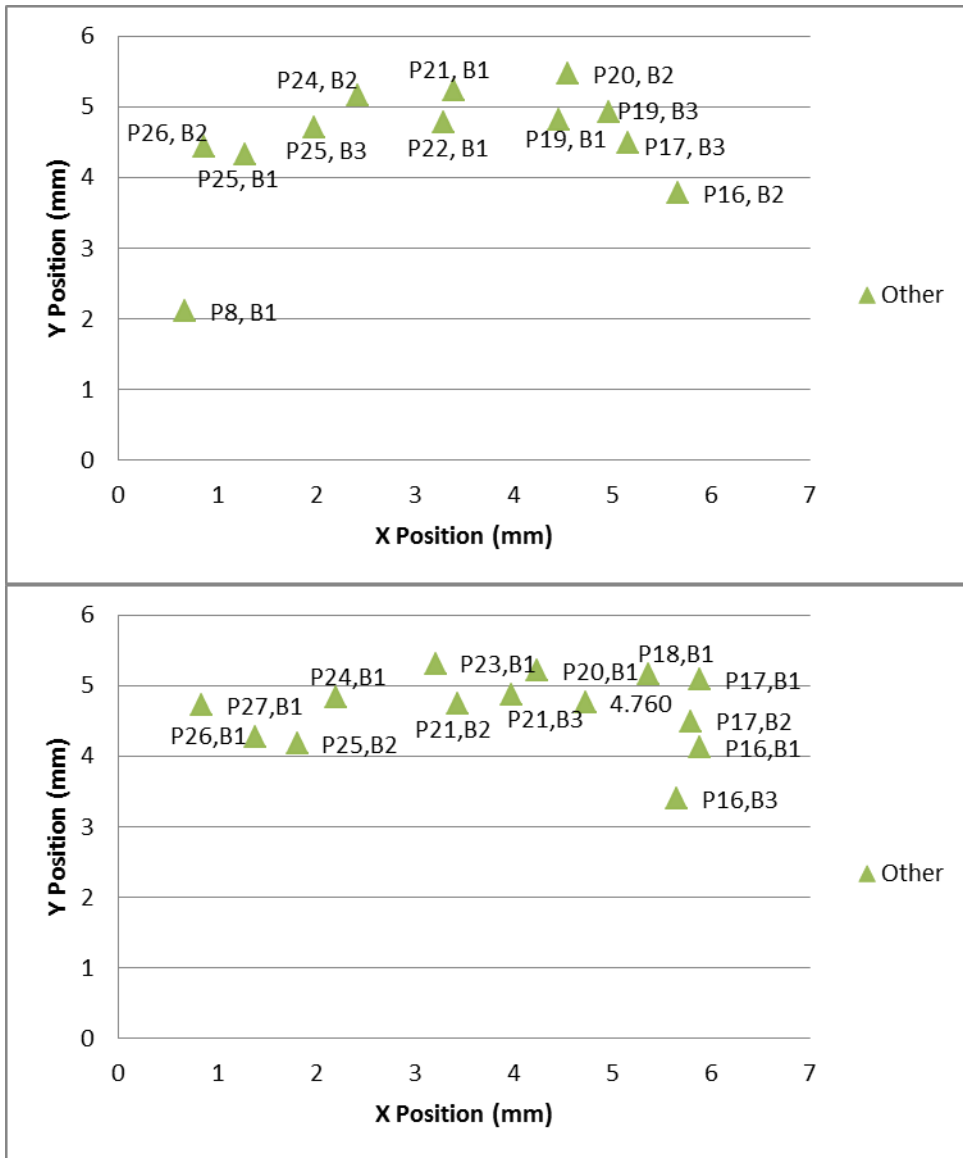




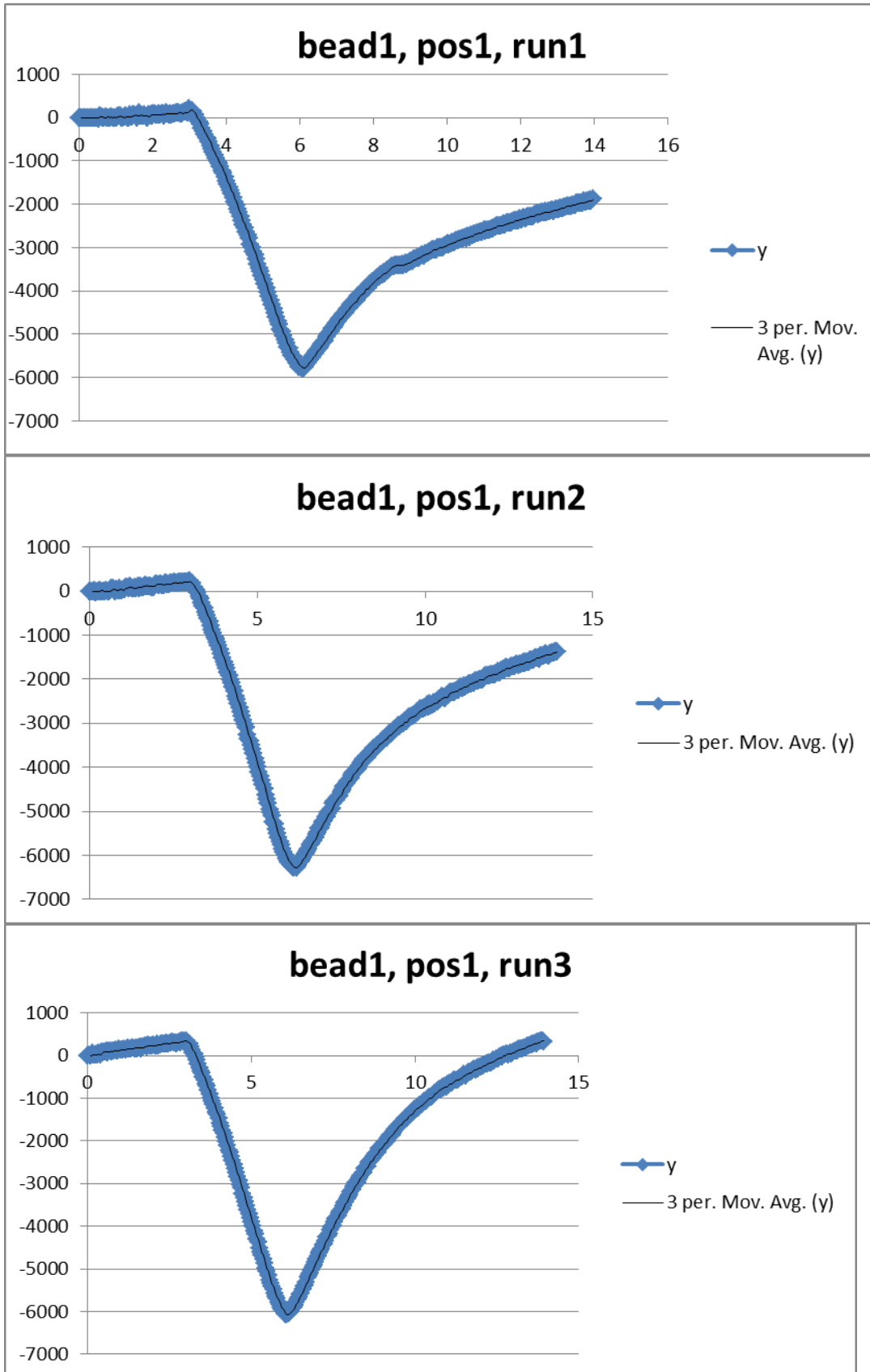
Appendix C: Bead displacement data for 0.2 kPa Hydrogel

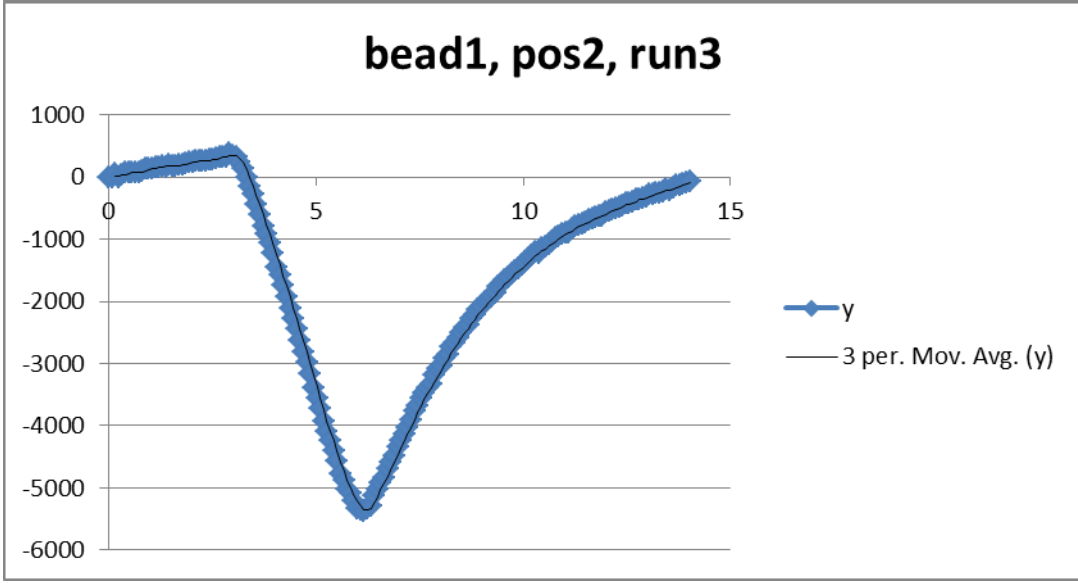
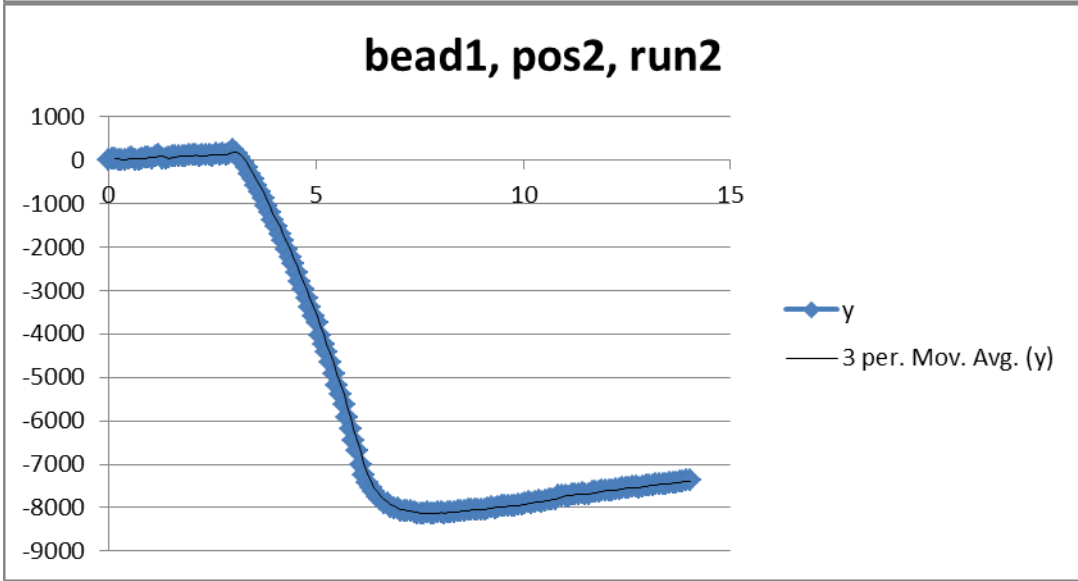
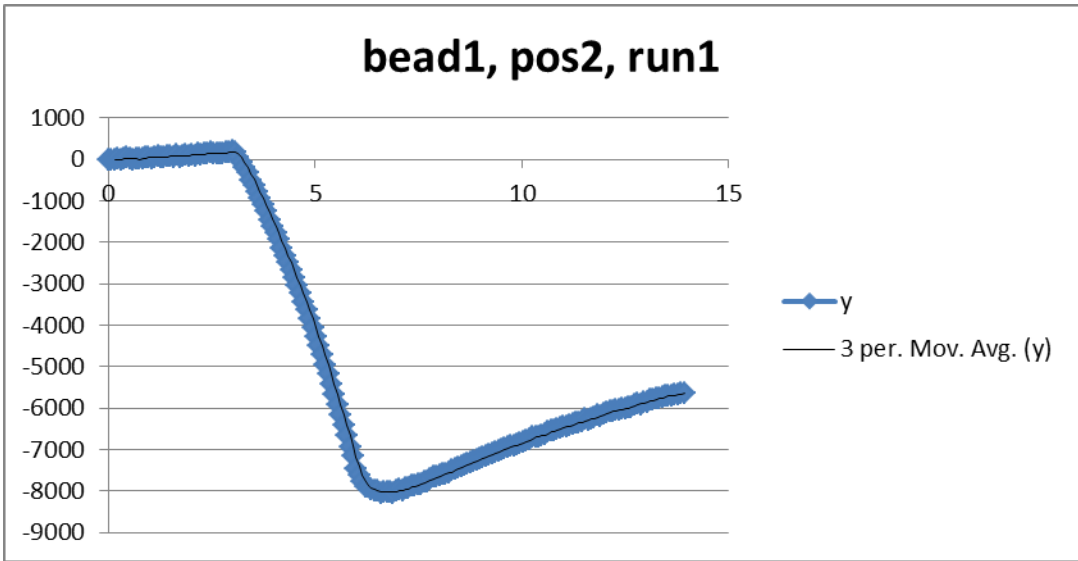
For reference, beads are labeled by Position (P) and Bead (B) on the spatial distribution plots below.

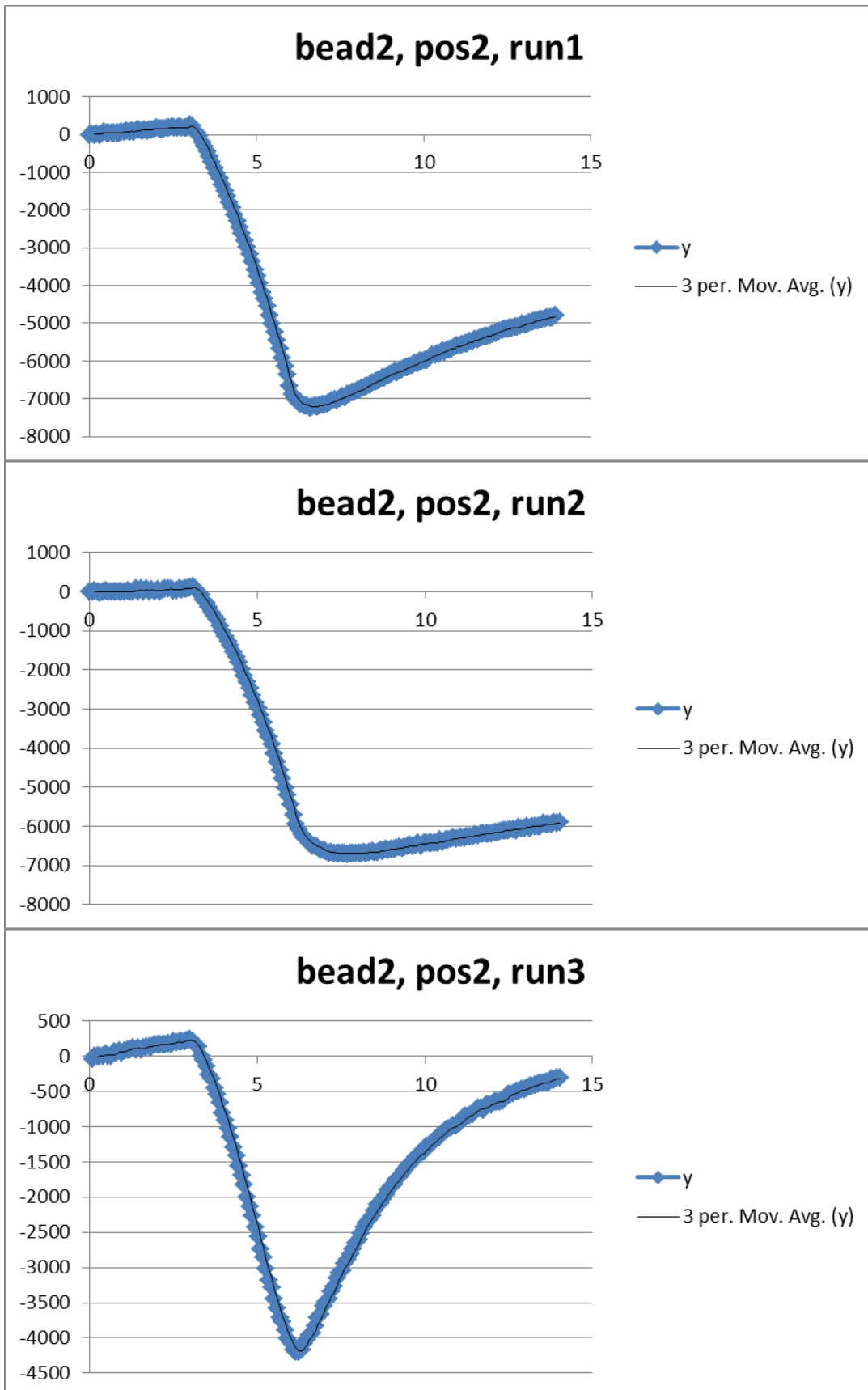


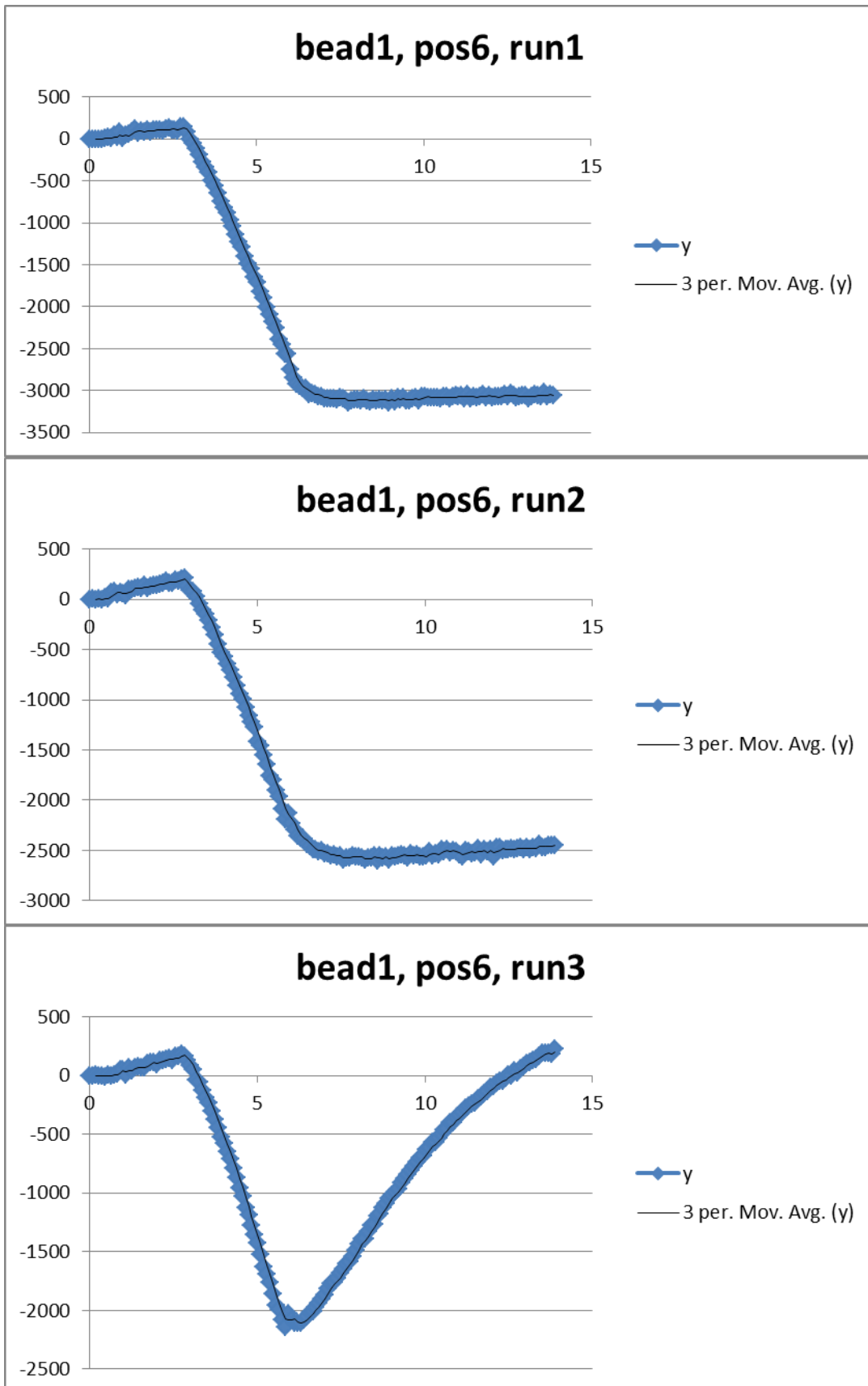


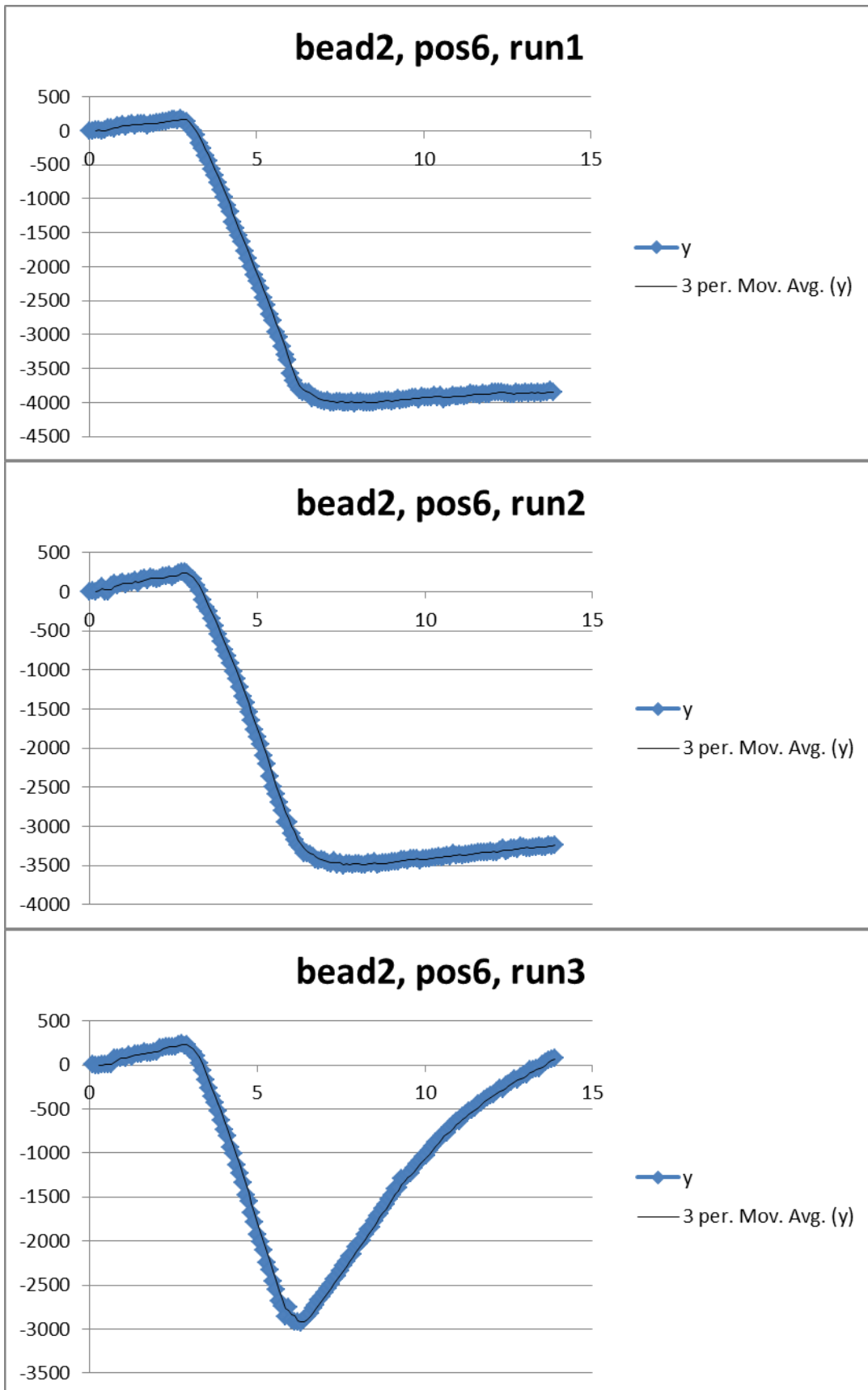
All plots represent Y-Displacement (nm) vs. Time

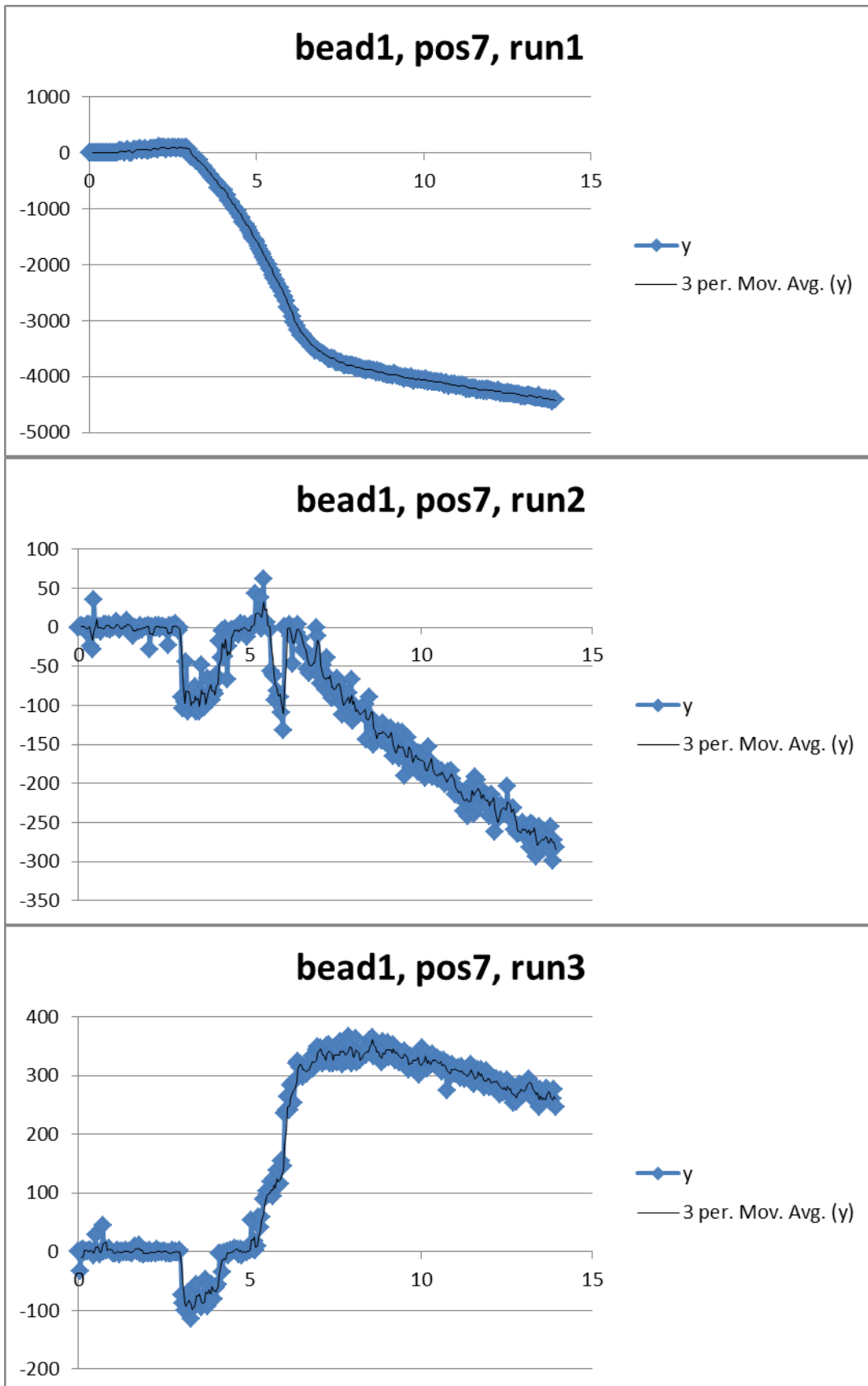


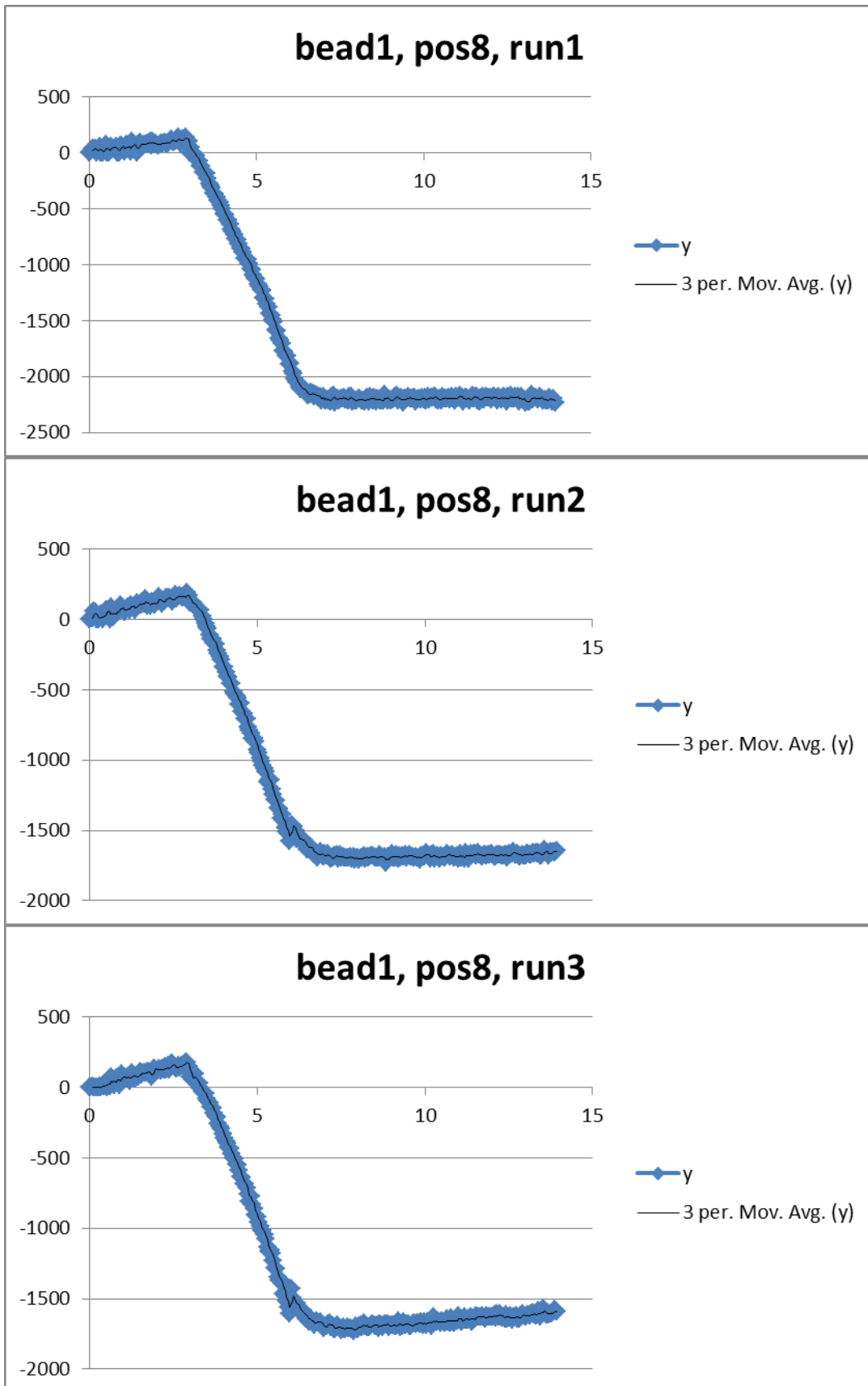


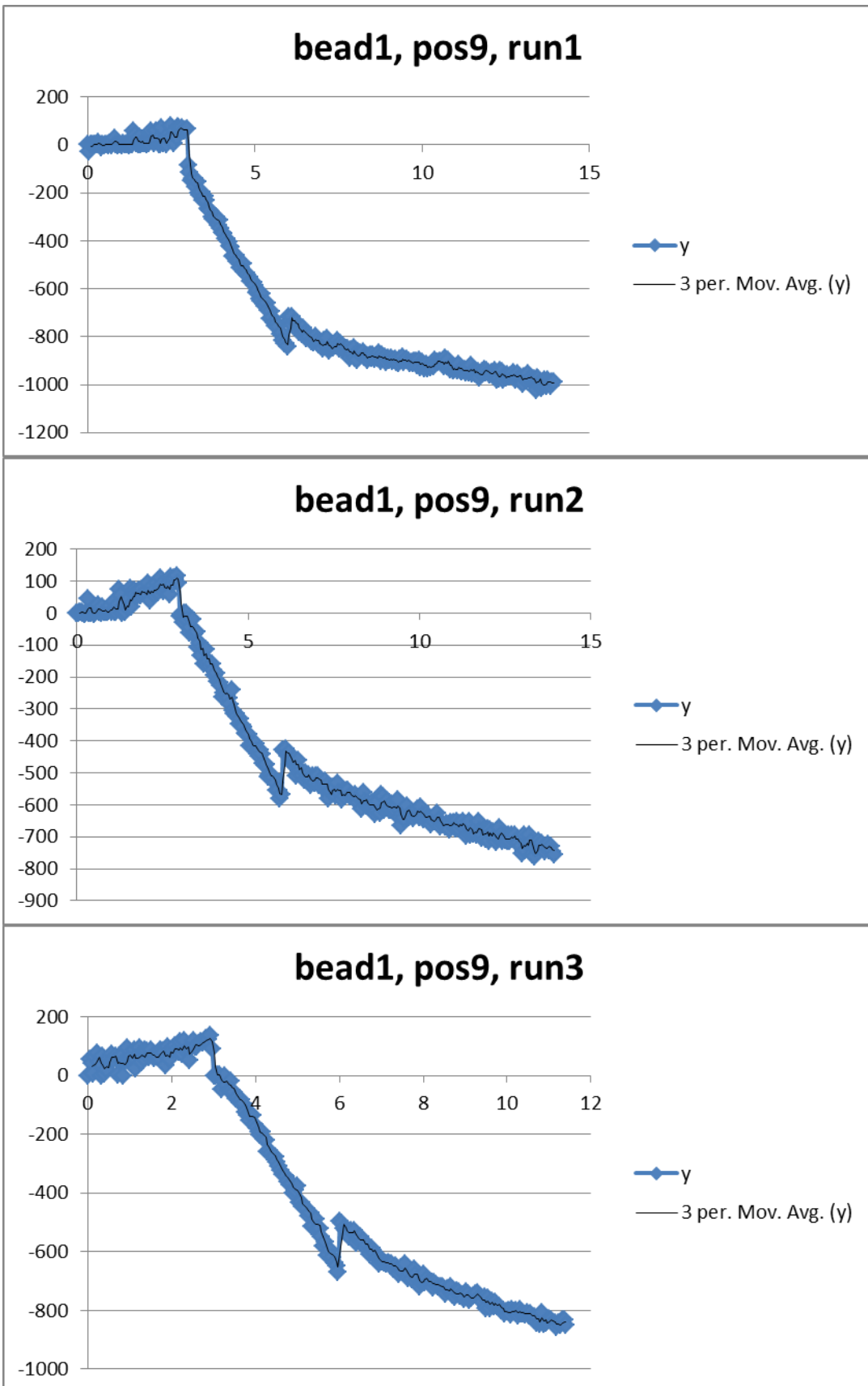


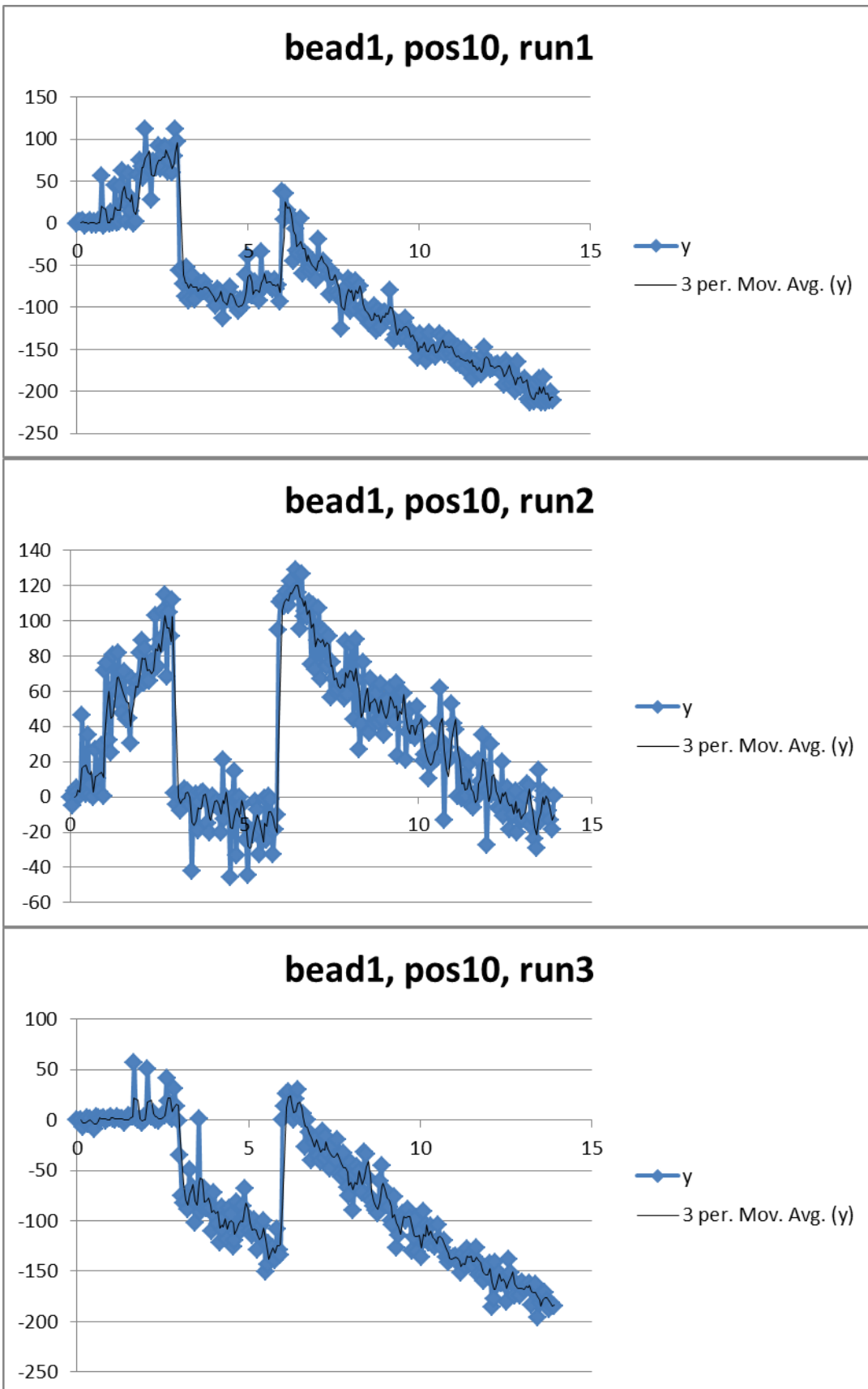


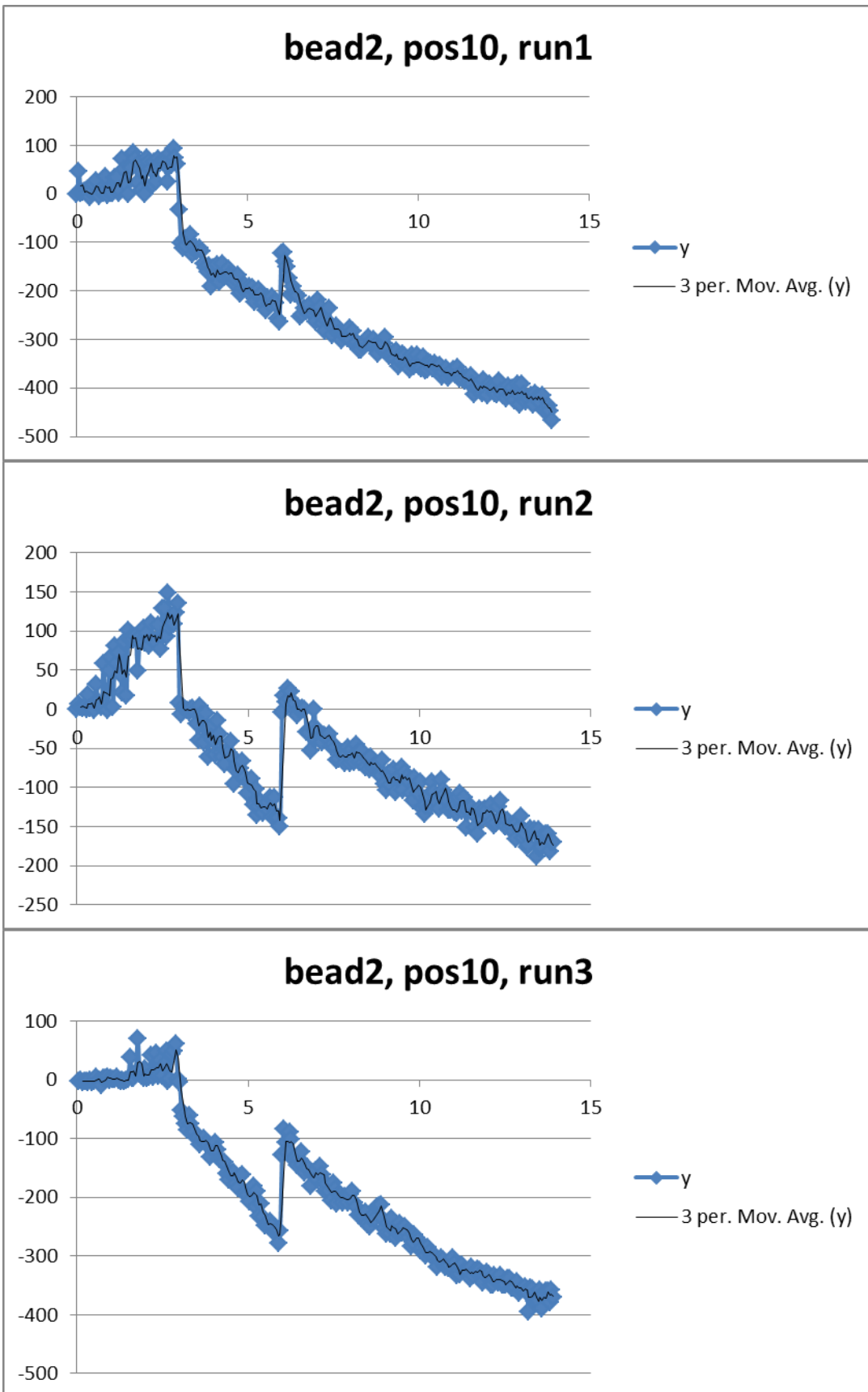


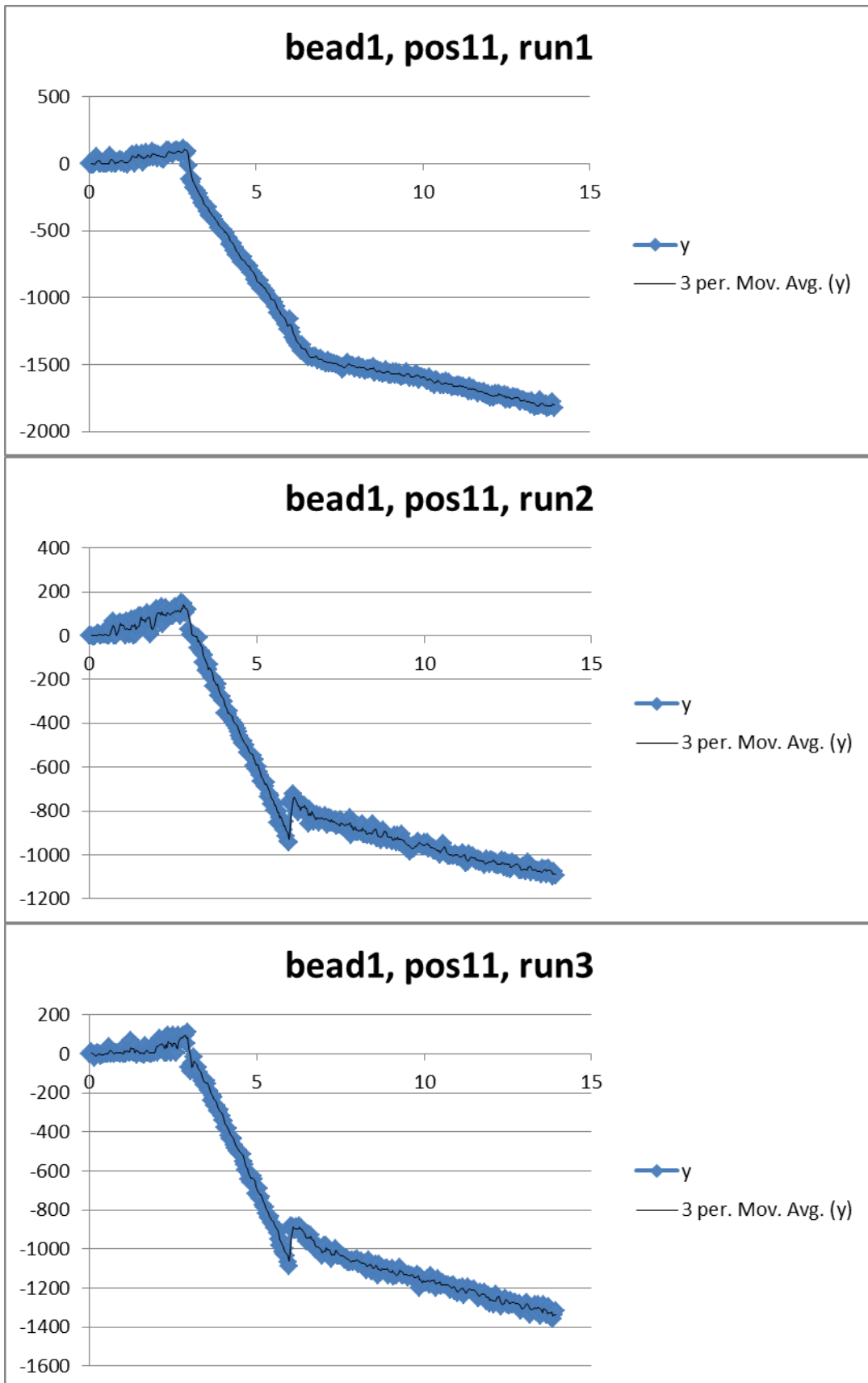


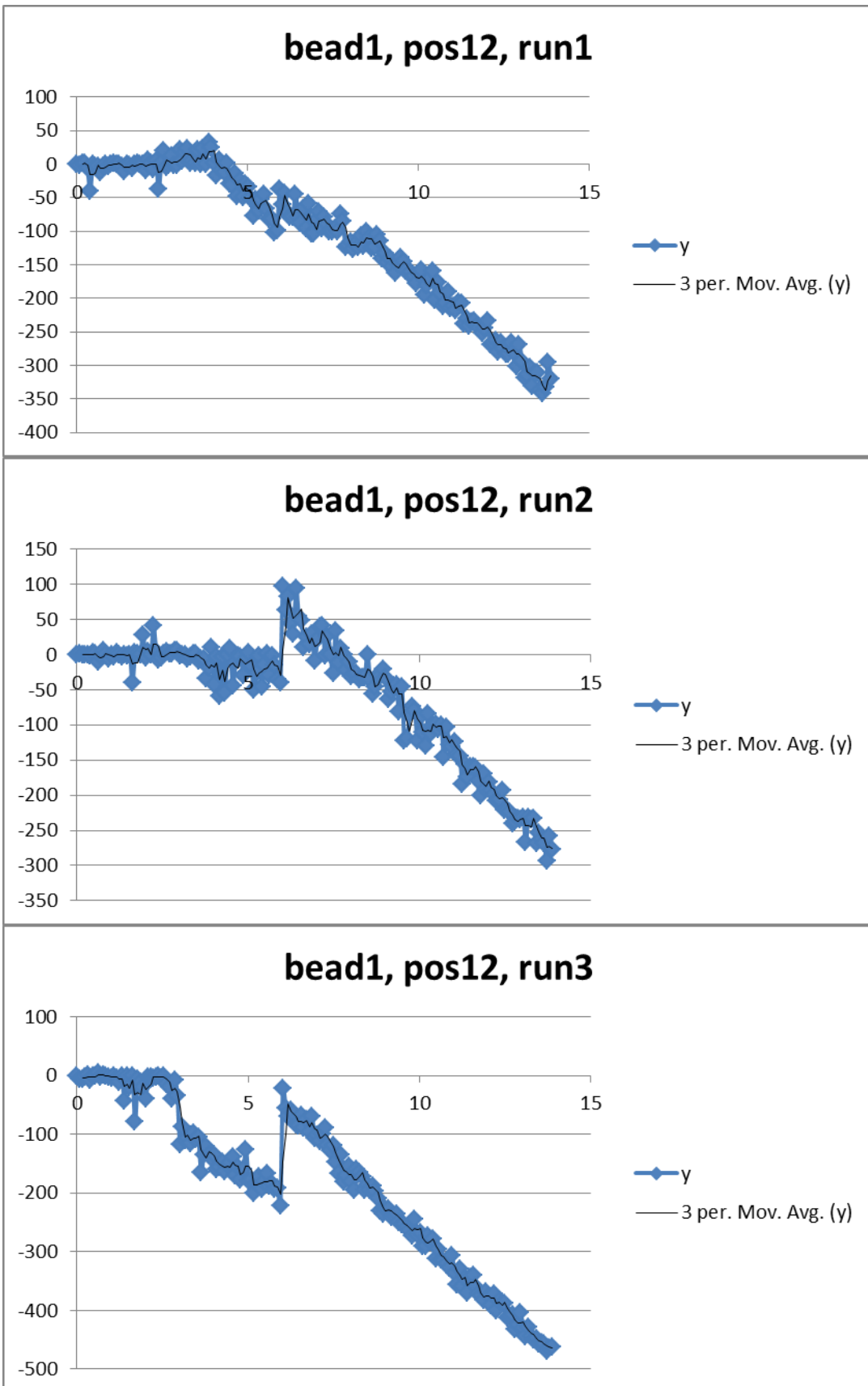


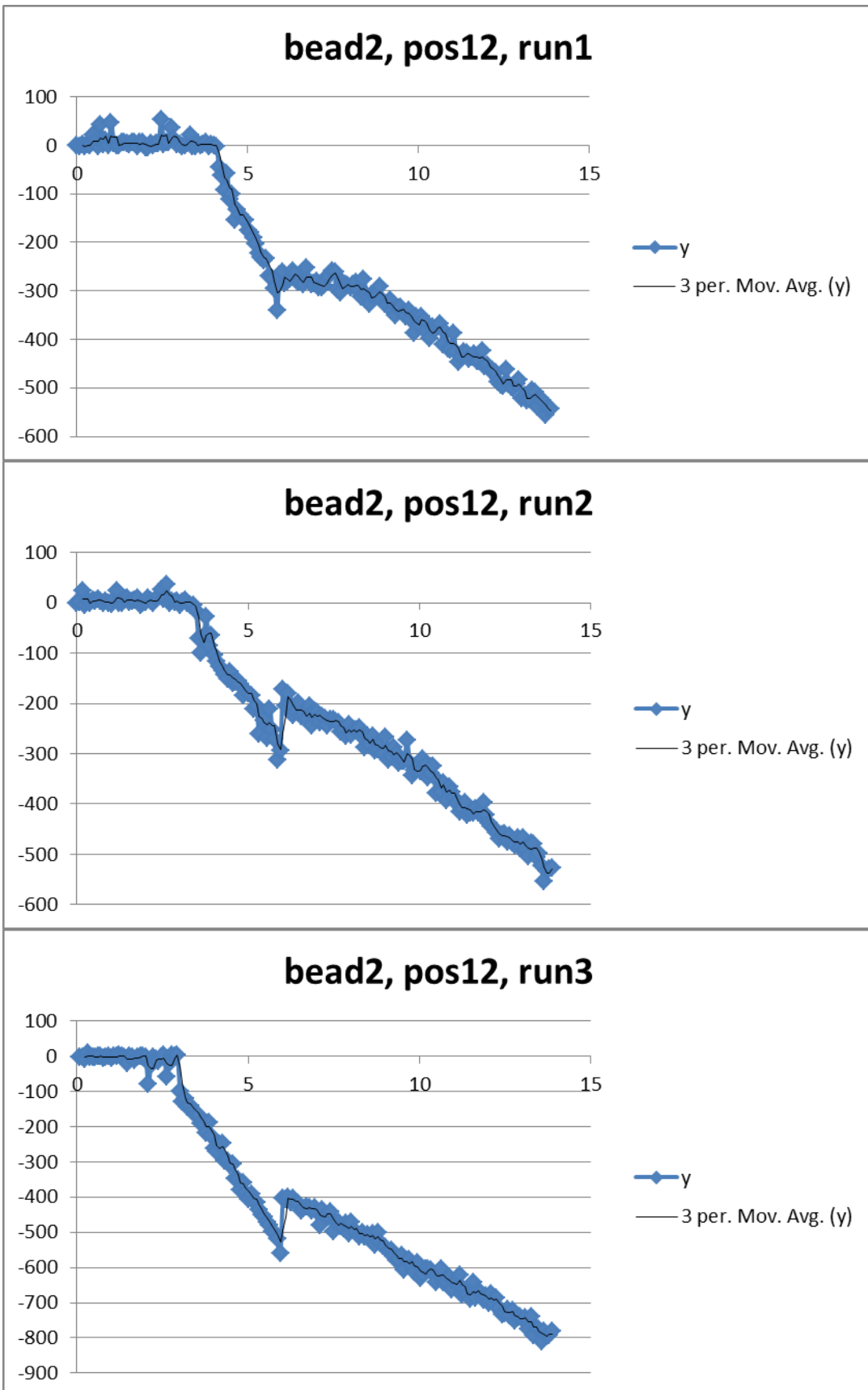


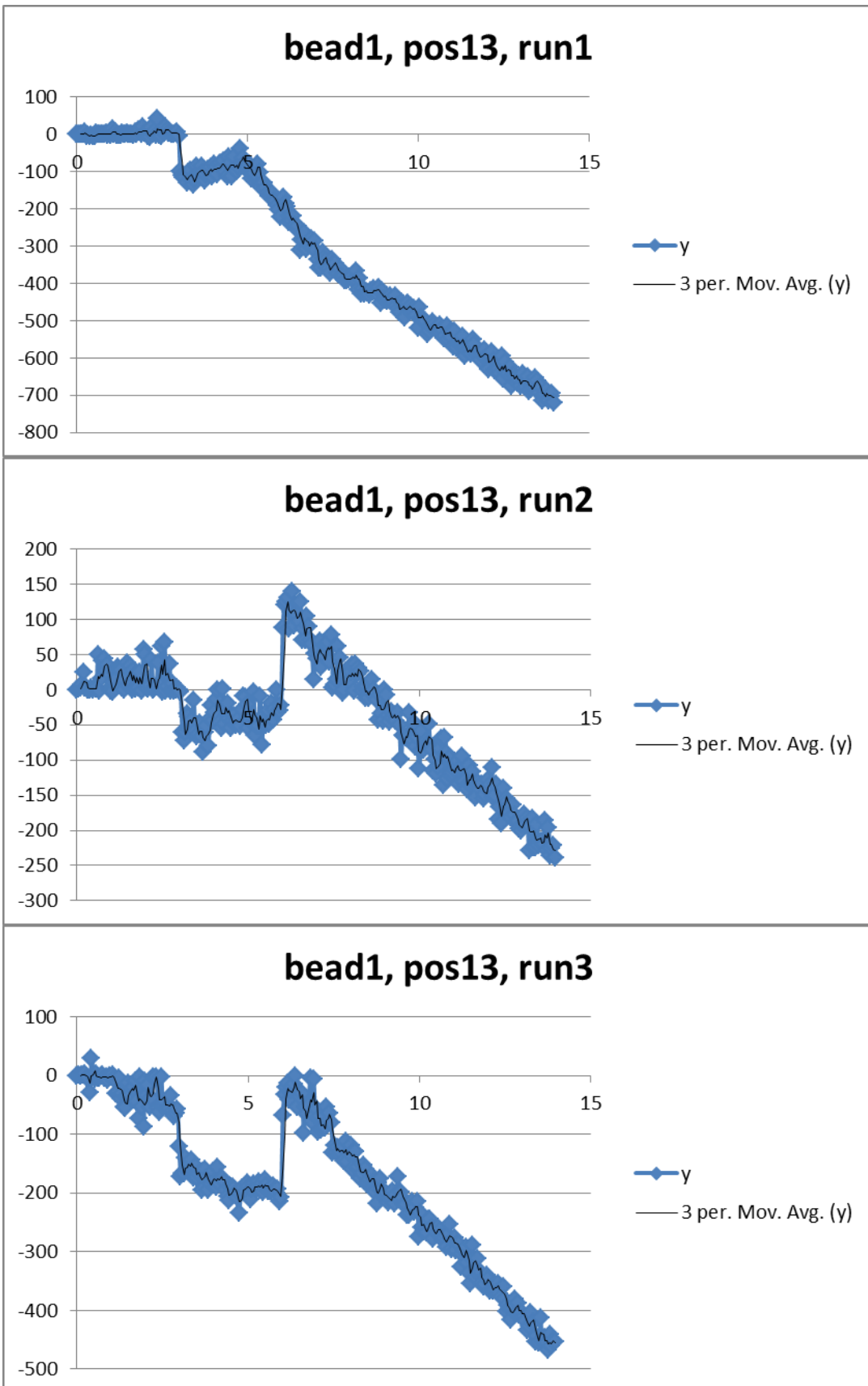


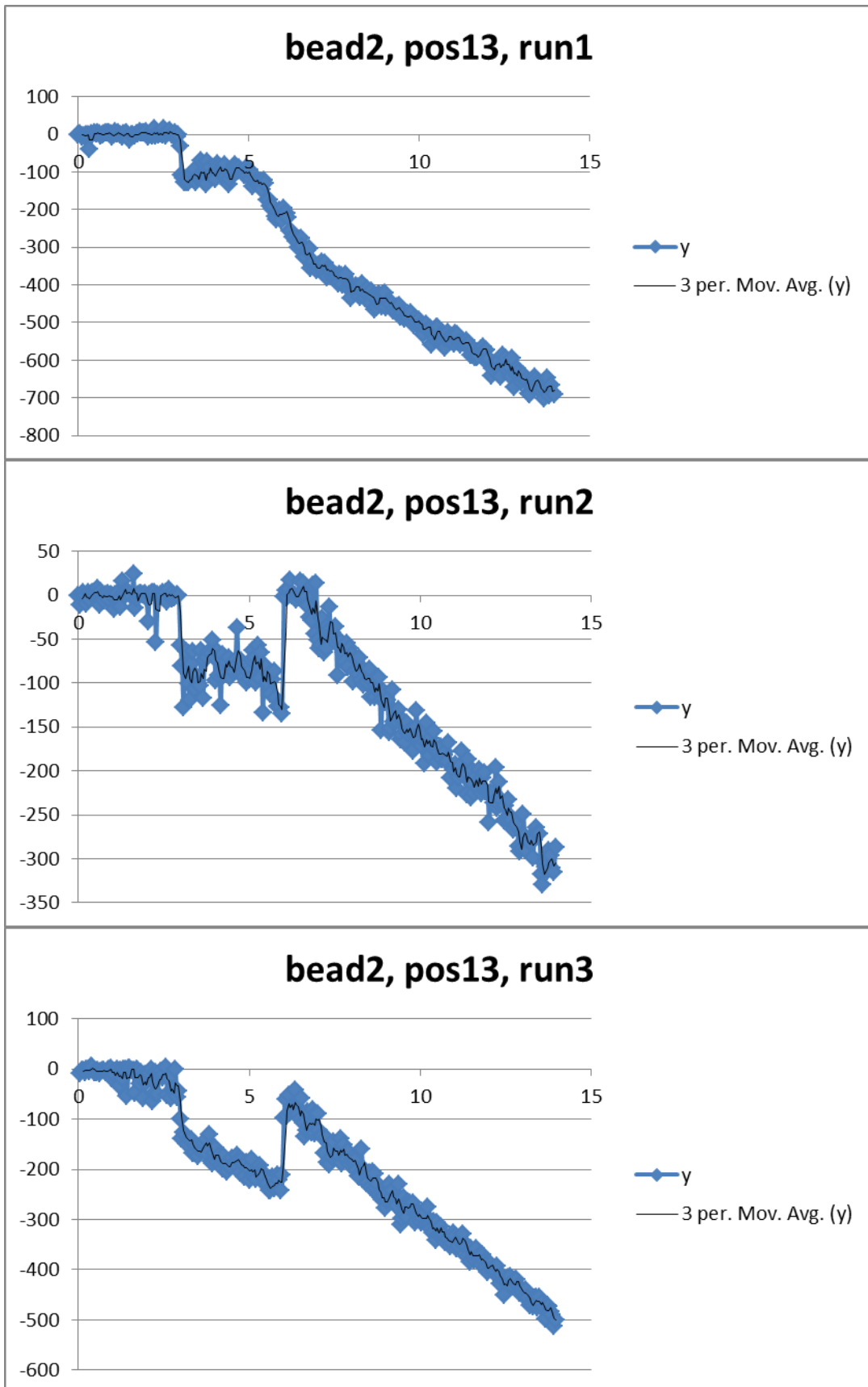


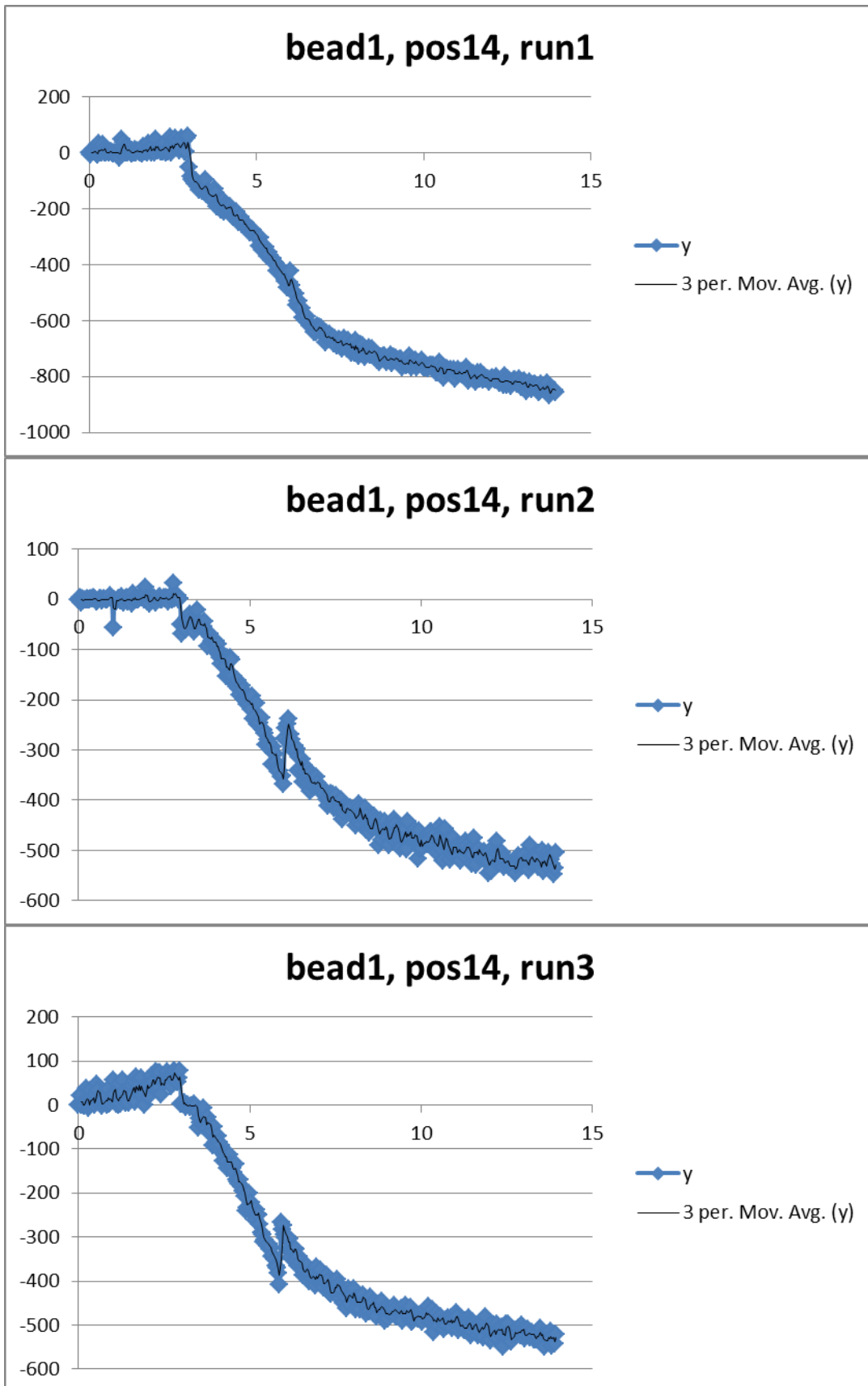


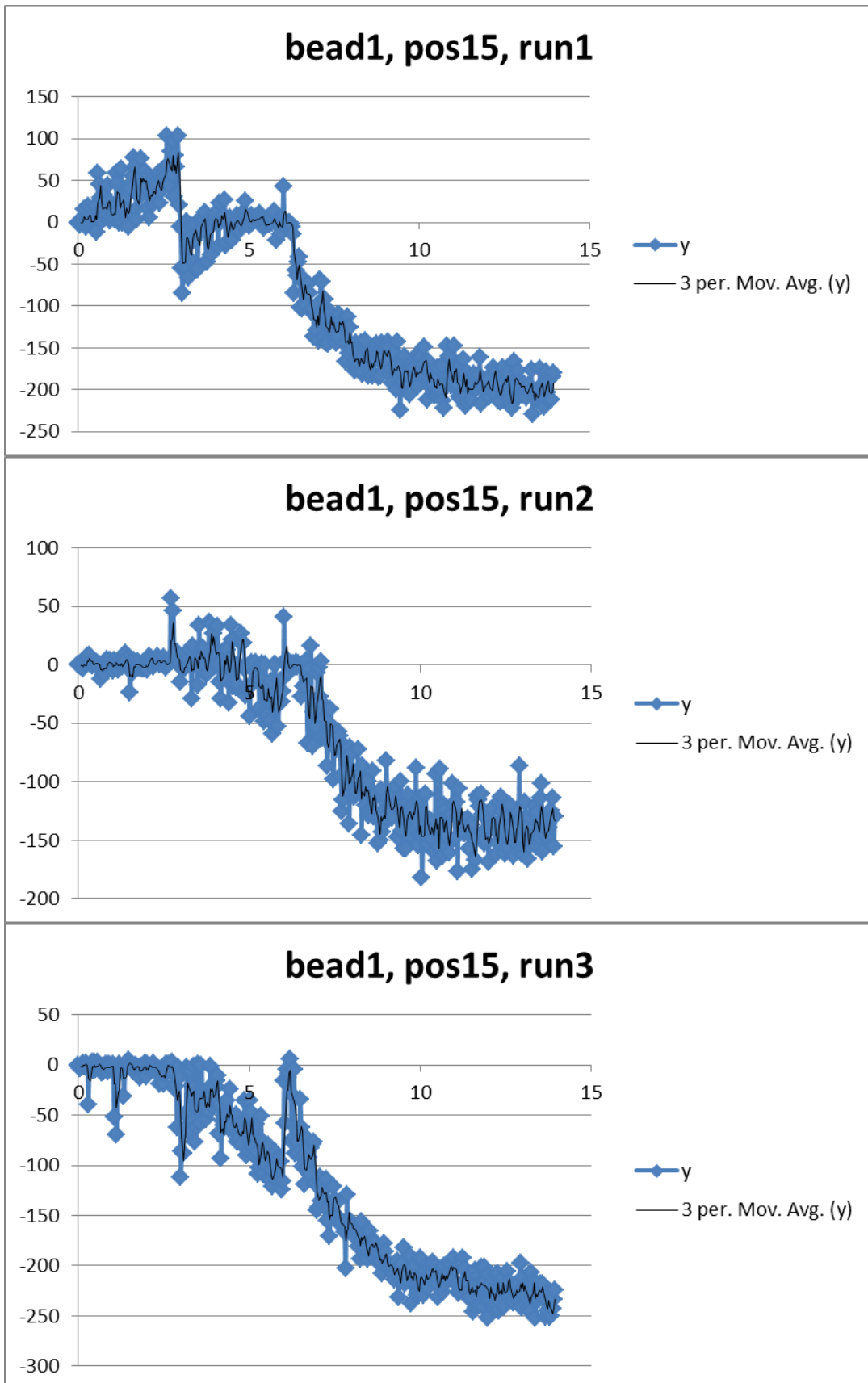


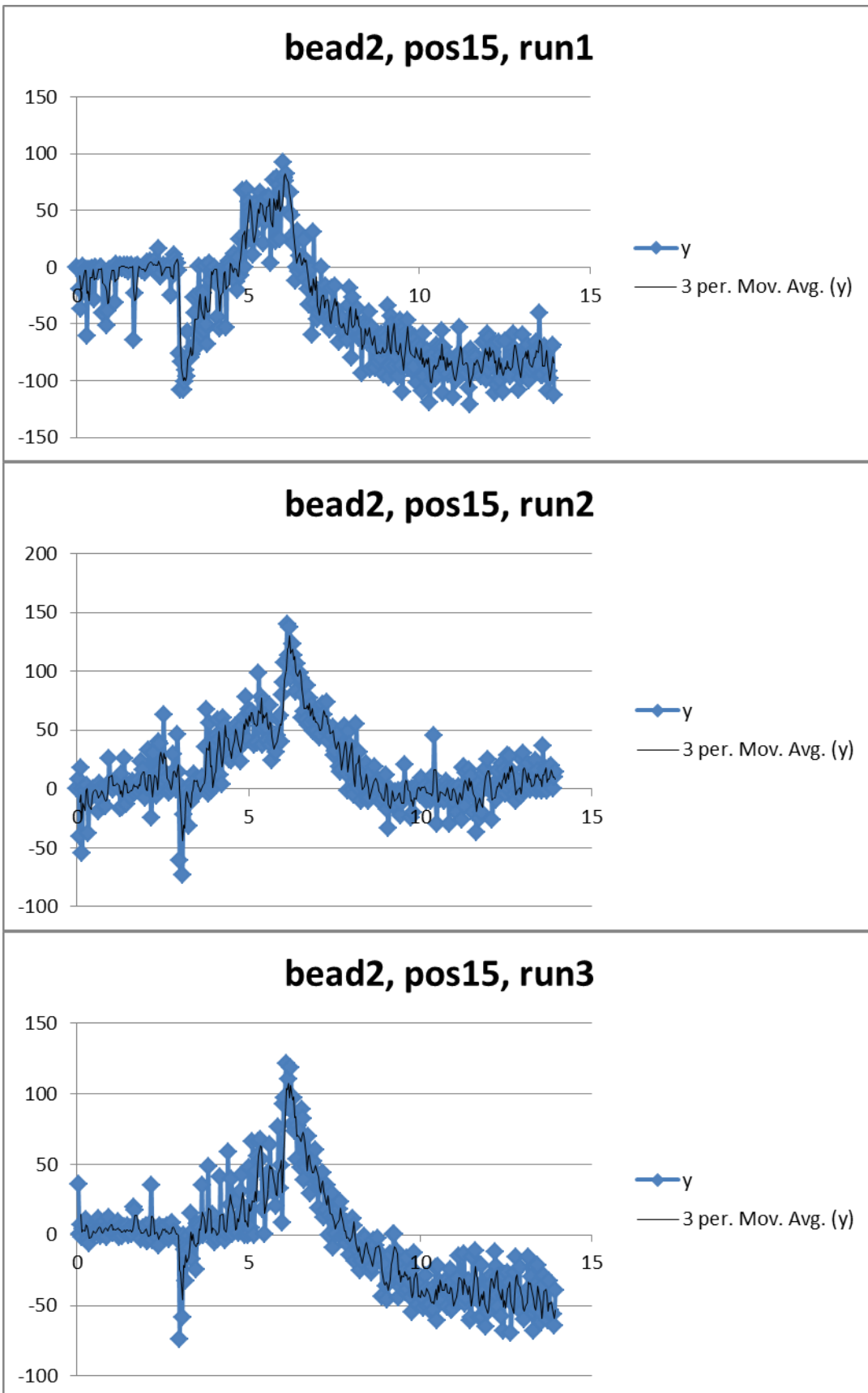


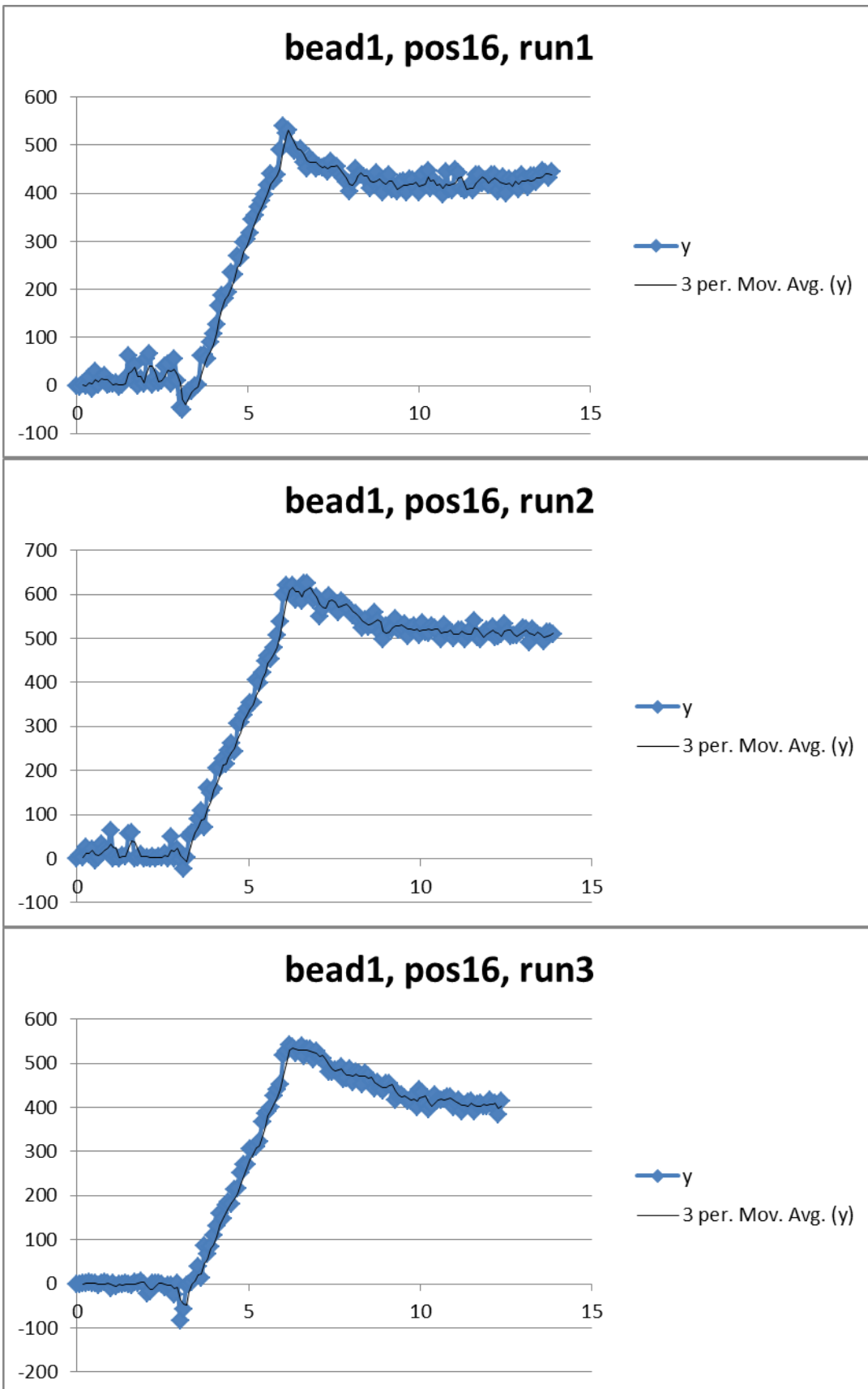


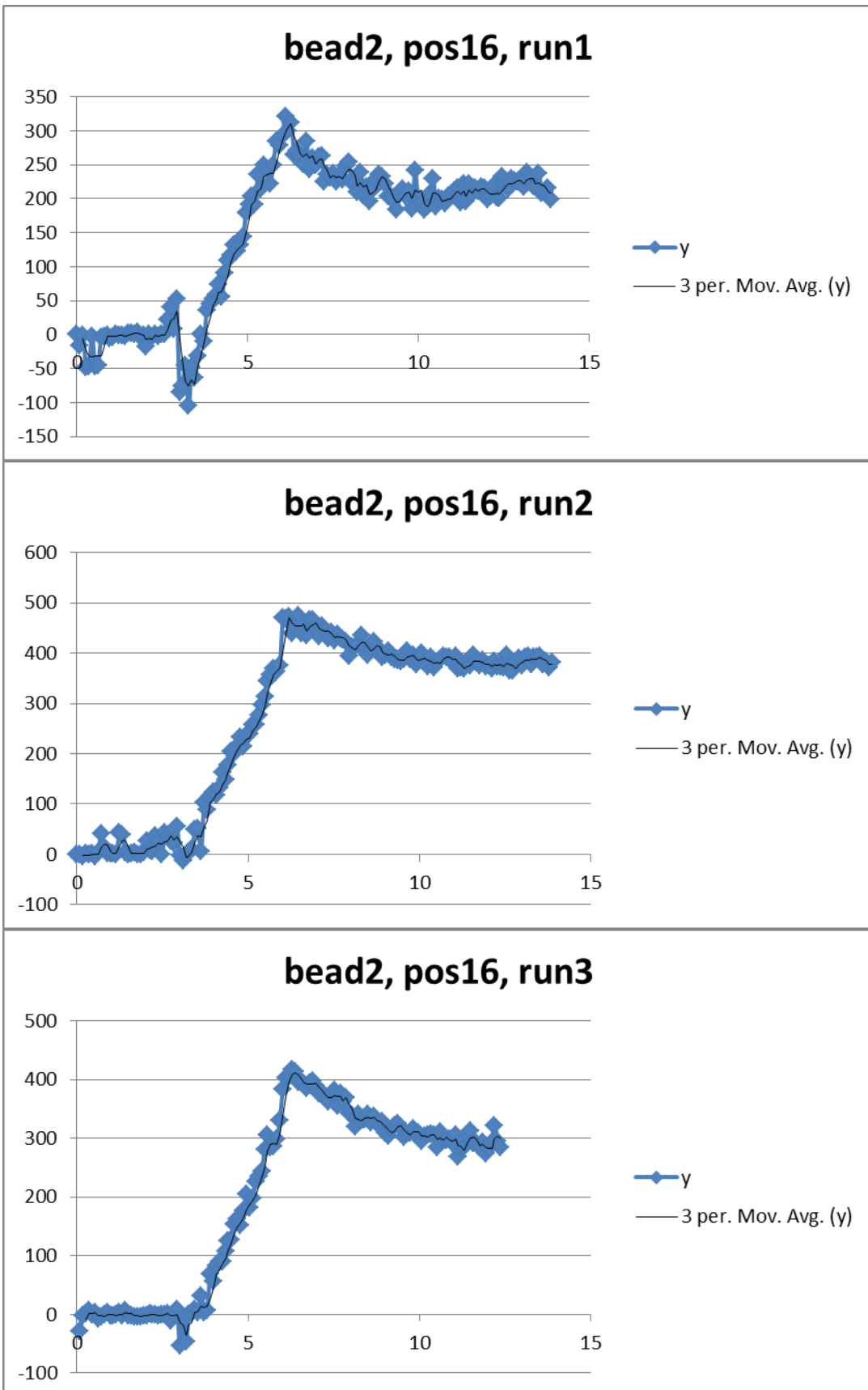


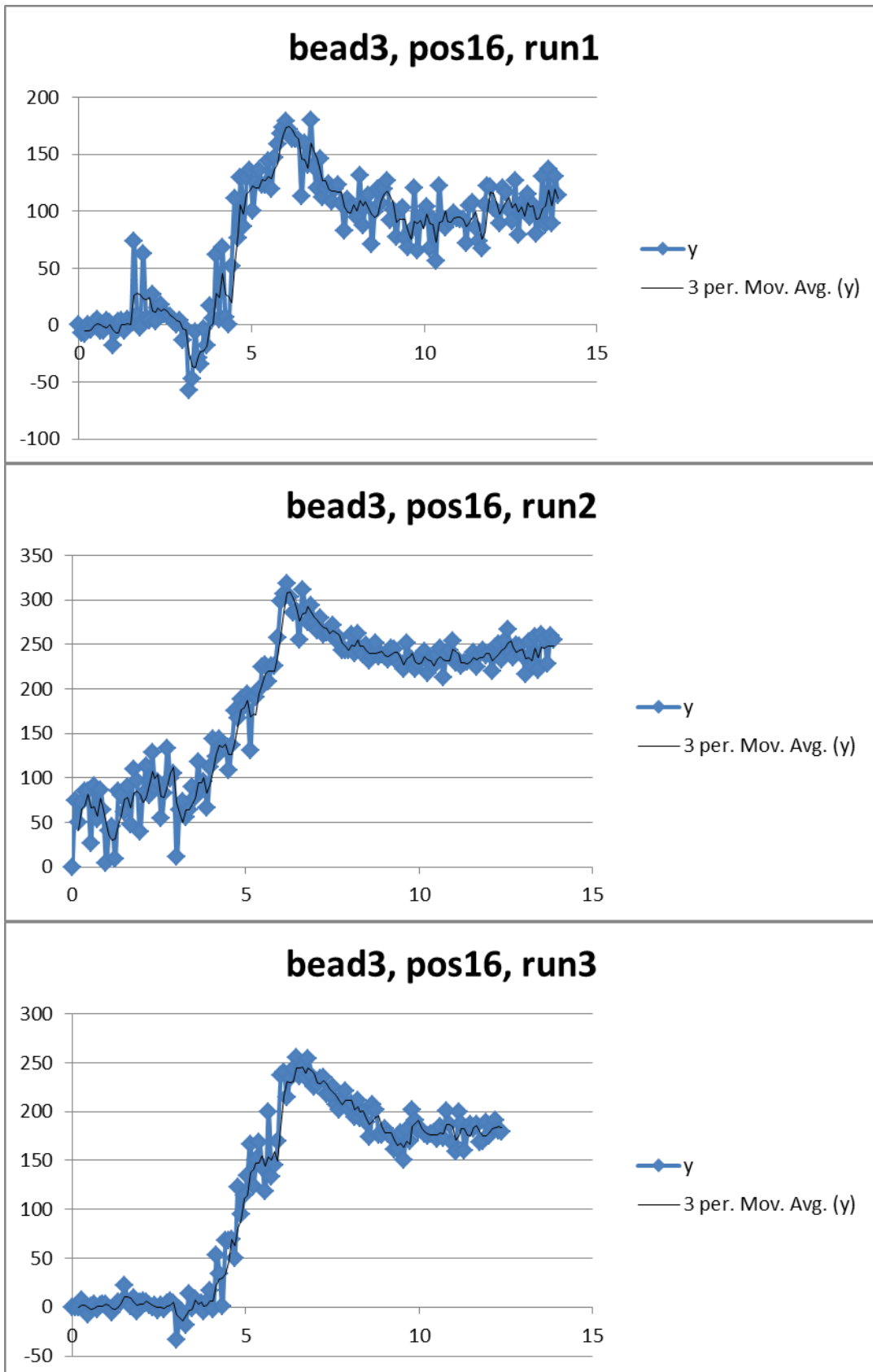


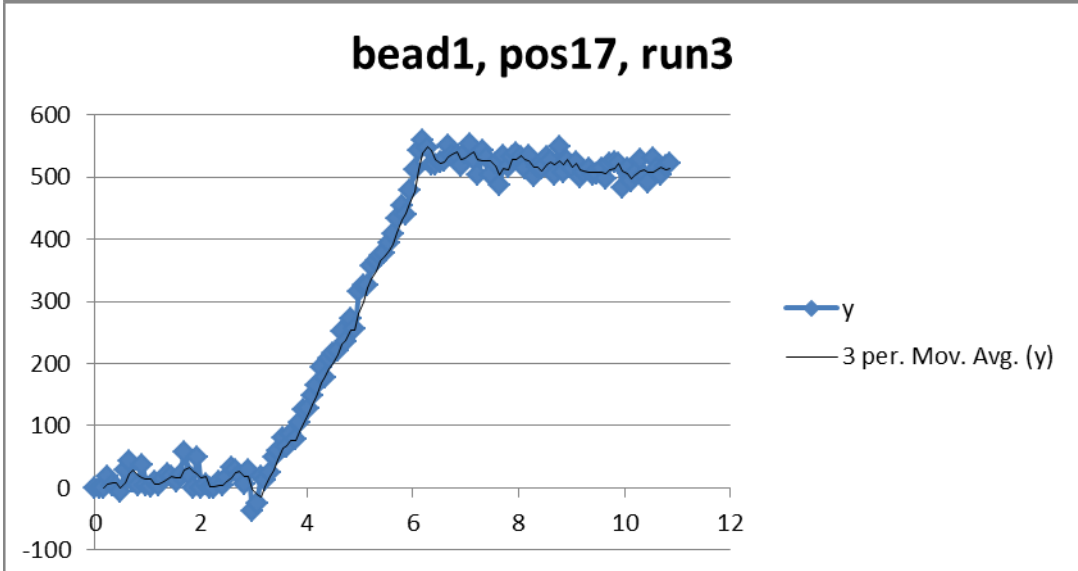
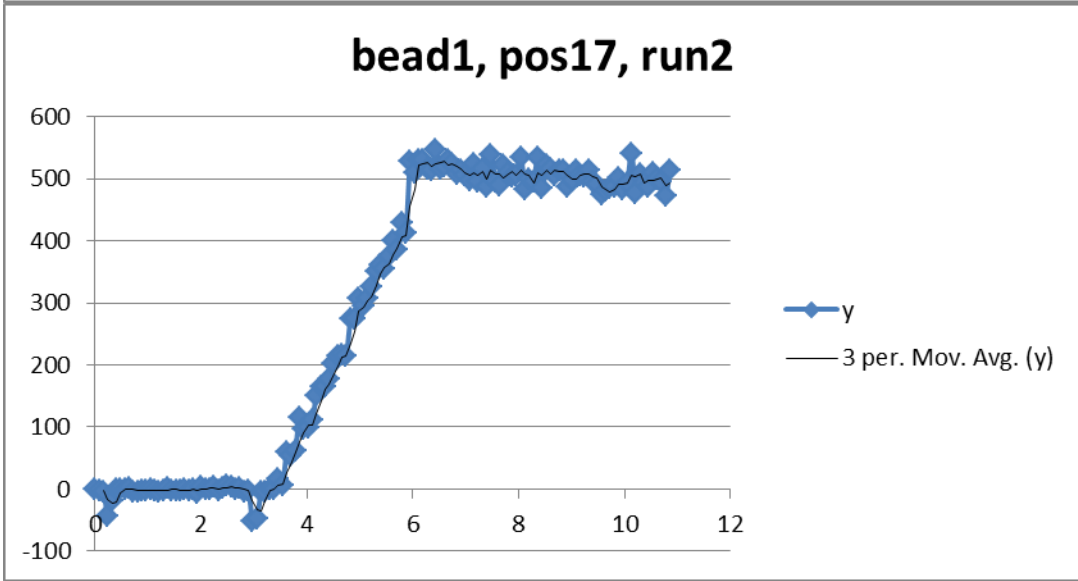
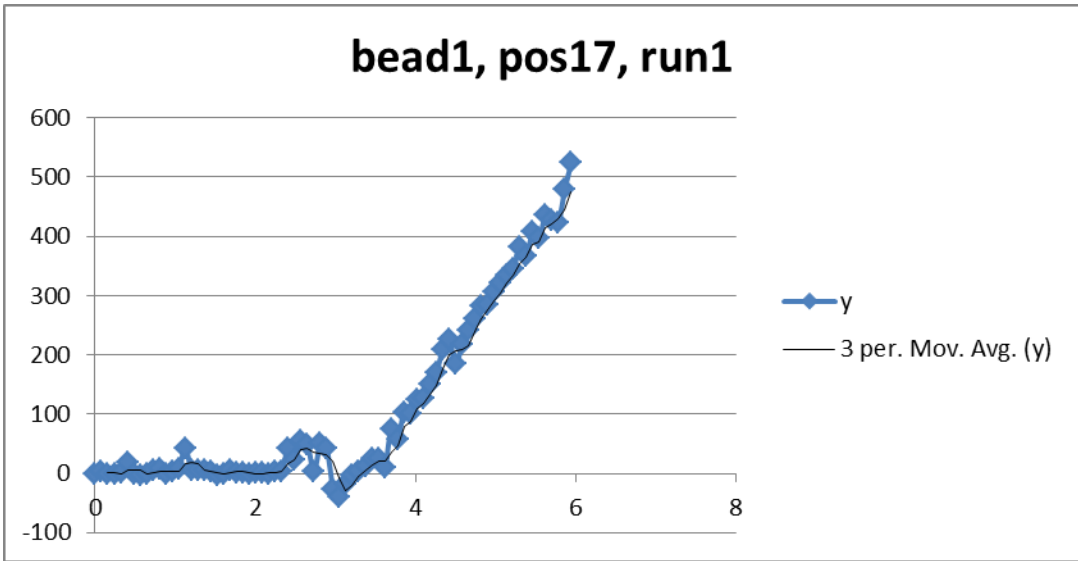


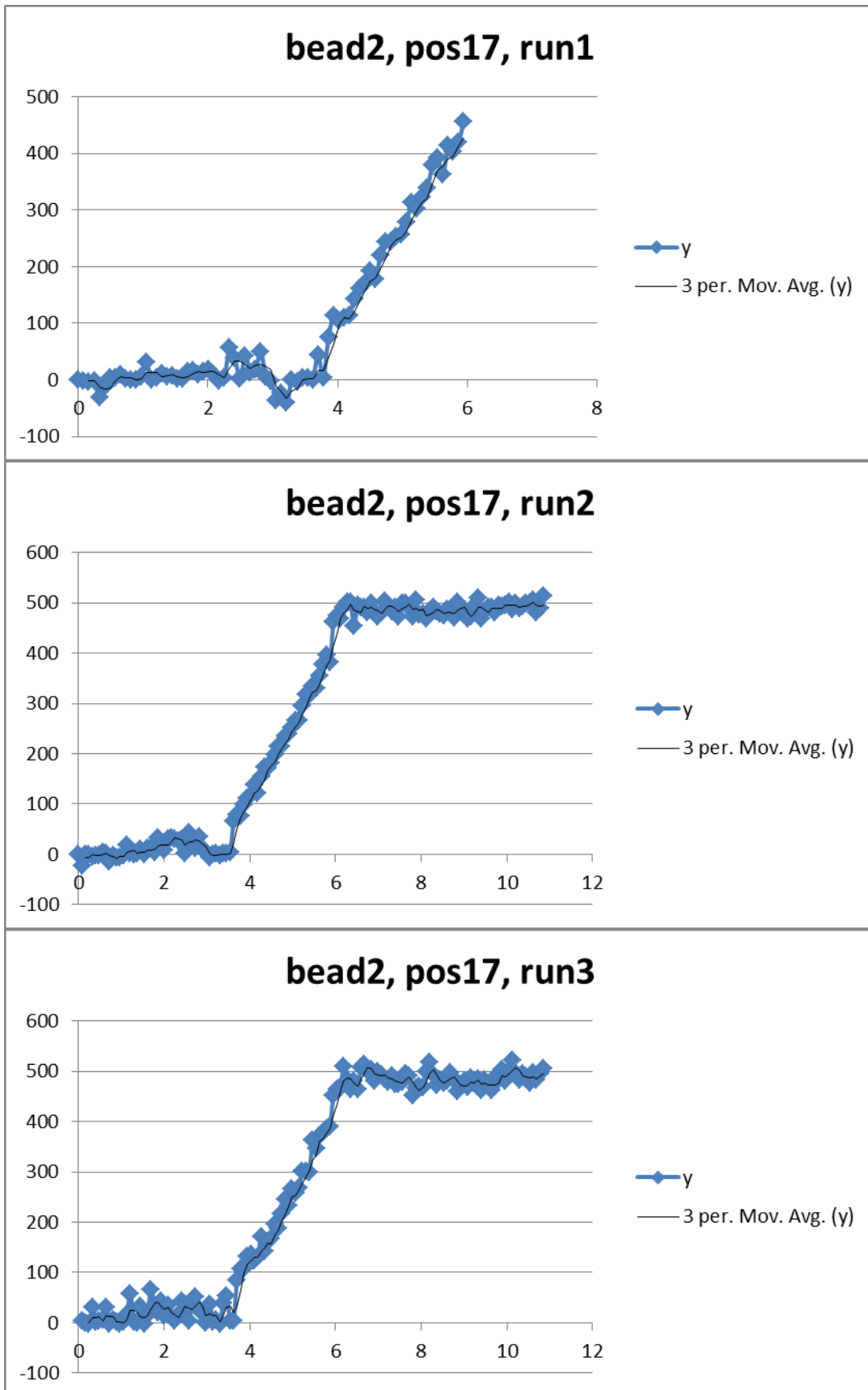


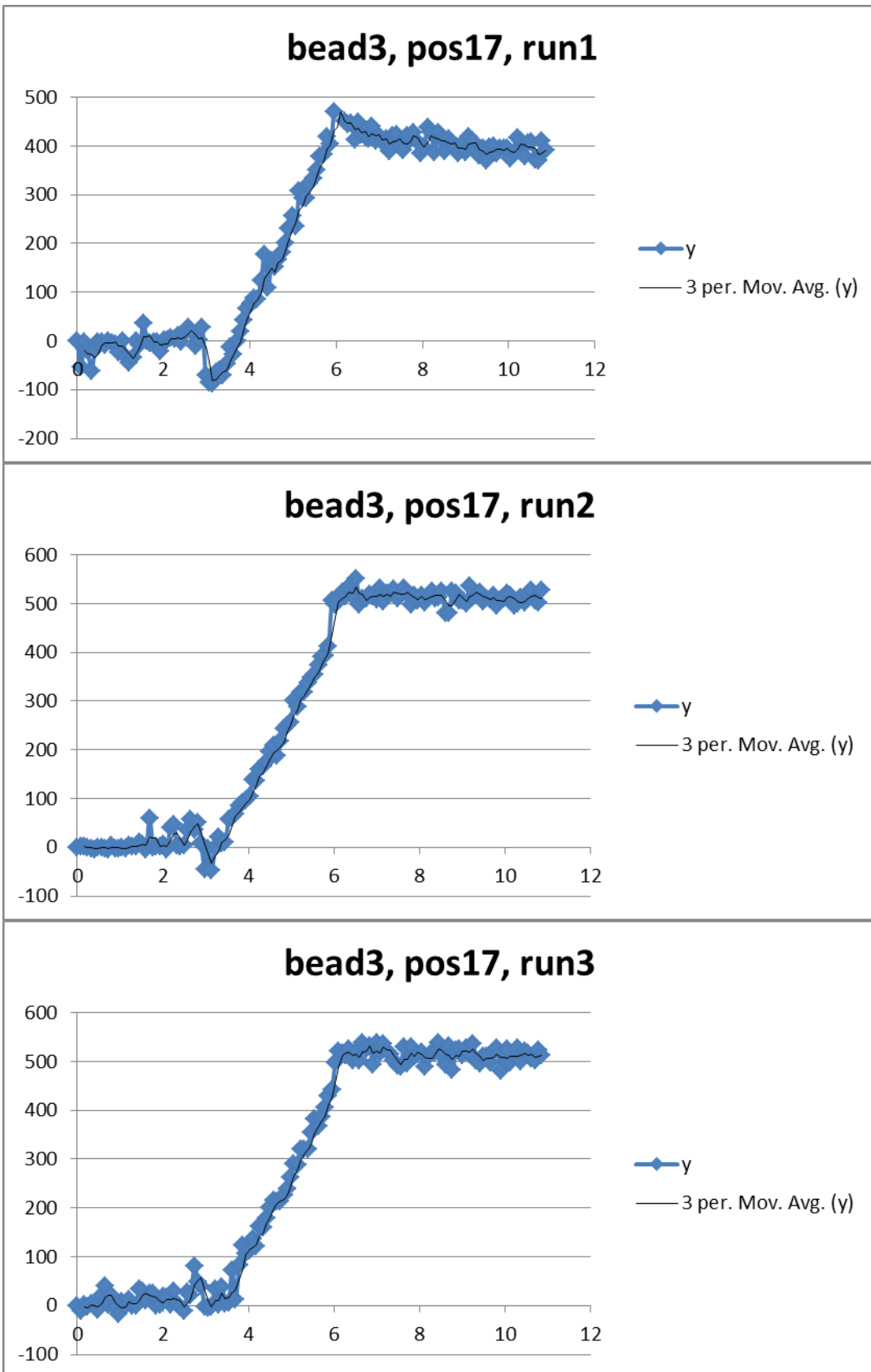


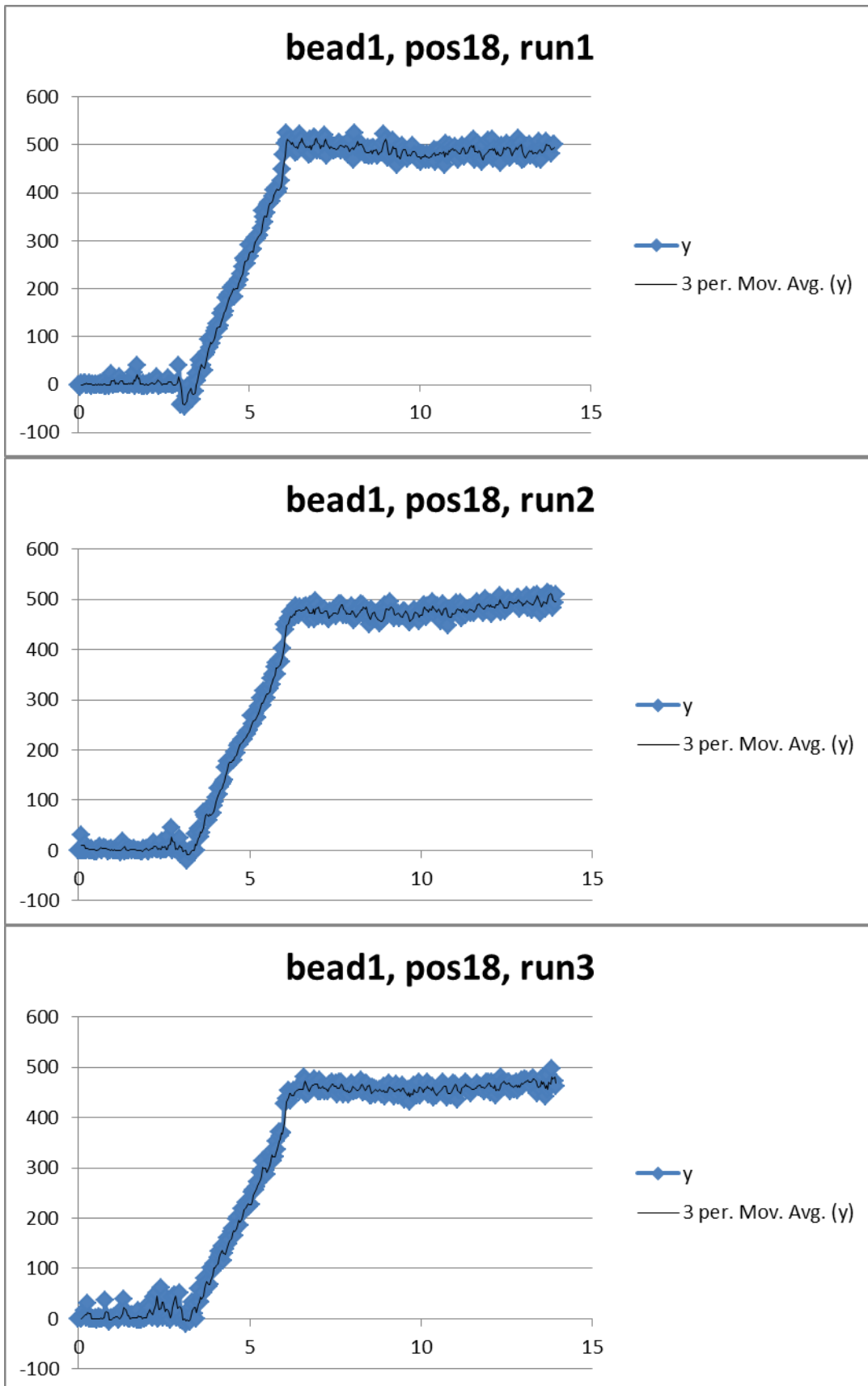


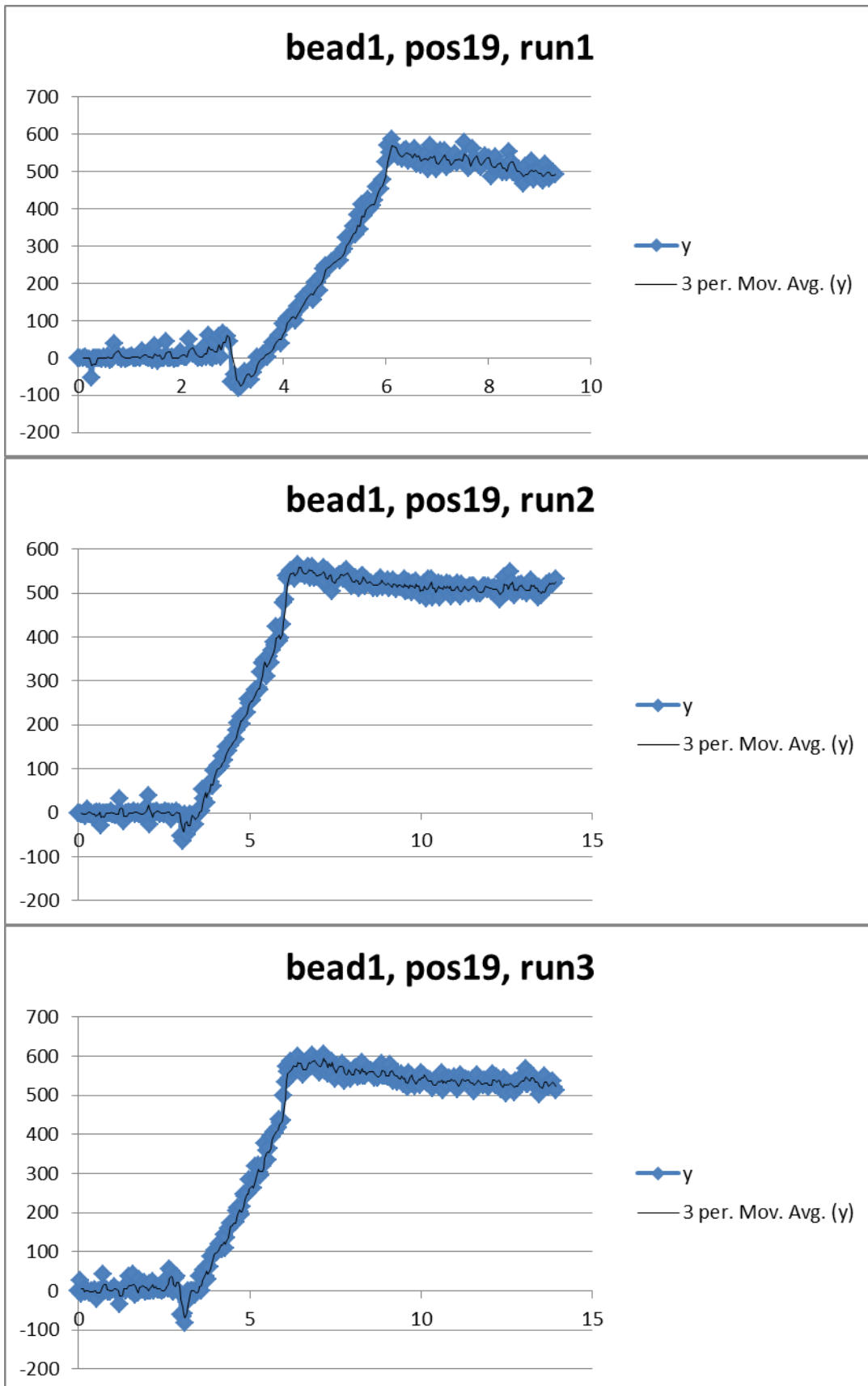


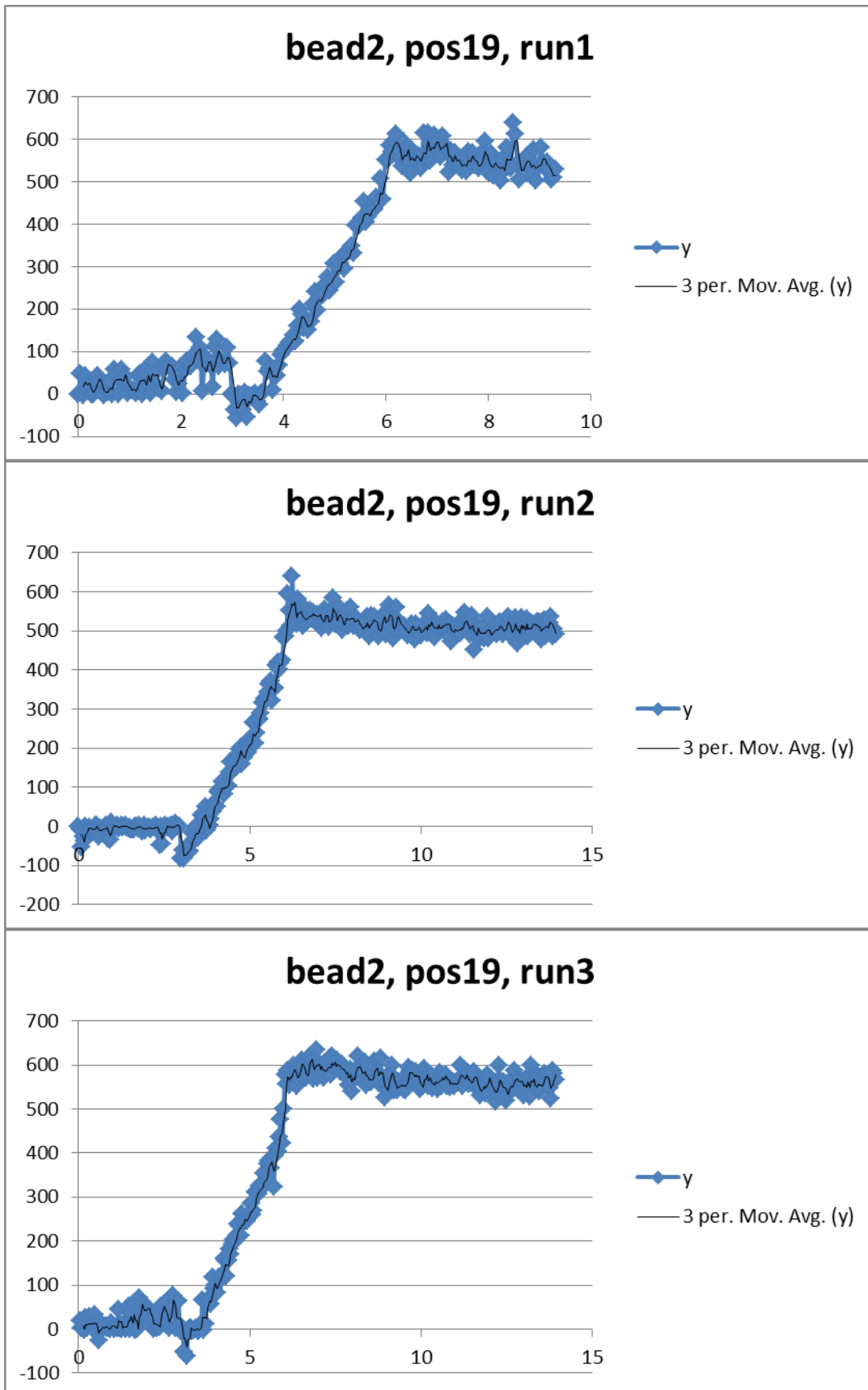


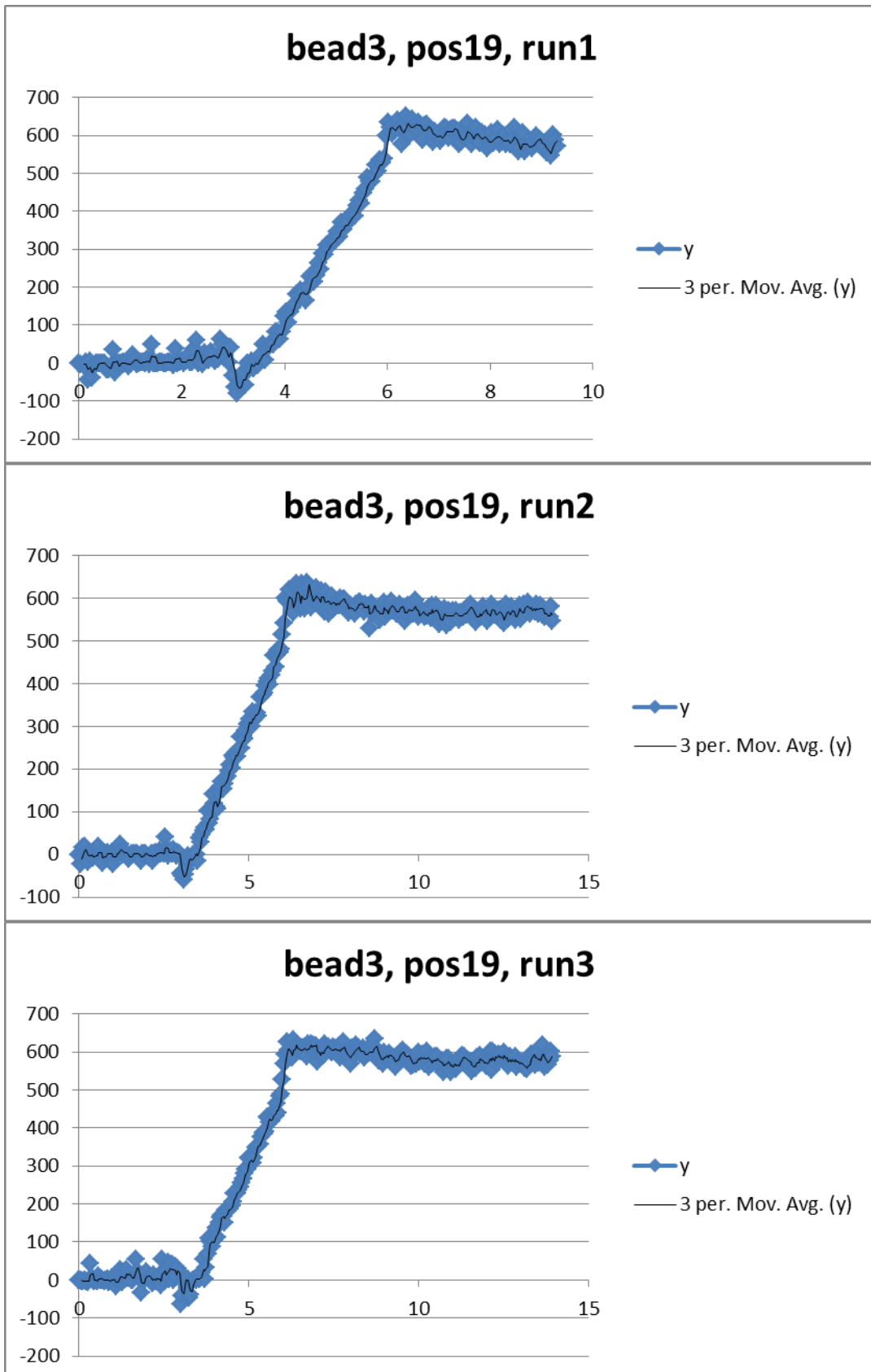


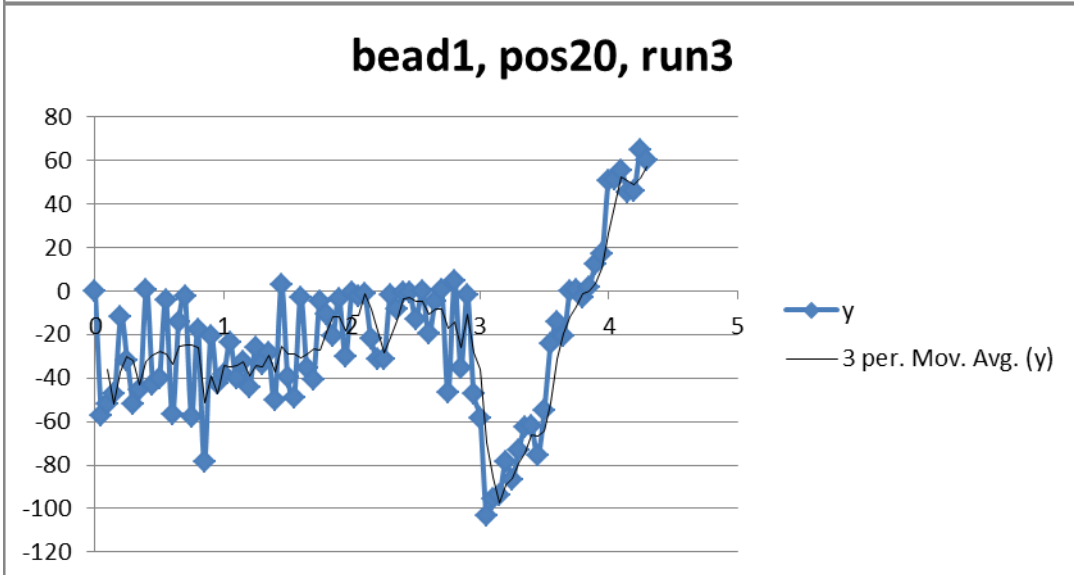
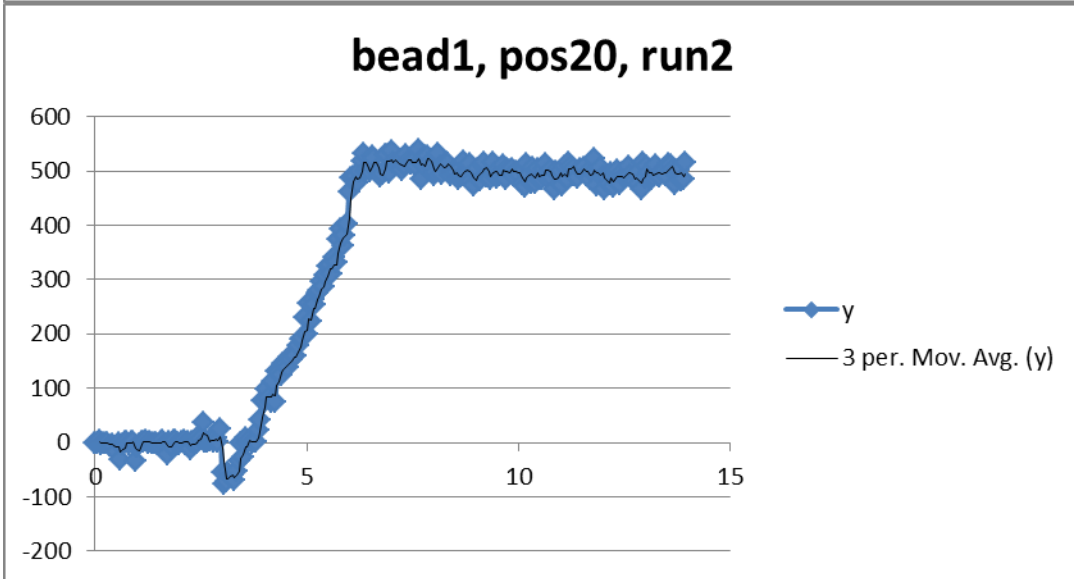
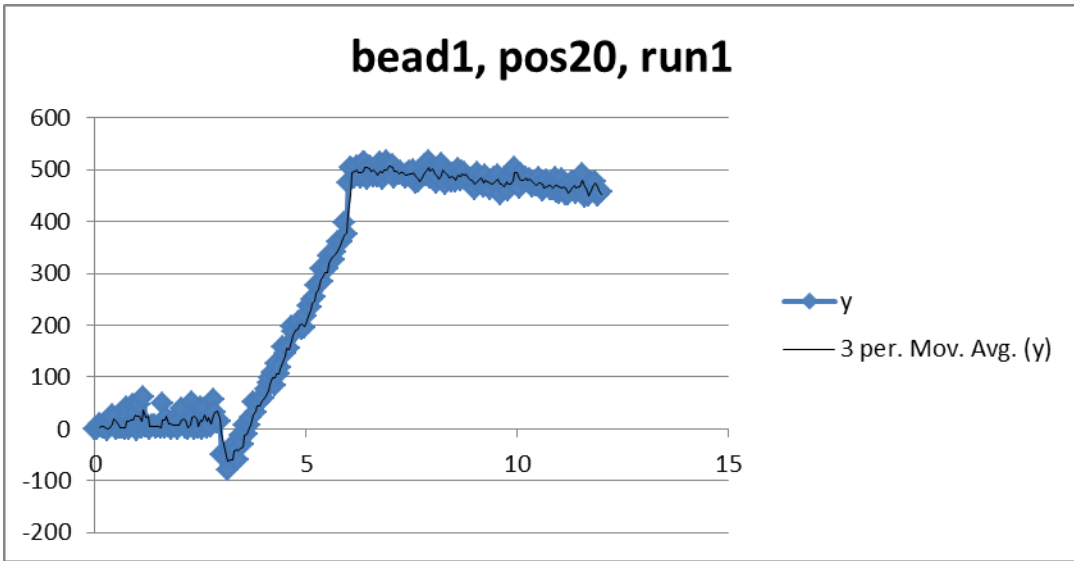


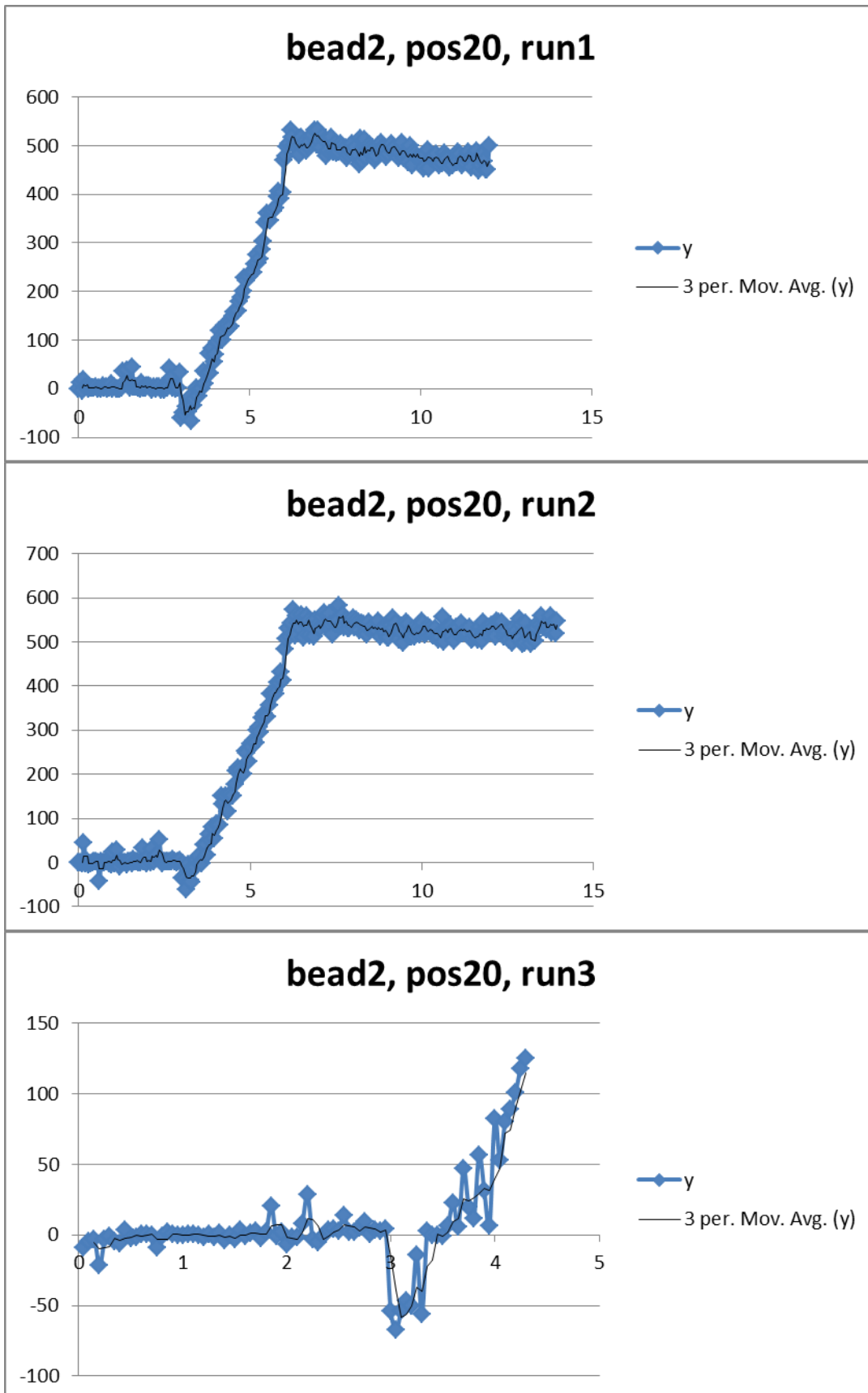


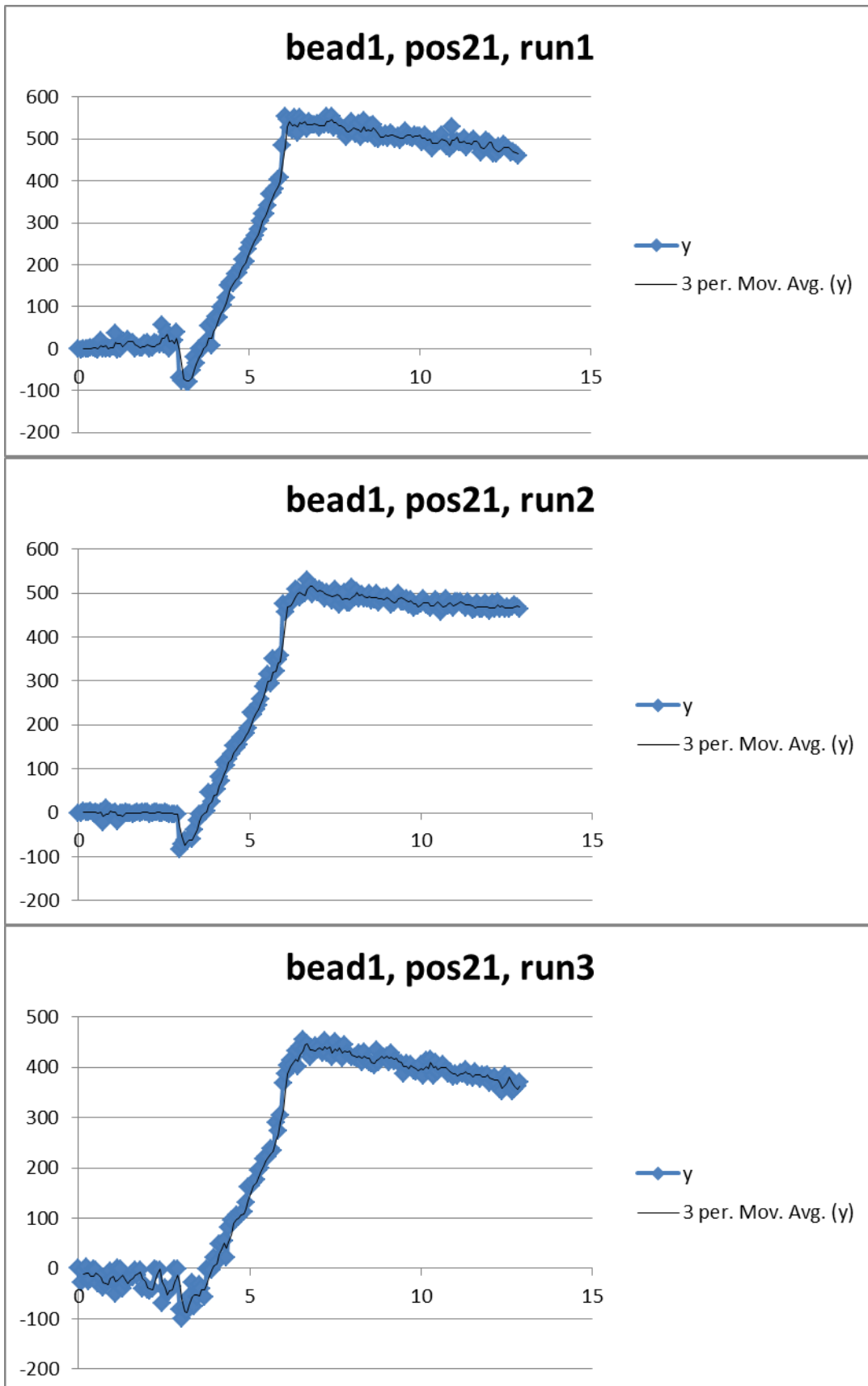


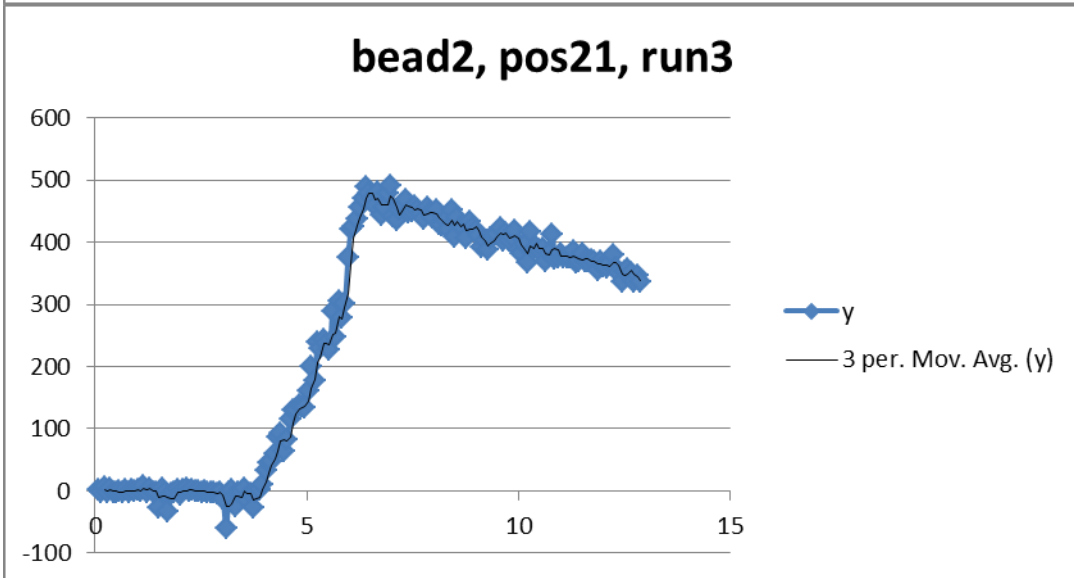
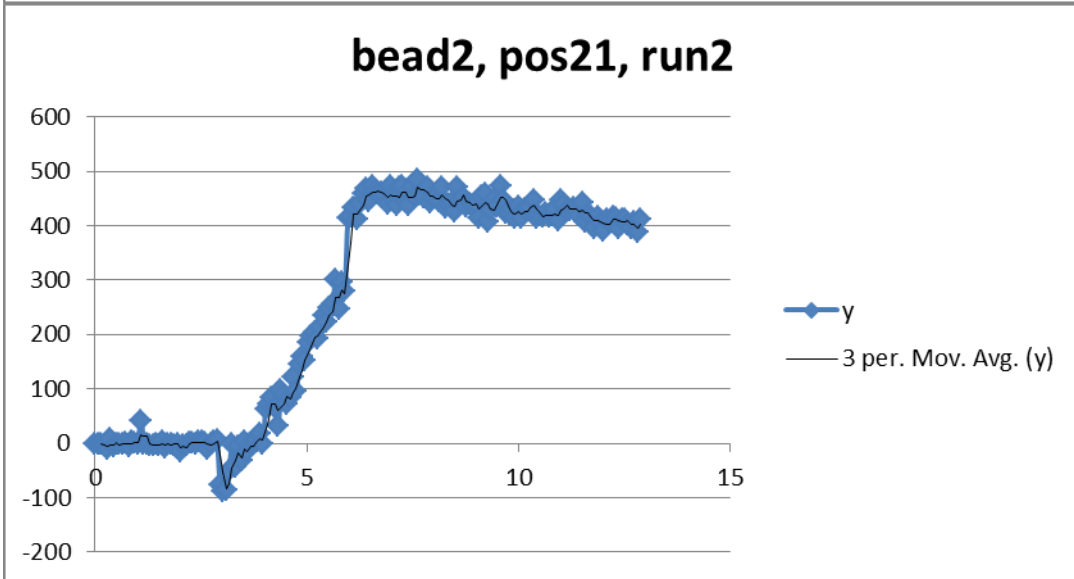
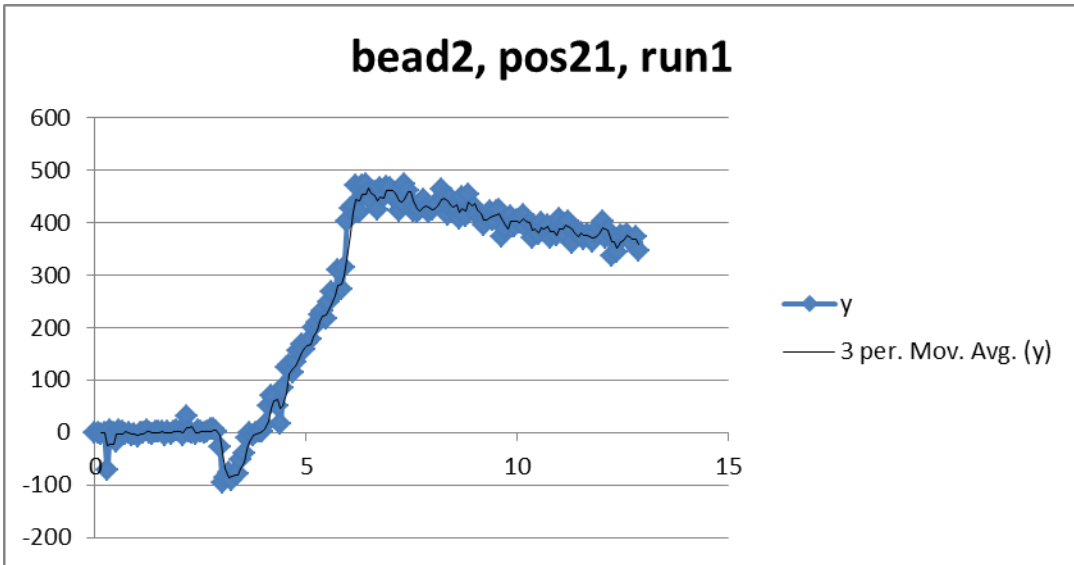


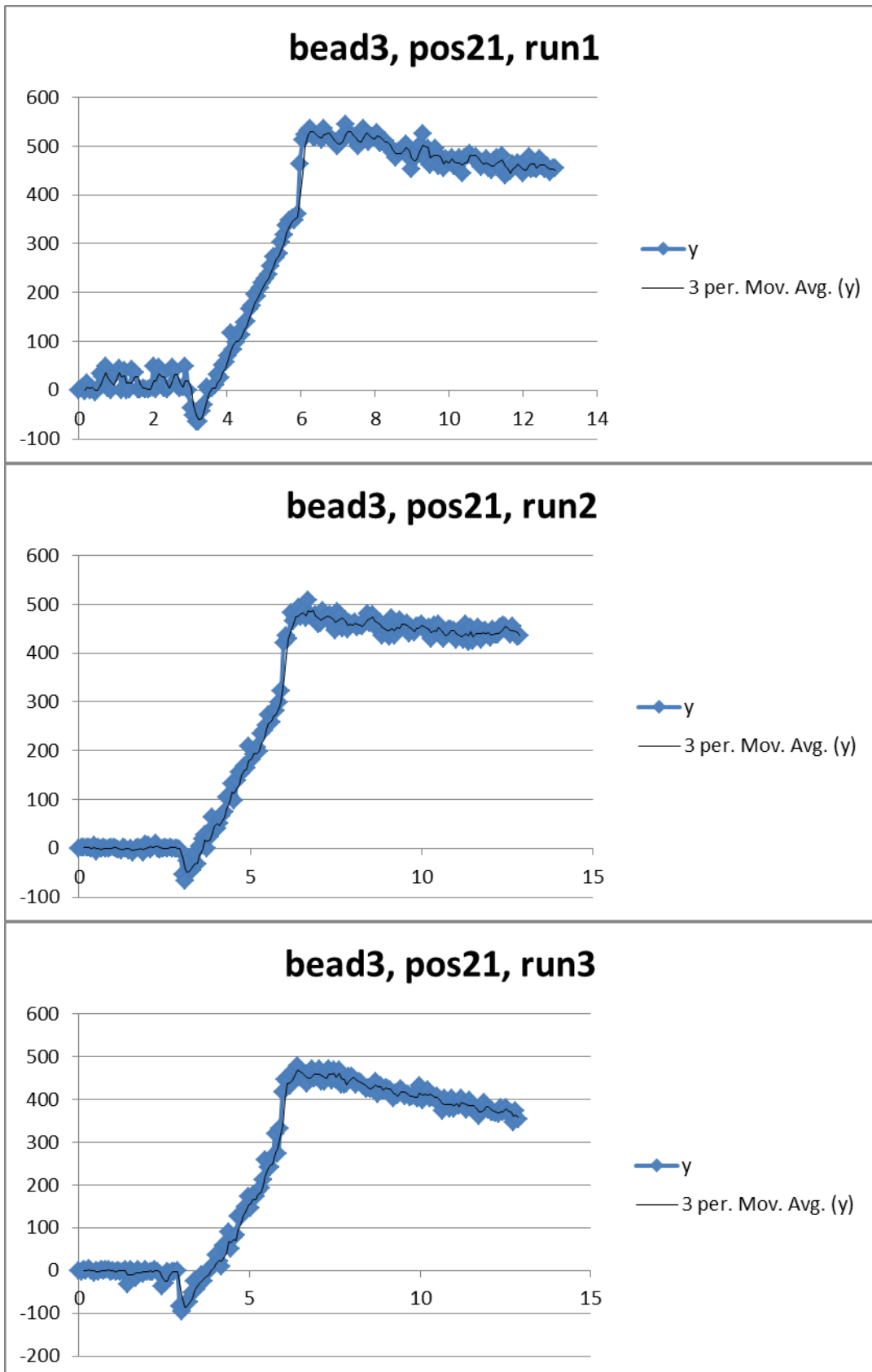


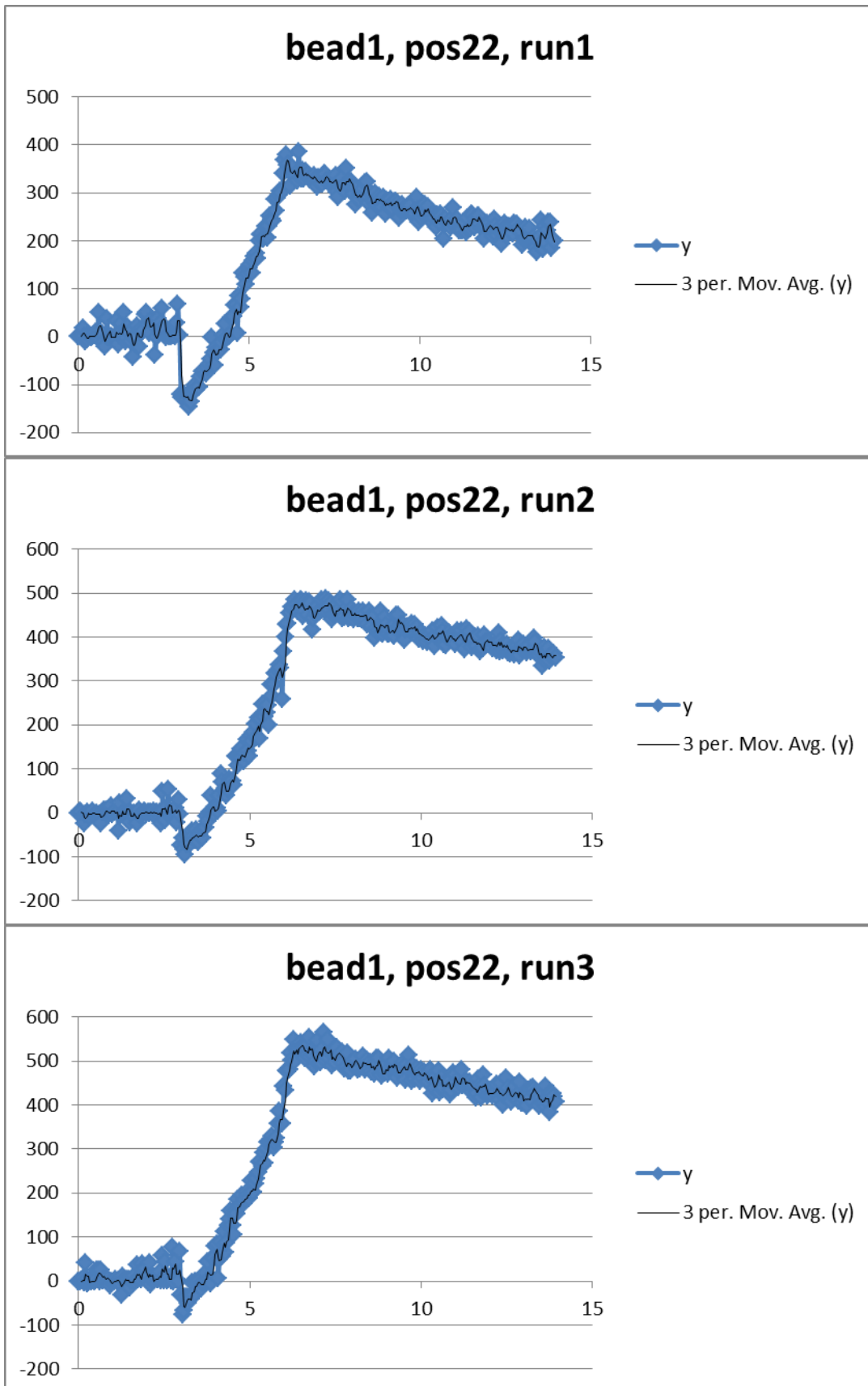


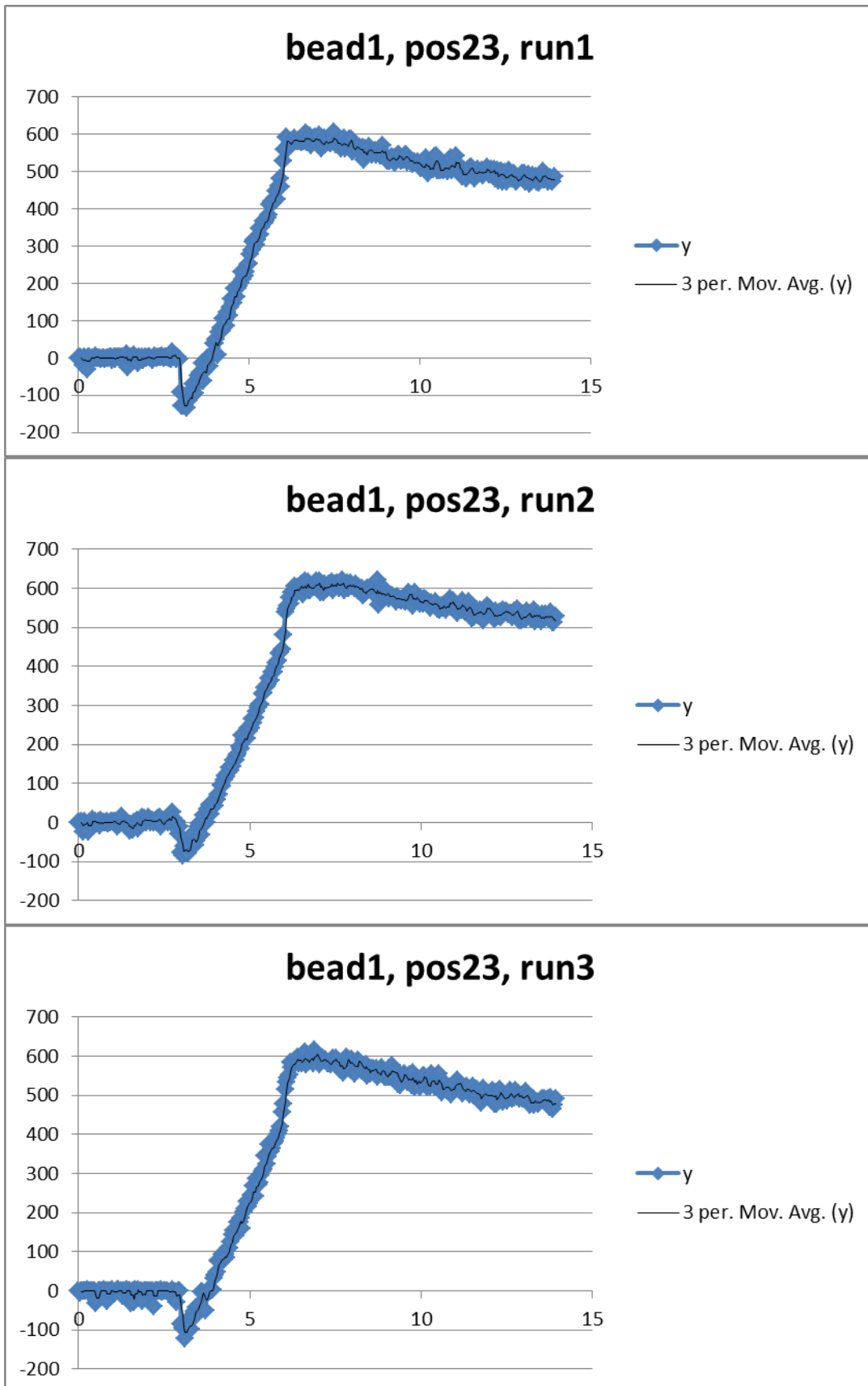


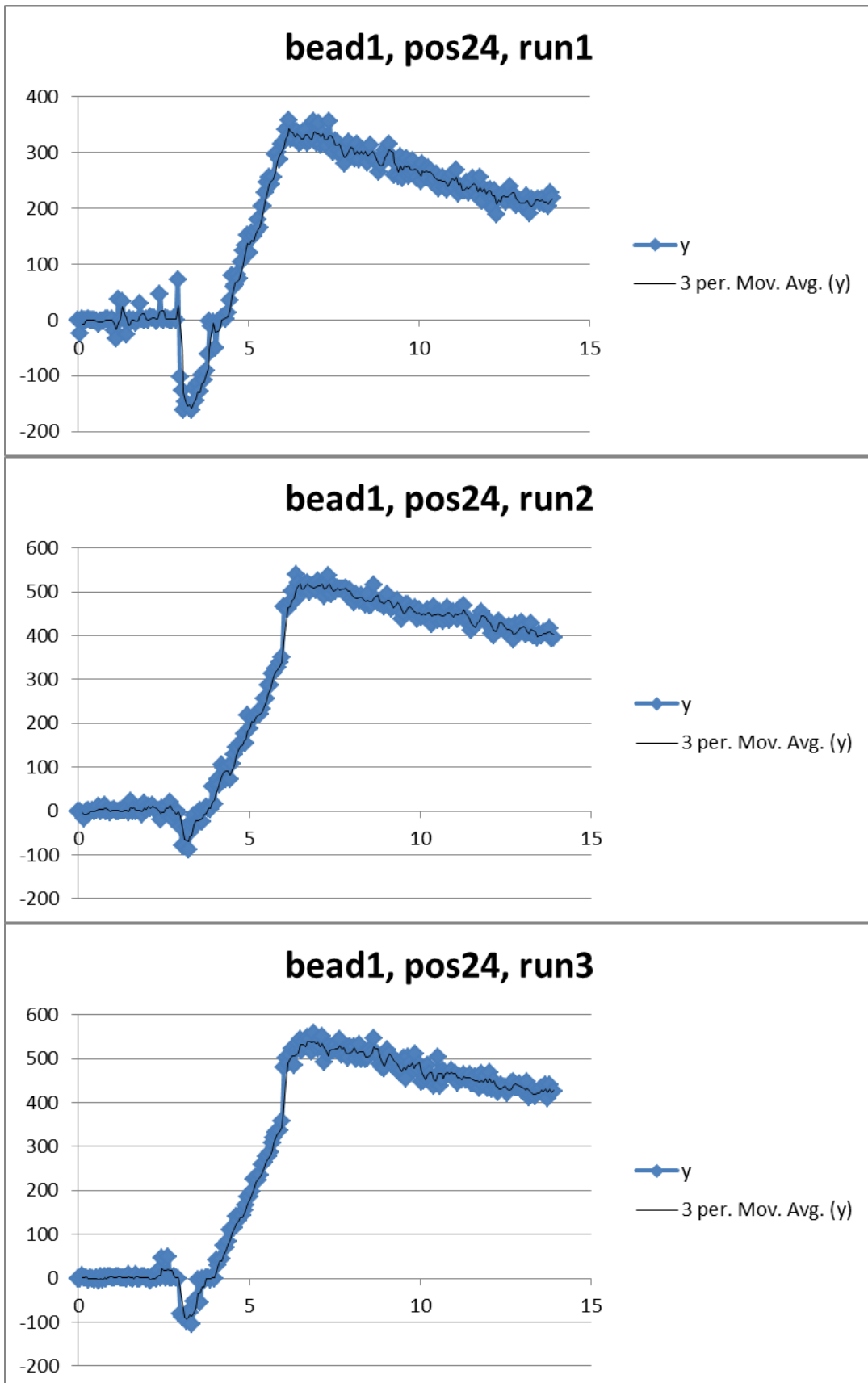


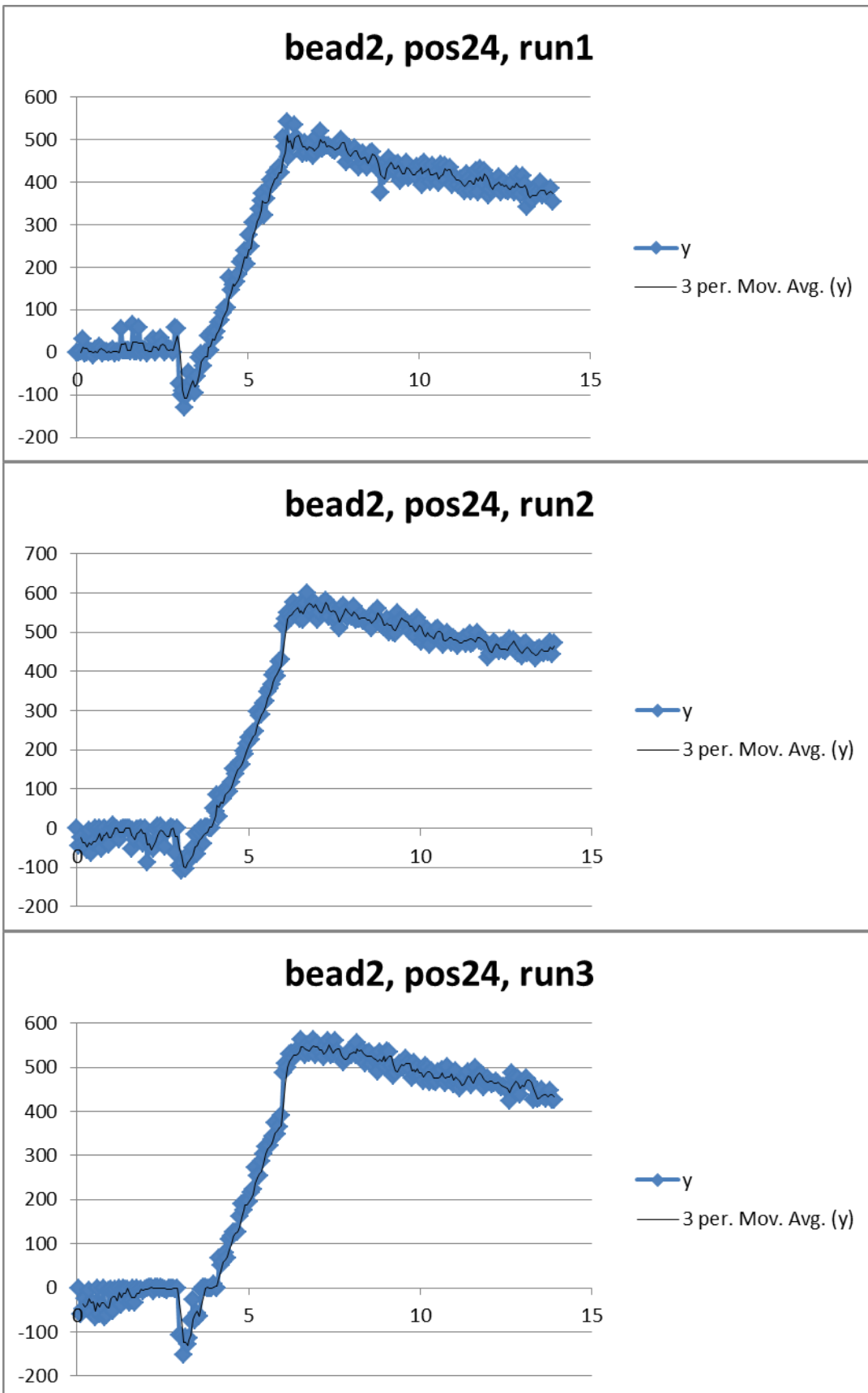


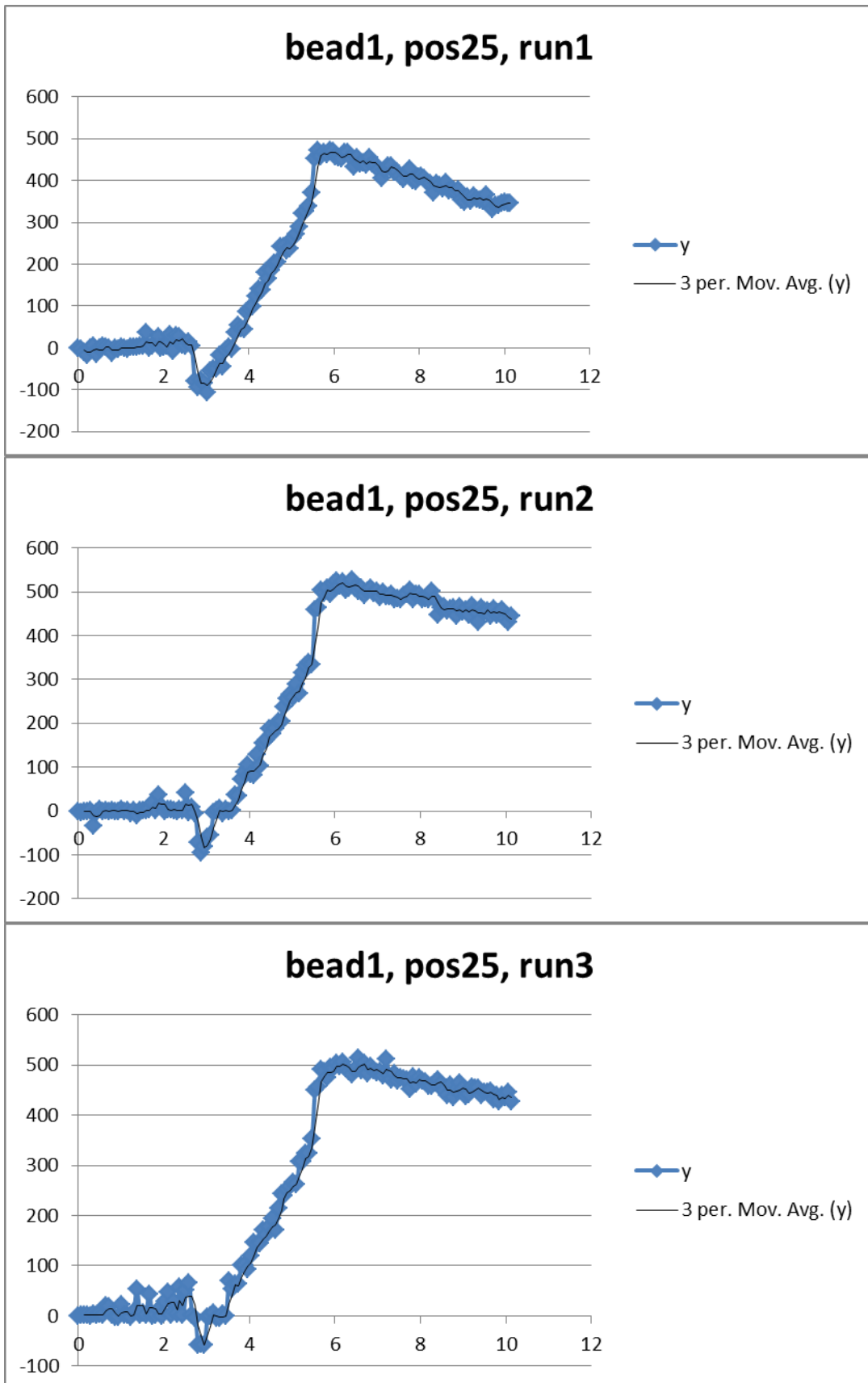


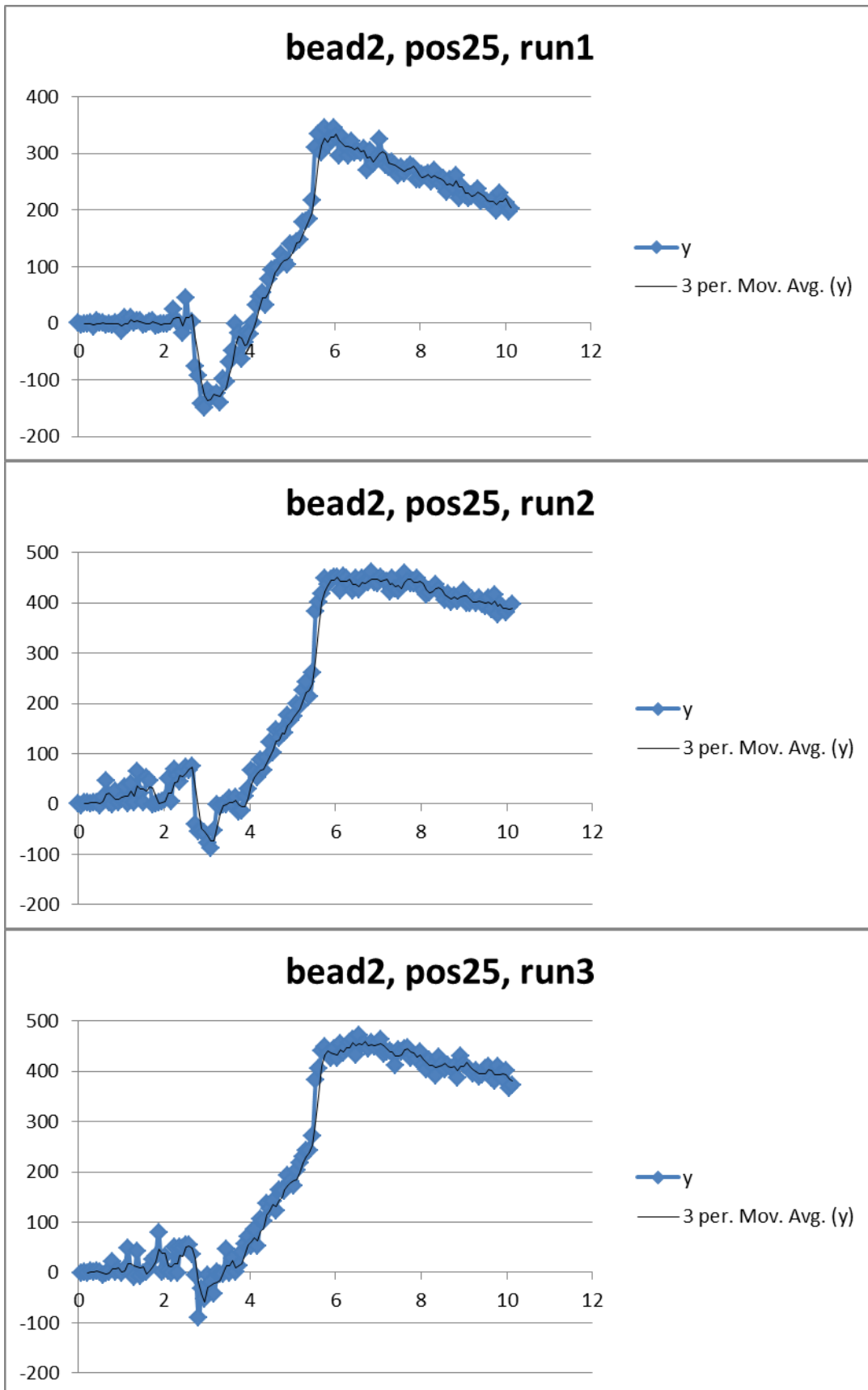


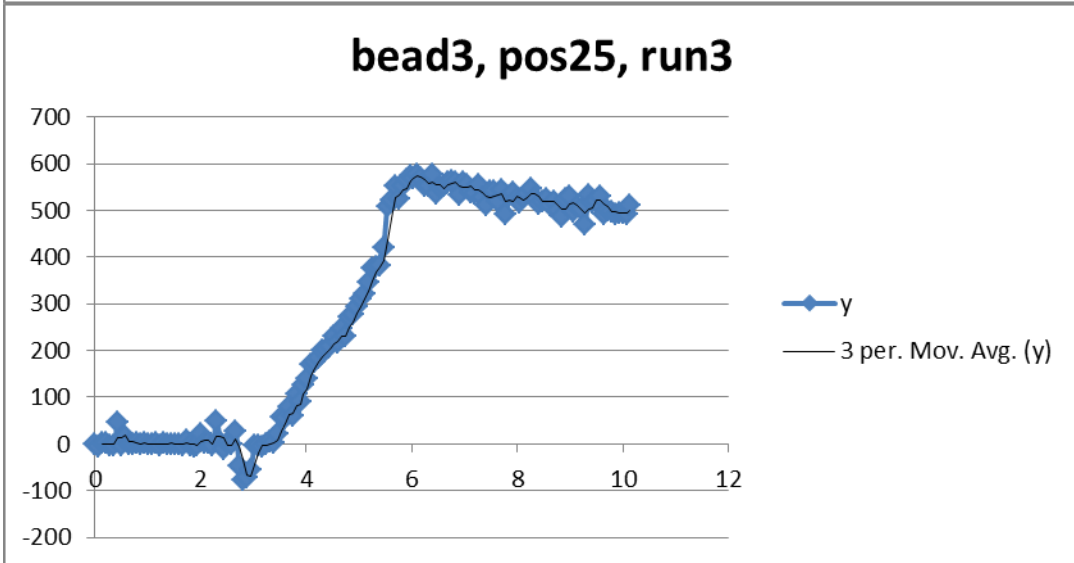
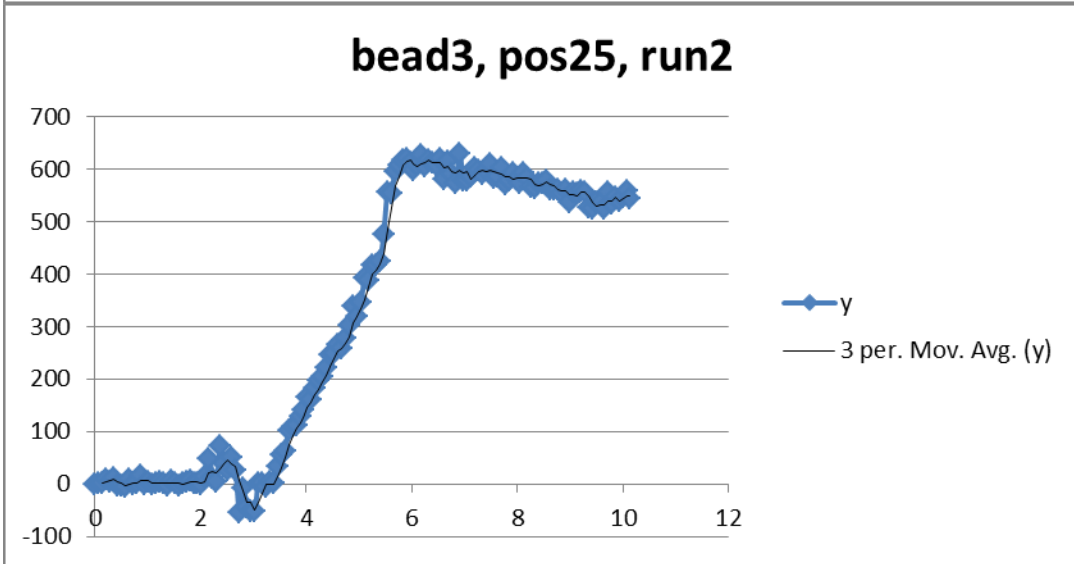
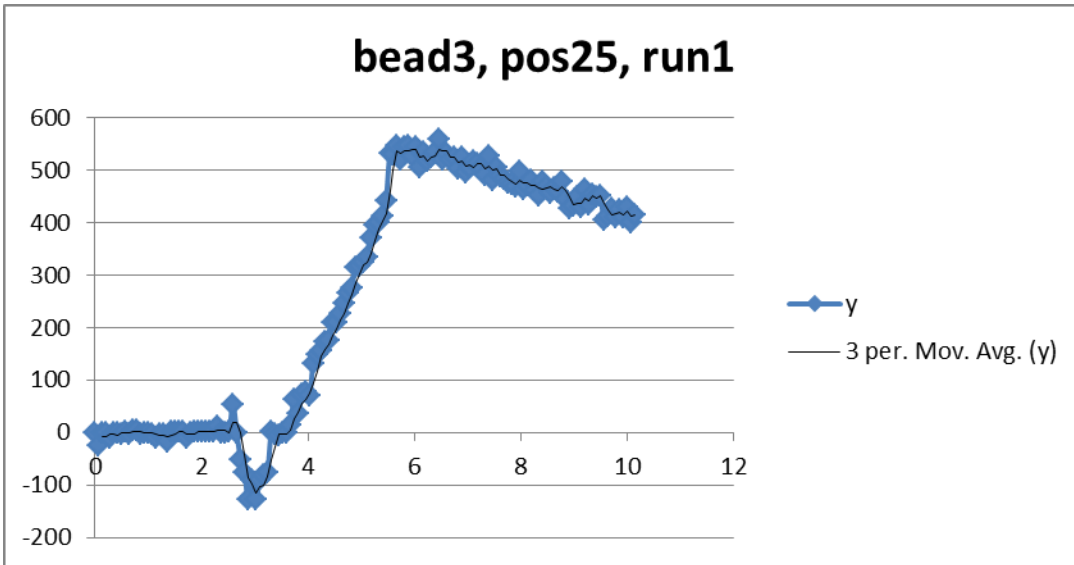


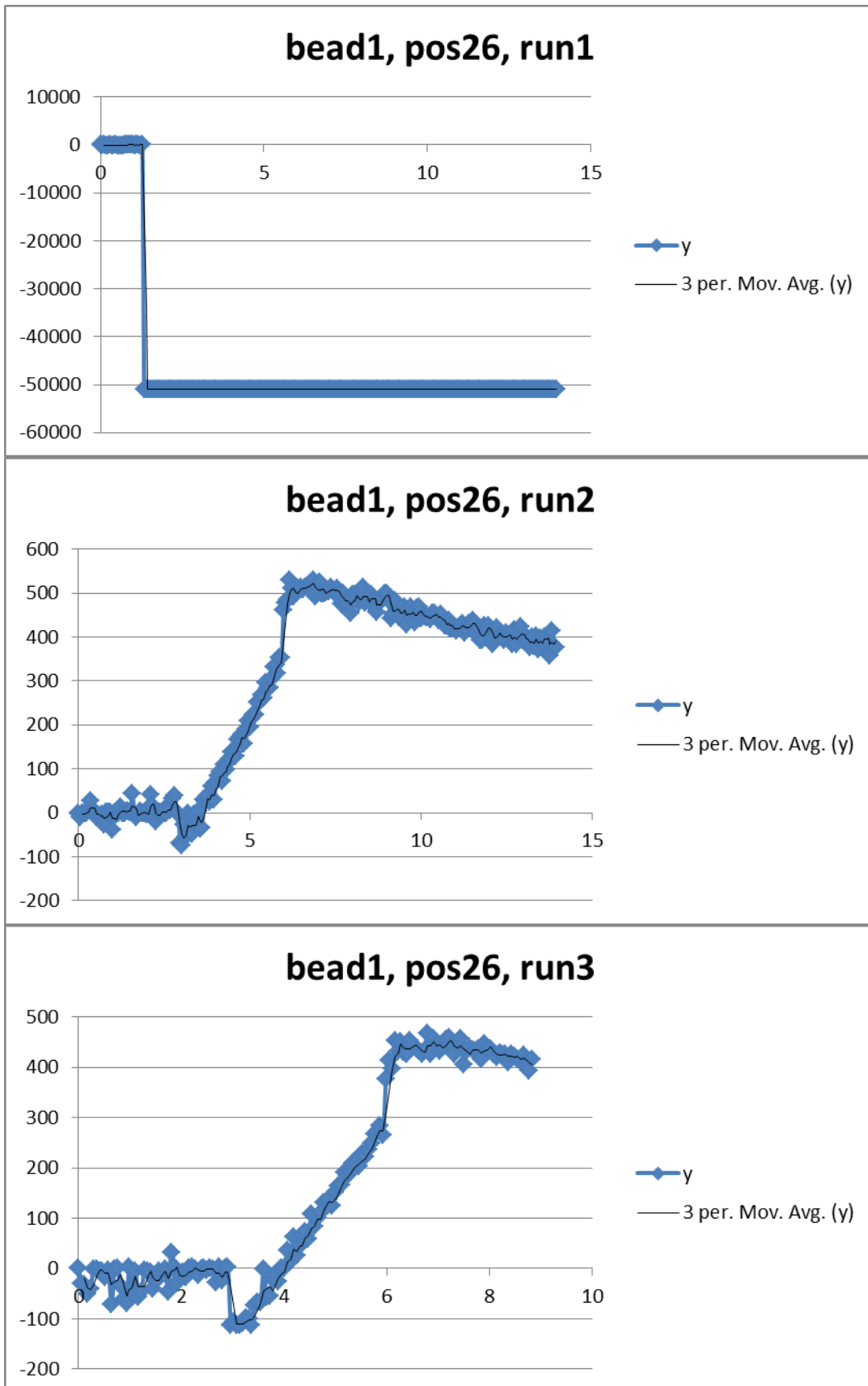


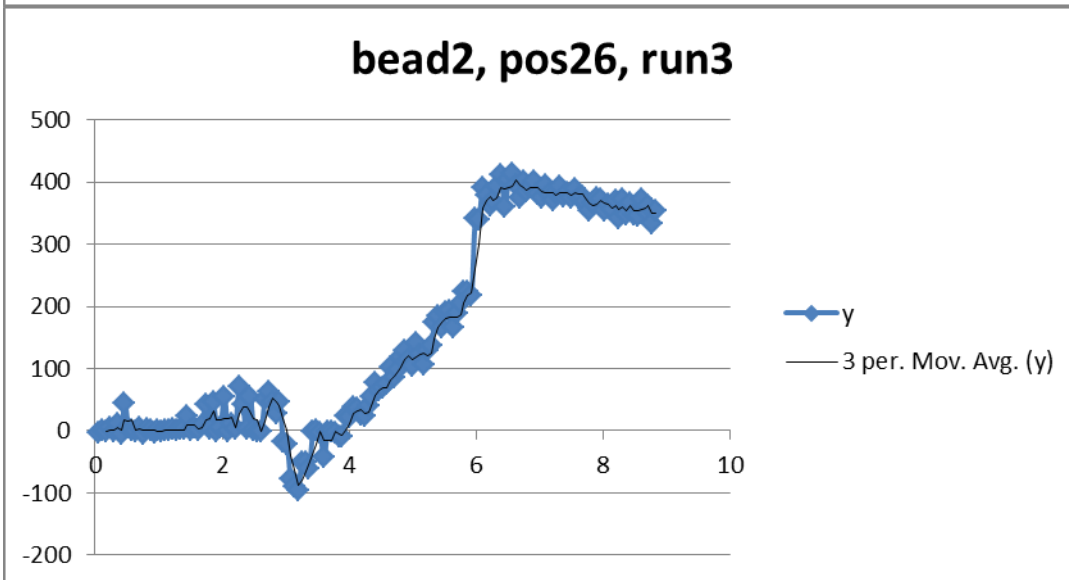
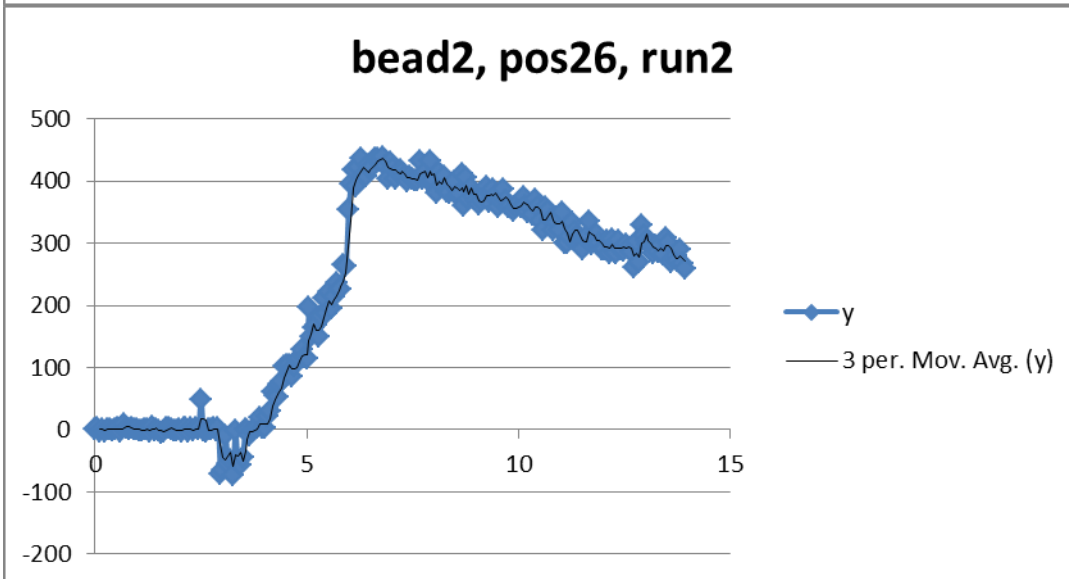


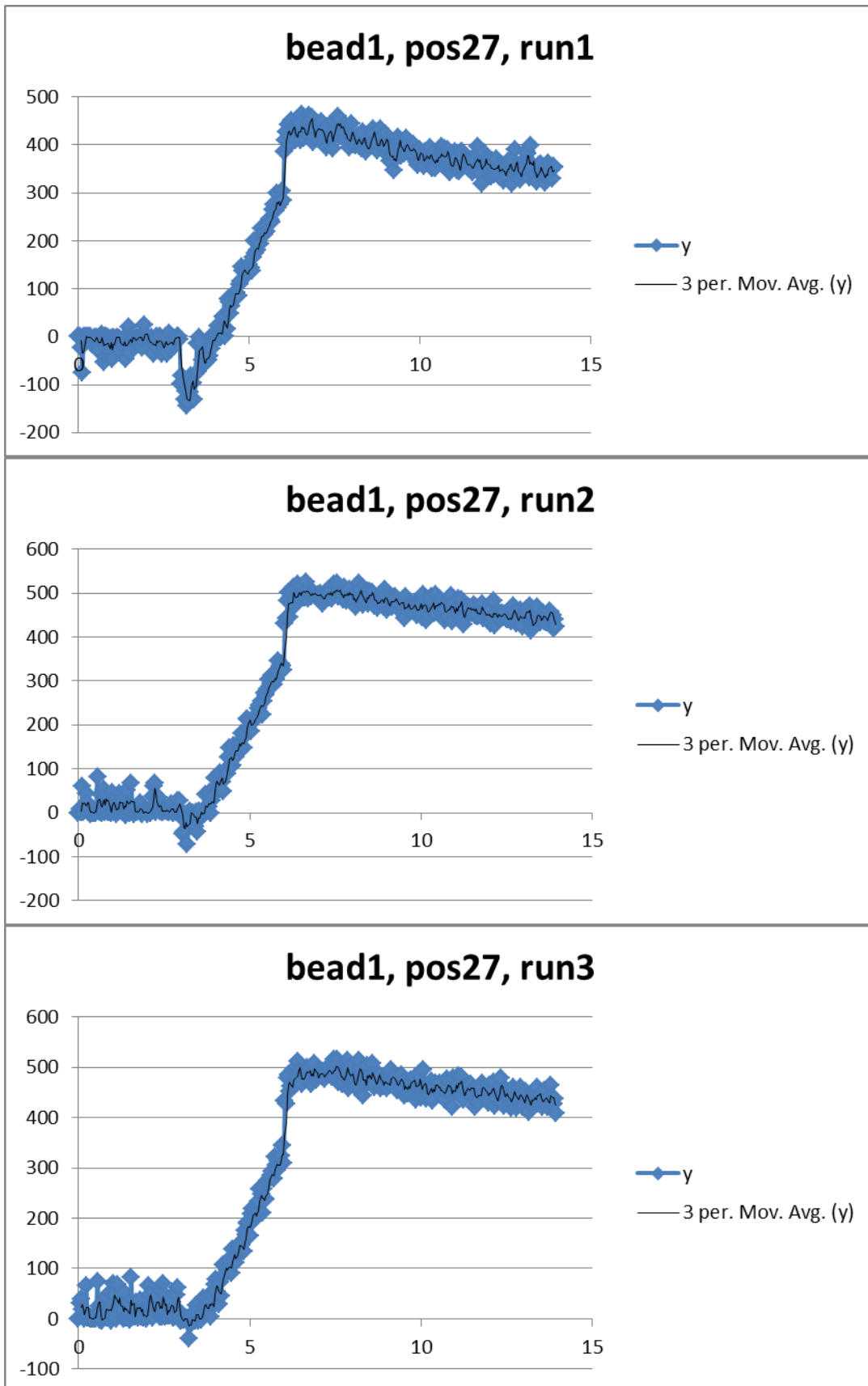












ACADEMIC VITA

Andrew Rogers

EDUCATION

- | | | |
|--------------|-----------------------------------|-------------------|
| 2009-present | The Pennsylvania State University | State College, PA |
|--------------|-----------------------------------|-------------------|
- College of Engineering
 - Schreyer's Honors College
 - Bachelor of Science, Bioengineering, Mechanical Engineering Option

RESEARCH AND MEDICAL EXPERIENCE

- | | | |
|-------------------|---------------------------------|---------------------|
| Fall 2011-present | Penn State Artificial Heart Lab | University Park, PA |
|-------------------|---------------------------------|---------------------|
- Undergraduate Research Assistant*
Primary Investigator: Dr. Keefe Manning
- Individual research project developing a magnetic bead microrheometry system to study blood clot elasticity
 - Experience with techniques such as blood flow loops, fluorescent microscopy, and histology
 - Received 2012 American Heart Association SURF grant

- | | | |
|--------------------------|-------------------------------------|-------------|
| Summers 2009, 2010, 2011 | Penn State Hershey Cancer Institute | Hershey, PA |
|--------------------------|-------------------------------------|-------------|
- Lab Assistant*

Loughran Lab, Primary Investigator: Dr. Xin Liu

- Experience with techniques related to immunohistochemistry, micropipetting, western blotting, MTT assay, flow cytometry, bacteria and cell culture, RT-PCR, blood processing, and animal studies
- Certified in handling mice and rats

- | | | |
|-----------|---|-------------|
| 2007-2009 | Pennsylvania Youth Apprenticeship Program, Hershey Medical Center | Hershey, PA |
|-----------|---|-------------|
- Intern*

- Daily internship shadowing doctors, nurses and technicians in over 22 rotations
- One full semester rotation (each) in Neurology and Sports Medicine

- | | | |
|---------------|---------------------------------|--------------------|
| November 2009 | Hearts for Ecuador Mission Trip | Guayaquil, Ecuador |
|---------------|---------------------------------|--------------------|
- Translator and Student*

- Traveled with Team of Pediatric Cardiologists and Cardiothoracic Surgeons
- Acted as a translator between the medical staff and Ecuadorians

PUBLICATIONS

- Liu X, Ryland L, Yang J, Liao AJ, Aliaga C, Watts R, Tan S, Kaiser J, **Rogers A**, Loughran K, Yuen J, Meng FX, Baab KT, Jarbaldan NR, Broeg K, Zhang R, Liao J, Kester M, Loughran TP JR. "Targeting of Survivin by Nanoliposomal Ceramide Induces Complete Remission in NK-LGL Leukemia." *Blood* 116.20 (2010): 4192-201.
- Liao AJ, Broeg K, Fox T, Tan S, Watts R, Shah M, Ryland L, Yang J, Aliaga C, **Rogers A**, Hirsch L, Jarbaldan NR, Baab KT, Liao J, Wang HG, Kester M, Desai D, Amin S, Loughran TP JR, Liu X. "Therapeutic Efficacy of FTY720 in a rat model of Large Granular Lymphocyte Leukemia" *Blood* 118.10 (2011): 2793-800.

ENGINEERING DESIGN PROJECTS

- Senior Capstone Design Project Spring 2013 - Present
- Developing an object avoidance visual feedback system for patients with Left Homonymous Hemianopsia
 - In collaboration with the University of Toronto and St. John's Rehabilitation Hospital
 - Team coordinator and contact person for our collaborators in Toronto
- Junior Design Project Spring 2012
- ENT Scope for the Mashavu Telemedicine System
 - Designed and built a prototype ENT scope designed for robust use in the developing world for less than \$10
 - Team coordinator and user interface programmer

OTHER WORK EXPERIENCE

- December 2010 - March 2011 Tussey Mountain Ski School Boalsburg, PA
Ski Instructor
- Worked with students between the ages of four and sixty
 - Taught a Penn State Beginner Kinesiology class
- 2003-2011 Rogers Lawn Service Hershey, PA
Owner
- Owner and operator of neighborhood lawn care service
 - Managed up to 8 accounts
 - Effective communication with clients

LEADERSHIP EXPERIENCE

- One Heart: Penn State Students Against The Sexual Abuse of Children
- Co-Founder and President 2011 – present
 - Led development of the organization initial conception
 - Led integration of other merged organizations and initiatives
 - Represented One Heart at the Penn State Child Sexual Abuse Conference
- Religious Education Teacher at Our Lady of Victory Catholic Church
- Taught 3rd grade Fall 2011 – Spring 2012
 - Taught 9th grade Fall 2012 – present
- Happy Pickles Flag Football
- Defensive Coordinator 2009-2011

AWARDS

- Awarded while at Penn State University
- The President's Freshman Award
 - The President Sparks Award